

Alma Mater Studiorum – Università di Bologna

DOTTORATO DI RICERCA IN

CHIMICA

Ciclo XXVIII

Settore Concorsuale di afferenza: 03/C1

Settore Scientifico disciplinare: CHIM/06

Design and synthesis of new luminescent materials:
from light sources to biological applications

Presentata da: Elia Matteucci

Coordinatore Dottorato

Prof. Aldo Roda

Relatore

Prof.ssa Letizia Sambri

Esame finale anno 2016

Index

Abstract	I
1. Luminescence	1
2. Why luminescent metal complexes matter	5
2.1 <i>Illuminating the World</i>	6
2.2 <i>Biological luminescent probes</i>	12
2.3 <i>Other important applications</i>	16
3. The role of the Ir(III)	18
3.1 <i>Ir(III) complexes for blue-light</i>	32
4. White light: goal for the future	34
5. Purpose of the work	38
6. Bibliography	40
7. A chelating diisocyanide ligand for cyclometalated Ir(III) complexes with strong and tunable luminescence	46
7.1 <i>Result and discussion</i>	46
7.1.1 <i>Synthesis of ligand 1 and complexes 2-4</i>	46
7.1.2 <i>Structural characterization</i>	48
7.1.3 <i>Electrochemical properties</i>	50
7.1.4 <i>Ground-state theoretical calculations</i>	51
7.1.5 <i>Photophysical properties and excited-state characterization</i>	53
7.2 <i>Conclusions</i>	57
7.3 <i>Experimental section</i>	57
7.4 <i>Bibliography</i>	62
8. Moving toward the blue: a new difluorophenyl-tetrazole as cyclometalating ligand for Ir(III) complexes	65
8.1 <i>Results and discussion</i>	66
8.1.1 <i>Synthesis</i>	66

8.1.2 Structural characterization	68
8.1.3 Photophysical properties	70
8.2 Conclusions	74
8.3 Experimental section	74
8.4 Bibliography	79
9. Heterometallic Ir(III)₂-Eu(III) complexes: white light emission from a single molecule	81
9.1 Results and discussion	82
9.1.1 Synthesis of ligand 2H	82
9.1.2 Synthesis of the Ir(III) dimers and Ir(III)-Eu(III) complexes	83
9.1.3 Photophysical properties	86
9.2 Conclusions	93
9.3 Experimental section	93
9.4 Bibliography	99
10. New organic white emitters: conjugated carbazole-terpyridine systems	100
10.1 Results and discussion	101
10.1.1 Synthesis	101
10.1.2 Photophysical properties	106
10.2 Conclusions	107
10.3 Experimental section	107
10.4 Bibliography	119
11. A mesoionic carbene as neutral ligand for phosphorescent cationic Ir(III) complexes	121
11.1 Results and discussion	122
11.1.1 Synthesis of complexes 3 and 5	122
11.1.2 Structural characterization	123
11.1.3 Electrochemical properties	127
11.1.4 Ground-state theoretical calculations	128
11.1.5 Photophysical properties and excited-state characterization	132

11.2 Conclusions	135
11.3 Experimental section	136
11.4 Bibliography	140
12. Ir complexes for in vitro imaging on glioblastoma cell line	143
12.1 Results and discussion	144
12.1.1 Synthesis of Iridium complex	144
12.1.2 Synthesis of the nanoparticles	145
12.1.3 ζ potential and hydrodynamic diameter	146
12.1.4 Photophysical characterization	146
12.1.5 Internalization of Ir(III)-NPs	147
12.2 Conclusions	148
12.3 Experimental section	148
12.4 Bibliography	151

Abstract

The synthesis of luminescent metal complexes is a very challenging task since they can be regarded as the starting point for many different areas. Luminescent complexes, in fact, can be used for technological, industrial, medical and biological applications. They consist of two main parts: the central core of the complex, a metal atom, and various organic ligands bonded to it.

Among all the transition metal complexes, Iridium(III) ones show the best photophysical properties: generally, they have high quantum yields, very long lifetimes and possess easily tunable emissions throughout the visible range.

During my PhD I prepared different families of Ir(III) complexes suitable for various applications.

In detail, my thesis deals with the synthesis of new functionalized chelating ligands that have been used to obtain phosphorescent Ir(III) complexes. In particular I synthesised isocyanides, phenyltetrazole and pyridil-triazolylidene derivatives and various corresponding Ir(III) complexes with peculiar photophysical properties, suitable for the preparation of electroluminescent devices.

Moreover, I synthesized pyridiltriazole chelating ligands for the preparation of Ir(III) complexes able to be embedded in nanoparticles. At the same time, I set up the synthesis of various carbazole-terpyridines systems containing substituent of different length and aromatic character.

During my studies, I enhanced my knowledges about the techniques for the spectroscopical characterization of the obtained compounds, such as mono- and bidimensional and VT- NMR, UV-vis and spectrofluorimetry.

1. Luminescence

The emission of light is a physical phenomenon that occurs in response to an external stimulus, which may be in the form of thermal, electrical or chemical energy. This phenomenon can be divided in two different family, depending on the type of the stimulus. If the energy source is thermal, the phenomenon is named incandescence, giving the so-called “hot-light”. On the contrary, when the energy source is of a different kind, the phenomenon take the name of luminescence, giving the “cold-light”. Luminescence can assumes different names, depending on the nature of the external stimulus (Table 1).

Table 1: Types of luminescence, according to the excitation source

<i>Name</i>	<i>Stimulus</i>
Bioluminescence	Enzymatic reaction
Chemiluminescence	Chemical reaction
Elettrochemiluminescence	Chemical reaction electrochemically induced
Elettroluminescence	Electricity
Photoluminescence	Photonons
Radioluminescence	Ionizing
Sonoluminescence	Sound waves
Triboluminescence	Mechanical efforts

The most well-known and studied phenomenon is the photoluminescence. A substance that is able to emit light after a luminous stimulus is called fluorophore.

According to the Boltzmann distribution, at room temperature the population of excited electronic states is neglectable compared to the one of the lowest energy level, the ground state. For this reason, it is assumed that almost all of the molecules are in the lower electronic state, with orbitals occupied by pairs of electrons with paired spins (antiparallel), in order to have total spin equal to 0 and multiplicity equal to 1 (singlet ground state S_0). When subjected to a stimulus, in this case to a light excitation, most of the molecules are promoted from the ground state to an electronic excited state, usually indicated as S_n . The just populate excited state is not stable, therefore the promoted molecules will return to the ground state thtough two different deactivation pathways: radiative or non-radiative decay mechanisms.

The non-radiative deactivation mechanism takes place without the emission of photons and consist of three main processes:

- *vibrational relaxation*: the excited molecule transfers vibrational energy through collisions with the surrounding molecules (time $\approx 10^{-12}$ s);
- *internal conversion*: transitions between electronic states of the same multiplicity (time $\approx 10^{-13}$ s);
- *intersystem crossing*: transition between two electronic states with different multiplicity, for example from singlet to triplet (time $\approx 10^{-8}$ s).

On the other hand, radiative deactivations mechanisms occur with an emission of photons, and can be of different nature:

- *fluorescence*: transition from the lowest excited singlet state (S_1) to the ground state (S_0), spin-allowed (time $\approx 10^{-9}$ s);
- *phosphorescence*: transition from the triplet lowest excited state (T_1) to the singlet ground state (S_0), spin-forbidden (time $\approx 10^{-6}$ s);
- *radiation of resonance*: emission with a frequency equal to that absorbed. Occurs only for low-pressure gas (time $\approx 10^{-8}$ s).

Comparing the typical lifetimes of the described processes, it is clear that there is always a competition between the non-radiative deactivation pathways and the radiative ones, so the latter may not be displayed at all. This can be due to several factors, such as a great flexibility of the molecular structure, the high temperature, that increase the mobility of the molecules favoring the collisions, or the presence of a solvent able to absorb the energy of the excited molecules. Accordingly, fluorescence or phosphorescence processes are rarely observed and most of the substances present in nature does not present these phenomena at all.

All the above described mechanisms are well schematized in the Jablonski diagram (Figure 1).¹ When irradiate with the right energy, a molecule can absorb light and can be promoted to an excited state, generally called S_n . The molecule can then decay to the lowest excited state S_1 , through internal conversion (non-radiative deactivation pathway).² From this state, two different mechanisms can occur: a) the molecule in the S_1 state can relax to the S_0 ground state through the emission of a photon, giving the fluorescence process; it's important to underline that fluorescence can be observed only for $S_1 \rightarrow S_0$ transitions;³ b) the internal conversion takes place, leading to the population of triplet state T_1 . When the molecule is in the T_1 state, phosphorescence can occur.

Obviously, the phosphorescence emission can be observed only if the intersystem crossing process is efficient enough to compete with other deactivation mechanisms, allowing the population of the triplet state. Indeed, based on the selection rules,⁴ transitions between states with different spin are forbidden, but these are promoted by the presence of a heavy atom with a large spin-orbit coupling constant. Furthermore, based on the Hund's rules (or maximum multiplicity principles),⁵ the triplet states have lower energies compared to the corresponding singlet states, therefore the phosphorescence emission always occurs at longer wavelengths than fluorescence. Moreover, because phosphorescence is a spin-forbidden process (from the triplet T_1 state to the singlet S_0 ground state), the emission is always observed with longer relaxation time than the fluorescence emission.

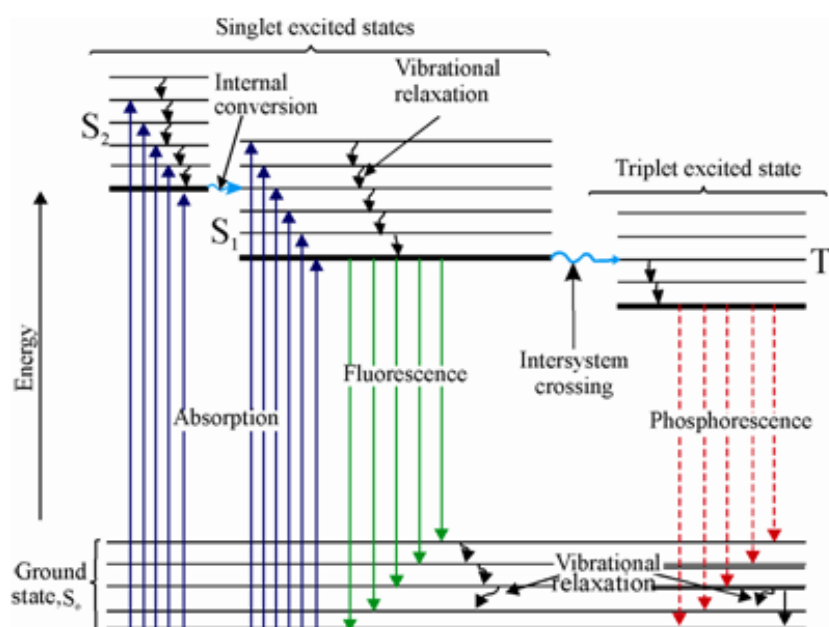


Figure 1: The Jablonski diagram

A further deactivation pathway for the excited state is the quenching. Three different types of quenching can be observed:

- collisional quenching: generally it is a bimolecular process that occurs when a substance (quencher), different from the fluorophore and able to absorb the energy possessed by the excited molecule, and the fluorophore hit each other; the result is the excitation of the quencher (that usually decay through a non-radiative deactivation pathway) and the relaxation of the fluorophore to the ground state;
- static quenching: occurs when there is the formation of a non-fluorescent complex between the fluorophore and the quencher;

- self-quenching: it is a typical phenomenon that occur when molecules of the same fluorophore act as quenchers; alternatively, it can be observed in the presence of substances that can absorb light at the same wavelength of that emitted by the fluorophore.

The ability of a substance to emit light can be quantified with the quantum yield (Φ), which is calculated as the ratio between the energy emitted by radiation and the total absorbed energy:

$$\Phi = k_r / (k_r + k_{nr} + k_q[Q])$$

where k_r , k_{nr} and k_q are the rate constants of radiative, non-radiative and quenching processes, respectively. It is evident that, in order to maximize the emission of light from a substance, the speed of all the other processes, responsible for the non-radiative deactivation of the excited state, should be reduced as much as possible.

Another important parameter that should be taken in consideration is the lifetimes, or decay time (τ) of the excited state, that represent the average time that an excited molecule spends in the excited state before decaying in a radiative way. It can be calculated as:

$$\tau = 1 / (k_r + k_{nr} + k_q[Q])$$

This parameter is essential for the evaluation of the possible applications of different luminescent compounds. Fluorescence and phosphorescence can be easily distinguished based on the difference lifetime of the excited state: in the first case, the typical value observed is of the order of nanoseconds (ns), while for the phosphorescence, lifetimes are usually of the order of microseconds (μ s).

2. Why luminescent metal complexes matter

The design and synthesis of luminescent substances is nowadays a very current topic of interest in different fields of the scientific research. In fact, many publications can be found in chemical journals, but also in medical, biological and technological reviews, demonstrating how this topic can be considered as a starting point for various studies.

Despite the considerable interest, the obtainment of substances for the preparation of new materials or devices still presents many problems, principally due to the high production costs and the poor durability of the finished products. For this reason, the research in this topic is still going on, trying to synthesize new organic functionalized molecules, which can be used as low costs and highly available ligands for metal cations, to form luminescent complexes.

In this context, it has been observed a significant increase of interest in the synthesis of transition metal complexes (Ir(III), Re(I), Ru(II), Pt(II) and Os(II)) with organic ligands.⁶ The reason for such expansion can be attributed to their unique luminescent properties together with high photochemical and thermal stability and a potential internal quantum efficiency of 100%. These complexes are able to exploit the fluorescence emission from singlet excited states as well as the phosphorescence from triplet states, generated by a high spin-orbit coupling, typical of the elements belonging to the second and third transition series, which allows an efficient intersystem crossing.

Among the plethora of transition metals complexes, Iridium (III) complexes play a very important role in different applications.⁷ However, also other transition metal derivative, *i.e.* Rhenium (I) and Zinc (II) complexes, or lanthanide derivative, *i.e.* Europium (III) complexes, have found a wide range of applications in different fields. Typically, all these metal complexes are used as sensitizers for outer-sphere electron-transfer reactions,⁸ photocatalysts,⁹ photoreductants or photooxidants,¹⁰ pH sensor,¹¹ biological luminescent probes and assays, medical diagnostics and optical imaging devices.¹² Nevertheless, the main application for this class of compound is the employment as emissive dopants in multicolor electroluminescent displays based on organic light emitting devices (OLEDs) and light-emitting electrochemical cells (LECs).

During my Ph.D. studies, I focalized the attention on the application of this class of molecules in two different fields, namely their use in electroluminescent devices (OLEDs and LECs) and as biological probes for medical diagnostics and optical imaging.

2.1 Illuminating the World

The diffusion of artificial lighting is one of the greatest achievements of the 20th century, in fact for millennia artificial lighting was generated by open fires first, and by oil lamps or gas light later. In 1879, taking advantage of the work of many other inventors and after having tested hundreds of different materials as filaments, Thomas A. Edison patented the incandescent carbon filament lamp, a milestone of modern lighting. Edison's device converted just 0.2% of electricity into light, but it was 20-times more efficient than a candle in converting chemical energy into useful photons.¹³ In the following decades, electric lighting devices underwent substantial progress in terms of efficiency and all the systems that are still used nowadays were introduced: the tungsten lamp (1906), that dominated residential lighting for one century, the sodium vapor lamp (1930s), now utilized for street illumination in its modern high-pressure variant, and the fluorescent tubes (1940s), very popular in large internal environments, such as offices and factories.¹⁴

The evolutions of these three fundamental designs were introduced in relatively recent times: the halogen lamp, an advanced filament system, entered the market in the 1960s and the compact fluorescence lamp, a sort of hybrid between bulbs and fluorescent tubes, appeared in the 1980s. The tremendous progress made during the 20th century in improving the quality and availability of artificial lighting was accomplished through the use of two main technologies: incandescent- and discharge-based lamps.¹⁵ Incandescent lamps consist of a bulb containing a wire filament that emits light upon heating in a vacuum. They emit up to 95% of the energy as infrared photons (heat) hence their efficiency is intrinsically low. Discharge lamps generate light by means of an internal electrical discharge between electrodes that produces ultraviolet (UV) radiation, which is then downconverted into visible light by solid or gaseous compounds; they can be substantially more efficient than the incandescent counterpart but often at the expense of color quality. There is a variety of both type of lamps, but these two traditional lighting concepts have been exploited near to their limit; thus, new lighting approaches have emerged in the last two decades (Figure 2).¹⁶

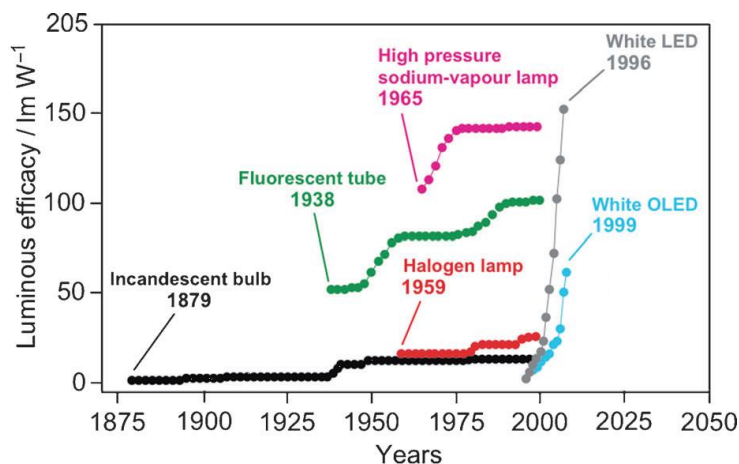


Figure 2: Historical trend of luminous efficacy of the most common light sources

The emerging concept for illumination is solid-state lighting (SSL),¹⁷ in which selected semiconductor materials are stimulated to produce visible light under the action of an electrical field (electroluminescence), in appropriately engineered devices where the transport of charge occurs in one specific direction (diodes). In traditional sources, visible light is essentially a byproduct of other processes, such as heating or discharging, while, through this approach, photon itself is the primary product of these lighting devices. As a result, SSL creates visible light with reduced heat generation or parasitic energy dissipation, while its solid-state nature provides for greater resistance, increasing significantly the lifespan of appliances.¹⁸

There are two main families of SSL devices, namely light emitting diodes (LEDs)¹⁹ and organic light-emitting diodes (OLEDs).^{20,21} The first example of LED was developed in 1962 by Nick Holonyak Jr. at General Electric Company.²² LED technology is based on inorganic semiconductors made from combination of several elements, and represent a basic pn-junction diode, which emits light when activated. When a fitting voltage is applied, electrons are able to recombine with electron holes within the device, releasing energy in the form of photons. The color of the light (corresponding to the energy of the photon) is determined by the energy band gap of the semiconductor. LEDs are now standard for screen backlighting, automotive applications, traffic signaling, advertising, and decoration.¹⁷ Notably, they are acquiring an increasing market share in ambient illumination thanks to the consolidation of white LED concepts.²³

OLEDs differ from classic LEDs for the nature of the emissive layer, typically organic or organometallic. This variation allows OLEDs to be particularly flexible and transparent.

The earliest OLEDs work was reported in 1987 by Tang and Van Slyke from Eastman Kodak labs. They made the first double heterostructure device in which its structure comprised of ITO / diamine HTL / Alq₃ / Mg:Ag.²⁴ A glass substrate was coated with a transparent indium tin oxide (ITO) acting as the anode. A diamine was used as the hole transporting material (HTL) and Alq₃ (tris(8-hydroxyquinoline) aluminum(III)) served as both an electron transporting layer (ETL) and an emissive layer (EML). Electrons were injected from a Mg:Ag alloy cathode with an additional layer of Ag to protect the Mg from oxidation. In this double layer device, electrons and holes combined at the diamine/Alq₃ interface (Figure 3, left). This double layer device utilized HTL and ETL to confine excitons and prevent dispersion. The utilization of HTL and ETL could lead to efficient charge carrier injections. The significant problem with this double layer device is that the excitons emitting from a dense and pure matrix typically go through significant self-quenching that leads to poor external quantum efficiency (~1%). In 1989, Tang, Van Slyke and Chen showed that it was possible to add small quantities of a highly fluorescent dye (green Coumarin 540 or red DCM (4-(Dicyanomethylene)-2-ethyl-6-(4-dimethylaminostyryl)-4H-pyran) fluorescent dyes) to a charge transporting material (Alq₃) in the double layer device to easily tune the OLED emission color. By introducing the fluorescent dopant, they were able to improve the device efficiency up to 2.5%.²⁵ Inside the emissive layer, energy will transfer

readily from the host (Alq_3) to a dopant with a smaller optical gap resulting in efficient emission from the dopant (Figure 3, right). The self-quenching of excitons is also suppressed by lowering the concentration of excitons and the device efficiency is so improved. An additional benefit of doping processes is to control emission colors of OLEDs by doping the EML with different emissive dyes.

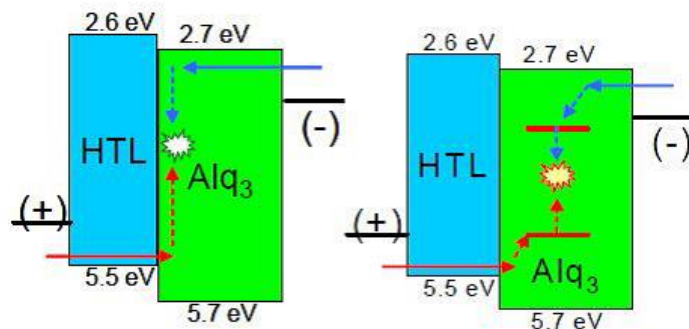


Figure 3: (left) Double layer OLED; (right) Doped-double layer OLED

Over the following years, research on multilayers OLEDs have led to the development of even more efficient devices, with the features of flexibility, low power consumption, lightweight. The basic structure of a multilayer OLED consists of a stack of two or more thin organic layers with a total thickness of about 1000 Å sandwiched between a transparent anode and a metallic cathode, placed on a glass or plastic support (Figure 4). The organic layers consist of a hole transporting layer (HTL), an emissive layer containing a dopant and a host material (EML), and an electron transporting layer (ETL). When an external driving voltage is applied, the introduced positive and negative charges are injected into the organic materials. The positive (holes) and negative (electrons) charges both migrate through the device and recombine to form excitons in the emissive layer. The device lights up (produces electroluminescence) when the excitons decay radiatively. The emission color depends on the energy of the exciton. Particular structures of the organic layers and the choice of anode and cathode should be considered to highly maximize the recombination process in the emissive layer, thus maximizing the light output from the OLED device.

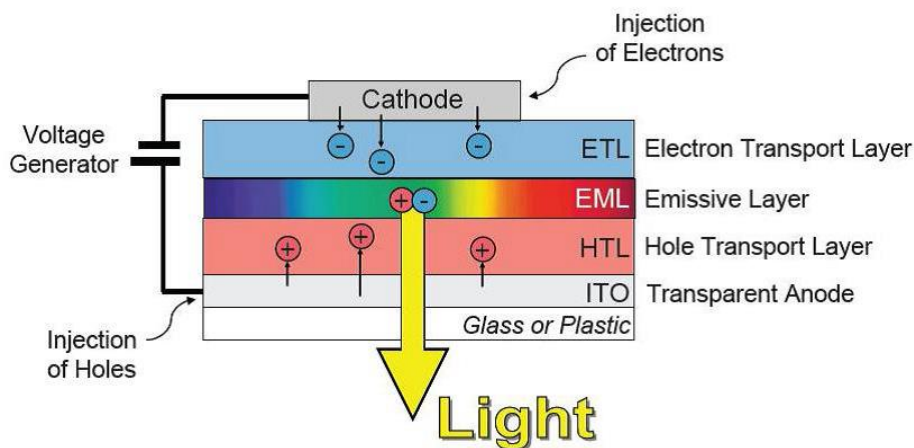


Figure 4: Typical multilayer OLED structure

Excitons in OLEDs are created in a ratio of about 3:1 (Figure 5), *i.e.*, approximately 75% triplets (spin parallel) and 25% singlets (spin antiparallel).²⁶ A fluorescence device only utilizes singlet excitons, while the energy of triplet excitons is generally lost to non-radiative decay processes that heat up the device. This inefficient utilization of triplet excitons limits the internal quantum efficiency of fluorescence-based devices to only 25%. Contrary to fluorescence-based devices, OLEDs utilizing phosphorescent materials that emit from triplet excited states are expected to result in higher internal quantum efficiency.

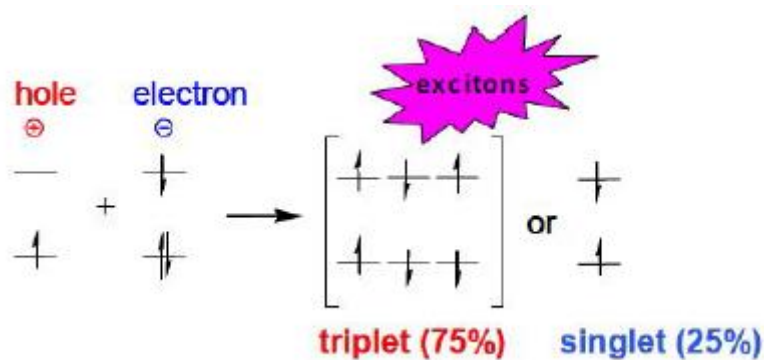


Figure 5: Exciton formation by hole-electron recombination

OLED devices can be fabricated on different types of substrates ranging from rigid glass to flexible polymers which are usually coated with a transparent conductive anode material, indium tin oxide (ITO). Since most organic molecules have low charge transport mobilities ($<10^{-2}\text{cm}^2/\text{Vs}$),²⁷ the films are required to be very thin ($\sim 1000\text{ \AA}$) in order to allow the passage of enough currents at low operating voltages. Organic films comprised of small molecules are usually grown by vapor deposition (sublimation) onto the substrate under high vacuum conditions ($< 10^{-6}$ torr). On the other hand, high molecular weight polymers, that are not

volatile enough for vapor deposition, are typically spincoated or printed onto the substrate. A low work-function metal (e.g. Ca, Al, or Mg) is vapor deposited on top of the organics to serve as the cathode. To improve the device performance, multi-layered materials are used, each of which serves different functions, *i.e.* hole carrier, emissive layer, or electron carrier. The most commonly used hole-transporters consist of an organic triarylamine-based compound. A series of metal quinolates are widely utilized as electron transporting materials. The chemical structure of several typical HTL and ETL molecules, *i.e.* 4,4'-(cyclohexane-1,1-diyl)bis(*N,N*-di-*p*-tolylaniline) (Cta), *N,N'*-bis-(1-naphthyl)-*N,N'*-diphenylbenzidine (α -NPD), Aluminum tris(8-hydroquinolate) (Alq₃), are shown in Figure 6.

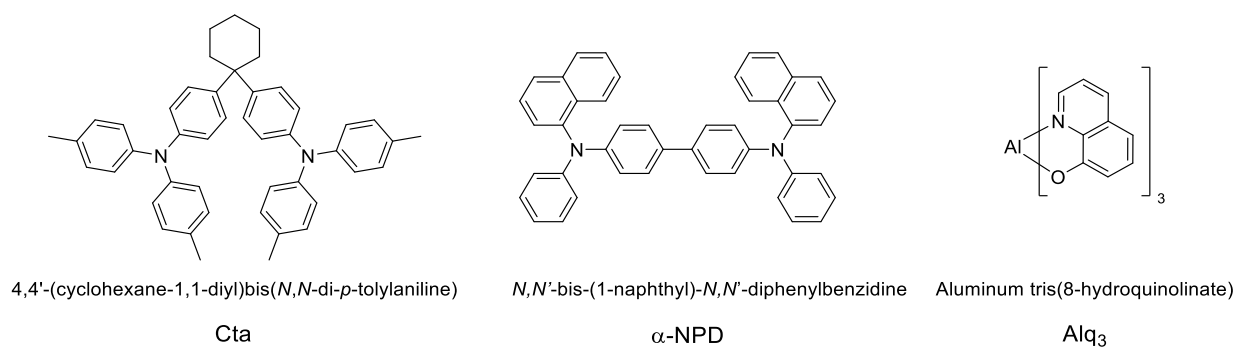


Figure 6: Structures of typical HTL and ETL materials used in OLEDs

In the electroluminescent displays industry it is now accepted that phosphorescence-based OLEDs offer many advantages over existing display technologies. The most common display technology used for portable applications to flat panel display (FPD) TVs is liquid crystal displays (LCDs). A non-organic LCD display does not emit light; a white fluorescent backlight sitting behind the LCD panel is filtered by switchable polarizers in order to generate the pixel colors and to create the image on the screen. Individual liquid crystals allow light to pass or block it. Since the polarize filter is employed in LCD, this leads to a loss in efficiency since most of the light is absorbed by the color filters, and creates viewing angle problems due to the polarized emission. On the other hand OLED displays do not need a backlight since the organic material self-generates light, requiring very low external power and showing, generally, more efficient than LCDs. Additionally, OLEDs do not suffer from viewing angle problems, thus they always display sharp quality images independent of viewing angles.

Nowadays, OLEDs can be utilized for display and illumination but their manufacturing still needs costly and complex procedures in an inert environment that must be followed by a rigorous encapsulation of the final device, particularly because of the presence of low work-function metals or doped injection layers which are extremely sensitive to ambient oxygen and moisture.^{21,28} The multilayer structure, additionally, makes large-area processing extremely difficult, and ultimately imposes a production cost of OLEDs still incompatible with widespread applications in the general lighting market. These limitations have

stimulated the exploitation of new concepts for flat electroluminescent lighting devices;²⁹ among these, LECs (light-emitting electrochemical cells) are the most popular.^{30,31,32} LECs have a much simpler architecture than OLEDs (Figure 7), are processed from solution, do not rely on air-sensitive charge-injection layers or metals for electron injection and hence require less stringent packaging procedures. The concept of LEC was introduced in 1995 by Pei et al.,³³ and consist of an ionic luminescent material in an ionic environment sandwiched between two electrodes. The luminescent material is either a conjugated light-emitting polymer or an ionic transition metal complex (iTMC). The first type is referred to as polymer-LECs (P-LECs).^{33,34} The second type is even simpler as it uses an ionic emitter that enables single-component devices; this type of LECs is referred to as iTMC-LECs.^{35,36,37,38} In this context, the most promising luminescent materials for iTMC-LECs are ionic Ir(III) complexes.³⁹

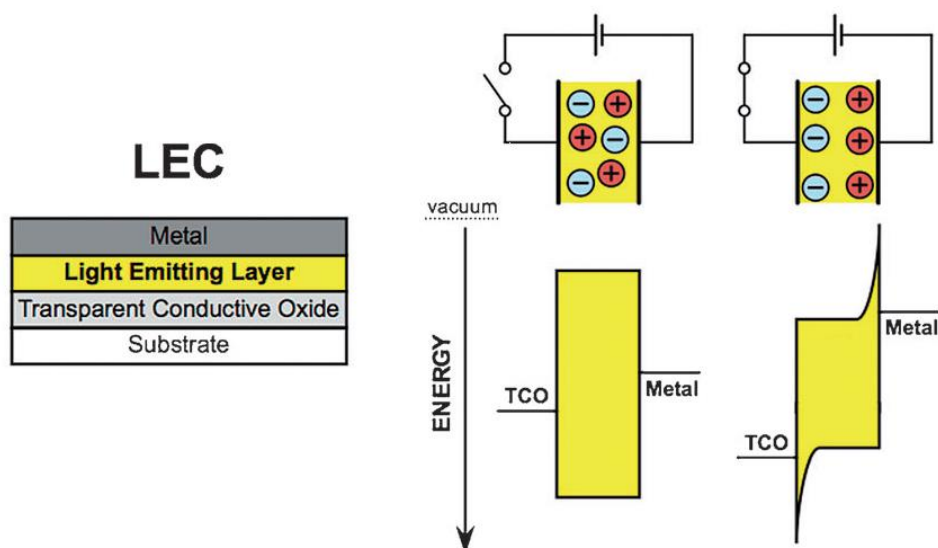


Figure 7: Schematic representations of a typical LEC

A crucial benefit in the use of ionic compounds is their processability: iTMCs dissolve in polar benign solvents, allowing the devices to be prepared by facile coating or printing processes. In addition, the insensitivity of LEC devices to the work function of the electrode material allows air-stable metals to be used as anode and cathodes, greatly decreasing the severe technical requirements for the encapsulation of devices. Moreover, graphene⁴⁰ or a blend of carbon nanotubes and polymers⁴¹ have been used as electrodes, eliminating the need for using ITO for a transparent electrode. Taken in concert, these characteristics facilitate large-area processing and might give entry to flat electroluminescent devices at more affordable costs.

2.2 Biological luminescent probes

Biomedical imaging is a process that allows the acquisition of an image of a target inside a living organism, in a non-invasively way. These type of images can be obtained for scientific purposes, allowing the study of the anatomy and the physiology of an organism, as well as for clinical purposes, in order to detect, to diagnose or to study a certain disease. In the recent years, imaging has become an indispensable tool in cancer research, clinical trials and medical practice.

Biomedical imaging includes several analysis techniques, illustrated in Figure 8.

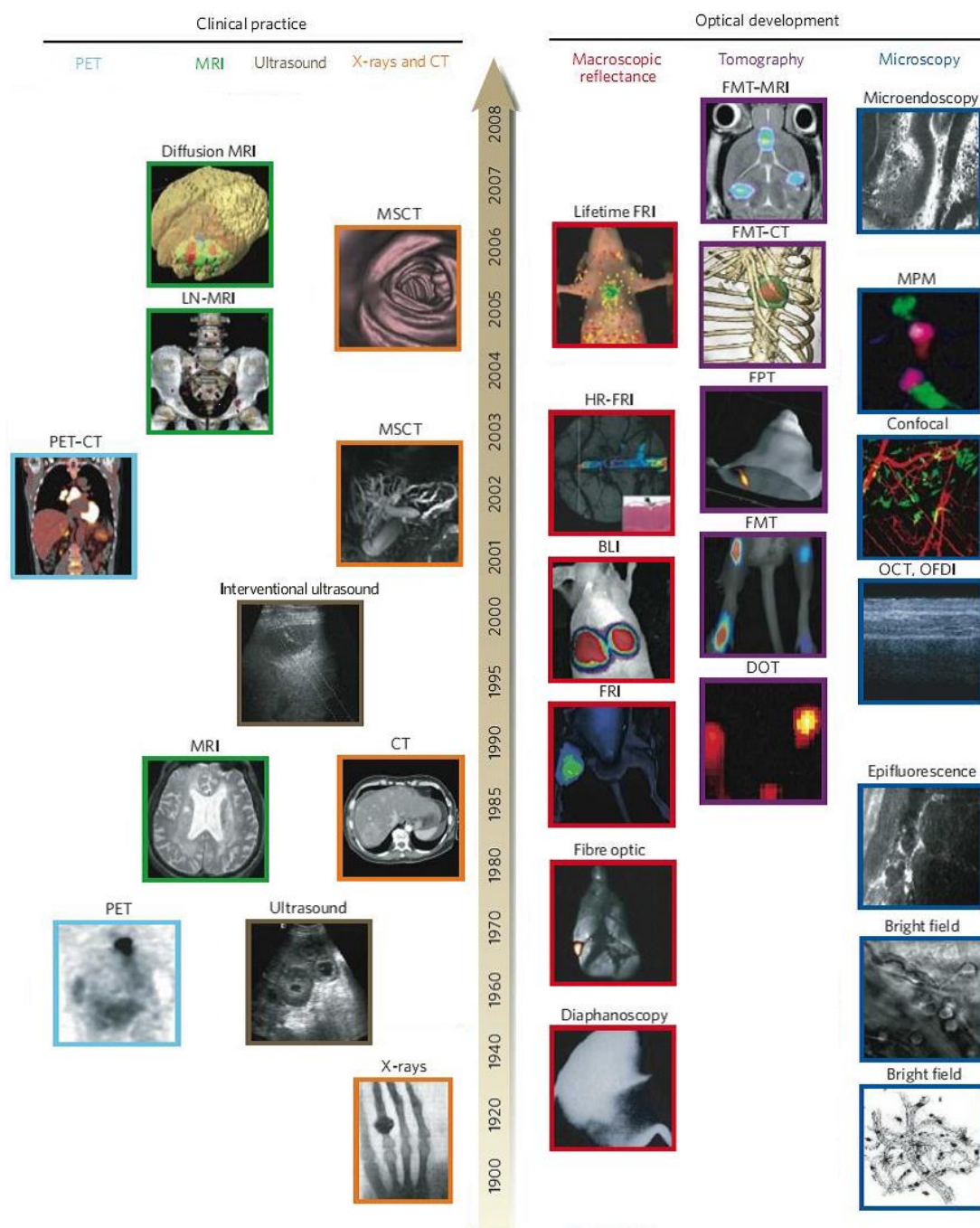


Figure 8: Evolution of biomedical imaging

The reported techniques can be grouped by the energy used to derive visual information (X-rays, positrons, photons or sound waves), the spatial resolution that can be achieved (macroscopic, mesoscopic or microscopic) or the type of information that can be obtained (anatomical, physiological, cellular or molecular).⁴² Macroscopic imaging systems that provide anatomical and physiological information, such as computed tomography (CT), ultrasound and magnetic resonance imaging (MRI), are now routinely used in clinical and preclinical analysis. By contrast, systems that allow the collection of molecular information are just emerging. They include the positron emission tomography (PET), the fluorescence reflectance, and the bioluminescent imaging.

The *in vivo* and *in vitro* imaging on biological samples has been carried out for several years, using optical microscopy. Among all the available optical imaging techniques, fluorescence microscopy is one of the most exploited, due to the possibility to observe the luminescence of a sample within good resolution.⁴³ The optical imaging techniques rarely exploit the intrinsic fluorescence of the biological sample, but usually employed luminescent organic or organometallic compound.

Luminescent derivatives, in fact, can act as molecular probes interacting with specific biological receptors, in a process named bioconjugation. This process usually occurs between a suitable functional group present on the luminophore and a receptor present on the target to detect; the observable result is a variation of the emitting properties of the dye. However, the complexity of the biological matrix makes the selectivity of this process very difficult. Usually, this problem can be solved in three different ways:

- functionalization of the luminophore: the emitting molecule is decorated with a particular functional group, able to easily react with the target molecule;
- exploiting the metabolism way: this approach is very used for cell imaging. The probe is equipped with a molecule that can be recognized by the cells and can so enter in the cell cycle, bringing the luminophore to accumulate in certain organelles rather than in other;
- *key-lock* approach: exploits the particular affinity of some protein within certain organic molecules. The luminophore is bound to the 'key' molecule and can be related only to a specific 'lock' protein.

Besides, it is essential that the luminophore is able to maintain some photophysical properties after the coordination with the target molecule. Moreover, it is important that no quenching processes occur, and this can be obtained by the inset of a suitable spacer between the biomolecule and the target, in order to opportunely outdistance the groups responsible for the coordination and the emission.

The probes labeled with luminophores are detected by spectroscopic measurements using the absorption and emission wavelengths typical of the fluorophore. The sensitivity of the method is strictly correlated to the molar extinction coefficient (ϵ) and the quantum yield (Φ) of the luminophore.

An essential feature in order to achieve high efficiency is that the both the absorption and the emission maxima should be located in a spectrum region where the auto-fluorescence of the biological matrix is

negligible. Furthermore, it is necessary to reduce scattering phenomena due to the presence of macromolecules, such as proteins. Scattering and auto-fluorescence, particularly detectable in the visible region, strongly reduce the sensitivity of the method. Therefore, a good luminophore suitable for bioimaging should display the following features:

- high photochemical stability
- high quantum yield
- possibility to tune the emission in the visible region
- high solubility in biological environment, in order to avoid phenomena of self-aggregation and quenching

Molecules possessing fluorescent properties have been widely exploited for these applications.

Organic fluorophores are commonly used due to the strong structural versatility and the possibility of simple modifications and derivatizations. Moreover, they display strong emissions all over the visible region of the spectra, with typical values of ϵ in the range of $10^5 \text{ M}^{-1}\text{cm}^{-1}$ and Φ close to 1.0 (100%).⁴⁴ Among the most known fluorophores, Xanthene derivatives, such as Rhodamine and Fluorescein (Figure 9), have a very important role.

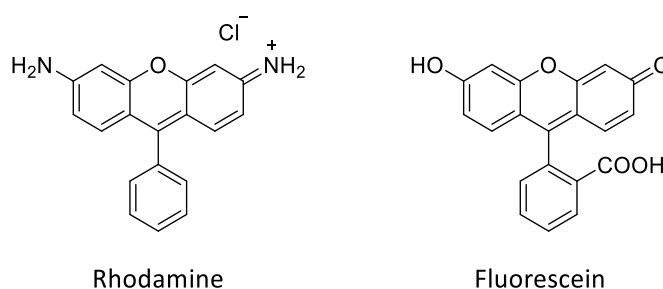


Figure 9: Typical organic fluorophore for optical imaging

Despite the above mentioned suitable properties, typical organic fluorophores also present some limitations. The most important restriction is their lifetime: usually purely organic fluorophores show an emission lifetime in the order of nanoseconds, too short for the use of time-resolved imaging techniques. Another important limitation is their fast photodegradation, which sensibly limits their use for long periods of observation. Moreover, each fluorophore can be excited only to a specific wavelength, and then the organic fluorophores cannot be used for multi-color imaging. Finally, biomolecules can absorb or scatter the UV/visible emission of the organic fluorophore, which can also be covered by the strong autofluorescence of the tissues.⁴⁵ For all these reasons, limited tissue penetration is observed, leading to a general decrease of the sensitivity of the method.

The use of transition metal complexes in biological imaging has rapidly grown in the last decades. Conversely to the described organic fluorophores, the use of phosphorescent organometallic complexes ensures high emission quantum yields together with long emission lifetimes, which are typically in the range

of submicroseconds to hundreds of microseconds. Such lifetimes are an obvious advantage because the phosphorescence of the probe can be readily differentiated from the background autofluorescence of the matrix and the tissues, by using simple time-resolved techniques with the effort to sensibly decrease the signal-to-noise ratio and so increase the sensitivity of the analysis. Again, the large Stokes shift and the possibility to cover the whole region of the visible light, join with their high photostability, make them perfect candidates for these applications.

The emissive properties of many transition metal complexes are readily perturbed by little change in their local environment, for example after interreactions with an external molecule. These changes usually results in a variation of the emission characteristics, including the emission intensity, the wavelength and the lifetime of the excited state. Although many phosphorescent transition metal complexes are kinetically inert under physiological conditions, their structure can be easily decorated with reactive moieties, which guarantee recognition capability and/or can represent binding sites for particular analytes.

Therefore, many transition metal complexes has been used as sensors for various analytes. Among all of them, a primary role is covered by Ir(III) complexes, that join good photophysical properties with the possibility to fine decorate the peripheral structure of the ligands in order to interact with different targets.

2.3 Other important applications

In recent years, the use of transition metal complexes have grown up in various application fields, such as the employment as sensitizers in artificial photosynthesis processes for energy production, and their use as photoredox catalysts for the synthesis of organic building blocks.

The consumption of energy is directly correlate with the human development. Nowadays, 84 % of the total energy coming from the combustion of fossil fuels,⁴⁶ but in the last decades a sensible shift towards more renewable energy sources has been observed. Among them, solar energy is clearly the most viable long-term solutions for this energetic demand; in fact, sun provide roughly 10^{22} J of insolation each hour, a value that correspond at the society's yearly energy demand.⁴⁷ In this optic, the critical aspect of using solar energy is the storage problem. In natural photosynthesis, solar energy is captured and stored by oxidizing H_2O and fixing CO_2 in order to produce sugars, in a series of light-and-dark reactions. In contrast, artificial photosynthesis involves the splitting of water into H_2 and O_2 , resulting in the conversion of harvested solar energy into storable solar fuels. Different technologies has been exploited, based on Si photovoltaic cell coupled to a Ni-based electrolyzer (efficiency around 10 %),⁴⁸ photoelectrochemical cells,⁴⁹ where the electrodes also absorb light, and fully-integrated molecular artificial photosynthetic systems, where supramolecular light-harvesting antennae power solar fuel producing catalysts in a homogeneous system. An idealized molecular artificial photosynthetic system consists of five essential components, a light-harvesting antenna, a photosensitized charge-separating site, an O_2 evolving catalyst, a H_2 evolving catalyst, and a membrane isolating the catalysts, as outlined in Figure 10. The light-harvesting antenna collects solar energy, and then funnels that energy to the photosensitizer (P) where initial charge separation takes place. A donor (D) and an acceptor (A) drive the electron and hole further apart to prevent back electron transfer and shuttle the respective charges to the catalysts. A membrane may also be placed somewhere between the O_2 and H_2 evolving catalysts to prevent a "short circuit".⁵⁰

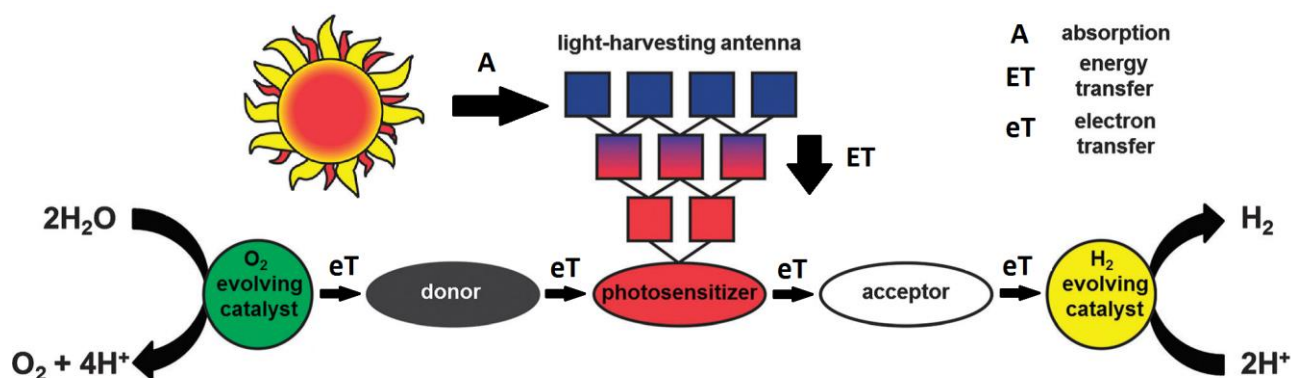


Figure 10: Schematic representation for a molecular artificial photosynthetic system

For photoinduced hydrogen production, photosensitizers with large molar extinction coefficients (to efficiently collect radiant energy) and relatively long excited-state lifetimes (to allow electron-transfer quenching to occur) would be desirable. Transition metal complexes completely fit these features.

The use of transition metal complexes as visible light photoredox catalysts for small molecule activation has rapidly grown since the pionieristic work of MacMillan.^{9a} In a general sense, this approach relies on the ability of metal complexes to engage in single-electron-transfer (SET) processes with organic substrates upon photoexcitation with visible light. Many of the commonly used photocatalysts are polypyridyl complexes of ruthenium(II) and iridium(III). These complexes absorb light in the visible region of the spectrum, giving stable and long-lived photoexcited states.

One of the major features of these compounds is the remarkable single-electron-transfer ability of the excited state, although they are poor single-electron-transfer oxidants and reductants in the ground state. The conversion from inactive complexes to highly redox-active species upon irradiation represent a key factor in their growing application, make them suitable to induce unique and valuable catalytic processes. Particularly, these derivatives can be employed in novel single-electron radical processes for C-C bond formation, as generators of radicals, opening the way to exotic bond constructions that are not possible using established protocols.⁵¹ Two different mechanistic pathways are accessible with these complexes, as reported in Figure 11 for the archetypal $\text{Ru}(\text{bpy})_3^{2+}$ complex. The excited specie $^*\text{Ru}(\text{bpy})_3^{2+}$ can be easily generate, and can act as both reductant and oxidant. In the oxidative quenching cycle, $^*\text{Ru}(\text{bpy})_3^{2+}$ functions as a reductant, reducing some electron acceptor (**A**) by a single electron. The products of this single-electron-transfer event are the radical anion of **A** and the oxidized form of the photocatalyst, $\text{Ru}(\text{bpy})_3^{3+}$. This species is a strong oxidant and may accept an electron from some donor **D** to give the radical cation of **D** and return the catalyst to the $\text{Ru}(\text{bpy})_3^{2+}$ ground-state species, completing the photocatalytic cycle. Alternatively, in the reductive quenching cycle, $^*\text{Ru}(\text{bpy})_3^{2+}$ functions as an oxidant, accepting an electron from **D** to give the reduced species $\text{Ru}(\text{bpy})_3^+$. This Ru(I) intermediate is a good reductant and may donate an electron to **A** to afford the ground-state species $\text{Ru}(\text{bpy})_3^{2+}$.

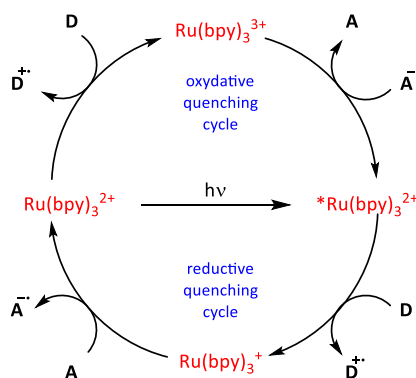


Figure 11: Oxidative and reductive quenching cycles of $\text{Ru}(\text{bpy})_3^{2+}$

3. The role of the Ir(III)

As shown above, a large number of Transition Metal Complexes (TMCs) have found a wide range of application in different fields. Among all of them, Ir(III) complexes cover a very important role for both luminescent devices and biological applications, thanks to a unique combination of physical and chemical properties, which provide the possibility to have high emission quantum efficiency in the whole visible spectrum, from blue to red, joint to a good photochemical stability.⁷ In particular, the reversible electrochemistry, synthetic versatility, and robust nature of Iridium(III) complexes render them appealing materials for a multitude of applications.

Ir(III) is a $5d^6$ metal center and its d orbitals are split by the interaction with the octahedral ligand field (ligand-field splitting energy (LFSE)⁵²) into three stabilized t_{2g} (d_{xy} , d_{xz} , d_{yz}) and two destabilized e_g orbitals (d_{z^2} , $d_{x^2-y^2}$), as shown in Figure 12. This splitting generates an energy difference between the levels, named Δ_o , which depends on:

- 1- the oxidation state of the metal center: the higher the oxidation state, the higher the splitting;
- 2- the size of the d orbitals: the splitting is small for 1st transition series (3d metals) and progressively increases with 4d and 5d metals, 2nd and 3rd series, respectively;
- 3- the field strength exerted by the ligands, following the spectrochemical series.

Ir(III) complexes exhibit a high Δ_o splitting because of the presence of a highly charged ion belonging to the third row of the d-block. As a result, the electronic configuration of the metal center is always in a low-spin state (t_{2g}^6 , e_g^0) and the ligand-field stabilization energy is maximized, which means that mostly Ir(III) complexes are generally stable and rather inert toward substitution. Accordingly, the configuration of the metal orbitals is closed-shell (A_{1g}) and, since the ligand orbitals are fully occupied, the ground-state of the complexes is a singlet (S_0).

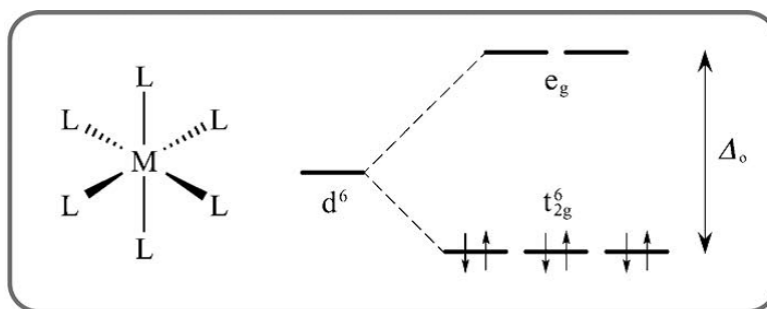


Figure 12: Low-spin d^6 orbital configuration in octahedral field

Also other Transition Metals ions show the same d^6 low-spin configuration of Ir(III), for examples Os(II), Ru(II) and, in some cases where particular ligands are present, even Fe(II). But none of their complexes exhibit such remarkable photophysical properties (*e.g.*, emission color tunability, high PLQYs, good photostability, etc.) because of the nature of their excited states (Figure 13). For Fe(II) complexes, the reason can be ascribed to the small Δ_o splitting, hence the lowest-lying excited state is 1MC in nature (*i.e.*, centered on e_g metal orbitals) and, therefore, not emissive.⁵³ In the case of Ru(II), the lowest emissive excited state is a metal-to-ligand charge transfer triplet (3MLCT), relatively close in energy to the non emissive 3MC states, that can be thermally populated, opening to competitive radiationless deactivation pathway; accordingly, the PLQY of Ru(II) complexes increase substantially with decreasing temperature.⁵⁴ The last example is Os(II), where the Δ_o splitting is considerable and the 3MC state are too high to affect the emission properties; although, the emissive 3MLCT excited states are very low in energy, typically in the red/infrared region of the spectrum, and this favors radiationless pathways, as described by the 'energy gap law'.⁵⁵ Accordingly, PLQYs of these complexes are typically low, often below 1-2%.⁵⁶

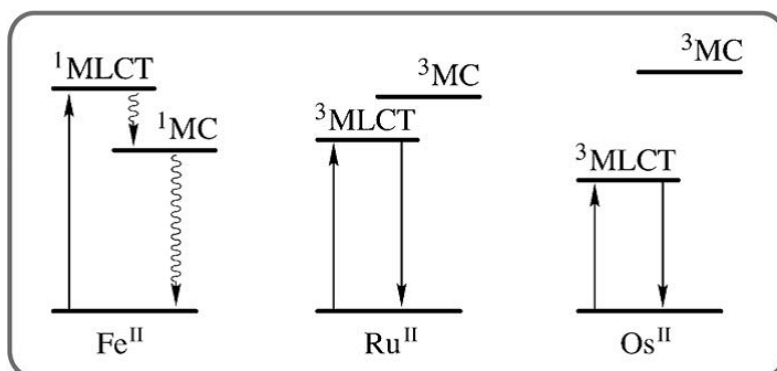


Figure 13: Qualitative electronic excited states description for Fe(II), Ru(II) and Os(II) metal complexes

Ir(III) complexes can be rationalized in two different families, according to the nature of the ligands bond to the metal centre: homoleptic, containing three identical cyclometalating ligands, or heteroleptic, containing two cyclometalated ligands and one ancillary ligand. The synthesis of homoleptic complexes is generally performed following two different approach, a direct one-step reaction or a two-steps synthesis.

The first reported efficient direct synthesis involved the reaction of $\text{Ir}(\text{acac})_3$, where acac is acetylacetonate, with an excess of the desired cyclometalating ligand, with the general formula $\text{HC}^{\wedge}\text{N}$ (*i.e.*, 2-phenylpyridine).⁵⁷ An alternative direct synthesis involves reaction of the $\text{IrCl}_3 \cdot x\text{H}_2\text{O}$ with a Silver(I) salt using the desired cyclometalating ligand as a solvent.⁵⁸ Both of these precedures are carried out at high temperature (>180 °C), but many potential cyclometallating ligands are intolerant to these conditions. Prior to these reports, Nonoyama described the efficient preparation of a μ -dichloro-bridged dimeric complex

with formula $[\text{Ir}(\text{C}^{\wedge}\text{N})_2\text{Cl}]_2$, in good yields and lower temperature (130 °C).⁵⁹ A large variety of these dimeric complexes can be synthesized in this way, and they can serve as precursors for the synthesis of tris-cyclometalated complexes by several routes. Silver ion can be used to abstract the bridging chlorides in the presence of a cyclometalating ligand to give the desired complex.⁶⁰ However, it has also been shown that silver ion is not required and good yields of complexes can be realized using a simple inorganic base in place of silver.⁶¹

The tris-cyclometalated complexes can present two different geometries, *facial (fac)*- or *meridional (mer)*-isomers (Figure 14, left and center). Typically, all the reported synthesis lead to the isolation of the *fac*-form as the major product. Also if Ir-dimers, that generally present a '*mer-like*' disposition of ligands (Figure 14, right), are used as precursors, the final isolated complex is the *fac*-isomer. This because the reactions are typically run at high temperatures (>180 °C) and the thermodynamically more stable *fac*-form is thus favored over the kinetic (*mer*-) product. However, if the synthesis is carried out at lower temperature (<130 °C), the *mer*-isomer can be obtained as the only product.⁶¹ The isolated *mer*-isomer can then be converted into the *fac*-form by either thermal or photochemical routes.^{62,63}

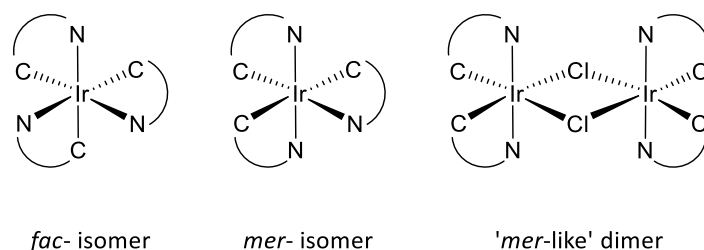


Figure 14: Geometry of homoleptic Ir(III) complexes and dimeric form

As regarding heteroleptic complexes, the synthesis proceeds via the isolation of the μ -dichloro-bridged dimer $[\text{Ir}(\text{C}^{\wedge}\text{N})_2\text{Cl}]_2$, in a typical two-step procedure. Following Nonoyama guidelines, $\text{IrCl}_3 \cdot n\text{H}_2\text{O}$ is reacted with an excess of the desired cyclometalating ligand using refluxing 2-ethoxyethanol as solvent ($T = 130$ °C), and the desired dimer can be obtained in good yields.⁵⁹ The isolated dimer can then be react with different ancillary ligands, giving the heteroleptic complex in high yields (Figure 15). When the direct addition of the ancillary ligands to the dimer affords low yields, an alternative synthetic route can be utilized, carrying out removal of chlorides by treating the μ -dichloro-bridged dimer with a soluble Silver(I)-based chloride-abstracting agent.⁶⁴ It is even possible to avoid this two-step procedure by directly treating the $[\text{Ir}(\text{C}^{\wedge}\text{N})_2\text{Cl}]_2$ dimer with a stoichiometric amount of neutral ligands in the presence of Ag_2O , to promote the removal of chloride during the reaction.⁶⁵

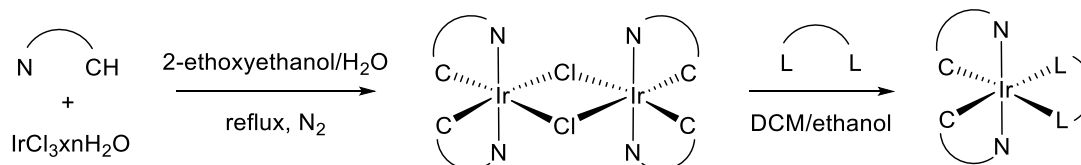


Figure 15: Typical two-step synthesis of a heteroleptic bis-cyclometalated Iridium(III) complex

Three different families of ancillary ligand can be involved in the preparation of heteroleptic Ir(III) complexes: monoanionic, dianionic and neutral (Figure 16). Depending on the ancillary ligand choose, the final Ir(III) complex will be neutral, anionic or cationic, respectively.

Monoanionic chelating ancillary ligand have been widely used in the preparation of neutral Ir(III) complexes suitable for OLEDs applications. Typical examples of this class of ligand are acac (acetylacetonone) and derivatives, and 2-pic (2-picolinic acid) and derivatives.

The most widely exploited class of neutral ligands are diimine, with general formula $\text{N}^{\wedge}\text{N}$. This class of molecules are able to chelate the metal ion through the formation of a dative-bond between the electronic doublet, located on the heteroatom, and an empty orbital of the metal centre. The main molecule belong to this class is 2,2'-bipyridine (bpy) and its derivatives, among with 1,10-phenantroline (phen). In recent years, two other families of neutral ligands have been reported, both containing a C atom as a neutral chelating atom, carbenes, such as biz (*N*-substituted bis-imidazolium derivatives), and isocyanides, such as *t*Bu-NC (*tert*-butylisocyanide).

Despite the previous family, anionic and dianionic ancillary ligand are still rather uncommon in Ir(III) complexes. First examples were reported by Thompson,⁶⁶ which used cyanide ions as ancillary ligand for the preparation of negative charged Ir(III) complexes. Some recent examples involving chelating dianionic $\text{C}^{\wedge}\text{C}$,⁶⁷ $\text{N}^{\wedge}\text{N}$, such as bipz (5,5'-(1-methylethylidene)-bis(3-trifluoromethyl-pyrazolate))⁶⁸ and $\text{S}^{\wedge}\text{S}$ ⁶⁹ chelators have been reported, leading to the preparation of more stable anionic complexes.

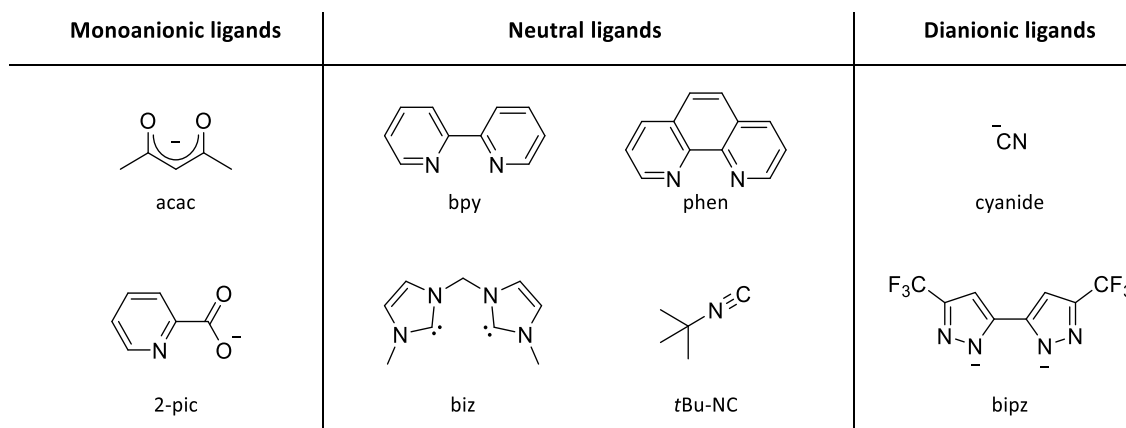


Figure 16: Most representative examples of ancillary ligands for the described classes

All the above mentioned classes of Ir(III) complexes show similar photochemical properties. The strongest absorption bands are ascribable to singlet ligand-centered (^1LC), metal-to-ligand ($^1\text{MLCT}$), and ligand-to-ligand ($^1\text{LLCT}$) charge-transfer transitions. In a typical absorption spectrum, the UV region is dominated by intense $^1\pi\text{-}\pi^*$ (^1LC) transitions involving the organic ligands. At longer wavelength (350-450 nm), less-intense $^1\text{MLCT}$ and $^1\text{LLCT}$ bands are present: the $^1\text{LLCT}$ transitions correspond to electron promotions from the aryl moiety of the cyclometalating ligands to the ancillary ligand. Additionally, the weak and long tails observed above 450 nm are due to direct spin-forbidden population of the triplet excited states, $^3\text{MLCT}$, $^3\text{LLCT}$, and ^3LC ($^3\pi\text{-}\pi^*$) transitions, enabled by the high spin-orbit coupling of the iridium metal core (spin-orbit coupling constant, $\xi = 3909\text{ cm}^{-1}$)⁷⁰ that allows the mixing of triplet states with the higher-lying $^1\text{MLCT}$ levels. The high spin-orbit coupling of Ir(III) yields almost unitary intersystem crossing efficiency from singlet to triplet excited states, therefore Ir(III) complexes always exhibit efficient spin-forbidden phosphorescence emissions. The emitting state is the lowest-energy triplet (T_1) which normally arises from 'mixed' triplet levels, due to the contributions of $^3\text{MLCT}$, ^3LC , and sometimes also $^3\text{LLCT}$ states.⁷ Depending on the extent of contribution of the charge-transfer (CT) states, the emission profile is substantially affected: the presence of vibrational features suggests a low charge-transfer (CT) character, whereas broader and less structured shapes are indicative of a high charge-transfer character. All the involved transition are schematically summarized in Figure 17.

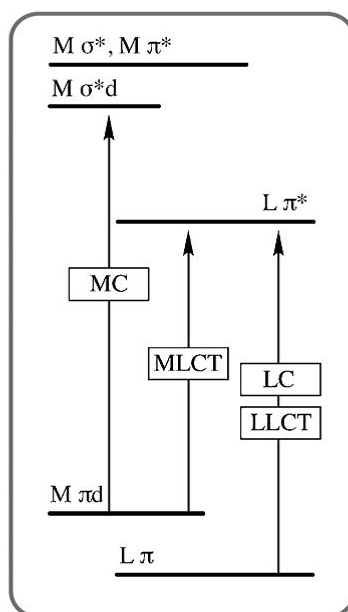


Figure 17: Electronic energy-level diagram for a generic Ir(III) complex. MC is metal-centered, LC is ligand-centered, LLCT and MLCT are ligand-to-ligand and metal-to-ligand charge transfer, respectively

To rationalize the photophysical properties of Ir(III) complexes, it is useful to determine the energy and atomic orbital composition of the highest-occupied (HOMO) and the lowest-unoccupied molecular orbitals (LUMO). Generally, in these type of complexes the HOMO is an admixture of Ir $d\pi$ orbitals (t_{2g}) and aryl π orbitals of the cyclometalated ($C^{\wedge}N$) ligands, whereas the LUMO is usually located on the ancillary ligand.⁷¹ Therefore, the emitting T_1 triplet usually has a mixed ${}^3MLCT/{}^3LLCT$ character. Based on this calculated evidences, it can be deduce that by changing or chemically modifying the ancillary ligand, it is possible to destabilize the LUMO, while keeping the HOMO relatively unperturbed. This practice is valid until the LUMO of the neutral ancillary ligand lies too high in energy; in this case, the LUMO+1 or the LUMO+2, usually located on the heterocyclic moiety of the $C^{\wedge}N$ ligand, becomes the new LUMO of the complex. In this way, the use of ancillary ligands with relatively inaccessible π^* orbitals (e.g., carbenes⁶⁵ or isocyanides^{72,73}) leads to low-lying emitting excited states centered on the cyclometalated ligands and the emitting T_1 state exhibits a more ligand-centered character. In such cases, highly structured emissions bands and strongly increased radiative lifetimes are found.

Despite the case of high-field-strength ancillary ligand, HOMO and LUMO are usually located on different ligands bonded to the Ir(III) metal centre. For this reason, the HOMO-LUMO energy gap can be fine-tuned by independently modifying the cyclometalated (HOMO) or the ancillary ligands (LUMO), or even both of them. As a general guideline, it can be assumed that:

- 1) electron-withdrawing substituents on the cyclometalated (C^N) ligands reduce the σ donation to the metal, decreasing the electron density on the iridium ion, so leading to a stabilization of the HOMO;
- 2) electron-donating substituents on the ancillary ligand, or generally the use of intrinsically electron-rich ligands, bring to a destabilization of the LUMO.

With this in mind, it's easy to understand that the Ir(III) complexes can furnish an almost illimitate color variety, with a broad range of excited-state lifetimes, from nanoseconds to several microsecond, as well as phosphorescent yields.

A parameter often used to describe the emission color of a given compound is the wavelength of the emission band maximum (λ_{\max}). It is a very practical parameter, but it can only give a rough estimation of the true emission color, which depends on the specific bandwidth. Moreover, to fully define a color, the sensitivity of the photoreceptors in the human eye has to be considered. The commonly used system suitable to describe and quantify a color is the CIE (Commission Internationale l'Eclairage) system.⁷⁴ CIE coordinates and CRI (color-rendering index) give a quantitative measurement of the quality of a color, in comparison with natural sunlight.⁷⁵ There are three different types of cone cells in the eye, responsible for color discrimination, with their absorption maxima centered at 419, 531, and 558 nm (Figure 18, left), represented by a set of three tristimulus functions (X , Y , and Z).⁷⁶ In order to represent the tristimulus values on a two-dimensional plot, X , Y , and Z are converted to their fractional contributions (*i.e.*, $x = X/(X+Y+Z)$, $y = Y/(X+Y+Z)$). A plot of x versus y is used to visualize how the colors are organized by the CIE system. This plot is termed the CIE chromaticity diagram (Figure 18, right). Monochromatic colors falls on the perimeter of the curve, while white or the neutral point is found at the center of the diagram. As a given point is moved toward the white point from the perimeter, the color remains constant, but becomes progressively more unsaturated. Mixing any two colors generates a new color, whose CIE coordinates fall on the line connecting the CIE coordinates of the two mixed colors. Similarly, three emissive colors can be combined to generate any color whose CIE coordinates fall within a triangle defined by the CIE coordinates of the three colors used.

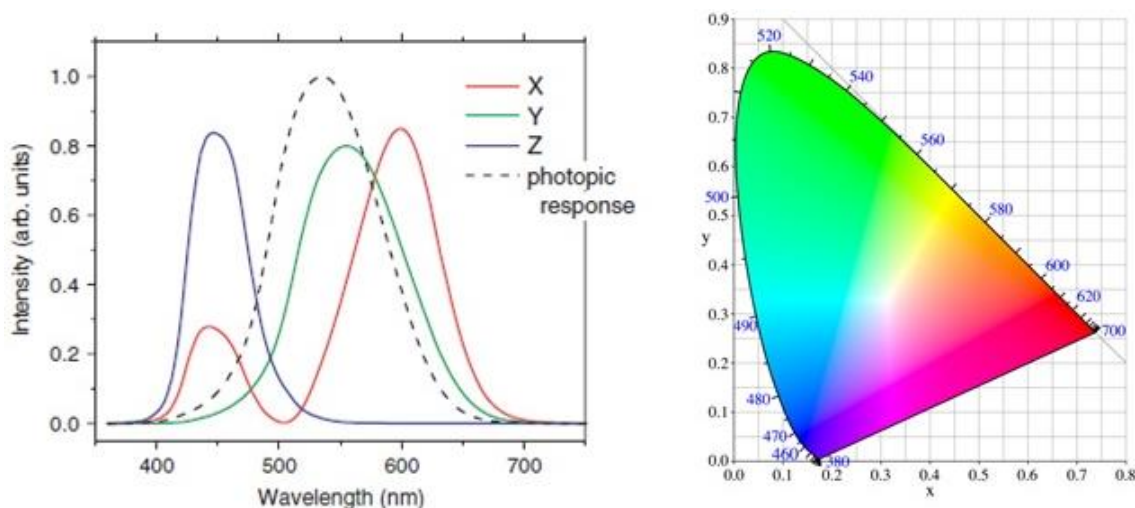


Figure 18: (left) Photopic response function and normalized tristimulus values; (right) CIE color space chromaticity diagram

Starting from the archetypal complex $[\text{Ir}(\text{ppy})_2\text{bpy}][\text{PF}_6]$, where Hppy is 2-phenylpyridine and bpy is 2,2'-bipyridine, different strategies can be pursued in order to move the emission color towards the red region of the visible spectrum rather than the blue region.

-moving to the red: a bathochromic shift of the emission color can be achieved by reducing the HOMO-LUMO gap of the complex (Figure 19). As shown above, this can be obtained by modifying independently both the cyclometalated anchor and the ancillary ligand. As regards the ancillary ligand, a *red shift* can be principally pursued by adding electron-withdrawing groups in *para*- position with respect to the coordination site, that are able to increase the electron affinity of the ligand toward the metal centre. The emission can be red shifted also by using ancillary ligand with a large π -system. Regarding the cyclometalated ligand, thus, a *red shift* is reached in three different ways:

- 1) adding electron-donating groups: the presence of these groups on the cyclometalated ligand, and particularly in *meta*- position related to the coordination site, can enhance the emission color up to several nanometers;
- 2) increasing the delocalization of the π -system: the expansion of the π -system leads to a marked bathochromic shift, the magnitude of which is dependent on the specific ligand used. The presence of fused rings gives rise to a red shift on the order of 80-100 nm;
- 3) presence of polarizable atoms: the incorporation of soft atoms, such as sulfur and nitrogen, in the cyclometalated ring system can significantly lower the emission energies of the complexes.

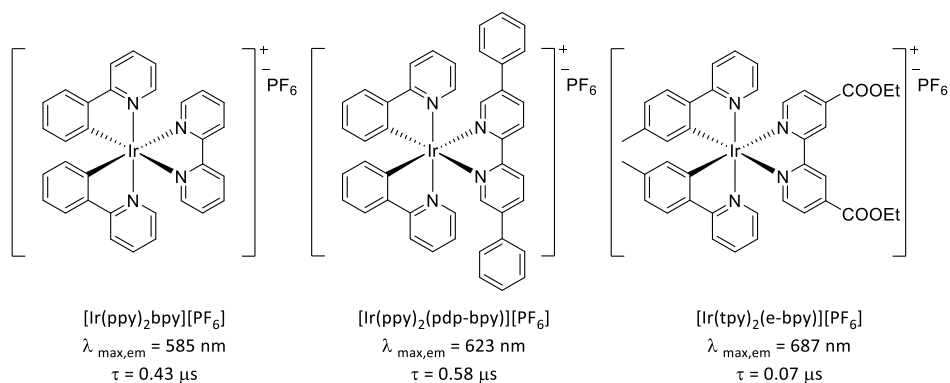


Figure 19: Effects of different ancillary and cyclometalated ligands toward *red shift* (data from literature)^{77,78}

- *moving to the blue*: a hypsochromic shift of the emission color can be achieved by enhancing the HOMO-LUMO gap of the complex (Figure 20). The LUMO of the complexes, located on the ancillary ligands, can be easily destabilized by adding electron-donating groups in *para*- position related to the coordination site, with the effect to decrease the electron affinity of the ligand toward the metal ion; alternatively, a *blue shift* can be obtained by using intrinsically electron-rich ancillary ligands. Instead, different approaches can be pursued in order to blue shift the emission color by modifying the cyclometalated ligand:

- 1) adding electron-withdrawing groups: the presence of electron-withdrawing groups in the cyclometalated ligand, typically -F or -CF₃ in *meta*- position with respect to the coordination site, leads to a considerable stabilization of the HOMO of the complex, and the result is a remarkable increase of the emission energies;
- 2) change the heterocyclic moiety of the C^N groups: the replacement of the typical pyridyl functionality with other heterocyclic groups can lead to a substantial enhancement of the emission energies. In particular, switching from pyridyl to a smaller heterocycle (*i.e.*, pyrazole) that has reduction potentials significantly higher, can decrease the emission wavelength up to 100 nm.
- 3) increase the number of nitrogen atoms in the heterocyclic moiety: by replacing the pyridyl moiety with pyrazolyl, triazolyl and tetrazolyl is possible to push the emission of the complex towards the blue.

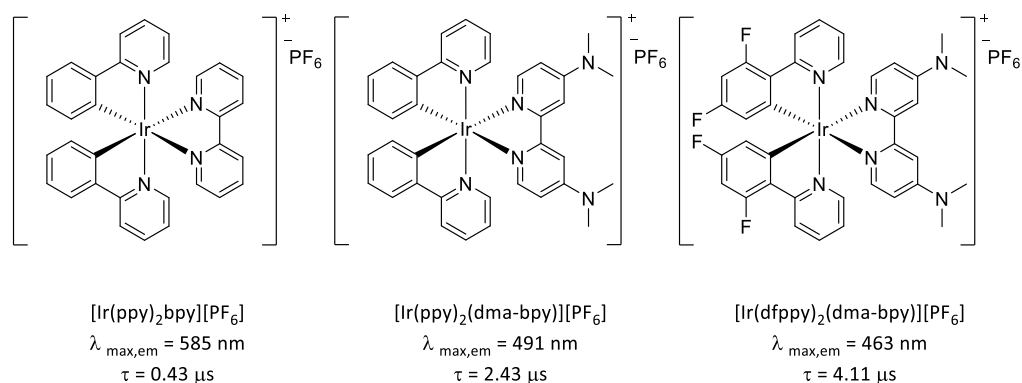


Figure 20: Effects of different ancillary and cyclometalated ligands toward *blue shift* (data from literature)^{79,80}

In this perspective, it's important to note that deep-blue emissions from Ir(III) complexes can be obtained also by introducing strong ligand-field-stabilizing ligands (*e.g.*, CO, isocyanides, or carbenes), so that the HOMO-LUMO transition involves only the cyclometalated C^N system, without any participation of the ancillary counterpart (Figure 21). In these cases, the HOMO orbital is predominantly located on the aryl moieties of the C^N ligands, while the LUMO is mostly found on the heteroaromatic rings of the same cyclometalating ligand, so the emission properties are fully controlled by the cyclometalated ligand only.

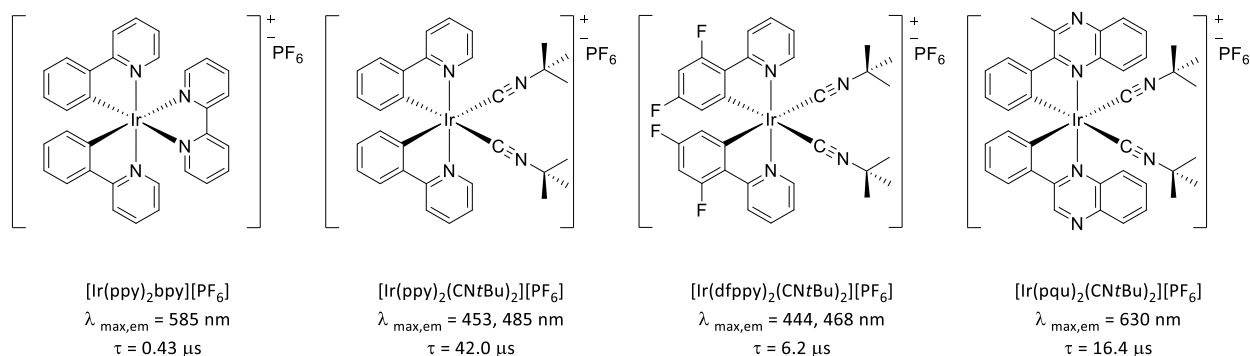


Figure 21: Effects of strong ligand-field-stabilizing ligands (data from literature)⁷²

Another feature of ancillary ligands is to modulate the redox potentials of the complexes, as a consequence of their different ligand strength and electron-withdrawal capability toward the metal d orbitals. Generally, for the majority of Ir(III) complexes, the first reduction usually occurs on the ancillary ligand, while the oxidation is centered on the aryl moiety of the cyclometalating ligand. This typical behaviour is observed when the LUMO is located on the ancillary ligand. In the other cases, so when strong ligand-field-stabilizing ligands are introduced in the complex, both the HOMO and the LUMO are localized on the cyclometalated ligands. In these cases, the oxidation process involves the aryl moiety of the cyclometalating ligands while

the reduction processes always involve the heteroaromatic moiety of the cyclometalating ligands and not the ancillary moiety.

As observed for the emissive properties, the same trend can be rationalized for the redox properties of Ir(III) complexes. Compared to the archetypal $[\text{Ir}(\text{ppy})_2\text{bpy}][\text{PF}_6]$, the nature of the cyclometalated and the ancillary ligand is responsible for variations in the redox properties (Figure 22).

Regarding the cyclometalated ligand, the presence of an electron-withdrawing group is able to enhancing the oxidation potential (stabilization of the HOMO), while the presence of an extended π -system leads to less positive potentials. However, the presence of electron-donating group in the structure of the ancillary ligand has the consequence of lowering the reduction potential (destabilization of the LUMO), while electron-withdrawing group or the presence of an extended π -system contributes to the enhancement of the reduction potential (less negative values).

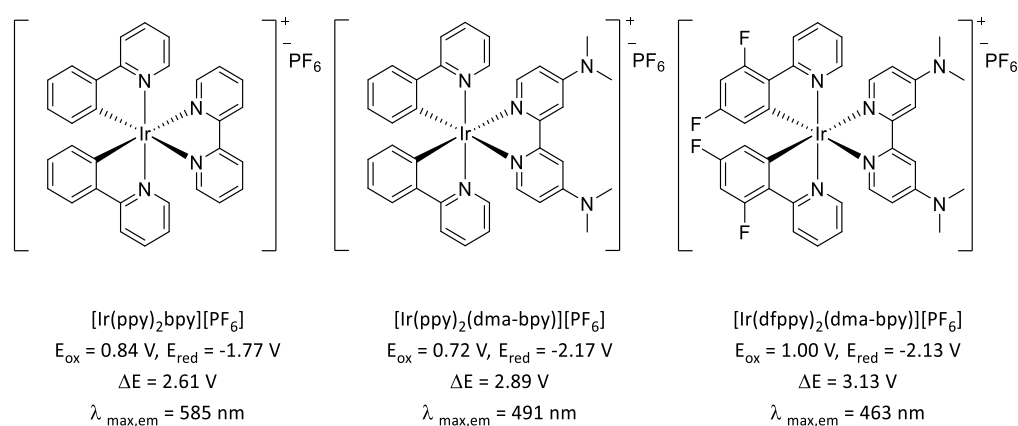


Figure 22: Effects of different substituents on electrochemistry properties (data from literature)^{79,80}

Ir-iTMCs (ionic Transition Metal Complex) has been well studied, and numerous Ir(III)-based LECs have been prepared, with emission colors all across the whole visible spectrum.

Red emitting LECs based on Ir-iTMCs are well known and have been reported since 2005, by Tamayo et al.⁸¹ Ancillary N[^]N ligands with low-energy LUMO levels have been employed, and the EQE (external quantum efficiency)¹⁸ is in the order of 10 % (Figure 23, left). As shown above, the attachment of electrodonating groups on the the ancillary ligands increase the HOMO-LUMO gap. Yellow-green emitting LECs have been prepared follow this strategy: starting from the archetypal $[\text{Ir}(\text{ppy})_2\text{bpy}][\text{PF}_6]$, the emission can blue shifts by adding methyl or dimethylamino group to the bpy moiety, leading to a 70 nm shift, but also to a significantly decrease in the EQE (0.2 %, $[\text{Ir}(\text{ppy})_2(\text{dma-bpy})][\text{PF}_6]$, Figure 22).⁷⁹ Green LECs were also achieved by using Ir-iTMCs with electron-withdrawing groups attached to the phenyl ring of the C[^]N

ligands, which stabilize the HOMO level of the complex. For example, Slinker et al. made a LEC using an Ir(III) complex with an emission maximum centred at 542 nm (Figure 23, centre).⁸² Finally, the first blue LEC was obtained by attaching electron-withdrawing groups to 2-phenylpyrazole (Hppz) cyclometalating ligand (Figure 23, right). The so prepared LEC exhibits electroluminescence at $\lambda_{\max} = 492$ nm and a remarkable EQE of 4.6%.⁸¹

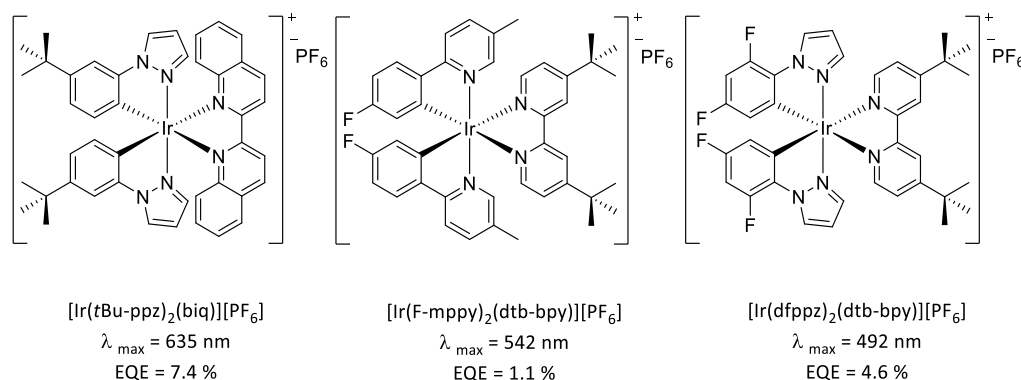


Figure 23: Ir(III) complexes used in fabrication of red (left),⁸¹ green (centre)⁸² and blue (right)⁸¹ devices

In 2014, my group reported the first example of highly efficient blue-emitting LEC device with non-fluorinated cyclometalating ligand. The classic 2-phenylpyridine was substituted by 2-methyl-5-phenyl-2*H*-tetrazole (Hptrz) as C^N ligands, while 4,4'-di-*tert*-butyl-2,2'-bipyridine (dtb-bpy) was used as ancillary ligand (Figure 24). The device built up with this complex as emitting material show an electroluminescence spectra with an emission maximum at 552 nm.⁸³

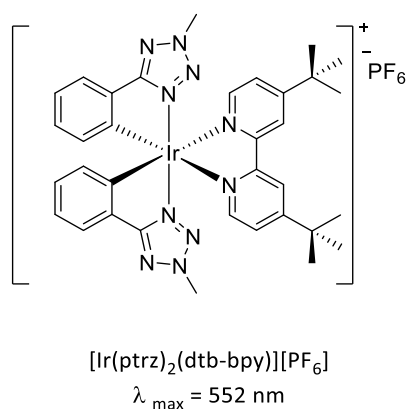


Figure 24: Ir(III) complex bearing Hptrz for the preparation of blue-LECs

Besides devices fabrication, Ir(III) complexes has been widely employed as biological sensor, in particular for sensing of intracellular simple oxygen- and nitrogen-containing compounds, such as molecular oxygen, nitric oxide,⁸⁴ cyanide anion,⁸⁵ hydrogen peroxide⁸⁶ and sulphite.⁸⁷ Ir(III) complexes decorated with proper appended group can also act as DNA and RNA intercalators,⁸⁸ for the sensing of intracellular pH,⁸⁹ for the detection of metal cation, such as Zn(II),⁹⁰ Cu(II)⁹¹ and Hg(II),⁹² and for the detection of reducing sugars.⁹³

The intracellular oxygen level is important in the regulation of many cellular processes. Notably, one of the most important features of this compound is the capability of efficiently quench the triplet state phosphorescence of metal complexes, generating reactive oxigens species (ROS), such as superoxide radical ($O_2^{\cdot-}$) and singlet oxygen (1O_2). The red emitting Ir(III) complex $[Ir(btp)_2(acac)]$, where Hbtp is 2-(benzo[*b*]thiophen-2-yl)pyridine and Hacac is acetylacetonate (Figure 25, left)⁹⁴ is reported to be extremely sensitive to the presence of molecular oxygen. When the complex is in presence of O_2 , both its emission intensity and lifetime are significantly decreased. The formed ROS are well-known to initiate chemical reactions with intracellular biomolecules, including amino acid residues in proteins, unsaturated lipids, and nucleic acid bases. These reactions cause damage to intracellular organelles, enzyme deactivation, and ultimately cell death.⁹⁵ Therefore, the design of a complex became very important, due to the possibility of localize the sensitizer in specific sub-cellular organelles, and, after photoactivation, make it useful as sensitizer for photodynamic treatments.

Another well-exploited feature of Ir(III) complexes is the possibility to decorate the peripheral structure with appropriate molecule able to interact with specific receptors. Among the possible structures that form specific interactions with appropriate receptors, the biotin is of great interest. This molecule is a vitamin (vitamin B₇ or vitamin H) and it is used in many energy cell cycles as a co-factor of ATP-dependent decarboxylase. Its most interesting feature is the ability to form strong non-covalent interaction with avidin, a specific glycoprotein.⁹⁶ Avidin is a tetrameric or dimeric protein⁹⁷ produced in the oviducts of birds, reptiles and amphibians deposited in the whites of their eggs. The tetrameric protein contains four identical subunits (homotetramer), each of which can bind to biotin with a high degree of affinity and specificity. The dissociation constant of avidin is measured to be $K_D \approx 10^{-15}$ M, making it one of the strongest known non-covalent bonds.⁹⁸

Owing to the extraordinarily high affinity of biotin to avidin, strong interactions are observed and such system has been widely exploited as a powerful tool in a variety of bioanalytical applications. Recently various examples of Ir(III) biotin complexes (Figure 25, right) have been utilized as luminescent probes since, in contrast to biotin-fluorophore conjugates, they show increased emission intensity and lifetimes when bound to avidin.^{99,100}

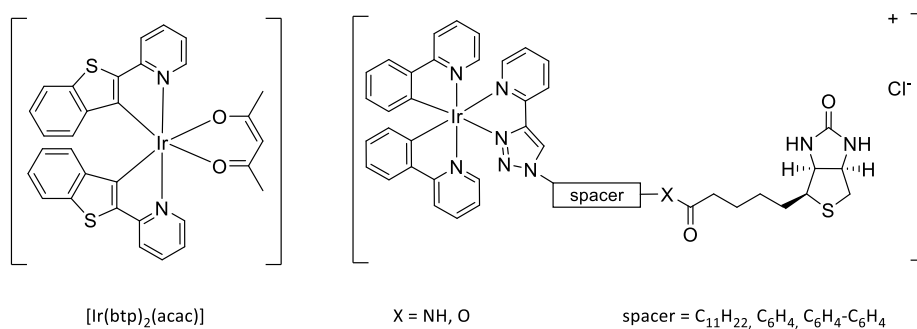


Figure 25: Ir(III) complexes for molecular oxygen sensing (left) and for avidin detection (right)

As reported above, Ir(III) complexes are now employed also for water splitting processes and H_2 production, and as visible light photocatalysts. As regarding this last field, a particular Ir(III) complex reported by Bernhard¹⁰¹ has become particularly interesting. In detail, $[\text{Ir}(\text{dF}(\text{CF}_3)\text{ppy})_2(\text{dtb-bpy})][\text{PF}_6]$, where $\text{dF}(\text{CF}_3)\text{ppy}$ is 2-(2,4-difluorophenyl)-5-trifluoromethylpyridine and dtb-bpy is 4,4'-di-tert-butyl-2,2'-bipyridine (Figure 26) is able to combine a wide HOMO-LUMO band gap with a remarkable high-energy excited state. These two important features, joint with the pronounced photoluminescence quantum yield, the great stability and a significant reducing strength of the excited state, make it a promising candidate for the photoactivation of a wide range of reaction, unaccessible with conventional methods.¹⁰²

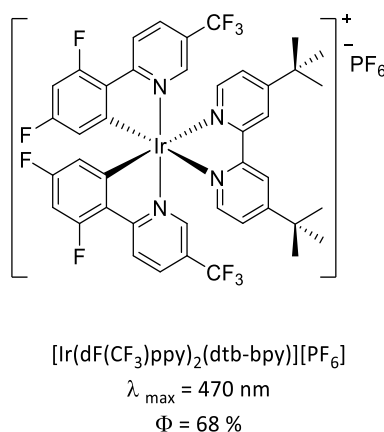


Figure 26: $[\text{Ir}(\text{dF}(\text{CF}_3)\text{ppy})_2(\text{dtb-bpy})][\text{PF}_6]$ used as visible light photocatalyst

3.1 Ir(III) complexes for blue-light

As shown above, the emission color of Ir(III) complexes can be readily tuned from blue to red by judicious modification of the cyclometalating ligands and/or ancillary ligands. In general, multicolor display applications require efficient and stable blue, green and red OLEDs. OLEDs have been manufactured with $[\text{Ir}(\text{C}^{\wedge}\text{N})_2(\text{L}^{\wedge}\text{L})]$ phosphor dopants, giving efficient green, yellow or red emission (Figure 27).¹⁰³

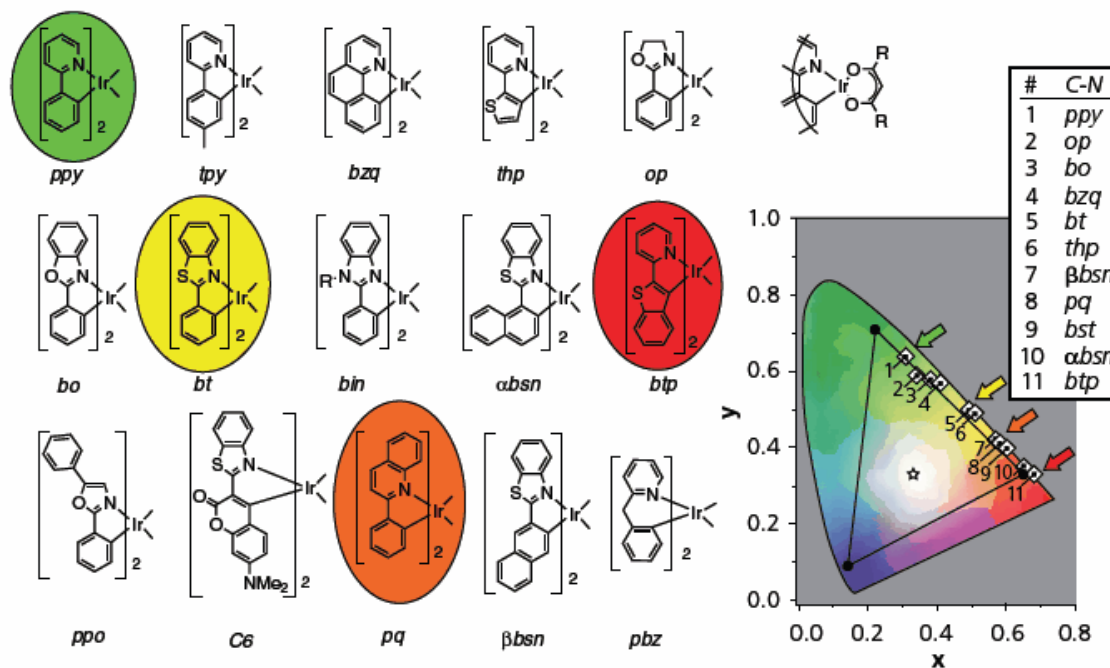


Figure 27: Green to red emission Ir(III) phosphors (from: <http://www.sigmaaldrich.com/technical-documents/articles/material-matters/achieving-high-efficiency.html>)

It is interesting to note that red and green iridium complexes have been well developed to be used in OLEDs, while blue iridium complexes are still less common. In this optic, the discover of efficient blue-emitting complexes is of a great importance, and many studies in this direction have been pursued.

As shown before, emission color tuning is conceptually easy to achieve. Simple modification of the ancillary ligand leads to a blue- or red-shift of several nanometers. A more remarkable effect can be obtained by variation of the $\text{C}^{\wedge}\text{N}$ cyclometalating ligands and this is the most employed strategy for the preparation of blue-emitting complexes. Although, blue-emitting complexes are not so easy to prepare, because wide HOMO-LUMO gaps are more difficult to obtain and, moreover, the high energy levels of blue emitters tend to be reactive under the device operating conditions.¹⁸ Two main modification strategies of the $\text{C}^{\wedge}\text{N}$ ligand have been pursued to stabilize the HOMO and shift the emission band of Ir(III) complexes to the blue: (i) addition of electron-withdrawing groups, typically fluorines;⁵⁸ (ii) reduction of the ring size of the aromatic

N-heterocycle. The latter approach has been well investigated, and several examples of Ir(III) complexes with cyclometalating ligands entailing 5-membered nitrogen-containing rings have been reported, namely, 1-aryl-1,2-pyrazoles,⁸¹ and phenyl imidazoles.¹⁰⁴ In addition, a few aryl triazoles have been also proposed, such as 5-aryl-1,2,4- triazoles¹⁰⁵ and aryl-1,2,3-triazoles.¹⁰⁶ Finally, only one example of tetrazole containing cyclometalated Ir(III) complexes have been reported in literature.⁸³

Compared to the prototypical $[\text{Ir}(\text{ppy})_2\text{bpy}]^+$, which has an emission maximum centred at 602 nm, a blue shift for the emission is observed in the case of $[\text{Ir}(\text{ppz})_2\text{bpy}]^+$, bearing 1-phenyl-1,2-pyrazoles (Hppz) as cyclometalating ligand (Figure 28), with $\lambda_{\text{max}} = 563 \text{ nm}$.⁸¹ However, the use of phenyl-triazoles did not further blue shift the emission band, as in the case of $[\text{Ir}(\text{phtl})_2\text{bpy}]^+$, where Hphtl = 1-phenyl-1,2,3-triazole, $\lambda_{\text{max}} = 580 \text{ nm}$ (Figure 28).¹⁰⁷ Therefore, an increase of the number of nitrogen atoms on the 5-membered heterocycle does not warrant an increase of the emission energy of the complexes, although one might expect that electron-rich triazoles in C^N ligands should enhance the ligand field splitting of Ir(III) d orbitals. In this perspective, an Ir(III) complex with 5-phenyltetrazole (Hptrz) as cyclometalated C^N ligand has been prepared. The emission observed for $[\text{Ir}(\text{ptrz})_2\text{bpy}]^+$ is shifted to 545 nm, resulting in the highest-energy emission bands ever reported for fluorine-free cyclometalating ligands (Figure 28, right).⁸³ This latter example presents three main advantages in respect with the previously reported luminescent Ir(III) complexes: (i) the high-field nature of phenyltetrazole that can lead to blue-shifted emissions without the need to use electron-deficient polyfluorinated ligands; (ii) the absence of reactive C(sp²)-F bonds that normally afford instability when the complex is used in LECs;¹⁰⁸ (iii) the higher radiative rate constants allows optimized performance in devices preventing exciton quenching.¹⁰⁹ These evidences now open the way for chemical modifications of the phenyl-tetrazole ligands, that will offer the possibility to further push the emission band toward the blue.

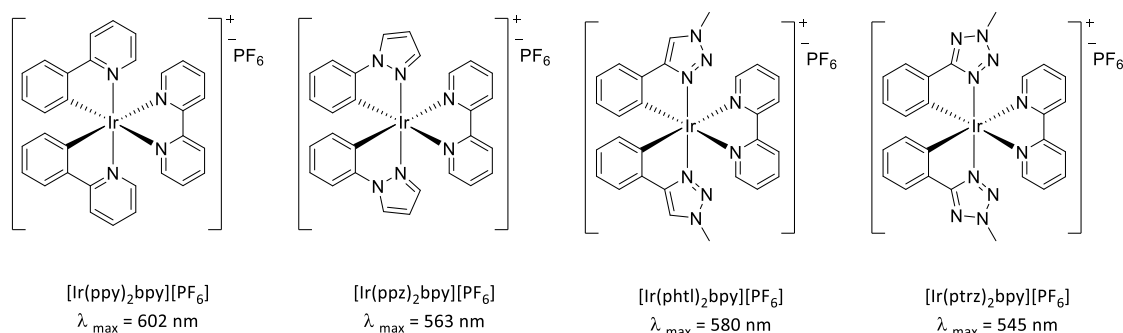


Figure 28: Selected examples for blue-emitting Ir(III) complexes

4. White light: goal for the future

In the recent years, a great attention has been devoted to the development of new innovative and low cost technologies for lighting and displays.¹¹⁰ In this context, one of the most challenging task is the obtainment of white light emitters, that are able to emit over the whole visible spectral region and surely offer the best visual comfort.

Molecular systems with white photoluminescence remain rather rare and their discovery is often serendipitous, although increasingly frequent.^{111,112} Various approaches to white emission can be pursued, where emission stems from multiple species which may be transient, generated in situ by an external stimulus, originated from intermolecular interactions or arranged in suitably designed multicomponent individual systems. In the latter case, the main challenge to obtain white emission is avoiding the complete funnelling of excitation energy to the lowest energy centre. This requires a rigorous molecular design and meticulous excited state engineering of the luminophoric species to be combined.

Individual white emitting molecules are very rare. They may display excited state intramolecular proton transfer (ESIPT), a phenomenon that enables dual emission due to enol-keto (E-K) tautomerism (Figure 29). ESIPT molecules exist in the ground state exclusively as E forms and, upon photoexcitation (E^*), they transform into the excited K form (K^*) which can exhibit a remarkably red-shifted luminescence. Typically, emission stems from K^* only but, if residual (higher energy) emission from E^* does occur, dual luminescence affording white-light is achievable.¹¹³

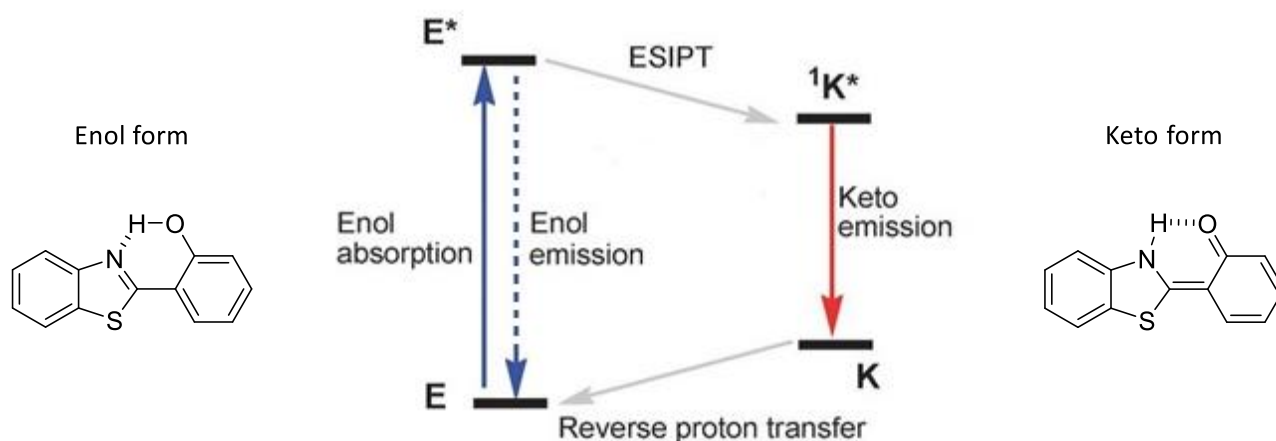


Figure 29: Principal photophysics of ESIPT molecules (illustrated for 2-(2-hydroxyphenyl)-benzothiazole, HBT)

Another approach is that based on partial protonation of simple molecules. This strategy can lead to dual emission, as reported by Strongin's group for a [a]benzofluorone derivative (Figure 30, left). The described compound exhibits dual emission bands that are pH-sensitive. In detail, the anionic form (A) is responsible for a red emission band centered at 620 nm, while the green emission band at 540 nm can be assigned to the neutral form (N). Modification of the solution pH lead to a fine tuning of the emitting response of the molecule, and in particular, upon increasing the solution pH is possible to increase the contribution of the red band, while decreasing the pH, the most stable form will be the neutral, resulting in a greener emission. By choosing the right solvent, the right solution pH and the right excitation wavelength, is possible to observe an almost pure with light emission, as reported in Figure 30, right.

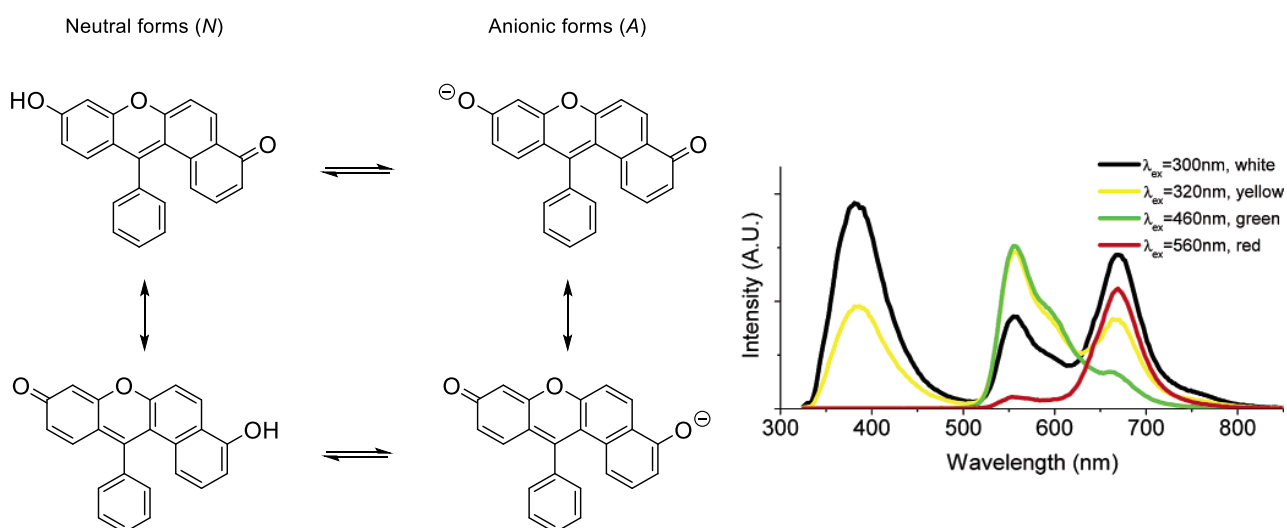


Figure 30: (left) A and N structures of [a]benzofluorone; (right) selected emission properties

On the other hand, a dyad containing two independent ESIPT organic systems combining blue and orange to give white has been obtained. Park's group prepare a single molecule made of two different fragment,¹¹⁴ HPI (2-(1,4,5-triphenyl-1*H*-imidazol-2-yl)phenol) and HPNI (3-(1,4,5-triphenyl-1*H*-imidazol-2-yl)naphthalen-2-ol) covalently linked by a diphenylether linking group, as shown in Figure 31, left. The two single fragment show a wide bandgap in the emission maxima ($\lambda_{\max} = 470$ nm for HPI and 570 nm for HPNI). When covalently linked in W1, the energy transfer between the two emitting centers is completely blocked by the presence of the ether, giving an emission that simply is the superimposition of those of the individual centers, resulting in a pure white light emission (Figure 31, right). However, this remarkable example remains virtually unique in the literature.

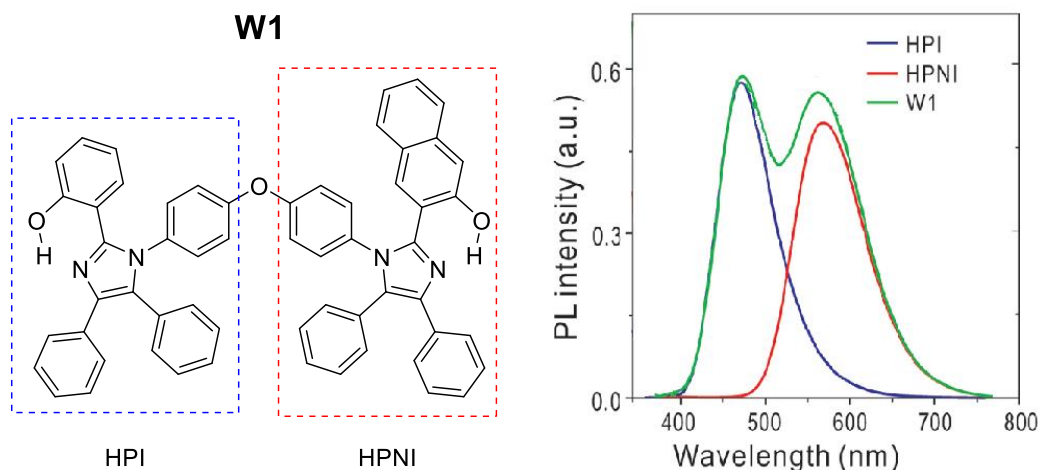


Figure 31: (left) Structure of the reported W1 emitter; (right) emission profiles of single component and W1

Dyad systems exhibiting partial energy transfer from a wide bandgap luminescent donor to an emitting acceptor with a smaller bandgap have also been reported. Higher energy (bluish-green) emission is maintained with concomitant sensitization of orange-red luminescence and generation of white light.

The first example of white emitting dyads system was reported by DeCola in 2005.¹¹⁵ In this work was firstly reported the use of an Ir(III) complex as sensitizer for the photoexcitation of an Eu(III)-terpyridine complex. In detail, a blue-emitting Ir(III) complex, with λ_{max} at 460 nm and 491 nm, has been opportunely functionalized with a terminal benzoic acid, able to chelate the Eu(III) moiety. This complex has then been reacted with an Eu(III) derivative, and the resulting dyad can actually emit over the whole visible spectrum. The emission profile show the contribution of both the metallic complexes, and this indicate that the Ir(III) complex is able to excite the Eu(III) center through a partial energy-transfer process. The structure of the described dyad and it emission spectrum is reported in Figure 32.

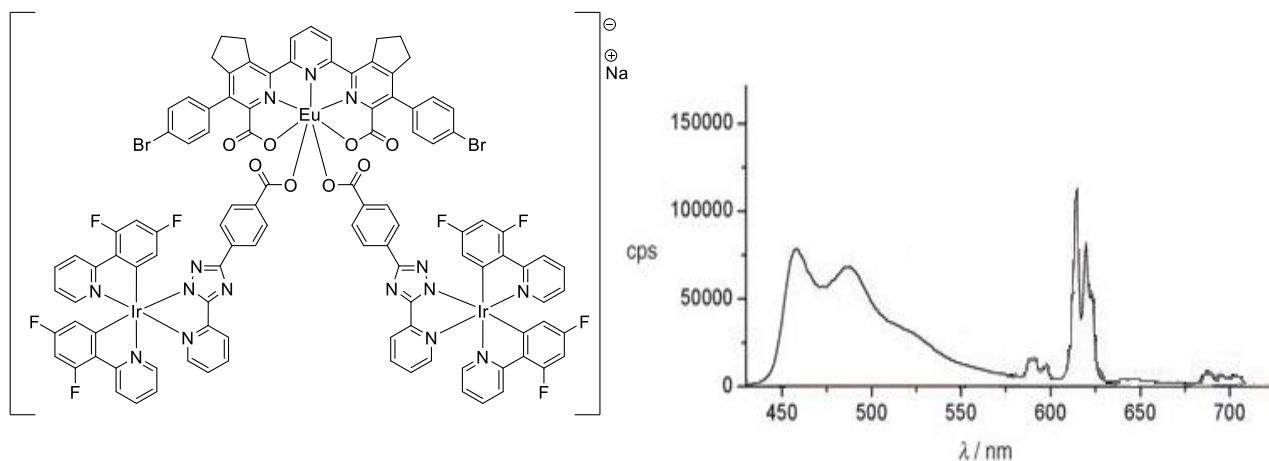


Figure 32: Ir(III)-Eu(III) dyad, structure and emission profile

White emission can be achieved also with other combination of metals. For instance, by carefully designing the cyclometalating ligands of an Ir(III) center, is possible to obtain white emission through partial energy-transfer to other Lanthanide metals, such as Gadolinium.¹¹⁶

Other interesting results have been obtained with molecules made of different units with particular properties, such as carbazole and terpyridine.¹¹⁷ These Donor-Acceptor architectures show a partial energy transfer between the two ending units, a carbazole, that act as a Donor, and a terpyridine moiety, that play the role of an Acceptor. Remarkably, the energy-transfer process can be controlled by varying the linking between the two subunit. In particular, passing from no linker to an acetylene-linker, is possible to obtain multiple emission, arising from the contribution of both the subunits, that afford white light luminescence under specific conditions of solvent and temperature. The structure of the studied systems and their emission profiles are reported in Figure 33.

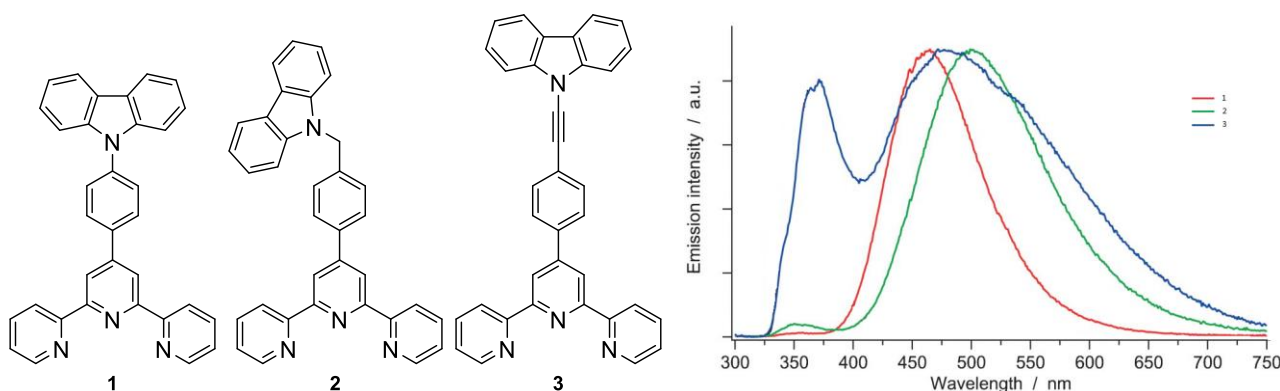


Figure 33: Structure and emission spectra in acetonitrile of carbazole-terpyridine derivatives

5. Purpose of the work

As illustrated in the previous sections, the synthesis of luminescent metal complexes is a very challenging task since they can be regarded as the starting point for many different areas. Luminescent complexes, in fact, can be used for technological, industrial, medical and biological applications. They consist of two main parts: the central core of the complex, a metal atom, and various organic ligands bonded to it.

Among all the transition metal complexes, Iridium(III) ones show the best photophysical properties: generally, they have high quantum yields, very long lifetimes and possess easily tunable emissions throughout the visible range.

During my PhD I prepared different families of Ir(III) complexes suitable for various applications.

The principal application of Ir(III) complexes is their use in the preparation of electroluminescent devices. In this context, the main feature of the complexes are their stability and their luminescent quantum yield. Remarkable features have been observed in Ir(III) complexes bearing isocyanides as ancillary ligand, but they are not very stable in devices' working conditions. In order to overcome these problems, I prepared a new class of more stable Ir(III) cyclometalated complexes equipped with a chelating diisocyanide moiety, with remarkable photoluminescent properties which can be used for the preparation of more performant electroluminescent devices.

In addition, one of the major interest in the research on luminescent complexes is the preparation of new compounds able to emit in the blue region of the visible spectra. Starting from this, and based on a work previously reported by my research group, I prepared a new class of Ir(III) complexes with a fluorine-tetrazole derivative as cyclometalated ligand, able to push the emission towards high energy.

Another well-investigated research field is the obtainment of white-light. This goal can be achieved in different ways, and one of the most investigated is the use of dyad architectures, generally based on a transition metal and a lanthanide. With this in mind, during my PhD I prepared different heterometallic Ir(III)₂-Eu(III) dyads able to emit an almost pure white-light.

In this context, we have demonstrate that a donor-acceptor system based on a carbazole moiety and a terpyridine can emit light covering all the visible spectra. In order to further study the relations between the structure and the luminescent properties of similar systems and with the aim to achieve white-light emission, I prepared a new family of compounds where the carbazole and the terpyridine moieties are connected with different conjugated linkers.

The research on new metal complexes with different ligands able to modify the photoluminescent properties of the central metal is an ongoing field. Recently, mesoionic carbens have emerged as a new class of ligand for the preparation of metal complex, typically to be used in the area of the homogenous

catalysis. During my PhD, I prepared an example of Ir(III) complex bearing a mesoionic carbene as donor ligand, with very interesting photoluminescent properties.

Ir(III) complexes have been used also for biological application, and particularly for the *in vitro* and *in vivo* imaging. In this field, the use of suitable biologically compatible nanocarriers is of a great importance, due to their ability to be internalized into cells. This capability has been exploited in order to permit the internalization of different molecules, such as agents for bioimaging or drugs. During my PhD, I prepared an Ir(III) complex equipped with a suitable ancillary ligand able to be linked to properly designed nanoparticles, able to carry the luminescent complex inside of cancer cells.

6. Bibliography

-
- ¹ P. Elumalai, P. Atkins, J. de Paula, *Atkins' Physical Chemistry*, Oxford University Press: Oxford (2002).
- ² J. R. Lakowicz, *Principles of Fluorescence Spectroscopy*, KA/PP: New York (1999).
- ³ R. C. Evans, P. Douglas, C. J. Winscom, *Coord. Chem. Rev.* **2006**, *250*, 2093.
- ⁴ D. C. Harris, M. D. Bertolucci, *Symmetry and Spectroscopy*. Oxford University Press, **1978**.
- ⁵ T. Engel, P. Reid, *Physical Chemistry* (Pearson Benjamin-Cummings, **2006**), 477.
- ⁶ (a) M. A. Baldo, D. F. O'Brien, Y. You, A. Shoustikov, S. Sibley, M. E. Thompson, S. R. Forrest, *Nature* **1998**, *395*, 151; (b) J. S. Wilson, A. S. Dhoot, A. J. A. B. Seeley, M. S. Khan, A. Köhler, R. H. Friend, *Nature* **2001**, *413*, 828; (c) I. Avilov, P. Minoofar, J. Cornil, L. De Cola, *J. Am. Chem. Soc.* **2007**, *129*, 8247; (d) H.-C. Su, F.-C. Fang, T.-Y. Hwu, H.-H. Hsieh, H.-F. Chen, G.-H. Lee, S.-M. Peng, K.-T. Wong, C.-C. Wu, *Adv. Funct. Mater.* **2007**, *17*, 1019.
- ⁷ L. Flamigni, A. Barbieri, C. Sabatini, B. Ventura, F. Barigelletti, *Top. Curr. Chem.* **2007**, *281*, 143.
- ⁸ T. J. Meyer, *Acc. Chem. Res.* **1978**, *11*, 94.
- ⁹ (a) D. A. Nicewicz, D. W. C. MacMillan, *Science* **2008**, *322*, 77; (b) J. Jin, D. W. C. MacMillan, *Angew. Chem. Int. Ed.* **2014**, *53*, 1; (c) J. L. Jeffrey, F. R. Petronijević, D. W. C. MacMillan, *J. Am. Chem. Soc.* **2015**, *137*, 8404.
- ¹⁰ K. A. King, P. J. Spellane, R. J. Watts, *J. Am. Chem. Soc.* **1985**, *107*, 1431.
- ¹¹ (a) C. Y.-S. Chung, S. P.-Y. Li, M.-W. Louie, K. K.-W. Lo, V. W.-W. Yam, *Chem. Sci.* **2013**, *4*, 2453; (b) V. Amendola, D. Bacchilega, I. Costa, L. Gianelli, M. Montalti, P. Pallavicini, A. Perotti, L. Prodi, N. Zaccheroni, *J. Photochem. Photobiol. A: Chem* **2003**, *159*, 249.
- ¹² K. K.-W. Lo, S. P.-Y. Li, *RSC Adv.* **2014**, *4*, 10560.
- ¹³ V. Smil, *Creating the Twentieth Century: Technical Innovations of 1867-1914 and Their Lasting Impact*, Oxford University Press, Oxford, **2005**.
- ¹⁴ J. Brox, *Brilliant: The Evolution of Artificial Light*, Houghton Mifflin Harcourt, New York, **2010**.
- ¹⁵ International Energy Agency, *Light's Labour's Lost-Policies for Energy-Efficient Lighting*, <http://www.iea.org/>, **2006**.
- ¹⁶ G. Zissis, S. Kitsinelis, *J. Phys. D* **2009**, *42*, 173001.
- ¹⁷ C. J. Humphreys, *MRS Bull.* **2008**, *33*, 459.
- ¹⁸ R. D. Costa, E. Orti, H. J. Bolink, F. Monti, G. Accorsi, N. Armaroli, *Angew. Chem. Int. Ed.* **2012**, *51*, 8178.
- ¹⁹ M. H. Crawford, *IEEE J. Sel. Top. Quantum Electron.* **2009**, *15*, 1028.
- ²⁰ J. H. Burroughes, D. D. C. Bradley, A. R. Brown, R. N. Marks, K. Mackay, R. H. Friend, P. L. Burns, A. B. Holmes, *Nature* **1990**, *347*, 539.
- ²¹ *Organic Light Emitting Devices: Synthesis, Properties and Applications* (Eds.: K. Müllen, U. Scherf), Wiley-VCH, Weinheim, **2006**.
- ²² N. Holonyak Jr., Lemelson-MIT Prize Winner. Lemelson-MIT Program. Retrieved August 13, **2007**.

-
- ²³ T. Jüstel in *Luminescence* (Eds.: C. Ronda), Wiley-VCH, Weinheim, **2008**, 179.
- ²⁴ C. W. Tang, S. A. Van Slyke, *Appl. Phys. Lett.* **1987**, *51*, 913.
- ²⁵ C. W. Tang, S. A. Van Slyke, C. H. Chen, *J. Appl. Phys.* **1989**, *65*, 3610.
- ²⁶ M. A. Baldo, D. F. O'Brien, M. E. Thompson, S. R. Forrest, *Physical Review B* **1999**, *60*, 14422.
- ²⁷ (a) C. W. Tang, *Inf. Disp.* **1996**, *10*, 16; (b) S. Sibley, M. E. Thompson, P. E. Burrows, S. R. Forrest, "Optoelectronic Properties of Inorganic Complexes", D. M. Roundhill, J. Fakler, Eds.; Plenum Press: New York; (c) P. E. Burrows, G. Gu, V. Bulovic, S. R. Forrest, M. E. Thompson, *IEEE Trans. Electron. Dev.* **1997**, *44*, 1188.
- ²⁸ Z. Li, H. Meng, *Organic Light-Emitting Materials and Devices*, CRC, Boca Raton, FL, **2007**.
- ²⁹ M. Sessolo, H. J. Bolink, *Adv. Mater.* **2011**, *23*, 1829.
- ³⁰ K. M. Maness, R. H. Terrill, T. J. Meyer, R. W. Murray, R. M. Wightman, *J. Am. Chem. Soc.* **1996**, *118*, 10609.
- ³¹ J. Slinker, D. Bernards, P. L. Houston, H. D. Abruña, S. Bernhard, G. G. Malliaras, *Chem. Commun.* **2003**, 2392.
- ³² H.-C. Su, K.-T. Wong, C.-C. Wu in *WOLEDs and Organic Photovoltaics-Recent Advances and Applications* (Hrsg.: V. W.W. Yam), Springer, Berlin, **2010**.
- ³³ Q. Pei, G. Yu, C. Zhang, Y. Yang, A. J. Heeger, *Science* **1995**, *269*, 1086.
- ³⁴ Q. J. Sun, Y. F. Li, Q. B. Pei, *J. Disp. Technol.* **2007**, *3*, 211.
- ³⁵ T. Hu, L. He, L. Duan, Y. Qiu, *J. Mater. Chem.* **2012**, *22*, 4206.
- ³⁶ J. D. Slinker, J. Rivnay, J. S. Moskowitz, J. B. Parker, S. Bernhard, H. D. Abruña, G. G. Malliaras, *J. Mater. Chem.* **2007**, *17*, 2976.
- ³⁷ K. M. Maness, H. Masui, R. M. Wightman, R. W. Murray, *J. Am. Chem. Soc.* **1997**, *119*, 3987.
- ³⁸ J.-K. Lee, D. Yoo, M. F. Rubner, *Chem. Mater.* **1997**, *9*, 1710.
- ³⁹ M. S. Lowry, S. Bernhard, *Chem. Eur. J.* **2006**, *12*, 7970.
- ⁴⁰ P. Matyba, H. Yamaguchi, G. Eda, M. Chhowalla, L. Edman, N. D. Robinson, *ACS Nano* **2010**, *4*, 637.
- ⁴¹ Z. Yu, L. Hu, Z. Liu, M. Sun, M. Wang, G. Grüner, Q. Pei, *Appl. Phys. Lett.* **2009**, *95*, 203304.
- ⁴² R. Weissleder, M. J. Pittet, *Nature* **2008**, *452*, 580.
- ⁴³ H. R. Petty, *Microsc. Res. Tech.* **2007**, *70*, 687.
- ⁴⁴ (a) M. Fernandez-Suarez, A. Y. Ting, *Nat. Rev. Mol. Cell Biol.* **2008**, *9*, 929; (b) T. Terai, T. Nagano, *Curr. Opin. Chem. Biol.* **2008**, *12*, 515; (c) L. Yuan, W. Lin, K. Zheng, L. He, W. Huang, *Chem. Soc. Rev.* **2013**, *42*, 622.
- ⁴⁵ (a) R. Weissleder, *Nat. Biotechnol.* **2001**, *19*, 316; (b) R. Weissleder, V. Ntziachristos, *Nat. Med.* **2003**, *9*, 123.

-
- ⁴⁶ U.S. Energy Information Administration (EIA); International Energy Statistics database; <http://www.eia.gov/cfapps/ipdb project/IEDIndex3.cfm> (accessed on May 20, 2012).
- ⁴⁷ N. S. Lewis, *Science* **2007**, *315*, 798.
- ⁴⁸ R. E. Blankenship, D. M. Tiede, J. Barber, G. W. Brudvig, G. Fleming, M. Ghirardi, M. R. Gunner, W. Junge, D. M. Kramer, A. Melis, T. A. Moore, C. C. Moser, D. G. Nocera, A. J. Nozik, D. R. Ort, W. W. Parson, R. C. Prince, R. T. Sayre, *Science* **2011**, *332*, 805.
- ⁴⁹ O. Khaselev, J. A. Turner, *Science* **1998**, *280*, 425.
- ⁵⁰ V. Balzani, A. Credi, M. Venturi, *Curr. Opin. Chem. Biol.* **1997**, *1*, 506.
- ⁵¹ C. K. Prier, D. A. Rankic, D. W. C. MacMillan, *Chem. Rev.* **2013**, *113*, 5322.
- ⁵² G. L. Miessler, D. A. Tarr, *Inorganic Chemistry* (**2003**, 3rd ed.) Pearson Prentice Hall.
- ⁵³ A. Juris, V. Balzani, F. Barigelletti, S. Campagna, P. Belser, A. Von Zelewsky, *Coord. Chem. Rev.* **1988**, *84*, 85.
- ⁵⁴ V. Balzani, G. Bergamini, S. Campagna, F. Puntoriero, *Top. Curr. Chem.* **2007**, *280*, 1.
- ⁵⁵ R. Englman, J. Jortner, *Mol. Phys.* **1970**, *18*, 145.
- ⁵⁶ D. Kumaresan, K. Shankar, S. Vaidya, R. H. Schmehl, *Top. Curr. Chem.* **2007**, *281*, 101.
- ⁵⁷ K. Dedeian, P. I. Djurovich, F. O. Garces, G. Carlson, R. J. Watts, *Inorg. Chem.* **1991**, *30*, 1685.
- ⁵⁸ V. V. Grushin, N. Herron, D. D. LeCloux, W. J. Marshall, V. A. Petrov, Y. Wang, *Chem. Commun.* **2001**, *16*, 1494.
- ⁵⁹ M. Nonoyama, *Bull. Chem. Soc. Jpn.* **1974**, *47*, 767.
- ⁶⁰ M. G. Colombo, T. C. Brunold, T. Riedener, H. U. Gudel, M. Fortsch, H. B. Burgi, *Inorg. Chem.* **1994**, *33*, 545.
- ⁶¹ A. B. Tamayo, B. D. Alleyne, P. I. Djurovich, S. Lamansky, I. Tsyba, N. N. Ho, R. Bau, M. E. Thompson, *J. Am. Chem. Soc.* **2003**, *125*, 7377.
- ⁶² K. Dedeian, J. M. Shi, N. Shepherd, E. Forsythe, D. C. Morton, *Inorg. Chem.* **2005**, *44*, 4445.
- ⁶³ T. Karatsu, T. Nakamura, S. Yagai, A. Kitamura, K. Yamaguchi, Y. Matsushima, T. Iwata, Y. Hori, T. Hagiwara, *Chem. Lett.* **2003**, *32*, 886.
- ⁶⁴ B. Schmid, F. O. Garces, R. J. Watts, *Inorg. Chem.* **1994**, *33*, 9.
- ⁶⁵ C. H. Yang, J. Beltran, V. Lemaire, J. Cornil, D. Hartmann, W. Sarfert, R. Frohlich, C. Bizzarri, L. De Cola, *Inorg. Chem.* **2010**, *49*, 9891.
- ⁶⁶ C. Wu, H.-F. Chen, K.-T. Wong, M. E. Thompson, *J. Am. Chem. Soc.* **2010**, *132*, 3133.
- ⁶⁷ K. R. Lee, M.-S. Eum, C. S. Chin, S. Lee, I. J. Kim, Y. S. Kim, Y. Kim, S.-J. Kim, N. H. Hur, *Dalton Trans.* **2009**, 3650.
- ⁶⁸ J.-L. Liao, Y. Chi, Z.-T. Sie, C.-H. Ku, C.-H. Chang, M. A. Fox, P. J. Low, M.-R. Tseng, G.-H. Lee, *Inorg. Chem.* **2015**, *54*, 10811.

- ⁶⁹ V. H. Nguyen, H. Q. Chew, B. Su, J. H. K. Yip, *Inorg. Chem.* **2014**, *53*, 9739.
- ⁷⁰ M. Montalti, A. Credi, L. Prodi, M. T. Gandolfi, *Handbook of Photochemistry*, 3rd ed., Taylor and Francis, Boca Raton, FL, **2006**.
- ⁷¹ R. D. Costa, E. Orti, H. J. Bolink, S. Graber, S. Schaffner, M. Neuburger, C. E. Housecroft, E. C. Constable, *Adv. Funct. Mater.* **2009**, *19*, 3456.
- ⁷² J. Li, P. I. Djurovich, B. D. Alleyne, M. Yousufuddin, N. N. Ho, J. C. Thomas, J. C. Peters, R. Bau, M. E. Thompson, *Inorg. Chem.* **2005**, *44*, 1713.
- ⁷³ N. M. Shavaleev, F. Monti, R. D. Costa, R. Scopelliti, H. J. Bolink, E. Orti, G. Accorsi, N. Armaroli, E. Baranoff, M. Grätzel, M. K. Nazeeruddin, *Inorg. Chem.* **2012**, *51*, 2263.
- ⁷⁴ CIE. *Commission internationale de l'Eclairage proceedings*, **1931**. Cambridge: Cambridge University Press.
- ⁷⁵ *Colorimetry - Understanding the CIE System* (Ed.: J. Schanda), Wiley, Hoboken, NJ, **2007**.
- ⁷⁶ H. Zollinger, *Color Chemistry*; Wiley-VCH: Weinheim, FDR, **1991**.
- ⁷⁷ S. Ladouceur, D. Fortin, E. Zysman-Colman, *Inorg. Chem.* **2010**, *49*, 5625.
- ⁷⁸ J. L. Rodriguez-Redondo, R. D. Costa, E. Orti, A. Sastre-Santos, H. J. Bolink, F. Fernandez-Lazaro, *Dalton Trans.* **2009**, 9787.
- ⁷⁹ M. K. Nazeeruddin, R. T. Wegh, Z. Zhou, C. Klein, Q. Wang, F. De Angelis, S. Fantacci, M. Grätzel, *Inorg. Chem.* **2006**, *45*, 9245.
- ⁸⁰ F. De Angelis, S. Fantacci, N. Evans, C. Klein, S. M. Zakeeruddin, J. E. Moser, K. Kalyanasundaram, H. J. Bolink, M. Grätzel, M. K. Nazeeruddin, *Inorg. Chem.* **2007**, *46*, 5989.
- ⁸¹ A. B. Tamayo, S. Garon, T. Sajoto, P. I. Djurovich, I. M. Tsyba, R. Bau, M. E. Thompson, *Inorg. Chem.* **2005**, *44*, 8723.
- ⁸² J. D. Slinker, C. Y. Koh, G. G. Malliaras, M. S. Lowry, S. Bernhard, *Appl. Phys. Lett.* **2005**, *86*, 173506.
- ⁸³ F. Monti, A. Baschieri, I. Gualandi, J. J. Serrano-Pérez, J. M. Junquera-Hernández, D. Tonelli, A. Mazzanti, S. Muzzioli, S. Stagni, C. Roldan-Carmona, A. Pertegás, H. J. Bolink, E. Ortí, L. Sambri, N. Armaroli, *Inorg. Chem.* **2014**, *53*, 7709.
- ⁸⁴ R. Zhang, Z. Ye, G. Wang, W. Zhang, J. Yuan, *Chem. - Eur. J.* **2010**, *16*, 6884.
- ⁸⁵ J. Liu, Y. Liu, Q. Liu, C. Li, L. Sun, F. Li, *J. Am. Chem. Soc.* **2011**, *133*, 15276.
- ⁸⁶ J. Jing, J.-L. Zhang, *Chem. Sci.* **2013**, *4*, 2947.
- ⁸⁷ G. Li, Y. Chen, J. Wang, Q. Lin, J. Zhao, L. Ji, H. Chao, *Chem. Sci.* **2013**, *4*, 4426.
- ⁸⁸ K. Y. Zhang, S. P.-Y. Li, N. Zhu, I. W.-S. Or, M. S.-H. Cheung, Y.-W. Lam, K. K.-W. Lo, *Inorg. Chem.* **2010**, *49*, 2530.
- ⁸⁹ L. Murphy, A. Congreve, L.-O. Pålsson, J. A. G. Williams, *Chem. Commun.* **2010**, 46, 8743.
- ⁹⁰ Y. You, S. Lee, T. Kim, K. Ohkubo, W.-S. Chae, S. Fukuzumi, G.-J. Jhon, W. Nam, S. J. Lippard, *J. Am. Chem. Soc.* **2011**, *133*, 18328.

- ⁹¹ Y. You, Y. Han, Y.-M. Lee, S. Y. Park, W. Nam, S. J. Lippard, *J. Am. Chem. Soc.* **2011**, *133*, 11488.
- ⁹² Y. Wu, H. Jiang, Z. Dong, Q. Zhao, H. Wu, F. Li, *Inorg. Chem.* **2011**, *50*, 7412.
- ⁹³ H.-W. Liu, K. Y. Zhang, W. H.-T. Law, K. K.-W. Lo, *Organometallics* **2010**, *29*, 3474.
- ⁹⁴ S. Zhang, M. Hosaka, T. Yoshihara, K. Negishi, Y. Iida, S. Tobita, T. Takeuchi, *Cancer Res.* **2010**, *70*, 4490.
- ⁹⁵ (a) L. Lyras, R. H. Perry, E. K. Perry, P. G. Ince, A. Jenner, P. Jenner, B. Halliwell, *J. Neurochem.* **1998**, *71*, 302; (b) M. Valko, D. Leibfritz, J. Moncol, M. T. Cronin, M. Mazur, J. Telser, *Int. J. Biochem. Cell Biol.* **2007**, *39*, 44.
- ⁹⁶ N. M. Green, *Methods Enzymol.* **1990**, *184*, 51.
- ⁹⁷ K. P. Nurminen, S. H. Helppolainen, J. A. E. Määttä, K. K. Halling, J. P. Slotte, T. Huhtala, T. Liimatainen, S. Ylä-Herttua, *Biochemical Journal* **2007**, *405*, 397.
- ⁹⁸ N. M. Green, *The Biochemical Journal* **1963**, *89*, 585.
- ⁹⁹ K. K.-W. Lo, K. H.-K. Tsang, K.-S. Sze, C.-K. Chung, T. K.-M. Lee, K. Y. Zhang, W.-K. Hui, C.-K. Li, J. S.-Y. Lau, D. C.-M. Ng, N. Zhu, *Coord. Chem. Rev.* **2007**, *251*, 2292 and cited refs.
- ¹⁰⁰ A. Baschieri, S. Muzzioli, V. Fiorini, E. Matteucci, M. Massi, L. Sambri, S. Stagni, *Organometallics* **2014**, *33*, 6154.
- ¹⁰¹ M. S. Lowry, J. I. Goldsmith, J. D. Slinker, R. Rohl, R. A. Pascal, Jr., G. G. Malliaras, S. Bernhard, *Chem. Mater.* **2005**, *17*, 5712.
- ¹⁰² L. Chu, C. Ohta, Z. Zuo, D. W. C. MacMillan, *J. Am. Chem. Soc.* **2014**, *136*, 10886.
- ¹⁰³ S. Lamansky, P. Djurovich, D. Murphy, F. Abdel-Razzaq, H.-E. Lee, C. Adachi, P. E. Burrows, S. R. Forrest, M. E. Thompson, *J. Am. Chem. Soc.* **2001**, *123*, 4304.
- ¹⁰⁴ E. Baranoff, S. Fantacci, F. De Angelis, X. Zhang, R. Scopelliti, M. Grätzel, M. K. Nazeeruddin, *Inorg. Chem.* **2011**, *50*, 451.
- ¹⁰⁵ W.-Y. Lai, J. W. Levell, A. C. Jackson, S.-C. Lo, P. V. Bernhardt, I. D. W. Samuel, P. L. Burn, *Macromolecules* **2010**, *43*, 6986.
- ¹⁰⁶ B. Beyer, C. Ulbricht, D. Escudero, C. Friebe, A. Winter, L. Gonzalez, U. S. Schubert, *Organometallics* **2009**, *28*, 5478.
- ¹⁰⁷ S. Ladouceur, D. Fortin, E. Zysman-Colman, *Inorg. Chem.* **2011**, *50*, 11514.
- ¹⁰⁸ J. L. Kiplinger, T. G. Richmond, C. E. Osterberg, *Chem. Rev.* **1994**, *94*, 373.
- ¹⁰⁹ N. M. Shavaleev, F. Monti, R. Scopelliti, A. Baschieri, L. Sambri, N. Armaroli, M. Grätzel, M. K. Nazeeruddin, *Organometallics* **2013**, *32*, 460.
- ¹¹⁰ (a) J. Kido, M. Kimura, K. Nagai, *Science* **1995**, *267*, 1332; (b) Y. Sun, N. C. Giebink, H. Kanno, B. Ma, M. E. Thompson, S. R. Forrest, *Nature* **2006**, *440*, 908.
- ¹¹¹ Q.-Y. Yang, J.-M. Lehn, *Angew. Chem. Int. Ed.* **2014**, *53*, 4572.
- ¹¹² S. Mukherjee, P. Thilagar, *Dyes Pigm.* **2014**, *110*, 2.

-
- ¹¹³ J. Zhao , S. Ji , Y. Chen , H. Guo, P. Yang, *Phys. Chem. Chem. Phys.* **2012**, *14*, 8803.
- ¹¹⁴ S. Park, J. E. Kwon, S. H. Kim, J. Seo, K. Chung, S.-Y. Park, D.-J. Jang, B. M. Medina, J. Gierschner, S. Y. Park, *J. Am. Chem. Soc.* **2009**, *131*, 14043.
- ¹¹⁵ P. Coppo, M. Duati, V. N. Kozhevnikov, J. W. Hofstraat, L. De Cola, *Angew. Chem. Int. Ed.* **2005**, *44*, 1806.
- ¹¹⁶ D. Sykes, I. S. Tidmarsh, A. Barbieri, I. V. Sazanovich, J. A. Weinstein, M. D. Ward, *Inorg. Chem.* **2011**, *50*, 11323.
- ¹¹⁷ A. Baschieri, L. Sambri, I. Gualandi, D. Tonelli, F. Monti, A. Degli Esposti, N. Armaroli, *RSC Adv.* **2013**, *3*, 6507.

7. A chelating diisocyanide ligand for cyclometalated Ir(III) complexes with strong and tunable luminescence

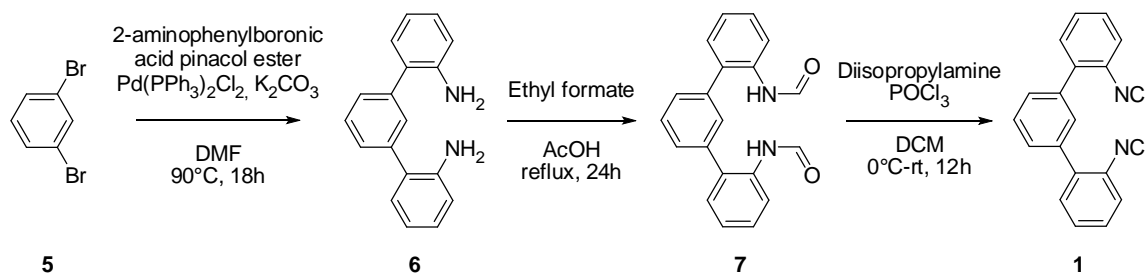
Cyclometalated Iridium (III) complexes represent one of the most widely exploited classes of triplet emitters for flat solid-state electroluminescent devices such as organic light-emitting diodes (OLEDs)^{1,2} and light-emitting electrochemical cells (LECs).^{3,4} The more important advantages of this class of complexes are the high photoluminescence quantum yields (PLQYs), the relatively short excited-state lifetimes and the extremely high versatility in tuning the emission color by little variation of the chemical nature of the ligands.³ Among all cyclometalated Ir(III) complexes, interesting features have been found in those bearing commercially-available monodentate isocyanide ancillary ligands. Isocyanides represents strong-field ancillary ligands, and they contribute to increase the *d*-orbital splitting of the iridium(III) metal centre, shifting the related complex emission towards blue with high photoluminescence quantum yields.^{3,5,6} However these luminophores display low stability in LECs if compared to analogous complexes containing bidentate ancillary ligands, such as conventional 2,2'-bipyridines or 1,10-phenanthrolines.³ This behaviour is principally due to the Ir-CN bond lability.

With the aim to overcome this problem, during my PhD, I designed and synthesised the first example of chelating diisocyanide ligand, which can actually act as a remarkably large, bidentate ancillary ligand.

7.1 Result and discussion

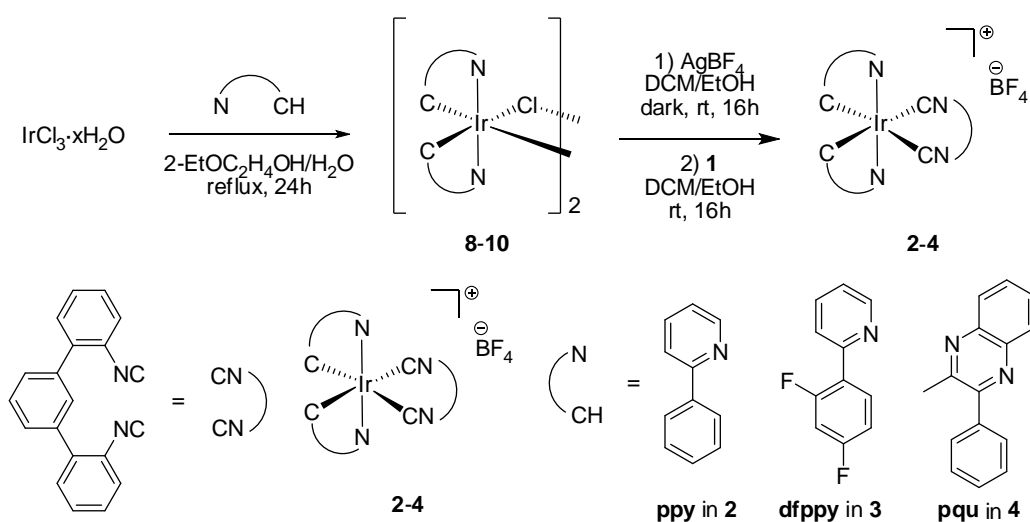
7.1.1 Synthesis of ligand 1 and complexes 2-4

The synthesis of chelating diisocyanide ligand **1** is reported in Scheme 1. The commercially available 1,3-dibromobenzene (**5**) was reacted with 2-aminophenylboronic acid pinacol ester under Suzuki-coupling conditions, giving the diamino derivative **6** in 85% yield. The amino groups of **6** were formylated with ethyl formate in refluxing acetic acid, resulted in the diformylated product **7** in almost quantitative yield (93%). This intermediate was subsequently dehydrated with POCl₃ to afford the desired ligand **1** in 50% yield.



Scheme 1: Synthesis of the bidentate diisocyanide ligand **1**

The diisocyanide **1** was used as ancillary ligand to prepare the cationic Ir(III) complexes **2-4** (Scheme 2). The cyclometalated μ -dichloro-bridged iridium precursors $[\text{Ir}(\text{C}^{\wedge}\text{N})_2\text{Cl}]_2$ (**8-10**) were prepared following a reported procedure^{7,8} by refluxing the $\text{IrCl}_3 \cdot x\text{H}_2\text{O}$ salt and the appropriate cyclometalating ligand $\text{HC}^{\wedge}\text{N}$, *i.e.* Hppy = 2-phenylpyridine for **8**, Hdffppy = 2-(2,4-difluoro-phenyl)pyridine for **9**, and Hpqu = 2-methyl-3-phenylquinoxaline for **10**, in a 2-ethoxyethanol/water mixture (3:1). Compounds **8-10** were treated with AgBF_4 and then, after filtration of the precipitated AgCl , ligand **1** was added dropwise to each solution and the reaction mixture was stirred at room temperature for 24 hours. Purification of the crudes by column chromatography on neutral alumina gave complexes **2-4** in good yields (57-60%).



Scheme 2: Synthesis of complexes **2-4** and related structures

The treatment of **8-10** with a soluble $\text{Ag}(\text{I})$ salt (*i.e.*, AgBF_4) to remove the chloride from the dichloro-bridged dimers is an essential step for the successful accomplishment of the reaction.⁹ In fact, in the absence of this step, compound **1** behaves as a monodentate ligand and coordinates two Ir(III)-fragments, both of them preserving one chloride ion in the metal coordination sphere.

7.1.2 Structural characterization

The complexes **2-4** were characterized by NMR spectroscopy and ESI mass spectrometry. For complex **3**, crystals were obtained and the structure was determined by single-crystal X-ray diffraction analysis. The structure is reported in Figure 1 and the corresponding crystallographic parameters in Table 1.

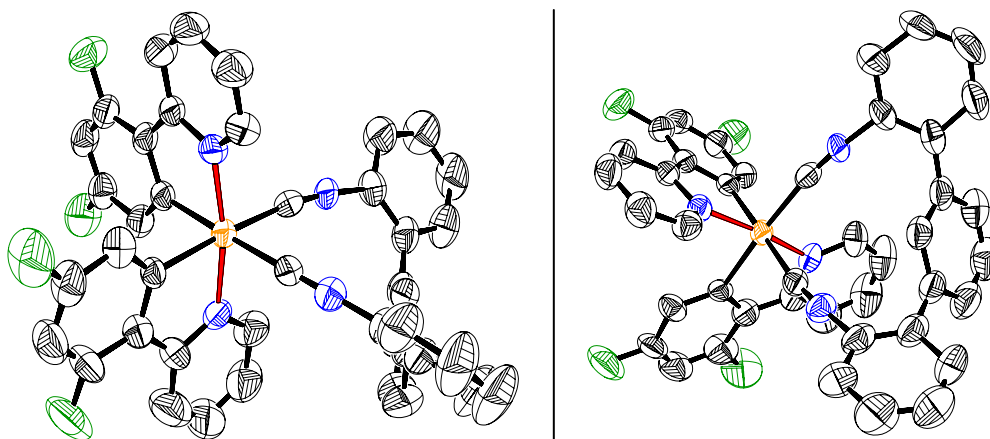


Figure 1: X-ray crystal structure of **3**. The BF_4^- counteranion, solvent molecules and hydrogen atoms are omitted for clarity. ORTEP representations are at the 50% probability

Table 1: Crystallographic parameters for **3**

3	
CCDC number	1062816
Formula	$\text{C}_{42}\text{H}_{23}\text{N}_4\text{F}_4\text{Ir}$, BF_4 , 2 CHCl_3 , CH_2Cl_2
F_w	1262.32
T , K	298
λ , Å	0.71073 (Mo- $\text{K}\alpha$)
Crystal system	Monoclinic
Space group	P_{21}/n
a , Å	9.2828(8)
b , Å	22.6451(19)
c , Å	24.351(2)
α , deg	90.000
β , deg	97.1920(10)
γ , deg	90.000
Cell volume, Å ³	5078.6(7)
Z	4
D_c , g cm^{-3}	1.651

μ , mm ⁻¹	3.115
F(000)	2460
h, k, l max	11,28,30
Crystal size, mm	0.20,0.16,0.11
θ limits, °	1.69 to 26.48
Reflections collected	52915
Independent reflections	10464
Data/restraints/parameters	10464/24/626
Weight. Scheme	0.071600 15.736697
GOF on F ²	1.131
R ₁ (I > 2 σ (I))	0.0589
wR ₂ (all data)	0.1568
Peak/hole, e Å ⁻³	1.466 and -1.186
Notes:	The cell contains 2 molecules of CHCl ₃ and one molecule of CH ₂ Cl ₂ , disordered over two positions (58:42 ratio).

As clearly visible from the crystal structure of **3** in Figure 1, the ancillary ligand **1** is not planar so the complex belongs to the C₁ point group. Accordingly, the two cyclometalating ligands are not equivalent. In fact, a splitting of the signal coming from the two C^N ligands is observed in the ¹H and ¹³C NMR spectra, when the motion of the terphenyl moiety on ligand **1** is sufficiently slow with respect to the NMR timescale. The dynamic behavior of this class of compounds was confirmed in the case of **4**. At room temperature the ¹H-NMR spectrum of this complex shows broad signals that can be resolved into pairs by lowering the temperature to -10°C, as reported in Figure 2.

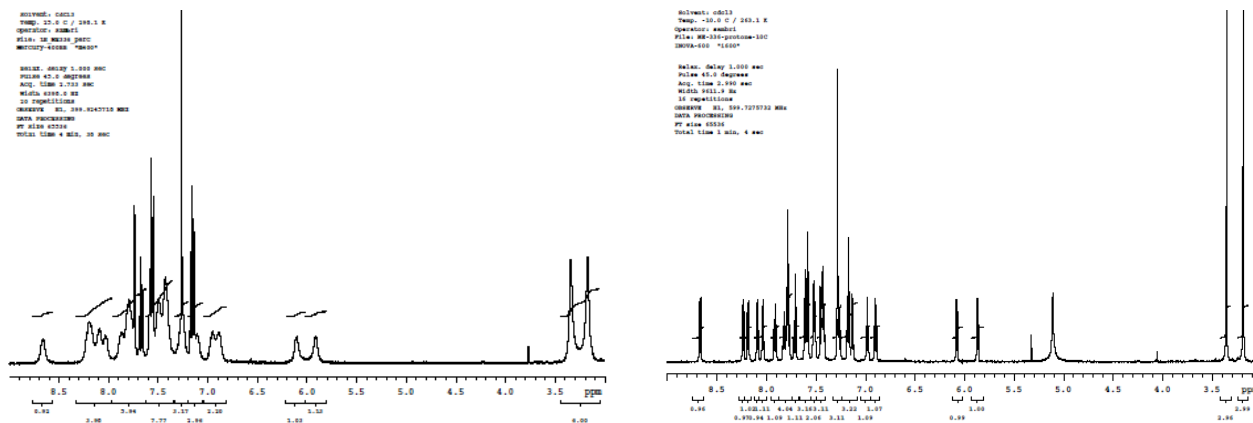


Figure 2: ¹H-NMR for complex **4**, recorded at room temperature (left) and -10°C (right)

7.1.3 Electrochemical properties

The electrochemical properties of complexes **2-4** were investigated by Osteryoung square-wave voltammetry (OSWV) and cyclic voltammetry (CV) in room-temperature acetonitrile solutions and reported relative to the Fc^+/Fc redox couple (Figure 3).

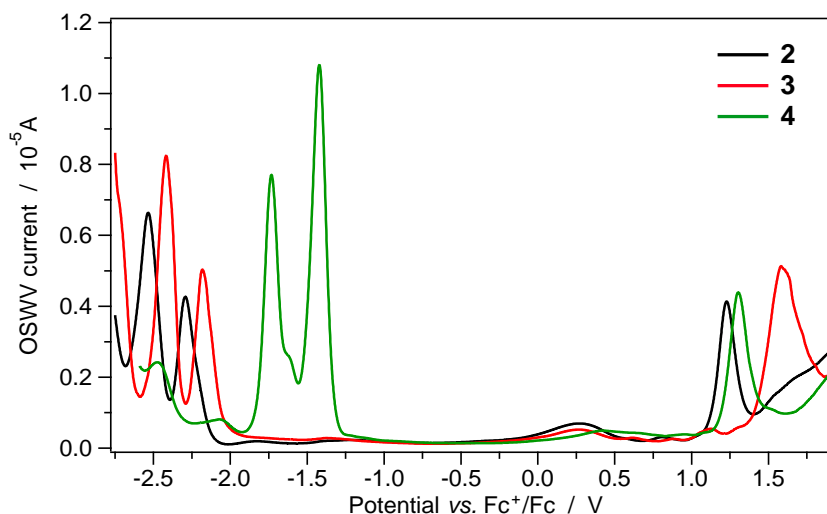


Figure 3: Square-wave voltammograms of **2-4** in room-temperature acetonitrile solutions recorded at a scan rate of 25 mV/s with a square-wave amplitude of ± 20 mV and a frequency of 25 Hz

All the observed redox processes were irreversible at any scan rate ($100\text{-}2000\text{ mV s}^{-1}$) as commonly observed for iridium(III) isocyanide complexes.^{5,10,11} Electrochemical data are reported in Table 2.

Table 2: Electrochemical data of **2-4** determined by OSWV in room-temperature acetonitrile solution + 0.1 M TBAPF₆. Ferrocene is used as internal reference

Complex	Electrochemical data ^a [V]		
	E_{ox}	E_{red}	$\Delta E_{\text{redox}}^b$
[Ir(ppy)₂(bpy)]⁺	+0.84 ^c	-1.77, ^c -2.60 ^c	2.61
2	+1.23	-2.29, -2.53	3.52
3	+1.60	-2.18, -2.42	4.02
4	+1.30	-1.42, -1.73	2.72

^a All redox processes were irreversible. Estimated errors: ± 50 mV. ^b $\Delta E_{\text{redox}} = E_{\text{ox}} - E_{\text{red}}$. ^c Data from literature.³

The oxidation process involves the Ir-phenyl moiety of the cyclometalating ligands. Complex **2** presents an oxidation potential of +1.23 V, 0.37 V lower than the one observed for **3** (+1.60 V), due to the presence of the electron-withdrawing fluorines in the dfppy ligands. The halogen substituents also induce a small

stabilisation of the LUMO, that results in slightly less negative reduction potentials for complex **3** with respect to **2** (0.11 V). The overall effect is an increase in the redox gap of around 0.50 V, passing from **2** (3.25 V) to **3** (4.02 V). A different trend is observed for complex **4**. The oxidation potential (1.30 V) is comparable to that of **2** (+1.23 V), while the reduction potential shifts positively by approximately +0.80 V, giving a redox gap of only 2.72 V. This reduced electrochemical gap should be predominantly ascribed to LUMO stabilisation due to the presence of the π -extended quinoxaline moiety on its cyclometalating ligands. This experimental evidence suggests that the reduction processes always involve the pyridyl (or quinoxaline) moiety of the cyclometalating ligands and not the chelating diisocyanide moiety, as also indicated by DFT calculations (*vide infra*).

7.1.4 Ground-state theoretical calculations

The molecular structures and the electronic properties of complexes **2-4** were investigated by density functional theory (DFT) calculations and compared to X-ray crystallographic structures (for **3**). The M06 hybrid meta exchange-correlation functional^{12,13} was used in combination with the 6-31G(d,p) basis set for all the atoms,¹⁴ except in the case of the Ir(III) metal centre where the LANL2DZ pseudopotential and the related basis-set was selected.¹⁵ The quality of the theoretically optimized geometries was evaluated by comparison with the available X-ray crystal structure of **3**, which can be reasonably utilized also as model for **2** and **4**. In Figure 4 the structural overlap between the X-ray crystal structure of **3** and the theoretically computed one is reported. No substantial differences are observed between the two geometries. This finding proves the effectiveness of the selected computational model and indicates that strong intermolecular interactions are not present in the crystal.

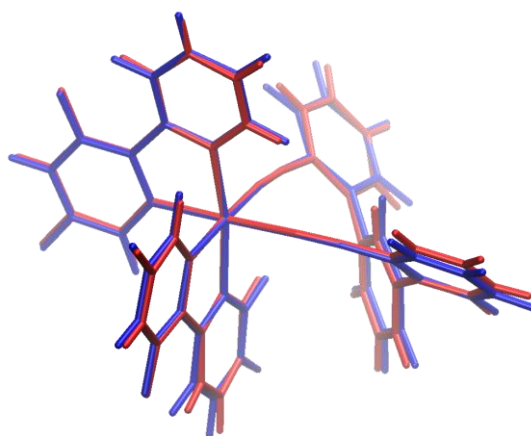


Figure 4: Structural overlay between the experimental X-ray structure (reported in red) of the cationic part of complex **3** and the theoretically computed one (in blue). The structural overlay is calculated by minimizing the root-mean-square deviation (RMSD) of all the atomic positions, except hydrogen atoms: RMSD = 0.127 Å

The frontier molecular orbitals of **2-4** are reported in Figure 5. The HOMO orbital is localized on the Ir(III) metal centre and on both the phenyl moiety of the two cyclometalating C^N ligands, while the LUMO and the LUMO+1 are mainly located on the nitrogen-containing ring of each cyclometalating ligand. The chelating diisocyanide ligand **1** exhibits relatively inaccessible π^* orbitals. Consequently, the lowest unoccupied molecular orbitals centred on this ancillary ligand are the LUMO+2 and LUMO+3 for all of the three complexes.

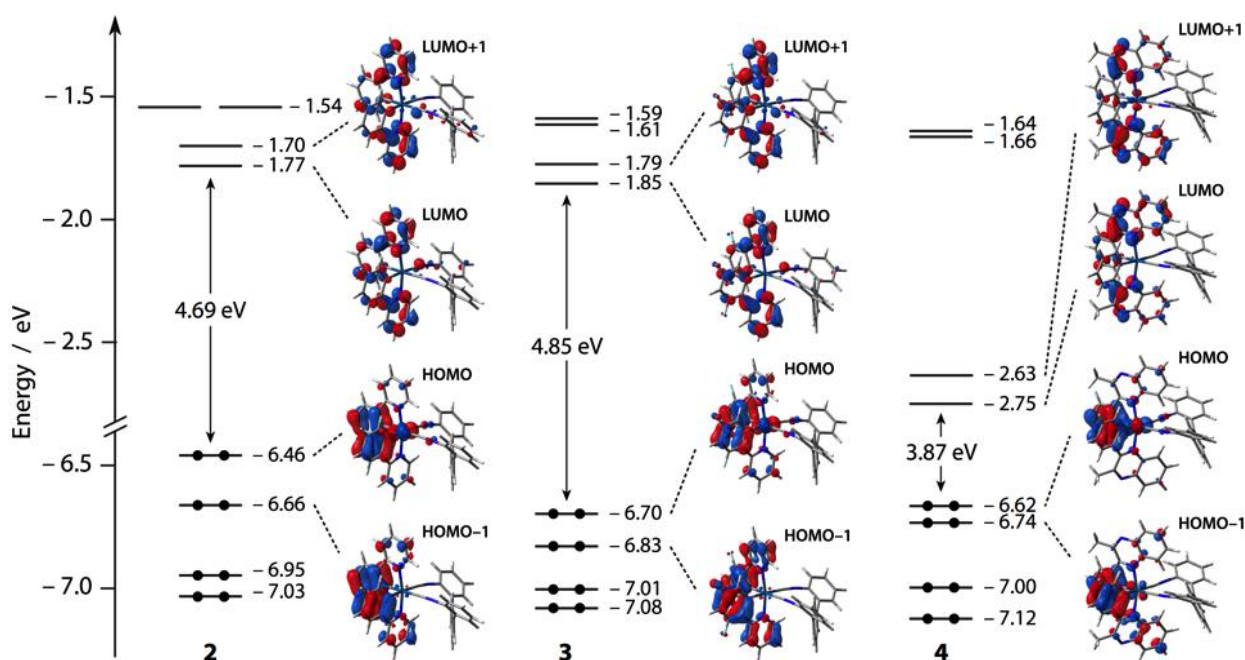


Figure 5: Energy diagram showing the frontier Kohn-Sham molecular orbitals of complexes **2-4** in acetonitrile calculated at the PCM-M06/6-31G(d,p)&LANL2DZ(Ir) level of theory

The presence of a strong-field ligand such as **1** induces a remarkable stabilisation of the HOMO in **2-4** if compared to $[\text{Ir}(\text{ppy})_2(\text{bpy})]^+$ complex. This stabilisation is maximized in the case of **3** (-0.84 eV) due to the fluorine substituents on the dfppy cyclometalating ligands. On the other hand a pronounced LUMO (and LUMO+1) stabilisation is observed in complex **4** (-0.47 eV), due to the π -extended quinoxaline moiety on the cyclometalating ligands. All the calculated energy levels are reported in Table 3.

Table 3: HOMO and LUMO energy levels calculated by DFT

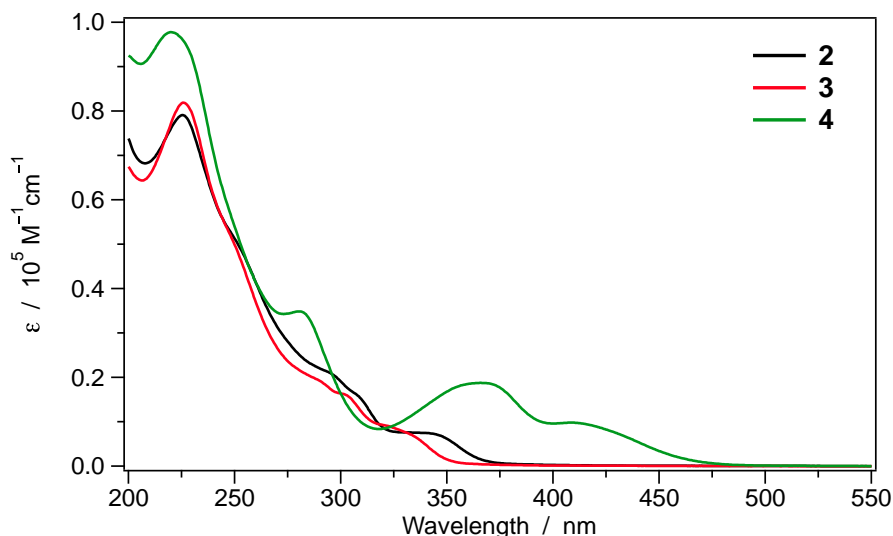
Complex	DFT calculated energy ^a [eV]		
	E_{HOMO}	E_{LUMO}	ΔE_{DFT}^b
[Ir(ppy)₂(bpy)]⁺	-5.86	-2.28	3.58
2	-6.46	-1.77	4.69
3	-6.70	-1.85	4.85
4	-6.62	-2.75	3.87

^a DFT calculations were carried out at the M06/6-31G(d,p)&LANL2DZ(Ir) level of theory in acetonitrile, using PCM. ^b $\Delta E_{\text{DFT}} = E_{\text{LUMO}} - E_{\text{HOMO}}$.

Theoretical calculations predict that the HOMO-LUMO energy gap increases along the series [Ir(ppy)₂(bpy)]⁺ (3.58 eV) < **4** (3.87 eV) < **2** (4.69 eV) < **3** (4.85 eV). This trend is in full agreement with the electrochemical gaps obtained from OSWV measurements (Table 2).

7.1.5 Photophysical properties and excited-state characterization

All the complexes are stable in acetonitrile solution for several months and do not show degradation under standard laboratory conditions. The room-temperature electronic absorption spectra of **2-4** are reported in Figure 6.

**Figure 6:** Absorption spectra of **2-4** in acetonitrile solution at 298 K

The spectral window between 200 and 300 nm shows intense absorption bands ($\epsilon \approx 2\text{-}10 \cdot 10^4 \text{ M}^{-1} \text{ cm}^{-1}$) that are assigned to spin-allowed ligand-centred (LC) $\pi\text{-}\pi^*$ transitions involving both the cyclometalating

and the ancillary ligand **1**. The weaker bands at longer wavelength could also display a contribution from the iridium *d* orbitals and arise from transitions of both singlet and triplet spin multiplicity, due to the high spin-orbit coupling constant of the iridium metal centre. For complex **2**, the lowest-energy band in the 325-375 nm region is attributed to an almost pure HOMO→LUMO transition and is consequently LC in nature with a small metal-to-ligand charge-transfer (MLCT) contribution. The shoulder centred at 300 nm is actually composed by four electronic transitions. The first two excitations can be described as HOMO-1 to LUMO and LUMO+1 excitations, so they are basically LC in nature and involve the cyclometalating ligands. On the other hand, the last couple of excitations concern transitions from the HOMO to the LUMO+2 and LUMO+3 (the lowest-laying π^* orbitals of ligand **1**) and they are consequently MLCT in nature with a remarkable ligand-to-ligand charge-transfer (LL'CT) character.

In the case of **3**, a remarkable blue shift of approximately 20 nm is observed for the lowest-energy absorption bands due to the presence of the fluorine substituents on the cyclometalating ligands that strongly stabilize the HOMO with respect to complex **2**.

The absorption spectrum of complex **4** extends up to 475 nm due to the presence of the phenyl-quinoxaline cyclometalating ligands. The lowest-energy broad absorption band between 380 and 450 nm involves electronic excitations from the HOMO-1 and HOMO to the LUMO and LUMO+1, so they present a mixed MLCT/LC character. The second absorption band in the 325-400 nm range can be describe as almost pure LC transitions involving the promotion of one electron from the phenyl moiety of the cyclometalating ligands to their quinoxaline subunit, with virtually no contribution of the iridium *d* orbitals.

The emission spectra of **2-4** are reported in Figure 7 both in acetonitrile solution at 298 K (full lines) and at 77 K (dashed lines), while in Table 4 are summarized the luminescence properties and photophysical parameters of all the complexes, including solid-state PMMA matrix.

Table 4: Luminescence properties and photophysical parameters of **2-4**

	Oxygen-free CH ₃ CN solution, 298 K					Rigid matrix CH ₃ CN, 77 K		1% PMMA matrix, 298 K				
	λ_{em}^a [nm]	Φ_{em}^b [%]	τ^c [μ s]	k_r^d [$10^3 s^{-1}$]	k_{nr}^e [$10^4 s^{-1}$]	λ_{em}^a [nm]	τ^c [μ s]	λ_{em} [nm]	Φ_{em}^f [%]	τ^c [μ s]	k_r^d [$10^3 s^{-1}$]	k_{nr}^e [$10^4 s^{-1}$]
2	452, 483	24	27.5	8.86	2.75	465, 485, 498	6.3 (62%) 40.1 (38%)	453, 484	68	36.4	18.6	0.89
3	438, 468	37	45.0	8.27	1.40	446, 469, 477	46.5 (33%) 57.3 (67%)	440, 469	79	59.7	13.1	0.36
4	630	25	16.4	15.0	4.60	596, 633	12.7 (60%) 29.9 (40%)	618	19	19.9	9.75	4.05

^a $\lambda_{exc} = 325$ nm; ^b $\lambda_{exc} = 325$ nm, quinine sulfate in 1 N H₂SO₄ aqueous solution as reference; ^c $\lambda_{exc} = 370$ nm; ^d $k_r = \Phi/\tau$; ^e $k_{nr} = \Phi/\tau$; ^f determined using an integrating sphere.

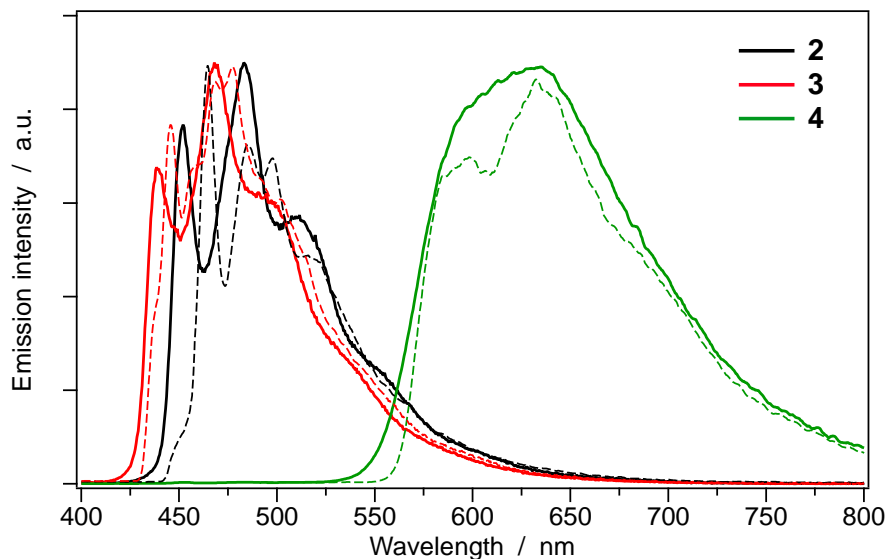


Figure 7: Normalized emission spectra of **2-4** in acetonitrile solution at 298 K (full lines) and at 77 K (dashed lines). Excitation wavelength: 325 nm

The room-temperature luminescence spectra of complexes **2** and **3** display a strongly pronounced vibronic structure, indicating the LC character of the emitting state, that is not present in the case of **4**, where the spectrum is broad and unstructured, with no vibronic progression. A blue shift is observed in the case of **3** ($\lambda_{\text{max}} = 438$ nm), if compared to **2** ($\lambda_{\text{max}} = 452$ nm). On the contrary, an orange emission is recorded for complex **4** ($\lambda_{\text{max}} = 630$ nm). Also in this case the emission arises from a LC triplet state centred on the 2-phenylquinoxaline cyclometalating ligands, with minimal admixture of metal-to-ligand charge-transfer character. This assumption is corroborated by the absence of any spectral shift in the emission profile of **4** when going from room temperature to 77 K, where the only observed difference is a better spectral resolution. At low temperature, also **2** and **3** again exhibit very similar behaviour.

These experimental data are in excellent agreement with the spin-unrestricted DFT calculations carried out by fully optimizing the lowest triplet state (T_1) of **2-4**. After relaxation, the T_1 state of all the complexes preserves its ligand-centred character, as revealed by the spin-density distribution shown in Figure 8.

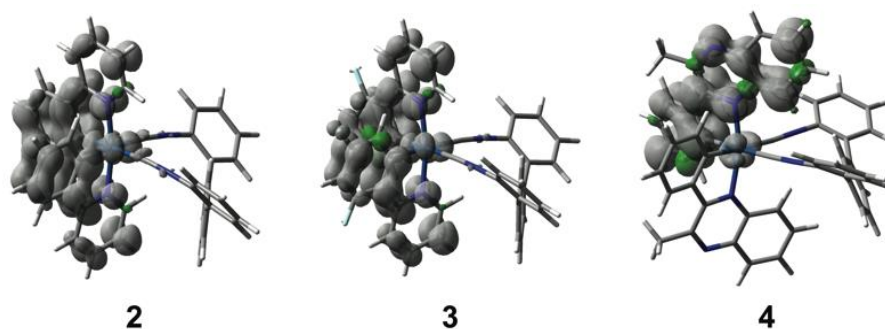


Figure 8: Spin-density distributions calculated for the fully relaxed lowest triplet state (T_1) of complexes **2-4** in acetonitrile at the PCM-UM06/6-31G(d,p)&LANL2DZ(Ir) level of theory

For all the complexes, the spin-density distribution confirms that the excited state is centred on the cyclometalating ligand only, without involving the chelating diisocyanide moiety **1**. The calculated emission energies are 3.00 eV (413 nm), 3.26 eV (380 nm) and 1.79 eV (692 nm) for **2**, **3** and **4**, respectively. These values correlate well with the experimental ones (Table 4).

The photoluminescence quantum yields (PLQYs) in room-temperature acetonitrile solution of **2-4** are around 30%. The bis-fluorinated complex **3** is the strongest emitter with a PLQY of 37% (Table 4), followed by complex **4** with a PLQY of 25% and complex **2** with 24%. These values are lower if compared to other iridium(III) complexes having monodentate isocyanides as ancillary ligands. Lower values can be tentatively ascribed to the nature of the ligand **1**: as shown above, the triphenyl moiety of **1** can ‘floppy’ between two different positions, promoting non radiative deactivation pathways, that are absent in rigid monodentate isocyanide ligands.

In Figure 9 are reported the room-temperature emission spectra of **2-4** in the solid state, dispersed in a poly(methyl methacrylate) (PMMA) matrix at a concentration of 1% by weight.

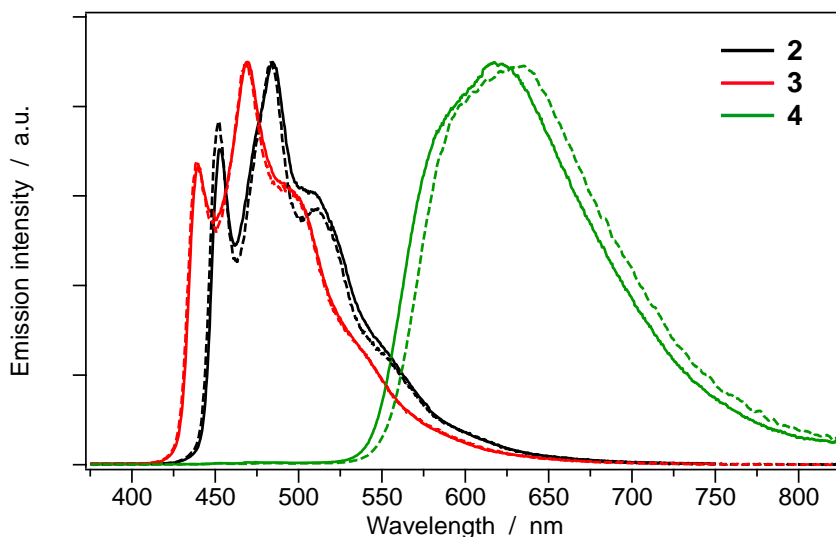


Figure 9: Normalized emission spectra of **2-4** in PMMA matrix 1% w./w. at 298 K (full lines). The emission spectra in RT acetonitrile solution are also reported (dashed lines) for comparison

The external environment does not affect the emission profiles and this confirms the ^3LC emitting state nature of the complexes. For **4**, PLQY and lifetime values in solid state are comparable with those observed in room-temperature acetonitrile, whereas the emission quantum yields of **2** and **3** in PMMA display approximately a two-fold increase, leading to 78.5% yield for complex **3** (Table 4). For both **2** and **3**, a three-fold decrease is observed in the non-radiative deactivation rate constant (k_{nr}) combined by a twice as fast

radiative decay rate (k_r), with respect to the solution. These findings can be rationalized in the PMMA solid matrix, where the rigidity of the ligand **1** may sensibly increase.

7.2 Conclusions

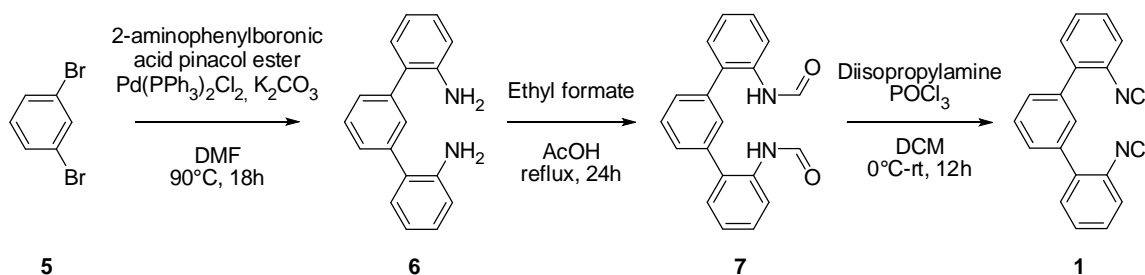
Complexes **2-4** are the first examples of stable Ir(III) cationic complexes bearing a chelating isocyanide as ancillary ligand.

HOMO and LUMO orbitals (as well as HOMO-1 and LUMO+1) of **2-4** only involve the cyclometalating ligands and the iridium *d* orbitals. Therefore, **1** has a key structural role but does not affect the energy and nature of the lowest electronic excited states of the complexes. This combination of structural and electronic properties enables tuning of the emission colour of **2-4** by simple modification of the C^N ligands, going from blue to orange upon extension of π -conjugation from phenylpyridine to phenylquinoxaline. Notably, PLQY of these complexes goes from moderate to very high (\approx 20-80%). This makes them very interesting candidates for optoelectronic applications.

7.3 Experimental section

General synthetic procedures

Analytical grade solvents and commercially available reagents were used as received, unless otherwise stated. Chromatographic purifications were performed using 70-230 mesh silica. Solvents were dried and distilled according to standard procedures and stored under nitrogen. ¹H, ¹³C, ¹⁹F NMR spectra were recorded on a Varian Inova 300 MHz, on a Mercury 400 MHz or on an Inova 600 MHz spectrometer. Chemical shifts (δ) are reported in ppm relative to residual solvent signals for ¹H and ¹³C NMR (¹H NMR: 7.26 ppm for CDCl₃; ¹³C NMR: 77.0 ppm for CDCl₃). ¹³C NMR spectra were acquired with ¹H broadband decoupling mode. Mass spectra were recorded on a micromass LCT spectrometer using electrospray (ES) ionisation techniques.

Synthesis of the ligand (1)**(1,1':3',1''-terphenyl)-2,2''-diamine (6)**

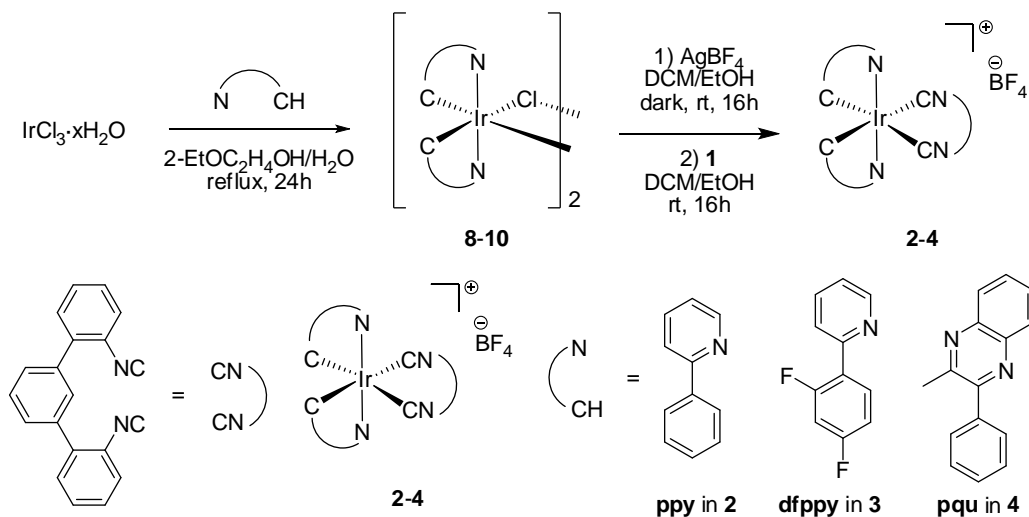
1,3-Dibromobenzene (**5**) (120.0 mg, 0.49 mmol) and 2-aminophenylboronic acid pinacol ester (440.0 mg, 2.0 mmol) were dissolved in dimethylformamide (8 mL). The resulting solution was degassed with nitrogen for 10 minutes. Then K_2CO_3 (2M in water, 2.5 mL, 5.0 mmol) was added, and the solution was degassed for additional 30 minutes. $Pd(PPh_3)_2Cl_2$ (18.0 mg, 0.05 mmol) was then added and the mixture was heated under nitrogen atmosphere at 90°C for 18 hours. After this time, water (30 mL) was added and the resulting mixture was extracted with ethyl acetate (4 x 15 mL). The collected organic phase was washed with water (30 mL) and brine (30 mL), dried over Na_2SO_4 and concentrated. The crude was purified on silica gel flash chromatography using a mixture of *n*-hexane/ethyl acetate (8:2) to give product **6** in 85% yield (108 mg).¹⁶ 1H NMR ($CDCl_3$, 300 MHz) δ 7.58-7.42 (m, 4H), 7.18-7.13 (m, 4H), 6.83 (td, $J_{HH} = 7.4$ Hz, $J_{HH} = 1.2$ Hz, 2H), 6.78 (dd, $J_{HH} = 8.3$ Hz, $J_{HH} = 1.2$ Hz, 2H), 3.81 (bs, 4H).

2,2''-diisocyano-1,1':3',1''-terphenyl (1)

[1,1':3',1''-terphenyl]-2,2''-diamine (**2**) (130.0 mg, 0.5 mmol) was dissolved in ethyl formate (921 μ L, 12.5 mmol) and acetic acid (56 μ L, 1.0 mmol) was added. The resulting solution was refluxed for 24 hours. The solvent was then evaporated. Water (30 mL) was added and the mixture was extracted with ethyl acetate (4 x 15 mL). The collected organic phase was washed with water (30 mL) and brine (30 mL), dried over Na_2SO_4 and concentrated to give product **7** (147 mg). The crude was used in the next step without purification. It was dissolved in dry dichloromethane (5 mL) and the solution was cooled at 0°C. Diisopropylamine (981 μ L, 7.0 mmol) was added and the resulting mixture was stirred at 0°C for 15 min. Phosphorous oxychloride (137 μ L, 1.5 mmol) in 5 mL of dry dichloromethane was added dropwise over a period of 10 min. The resulting mixture was stirred from 0°C to room temperature for 12 hours. After this time, the reaction was quenched with saturated Na_2CO_3 aqueous solution at 0°C and the product was extracted with dichloromethane. The organic phase was washed with aqueous NH_4Cl , then dried over anhydrous Na_2SO_4 and the solvent evaporated. The residue was purified by silica gel flash chromatography using a mixture of dichloromethane/methanol (99:1) to give product **1** in 50% yield (70 mg). 1H NMR ($CDCl_3$, 300 MHz) δ 7.65 (bs, 1H), 7.61 (bs, 3H), 7.56-7.45 (m, 6H), 7.43-7.36 (m, 2H). ^{13}C NMR ($CDCl_3$, 75 MHz) δ

169.0 (C), 166.8 (C), 138.3 (C), 137.3 (C), 130.7 (CH), 129.8 (CH), 129.7 (CH), 129.0 (CH), 128.9 (CH), 128.4 (CH), 127.9 (CH). ESI-MS: 281 [M+H]⁺.

Synthesis of the Ir(III) complexes



General procedure

In a 10 ml flask, the desired Ir(III)-dimer (0.025 mmol) (**8-10**) was dissolved in dichloromethane (2 ml) and ethanol (2 drops). AgBF₄ (0.05 mmol, 9.8 mg) was added and the solution was stirred for 24 hours in absence of light. Then the formed solid was filtered off and the solution was slowly added to a solution of ligand **4** in dichloromethane (0.05 mmol, 14.5 mg in 13 ml). The resulting mixture was stirred for additional 24 hours. After this time, solvent was evaporated and the crude was purified by flash chromatography on Al₂O₃ using a mixture of dichloromethane/methanol (95:5) to give the expected product.

Complex **2**: 25.3 mg, yield = 58%. ¹H NMR (CDCl₃, 600 MHz, T= -10°C) δ 9.36 (d, *J*_{HH} = 6 Hz, 1H), 8.12 (t, *J*_{HH} = 8.4 Hz, 1H), 8.05 (d, *J*_{HH} = 8.4 Hz, 1H), 7.94-7.90 (m, 2H), 7.88-7.83 (m, 3H), 7.68 (t, *J*_{HH} = 6.6 Hz, 2H), 7.65-7.60 (m, 2H), 7.56-7.51 (m, 2H), 7.48-7.41 (m, 3H), 7.38 (t, *J*_{HH} = 7.8 Hz, 1H), 7.34-7.29 (m, 3H), 6.96 (q, *J*_{HH} = 7.8 Hz, 2H), 6.93 (t, *J*_{HH} = 7.8 Hz, 1H), 6.88 (t, *J*_{HH} = 7.8 Hz, 1H), 6.81 (t, *J*_{HH} = 7.8 Hz, 1H), 6.14 (d, *J*_{HH} = 7.8 Hz, 1H), 5.99 (d, *J*_{HH} = 7.8 Hz, 1H). ¹³C NMR (CDCl₃, 150 MHz, T= -10°C) δ 167.0 (C), 166.7 (C), 154.5 (CH), 153.1 (C), 152.0 (C), 151.4 (CH), 143.8 (C), 143.3 (C), 140.3 (C), 139.9 (C), 139.3 (CH), 138.8 (CH), 137.6 (C), 137.0 (C), 132.9 (C), 131.7 (C), 131.1 (CH), 131.0 (CH), 130.9 (CH), 130.8 (CH), 130.7 (CH), 130.6 (CH), 130.4 (CH), 130.3 (CH), 130.2 (CH), 129.7 (CH), 129.3 (CH), 129.2 (CH), 128.9 (CH), 128.8 (CH), 127.2 (CH), 126.4 (CH), 125.2 (CH), 124.6 (CH), 124.5 (CH), 124.1 (C), 123.9 (C), 123.8 (CH), 123.7 (CH), 123.6 (CH), 120.6 (CH), 120.5 (CH). ESI-MS: 781 (M-BF₄)⁺.

Complex **3**: 28.2 mg, yield = 60%. ^1H NMR (CDCl_3 , 600 MHz, $T = +25^\circ\text{C}$) δ 9.55 (d, $J_{\text{HH}} = 6.0$ Hz, 1H), 8.37 (d, $J_{\text{HH}} = 8.8$ Hz, 1H), 8.24 (d, $J_{\text{HH}} = 7.6$ Hz, 1H), 8.08 (t, $J_{\text{HH}} = 8.0$ Hz, 1H), 8.06 (t, $J_{\text{HH}} = 1.6$ Hz, 1H), 7.90 (t, $J_{\text{HH}} = 7.6$ Hz, 1H), 7.85 (d, $J_{\text{HH}} = 6.0$ Hz, 1H), 7.81 (t, $J_{\text{HH}} = 7.6$ Hz, 1H), 7.73 (d, $J_{\text{HH}} = 7.6$ Hz, 1H), 7.70 (t, $J_{\text{HH}} = 6.8$ Hz, 1H), 7.65 (d, $J_{\text{HH}} = 8.0$ Hz, 1H), 7.54 (t, $J_{\text{HH}} = 7.6$ Hz, 1H), 7.49-7.42 (m, 3H), 7.40 (t, $J_{\text{HH}} = 8.0$ Hz, 1H), 7.36 (d, $J_{\text{HH}} = 8.0$ Hz, 1H), 7.32 (d, $J_{\text{HH}} = 7.6$ Hz, 1H), 7.29 (d, $J_{\text{HH}} = 7.6$ Hz, 1H), 6.94 (t, $J_{\text{HH}} = 6.8$ Hz, 1H), 6.50-6.42 (m, 2H), 5.59 (dd, $J_{\text{HH}} = 1.8$ Hz, $J_{\text{HH}} = 8.0$ Hz, 1H), 5.42 (dd, $J_{\text{HH}} = 1.8$ Hz, $J_{\text{HH}} = 8.0$ Hz, 1H). ^{13}C NMR (CDCl_3 , 150 MHz, $T = +25^\circ\text{C}$) δ 164.2 (C, d, $J_{\text{CF}} = 6.1$ Hz), 163.7 (C, dd, $J_{\text{CF}} = 257.2$ Hz, $J_{\text{CF}} = 12.1$ Hz), 163.1 (C, d, $J_{\text{CF}} = 7.2$ Hz), 163.4 (C, dd, $J_{\text{CF}} = 257.3$ Hz, $J_{\text{CF}} = 10.8$ Hz), 161.4 (C, dd, $J_{\text{CF}} = 261.0$ Hz, $J_{\text{CF}} = 11.5$ Hz), 161.3 (C, dd, $J_{\text{CF}} = 261.0$ Hz, $J_{\text{CF}} = 11.5$ Hz), 157.0 (C, d, $J_{\text{CF}} = 6.0$ Hz), 156.2 (CH), 155.4 (C, d, $J_{\text{CF}} = 6.0$ Hz), 151.9 (CH), 140.7 (C), 140.1 (C), 140.0 (CH), 139.4 (CH), 138.0 (C), 137.3 (C), 131.3 (C), 131.22 (CH), 131.18 (CH), 130.96 (CH), 130.88 (CH), 130.7 (CH), 130.1 (CH), 129.8 (CH), 129.5 (C), 129.3 (CH), 129.1 (CH), 129.0 (CH), 128.1 (C), 127.9 (CH), 127.4 (C), 126.8 (CH), 126.0 (CH), 124.3 (CH, d, $J = 21$ Hz), 124.1 (CH, d, $J = 21$ Hz), 123.9 (CH), 113.0 (CH, dd, $J_{\text{CF}} = 32.8$ Hz, $J_{\text{CF}} = 18.3$ Hz), 100.4 (CH, t, $J_{\text{CF}} = 26.5$ Hz). ^{19}F NMR (CDCl_3 , 300 MHz, $T = +25^\circ\text{C}$) δ -153.0 (s, 4F), -108.2 (m, 2F), -105.9 (m, 1F), -104.6 (m, 1F). ESI-MS: 853 (M-BF₄)⁺.

Complex **4**: 28.5 mg, yield = 57%. ^1H NMR (CDCl_3 , 600 MHz, $T = -10^\circ\text{C}$) δ 8.67 (d, $J_{\text{HH}} = 9.0$ Hz, 1H), 8.24 (d, $J_{\text{HH}} = 8.4$ Hz, 1H), 8.19 (d, $J_{\text{HH}} = 8.4$ Hz, 1H), 8.09 (d, $J_{\text{HH}} = 8.4$ Hz, 1H), 8.04 (d, $J_{\text{HH}} = 8.4$ Hz, 1H), 7.91 (t, $J_{\text{HH}} = 7.8$ Hz, 1H), 7.82 (t, $J_{\text{HH}} = 7.8$ Hz, 1H), 7.80-7.76 (m, 1H), 7.71 (t, $J_{\text{HH}} = 7.8$ Hz, 1H), 7.63-7.57 (m, 3H), 7.54-7.50 (m, 2H), 7.46-7.41 (m, 3H), 7.30-7.24 (m, 2H), 7.17 (t, $J_{\text{HH}} = 7.8$ Hz, 2H), 7.13 (d, $J_{\text{HH}} = 7.8$ Hz, 2H), 6.98 (t, $J_{\text{HH}} = 7.8$ Hz, 1H), 6.90 (t, $J_{\text{HH}} = 7.8$ Hz, 1H), 6.08 (d, $J_{\text{HH}} = 7.2$ Hz, 1H), 5.87 (d, $J_{\text{HH}} = 7.2$ Hz, 1H), 3.35 (s, 3H), 3.19 (s, 3H). ^{13}C NMR (CDCl_3 , 150 MHz, $T = -10^\circ\text{C}$) δ 165.9 (C), 165.4 (C), 155.8 (C), 155.4 (C), 153.1 (C), 152.6 (C), 144.9 (C), 140.6 (C), 140.3 (C), 140.2 (C), 140.1 (C), 139.4 (C), 139.2 (C), 139.7 (C), 136.6 (C), 131.9 (CH), 131.8 (CH), 131.7 (CH), 131.6 (CH), 131.6 (CH), 131.3 (C), 131.3 (CH), 131.2 (CH), 131.1 (C), 131.0 (CH), 130.6 (C), 130.5 (CH), 130.4 (CH), 130.2 (CH), 130.1 (CH), 130.0 (CH), 129.4 (CH), 129.3 (CH), 128.0 (CH), 127.2 (CH), 127.1 (CH), 126.7 (CH), 124.3 (CH), 124.2 (CH), 123.1 (C), 123.0 (C), 27.6 (CH₃). ESI-MS: 911 (M-BF₄)⁺.

Electrochemistry

Voltammetric experiments were performed using a Metrohm AutoLab PGSTAT 302 electrochemical workstation in combination with the NOVA software package. All the measurements were carried out at room temperature in acetonitrile solutions with a sample concentration approx. 1 mM and using 0.1 M tetrabutylammonium hexafluorophosphate (electrochemical grade, TBAPF₆) as supporting electrolyte. Oxygen was removed from the solutions by bubbling argon for 20 minutes. All the experiments were carried out using a three-electrode setup (BioLogic SVC-2 cell, volume range: 5-20 ml) with a platinum disk (1.6 mm diameter) as working electrode, the Ag/AgNO₃ redox couple (0.01 M in acetonitrile with 0.1 M

TBAClO₄ supporting electrolyte) as reference electrode and a platinum wire as counter electrode. At the end of each measurement, ferrocene was added as internal reference. Cyclic voltammograms (CV) were recorded at a scan rate of 100 mV/s (up to 2000 mV/s to check reversibility), while Osteryoung square-wave voltammograms (OSWV) with scan rate of 25 mV/s, a SW amplitude of ± 20 mV and a frequency of 25 Hz.

Computational details

Density functional theory (DFT) calculations¹⁷ were carried out using the D.01 revision of the Gaussian 09 program package¹⁸ in combination with the M06 hybrid meta exchange-correlation functional.^{12,13} The 6-31G(d,p) basis set was selected for C, H, N and F atoms;¹⁴ on the other hand, the “double- ζ ” quality LANL2DZ basis set and the related pseudopotential was adopted for the Ir metal centre.¹⁵ All the complexes were fully optimised, without symmetry constraints, in acetonitrile both in the electronic ground state (S_0) and in the lowest triplet state (T_1) by using the polarisable continuum model (PCM) applying the integral equation formalism model (IEFPCM).^{19,20,21} A frequency calculation was always used to confirm that the stationary point found by the geometry optimisation was actually corresponding to a minimum on the potential energy surface (no imaginary frequencies). Time-dependent DFT calculations (TD-DFT), at the same level of theory used for the geometrical optimisations, were employed to simulate the absorption spectra of all the complexes in their optimized S_0 geometry.^{22,23,24} The first 100 singlet and 25 triplet vertical excitations were computed for the complexes using the non-equilibrium, linear response formalism. To investigate the nature of the T_1 state, geometry optimisations and related frequency calculations were performed at the spin-unrestricted UM06 level of theory, imposing a spin multiplicity of 3. The emission energy from the lowest triplet excited state was estimated by subtracting the SCF energy of the T_1 state in its minimum conformation from that of the singlet ground state having the same geometry of T_1 . All the pictures of molecular orbitals and spin-density surfaces were created using GaussView 5.²⁵ The structural overlap of the X-ray crystal structure of **3** and the theoretically computed one is obtained using the VMD program by minimising the root-mean-square deviation (RMSD) of all the atomic positions, except hydrogen.²⁶

Photophysical measurements

The spectroscopic investigations were carried out in spectrofluorimetric grade acetonitrile. The absorption spectra were recorded with a Perkin-Elmer Lambda 950 spectrophotometer. For the photoluminescence experiments, the sample solutions were placed in fluorimetric Suprasil quartz cuvettes (1 cm) and dissolved oxygen was removed by bubbling argon for 20 minutes. The uncorrected emission spectra were obtained

with an Edinburgh Instruments FLS920 spectrometer equipped with a Peltier-cooled Hamamatsu R928 photomultiplier tube (PMT) (185-850 nm). An Edinburgh Xe 900 (450 W xenon arc lamp) was used as the excitation light source. The corrected spectra were obtained via a calibration curve supplied with the instrument. The photoluminescence quantum yields (Φ_{PL}) in solution were obtained from the corrected spectra on a wavelength scale (nm) and measured according to the approach described by Demas and Crosby²⁷ using an air-equilibrated water solution of quinine sulfate in 1N H₂SO₄ as reference ($\Phi_{\text{PL}} = 0.546$).²⁸ The emission lifetimes (τ) in the microsecond time range were measured through the time-correlated single photon counting (TCSPC) technique using an HORIBA Jobin Yvon IBH FluoroHub controlling a spectrometer equipped with a pulsed SpectraLED ($\lambda_{\text{exc}} = 370$ nm; FWHM = 11 nm) as excitation source and a red-sensitive Hamamatsu R-3237-01 PMT (185-850 nm) as detector. The analysis of the luminescence decay profiles was accomplished with the DAS6 Decay Analysis Software provided by the manufacturer, and the quality of the fit was assessed with the χ^2 value close to unity and with the residuals regularly distributed along the time axis. To record the 77 K luminescence spectra, samples were put in quartz tubes (2 mm inner diameter) and inserted into a special quartz Dewar flask filled with liquid nitrogen. Solid samples were prepared by drop casting using a dichloromethane solution containing the poly(methyl methacrylate) (PMMA) matrix with 1% wt. of the complex; the thickness of the films was not controlled. Solid-state Φ_{PL} values were calculated by corrected emission spectra obtained from an Edinburgh FLS920 spectrometer equipped with a barium sulfate-coated integrating sphere (diameter of 4 in.) following the procedure described by Würth *et al.*²⁹ Experimental uncertainties are estimated to be $\pm 8\%$ for τ determinations, $\pm 20\%$ for Φ_{PL} , ± 2 nm and ± 5 nm for absorption and emission peaks, respectively.

7.4 Bibliography

- ¹ R. C. Evans, P. Douglas, C. J. Winscom, *Coord. Chem. Rev.* **2006**, *250*, 2093.
- ² L. Flamigni, A. Barbieri, C. Sabatini, B. Ventura, F. Barigelletti, *Top. Curr. Chem.* **2007**, *281*, 143.
- ³ R. D. Costa, E. Orti, H. J. Bolink, F. Monti, G. Accorsi, N. Armaroli, *Angew. Chem. Int. Ed.* **2012**, *51*, 8178.
- ⁴ T. Hu, L. He, L. Duan, Y. Qiu, *J. Mater. Chem.* **2012**, *22*, 4206.
- ⁵ N. M. Shavaleev, F. Monti, R. D. Costa, R. Scopelliti, H. J. Bolink, E. Orti, G. Accorsi, N. Armaroli, E. Baranoff, M. Gratzel, M. K. Nazeeruddin, *Inorg. Chem.* **2012**, *51*, 2263.
- ⁶ J. Li, P. I. Djurovich, B. D. Alleyne, M. Yousufuddin, N. N. Ho, J. C. Thomas, J. C. Peters, R. Bau, M. E. Thompson, *Inorg. Chem.* **2005**, *44*, 1713.
- ⁷ M. Nonoyama, *Bull. Chem. Soc. Jpn.* **1974**, *47*, 767.
- ⁸ S. Sprouse, K. A. King, P. J. Spellane, R. J. Watts, *J. Am. Chem. Soc.* **1984**, *106*, 6647.
- ⁹ B. Schmid, F. O. Garces, R. J. Watts, *Inorg. Chem.* **1994**, *33*, 9.

- ¹⁰ N. M. Shavaleev, F. Monti, R. Scopelliti, N. Armaroli, M. Gratzel, M. K. Nazeeruddin, *Organometallics* **2012**, *31*, 6288.
- ¹¹ N. M. Shavaleev, F. Monti, R. Scopelliti, A. Baschieri, L. Sambri, N. Armaroli, M. Gratzel, M. K. Nazeeruddin, *Organometallics* **2013**, *32*, 460.
- ¹² Y. Zhao, D. G. Truhlar, *Theor. Chem. Acc.* **2008**, *120*, 215.
- ¹³ Y. Zhao, D. G. Truhlar, *Acc. Chem. Res.* **2008**, *41*, 157.
- ¹⁴ M. M. Francl, W. J. Pietro, W. J. Hehre, J. S. Binkley, M. S. Gordon, D. J. Defrees, J. A. Pople, *J. Chem. Phys.* **1982**, *77*, 3654.
- ¹⁵ P. J. Hay, W. R. Wadt, *J. Chem. Phys.* **1985**, *82*, 299.
- ¹⁶ C. Poriel, R. Metivier, J. Rault-Berthelot, D. Thirion, F. Barriere, O. Jeannin, *Chem. Commun.* **2011**, *47*, 11703.
- ¹⁷ R. G. Parr and W. Yang, *Density Functional Theory of Atoms and Molecules*, Oxford University Press, Oxford, U.K., 1989.
- ¹⁸ M. J. Frisch, G. W. Trucks, H. B. Schlegel, G. E. Scuseria, M. A. Robb, J. R. Cheeseman, G. Scalmani, V. Barone, B. Mennucci, G. A. Petersson, H. Nakatsuji, M. Caricato, X. Li, H. P. Hratchian, A. F. Izmaylov, J. Bloino, G. Zheng, J. L. Sonnenberg, M. Hada, M. Ehara, K. Toyota, R. Fukuda, J. Hasegawa, M. Ishida, T. Nakajima, Y. Honda, O. Kitao, H. Nakai, T. Vreven, J. A. Montgomery Jr., J. E. Peralta, F. Ogliaro, M. J. Bearpark, J. Heyd, E. N. Brothers, K. N. Kudin, V. N. Staroverov, R. Kobayashi, J. Normand, K. Raghavachari, A. P. Rendell, J. C. Burant, S. S. Iyengar, J. Tomasi, M. Cossi, N. Rega, N. J. Millam, M. Klene, J. E. Knox, J. B. Cross, V. Bakken, C. Adamo, J. Jaramillo, R. Gomperts, R. E. Stratmann, O. Yazyev, A. J. Austin, R. Cammi, C. Pomelli, J. W. Ochterski, R. L. Martin, K. Morokuma, V. G. Zakrzewski, G. A. Voth, P. Salvador, J. J. Dannenberg, S. Dapprich, A. D. Daniels, O. Farkas, J. B. Foresman, J. V. Ortiz, J. Cioslowski and D. J. Fox, *Gaussian 09, Revision D.01*, (2009) Gaussian, Inc., Wallingford, CT, USA.
- ¹⁹ J. Tomasi, M. Persico, *Chem. Rev.* **1994**, *94*, 2027.
- ²⁰ J. Tomasi, B. Mennucci, R. Cammi, *Chem. Rev.* **2005**, *105*, 2999.
- ²¹ C. J. Cramer, D. G. Truhlar, in *Solvent Effects and Chemical Reactivity*, eds. O. Tapia and J. Bertrán, Springer Netherlands, 2002, vol. 17, pp. 1-80.
- ²² R. E. Stratmann, G. E. Scuseria, M. J. Frisch, *J. Chem. Phys.* **1998**, *109*, 8218.
- ²³ M. E. Casida, C. Jamorski, K. C. Casida, D. R. Salahub, *J. Chem. Phys.* **1998**, *108*, 4439.
- ²⁴ R. Bauernschmitt, R. Ahlrichs, *Chem. Phys. Lett.* **1996**, *256*, 454.
- ²⁵ R. Dennington, T. Keith and J. Millam, *GaussView, Version 5*, (2009) Semichem Inc., Shawnee Mission, KS, USA.
- ²⁶ W. Humphrey, A. Dalke, K. Schulten, *J. Mol. Graph Model.* **1996**, *14*, 33.
- ²⁷ G. A. Crosby, J. N. Demas, *J. Phys. Chem.* **1971**, *75*, 991.

²⁸ S. R. Meech, D. Phillips, *J. Photochem.* **1983**, *23*, 193.

²⁹ C. Wurth, M. Grabolle, J. Pauli, M. Spieles, U. Resch-Genger, *Nat. Protoc.* **2013**, *8*, 1535.

8. Moving toward the blue: a new difluorophenyl-tetrazole as cyclometalating ligand for Ir(III) complexes

In recent years, an increasing interest has been devoted to the development of new phosphorescent metal complexes and in their application as emitters in electroluminescent devices, such as organic light-emitting diodes (OLEDs) and light-emitting electrochemical cells (LECs) for displays and lighting applications.¹

Among all the heavy metal based luminescent complexes, those based on iridium are widely the most studied, due to their unique properties, such as the relatively short excited-state lifetime, the high emission quantum yield and the facile colour tuning.² Another very interesting feature is represented by the triplet character of the emission, induced by the strong spin-orbit coupling in these complexes. This character is of a great importance, since it allows for harvesting of both the singlet and the triplet excitons produced when electrons and holes recombine, reaching up to 100% internal efficiency.³

In order to develop full-colour displays and lighting technologies, a key factor is the possibility to have compounds able to emit primary colours (red, green and blue). In this context, one of the mayor features of cyclometalated Ir(III) complexes is the possibility to fine tune the emission colour by an appropriate design of the chemical structure and nature of the cyclometalating ligands.^{4,5,6} Efficient red- and green-emitting Ir(III) complexes are very common and have been greatly exploited, and some of them are now in their commercialization phase due to their very good stability in devices. On the contrary, finding stable and efficient blue emitters is still an issue.⁷

Among all the cyclometalating ligands, the most employed in the preparation of Ir(III) complexes are 2-phenylpyridine (Hppy) and its derivatives, in which a carbon of the phenyl ring acts as a donor, and the metallacyclo is completed by the nitrogen atom of the N-heterocycle ring.⁶ The final complex is then complete with a neutral or ionic appropriate ancillary ligand. Through rational design, it is possible to decorate both the cyclometalated and the ancillary ligands. In detail, these can be appended with electron-withdrawing and/or electron-donating substituents, which has important effects on both the HOMO and LUMO levels of the complex and, consequently, on the light emission. In order to obtain blue emitters, several options can be followed. One of the most employed approach is the stabilization of the HOMO, which can be pursued with different strategies: (i) addition of electron-withdrawing groups, typically fluorines, to the aryl moiety of the C^N ligand;⁸ (ii) reduction of the ring size of the aromatic N-heterocycle and increase of the number of N atoms.⁹ The latter approach has been well investigated, and several examples of Ir(III) complexes with cyclometalating ligands entailing 5-membered nitrogen-containing rings have been reported, namely, 1-aryl-1,2-pyrazoles,¹⁰ and phenyl imidazoles.¹¹ In addition, a few aryl triazoles have been also proposed, such as 5-aryl-1,2,4- triazoles¹² and aryl-1,2,3-triazoles.¹³

In this perspective, my group designed and synthesized the first example of cyclometalated Ir(III) complexes bearing 5-phenyltetrazole (Hptrz) as cyclometalated C[^]N ligands.¹⁴ The emission observed for [Ir(ptzr)₂bpy]⁺ is shifted to 545 nm, resulting in the highest-energy emission bands ever reported for fluorine-free cyclometalating ligands.

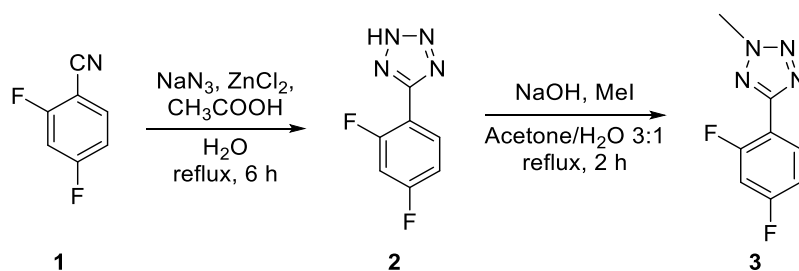
In order to further push the emission toward the blue, during my PhD we designed a fluorinated phenyltetrazole ligand and we used it in the preparation of blue-emitting Ir(III) complexes.

8.1 Results and discussion

8.1.1 Synthesis

Starting from the experience of my group, in order to further push the emission of Ir(III) complexes towards higher energies, we designed a new cyclometalating ligand equipped with two fluorine substituent in the aryl moiety.

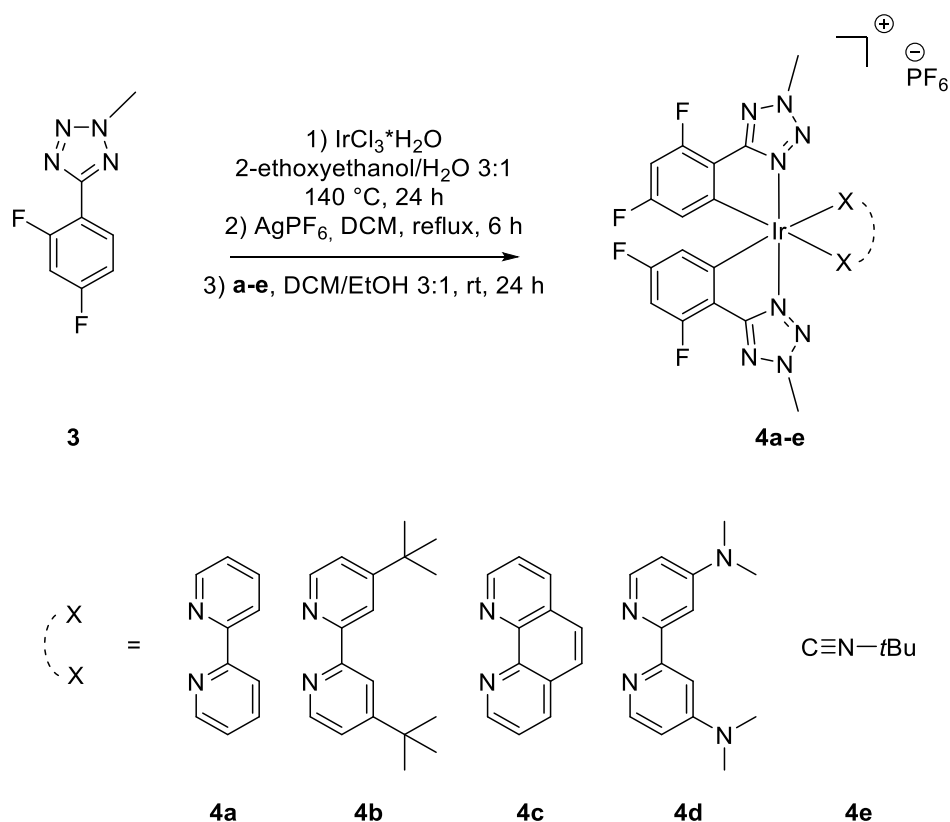
The synthetic route to the designed 5-(2,4-difluorophenyl)-2-methyl-2*H*-tetrazole (Hdfptrz, **3**) is reported in Scheme 1. Starting from commercially available 2,4-difluorobenzonitrile (**1**), tetrazole derivative (**2**) can be prepared within good yields (80%) by reaction with sodium azide in presence of ZnCl₂ and acetic acid as catalysts. The treatment of **2** with methyl iodide in presence of NaOH lead to the formation of two methylated derivative. The desired product can be successfully separated from the undesired isomer 5-(2,4-difluorophenyl)-1-methyl-1*H*-tetrazole by flash chromatography. Compound **3** can be isolated in 45% yield.



Scheme 1: Synthesis of cyclometalating ligand **3**

As already described for phenyltetrazole derivative,¹⁴ any attempt to obtain the classical cyclometalated Ir(III) μ -dichloro bridged dimer [Ir(dfptrz)₂(μ -Cl)] failed. This can be tentatively explained with the formation of an IrCl₃-tetrazole salt. Therefore, a further step involving a reagent able to promote the removal of a chlorine atom from the formed salt and favour the cyclometalation proved to be necessary. In detail, the

tetrazole derivative **3** was reacted with $\text{IrCl}_3 \cdot n\text{H}_2\text{O}$ in a refluxing mixture of 2-ethoxyethanol/water in 3:1 ratio. The obtained yellow salt was filtered off and refluxed in DCM in presence of AgPF_6 in order to satisfactory obtain the related solvato-complex. The solvato-complex was then reacted with the proper ancillary ligand, in order to prepare the desired complexes **4a-e**, as reported in Scheme 2. After purification of the crudes by column chromatography on neutral alumina, products **4a-e** were obtained in 46-54% yields.



Scheme 2: Synthesis and structures of complexes **4a-e**

8.1.2 Structural characterization

Slow diffusion of Et₂O vapour in a solution of **4b** in CH₃CN gave crystals suitable for X-rays analysis. The structure of the complex is reported in Figure 1.

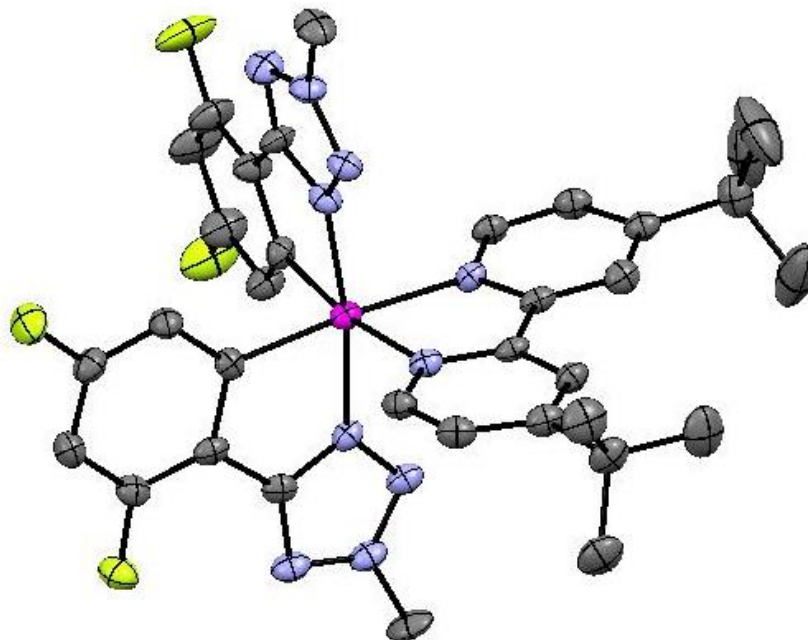


Figure 1: X-ray structure of complex **4b**. Counter anion, solvents, and hydrogen atoms are omitted for the sake of clarity. ORTEP representations are at the 50% probability

The compound crystallizes in the monoclinic $P2_1/c$ space group. The X-ray structure of complex **4b** showed an arrangement of the two difluorophenyl-tetrazole ligands around a pseudo-octahedral iridium ion (see Figure 1). One of the difluorophenyl-tetrazole is bound to two equatorial positions of the octahedral Ir(III) center, whereas the second one occupies an equatorial position with nitrogen and an axial position with carbon. This arrangement implies that the two nitrogens of the tetrazole rings are mutually in a *trans* position. The two nitrogen of the ancillary ligand fill the remaining equatorial and axial positions. The Ir–N and Ir–C distances are very similar to other iridium complexes reported in the literature.^{15,16,17} Therefore, the different geometry of the tetrazole with respect to heterocycles used previously does not alter the bonding distances.¹⁴ The crystallographic data are reported in Table 1.

Table 1: Crystallographic parameters for complex **4b**

	4b
Formula	C ₃₄ H ₃₄ N ₁₀ F ₁₀ PIr
F _w	995.88
T, K	298
λ, Å	0.71073 (Mo-Kα)
Crystal system	Monoclinic
Space group	P2 ₁ /c
a, Å	10.9234(13)
b, Å	19.252(2)
c, Å	17.806(2)
α, deg	90.000
β, deg	97.958(2)
γ, deg	90.000
Cell volume, Å ³	3708.6(8)
Z	4
D _c , g cm ⁻³	1.784
μ, mm ⁻¹	3.735
F(000)	1960
h, k, l max	9, 19, 21
Crystal size, mm	0.25, 0.15, 0.15
θ limits, °	1.57 to 26.00
Reflections collected	7073
Independent reflections	5923
Data/restraints/parameters	5923/0/513
Weight. Scheme	0.0549 9.7731
GOF on F ²	1.053
R ₁ (I > 4σ(I))	0.0366
wR ₂ (all data)	0.0990
Peak/hole, e Å ⁻³	2.502 and -1.999

8.1.3 Photophysical properties

All the complexes are stable in acetonitrile solution for several months and do not show degradation under standard laboratory conditions. The room-temperature electronic absorption spectra of **4a-e** are reported in Figure 2.

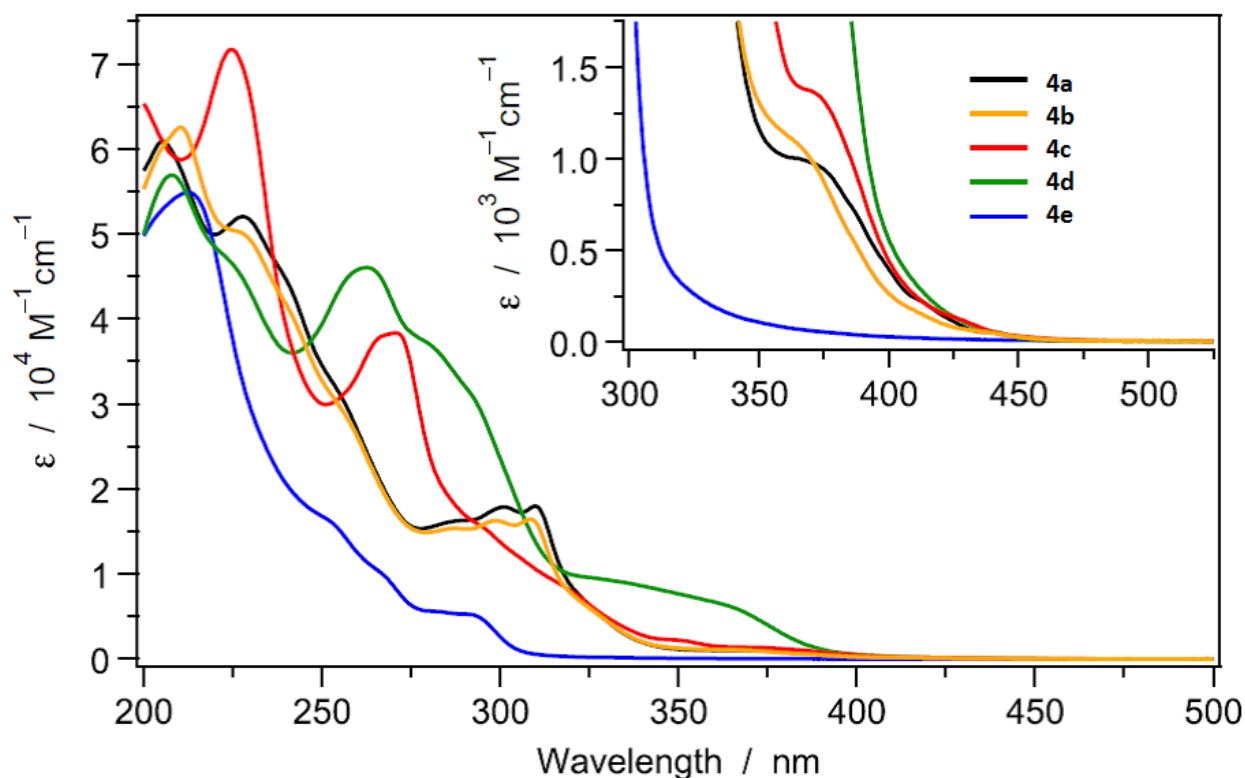


Figure 2: Absorption spectra of **4a-e** in acetonitrile solution at 298 K

All the reported complexes display strong absorption bands ($\epsilon \approx 2\text{-}7 \times 10^4 \text{ M}^{-1} \text{ cm}^{-1}$) in the spectral window between 200-275 nm. These bands can be assigned to spin-allowed ligand-centered (LC) $\pi\text{-}\pi^*$ transitions involving both the cyclometalating and the ancillary ligands. Moving at longer wavelengths, it is possible to observe weaker and broader bands (275-375 nm; $\epsilon \approx 1\text{-}15 \times 10^3 \text{ M}^{-1} \text{ cm}^{-1}$) which can be attributed to charge transfer transitions with mixed metal-to-ligand and ligand-to-ligand charge transfer (MLCT/LLCT) character.¹⁸ In the case of complex **4e**, the absorption band at 325-350 nm is absent because isocyanide ancillary ligands do not have low-energy π^* acceptor orbitals allowing MLCT transitions from the Iridium metal center; this is a common feature in cationic Ir(III) complexes with isocyanides.^{19,20,21} The weak and long tails observed in the spectra above 375 nm (inset, Figure 2) is due to direct spin-forbidden absorption from the singlet ground state (S_0) to the first triple excited state (T_1) of the complexes, enabled by the high spin-orbit coupling constant of the iridium metal core ($\xi_{\text{Ir}} = 3909 \text{ cm}^{-1}$). The band is stronger for **4a-d** ($\epsilon \approx 5\text{-}$

$10 \times 10^2 \text{ M}^{-1} \text{ cm}^{-1}$) where T_1 is expected to have a marked MLCT character, but it is completely absent in **4e**. This is in complete agreement with the fact that isocyanide-based Ir(III) complexes lack MLCT transitions and, accordingly, display only strong ligand-centered (LC) luminescence. A significant blue shift is observed for the lowest-energy absorption bands with respect to the fluorine-free phenyl-tetrazole already described by my group. This is perfectly in line other reported Ir(III) complexes, and it is due to the presence of the fluorine substituents on the cyclometalating ligands, which strongly stabilize the HOMO of the complexes.

The emission spectra of **4a-e** in acetonitrile solution at 298 K are reported in Figure 3, while in Table 1 are summarized the luminescence properties and photophysical parameters of all the complexes, including solid-state PMMA matrix.

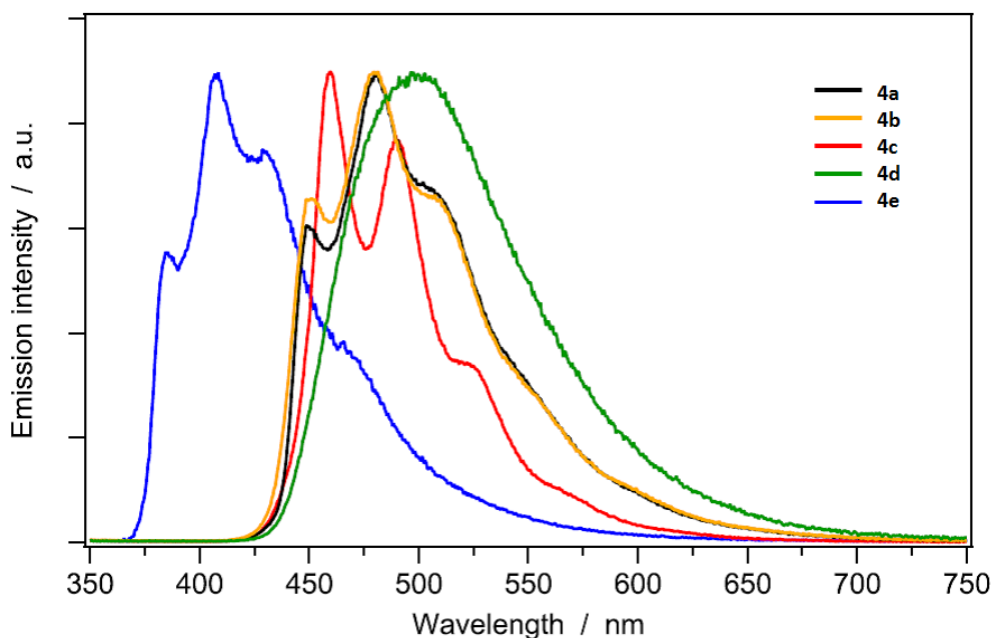


Figure 3: Normalized emission spectra of **4a-e** in acetonitrile solution at 298 K. Excitation wavelength: 290 nm

Table 2: Luminescence properties and photophysical parameters of **4a-e**

	Oxygen-free CH ₃ CN solution, 298 K				
	λ_{em}^a [nm]	Φ_{em}^b [%]	τ^c [μ s]	k_r [10^4 s^{-1}]	k_{nr} [10^4 s^{-1}]
4a	448, 481, 508 (sh)	76	4.11	18.5	5.86
4b	448, 481, 507 (sh)	58	4.90	11.7	8.66
4c	460, 488, 519 (sh)	56	43.77	1.29	0.99
4d	496	40	10.33	3.89	5.79
4e	384, 407, 429 (sh)	0.6	1.21	0.53	82.1

^a $\lambda_{exc} = 290 \text{ nm}$; ^b $\lambda_{exc} = 290 \text{ nm}$, quinine sulfate in 1 N H₂SO₄ aqueous solution as reference; ^c $\lambda_{exc} = 290 \text{ nm}$

All the complexes display a blue emission with maxima between 407 and 496 nm. In line with the absorption spectra, complexes **4a-c** show very similar emission properties with vibronically structured band, typical for an emitting triplet state T_1 with a predominant MLCT character with an admixture of LC contribute. On the contrary, complex **4d** exhibits a much greener emission and a broad and structureless band, indicating a triplet T_1 state with strong MLCT character. In addition, complex **4e** shows an emission maxima shift toward higher energy related to other complexes, with a vibronically structured emission, clearly indicating an emitting state with LC character.

The different nature of the emitting state is also crucially influencing the photoluminescence quantum yield (PLQY) of these complexes. Complexes **4a-d** show very high PLQYs (up to 76 %), whereas **4e** is almost non-emissive ($\Phi_{em} = 0.6$ %). In fact, complexes **4a-d** exhibit radiative constants similar to many others Ir(III) complexes ($k_r \approx 1-18 \times 10^4 \text{ s}^{-1}$), so the high PLQY values are primarily attributable to the lack of effective non-radiative pathways. The picture drastically changes if the T_1 state does not have a pronounced MLCT character, as in the case of **4e**. For this complex, in which the lowest electronic state has an LC character, the radiative constant drastically drops ($k_r \approx 5 \times 10^3 \text{ s}^{-1}$) making **4e** barely emissive. The photophysical properties of **4e** are very similar to those of $[\text{Ir}(\text{ppz})_2(\text{CN-}t\text{Bu})_2]^+$ and $[\text{Ir}(\text{ptrz})_2(\text{CN-}t\text{Bu})_2]^+$ that have been reported recently.^{20,14} Therefore, it can be concluded that 5-(2,4-difluorophenyl)-tetrazole (dfptrz), 5-phenyltetrazole (ptrz), 1-phenylpyrazole (ppz), and phenyl-[1,2,3]triazole (phtl) cyclometalating ligands act in a very similar way in cationic iridium(III) complexes bearing high-field ancillary ligands, that is, they exhibit faint luminescence.^{22,20,13} A totally different behavior is observed for $[\text{Ir}(\text{ppy})_2(\text{CN-}t\text{Bu})_2]^+$ and analogous 2-phenylpyridine complexes, where, in spite of rather small k_r values ($2-18 \times 10^3 \text{ s}^{-1}$), very high PLQYs ($\approx 30-70$ %) were found.^{19,23}

In Figure 4 are reported the emission spectra of complexes **4a-e** recorded in glass matrix of ACN at 77K. As shown, a remarkable blue shift is observed for **4e**, as expected for transitions with predominant LC character. For all the other complexes, more structured bands are observed, also in the case of **4d**, while a shift toward higher energies is generally observed. These shifts are not so remarkable, due to the high contribution of the MLCT transition to the emission, unaffected by matrix effects.

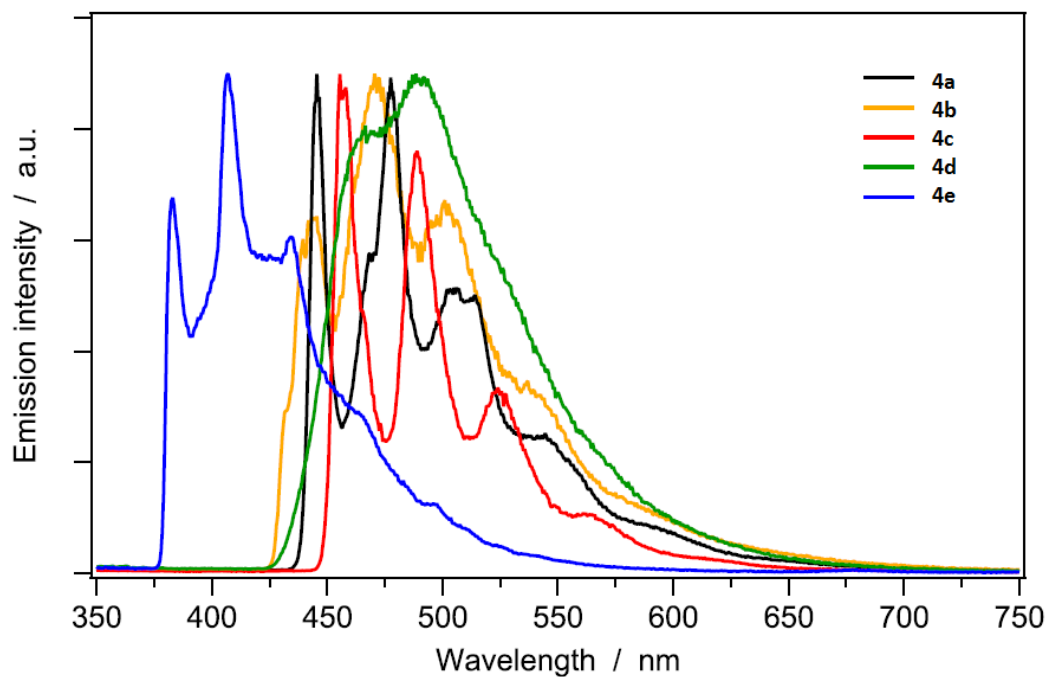


Figure 4: Normalized emission spectra of **4a-e** in acetonitrile glass matrix at 77 K. Excitation wavelength: 290 nm

In Figure 5 are reported the emission spectra of complexes **4a-d** in poly(methyl methacrylate matrix (PMMA, 1% by weight). The emission profiles are comparable with those recorded in acetonitrile solution at 298 K (see Figure 3).

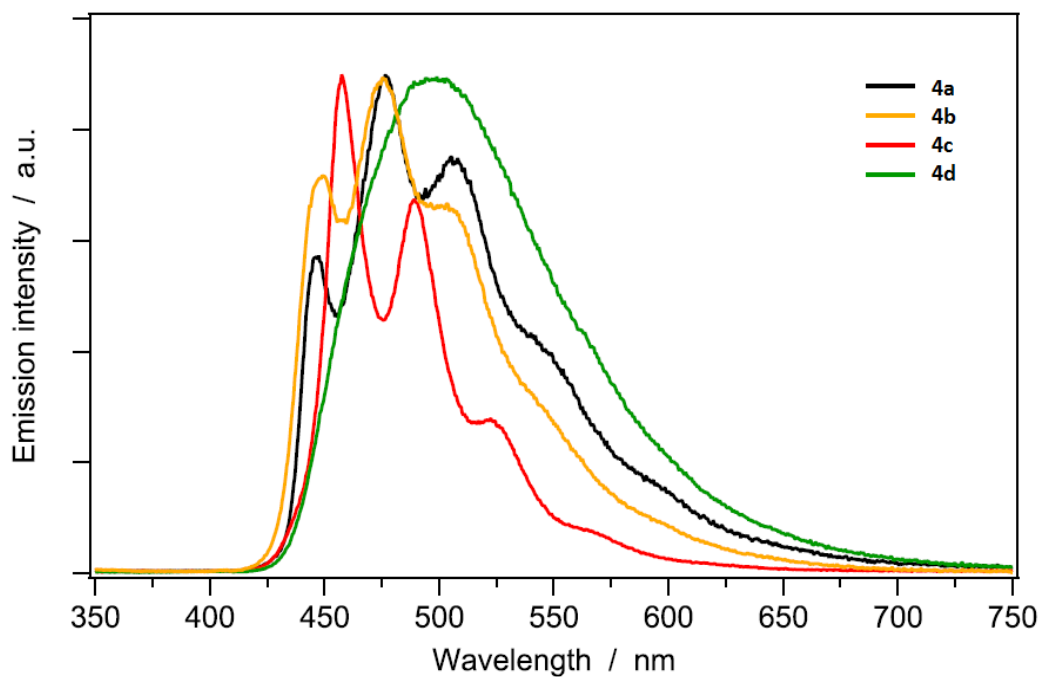


Figure 5: Corrected emission spectra of complex **4a-d** in 1% PMMA matrix recorded at 298 K

8.2 Conclusions

The complete characterization of the reported complexes **4a-e** is still going on. Here are reported only some preliminary results.

Ligand **3** represents the first example of fluorine-containing phenyl-tetrazole derivatives used as cyclometalating ligands for the preparation of Ir(III) complexes. The synthesis of complexes **4a-e** have been accomplished by a two-steps synthetic procedure, involving a silver-assisted cyclometalation reaction of ligand **3** with $\text{IrCl}_3 \cdot \text{H}_2\text{O}$. Reaction of the so obtained Ir-solvato complex with a proper ancillary ligands lead to the formation of the desired complexes within good yields.

As regarding the luminescent properties, complexes **4a-d** show strong PLQY with an emission in the blue-green region of the visible spectra. For complex **4e**, a weak photoluminescence is recorded, with an emission maximum centered at 407 nm. In this case, the complex show a PLQY of only 0.6 % due to the presence of favoured non-radiative deactivation pathways.

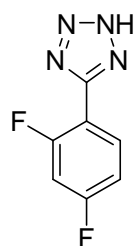
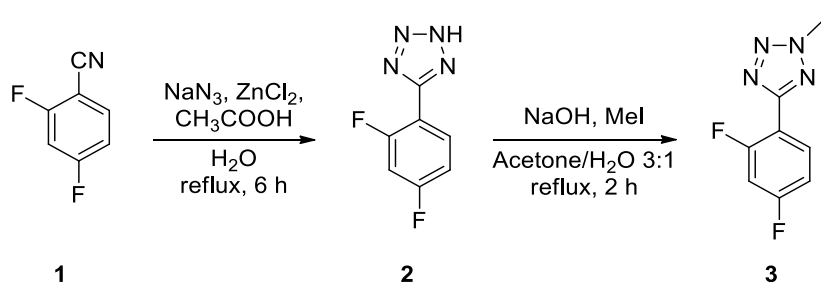
The primary objective of this work was the blue shift of the emission of already reported Ir(III) complexes equipped with phenyl-tetrazole as cyclometalating ligand by adding electron-withdrawing atom in the C^N fragments. We have successfully demonstrate that a blue shift can be pursued by add F- atoms in 2,4 positions of the phenyl moieties, without remarkably affect the photoluminescent properties of the complexes.

8.3 Experimental section

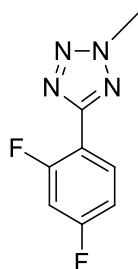
General synthetic procedures

Analytical grade solvents and commercially available reagents were used as received, unless otherwise stated. Chromatographic purifications were performed using 70-230 mesh silica. Solvents were dried and distilled according to standard procedures and stored under nitrogen. ^1H , ^{13}C , ^{19}F NMR spectra were recorded on a Varian Inova 300 MHz, on a Mercury 400 MHz or on an Inova 600 MHz spectrometer. Chemical shifts (δ) are reported in ppm relative to residual solvent signals for ^1H and ^{13}C NMR (^1H NMR: 7.26 ppm for CDCl_3 ; ^{13}C NMR: 77.0 ppm for CDCl_3). ^{13}C NMR spectra were acquired with ^1H broadband decoupling mode. Mass spectra were recorded on a micromass LCT spectrometer using electrospray (ES) ionisation techniques.

Synthesis of Ligand 3

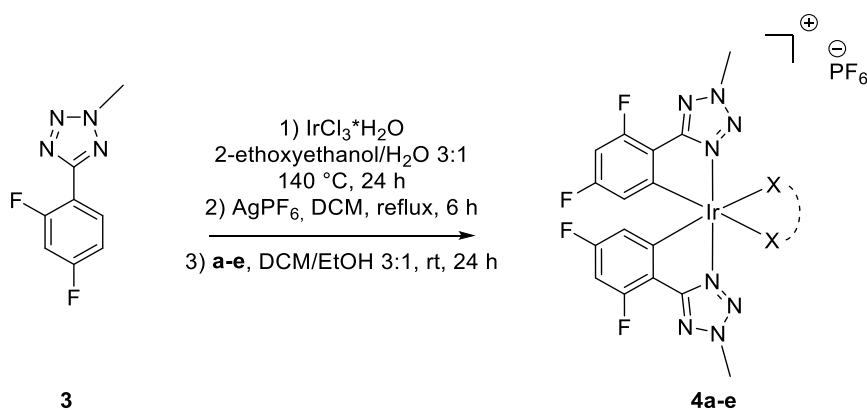


NaN₃ (546.0 mg, 8.4 mmol) was dissolved in H₂O (10 mL), then ZnCl₂ (1.14 g, 8.4 mmol) and CH₃COOH (1 mL) were added. The solution was stirred for 10 minutes. Then 2,4-difluorobenzonitrile (**1**) (1.17 g, 8.4 mmol) was added and the resulting mixture was refluxed for 6 hours. After this time the solution was cooled and HCl 1M (1 mL) was added. The resulting solid was filtered and washed with cold water. Product **2** was isolated in 80% yield (1.23 g) and used in the next step without further purifications. ¹H NMR (DMSO, 300 MHz) δ 7.88 (dt, *J*₁ = 6.9 Hz, *J*₂ = 8.6 Hz 1H), 7.29 (ddd, *J*₁ = 2.6 Hz, *J*₂ = 9.5 Hz, *J*₃ = 10.7 Hz, 1H), 7.12 (ddt, *J*₁ = 0.9 Hz, *J*₂ = 2.6 Hz, *J*₃ = 8.6 Hz, 1H). ESI-MS: 183 [M+H]⁺.

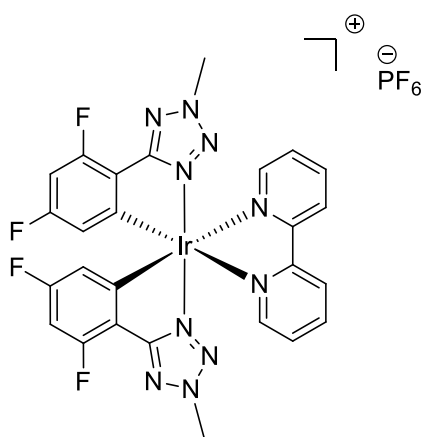


5-(2,4-difluorophenyl)-2H-tetrazole (**2**) (746.2 mg, 4.1 mmol) was dissolved in a mixture of Acetone/Water 3:1 (16 mL). Then NaOH (330.0 mg, 8.2 mmol) and MeI (510 μL, 8.2 mmol) were added and the resulting mixture was refluxed for 2 hours. After this time solvent was evaporated. Water (30 mL) was added and the mixture was extracted with DCM (4 x 15 mL). The collected organic phase was washed with water (30 mL) and brine (30 mL), dried over Na₂SO₄ and concentrated. The crude was purified on silica gel flash chromatography using a mixture of EP/DCM (50:50) and then DCM/methanol (95:5) to give product **3** in 40% yield (305.4 mg). ¹H NMR (CDCl₃, 400 MHz) δ 8.14 (dt, *J*₁ = 6.4 Hz, *J*₂ = 8.0 Hz, 1H), 7.06-6.97 (m, 2H), 4.44 (s, 3H). ¹³C NMR (CDCl₃, 100 MHz) δ 163.8 (C, dd, *J*_{CF} = 12 Hz, *J*_{CF} = 254 Hz), 160.7 (C, d, *J*_{CF} = 6 Hz), 160.4 (C, dd, *J*_{CF} = 12 Hz, *J*_{CF} = 254 Hz), 130.9 (CH, dd, *J*_{CF} = 4 Hz, *J*_{CF} = 10 Hz), 111.9 (C, d, *J*_{CF} = 4 Hz), 111.8 (CH, dd, *J*_{CF} = 4 Hz, *J*_{CF} = 24 Hz), 104.8 (CH, t, *J*_{CF} = 24 Hz), 39.4 (CH₃). ¹⁹F NMR (CDCl₃, 400 MHz) δ -107.44 (q, *J* = 8.0 Hz, 1F), -106.2 (quint, *J* = 8.0 Hz, 1F). ESI-MS: 197 [M+H]⁺.

Synthesis of complexes 4a-e

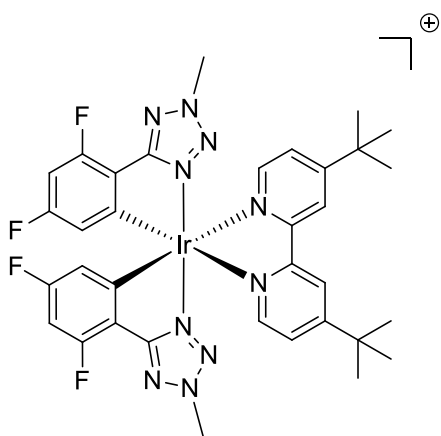


5-(2,4-difluorophenyl)-2-methyl-2H-tetrazole (**3**, 59.2 mg, 0.3 mmol) was dissolved in a mixture of 2-ethoxyethanol/Water 3:1 (1.2 mL) and the solution was degassed with N_2 for 20 minutes. Then, $\text{IrCl}_3 \cdot \text{H}_2\text{O}$ (30.0 mg, 0.1 mmol) was added and the resulting mixture was refluxed for 24 hours in N_2 atmosphere. After this time, water (1 mL) was added and the resulting precipitate was collected and washed with additional water (1 mL). The solid was then dissolved in DCM (5.0 mL) and AgPF_6 (50.6 mg, 0.2 mmol) was added. The resulting mixture was refluxed for 6 hours and the former precipitate was filtered off. The solvent was then evaporated and the solid added to the proper ligand **a-e** (0.3 mmol) dissolved in a mixture of DCM/Ethanol 3:1 (4 mL). The resulting solution was stirred for 24 hours. The solvent was then evaporated and the crude was concentrated. The crude was purified on Al_2O_3 gel flash chromatography using a mixture of CH_2Cl_2 /methanol (95:5) to give the desired products.

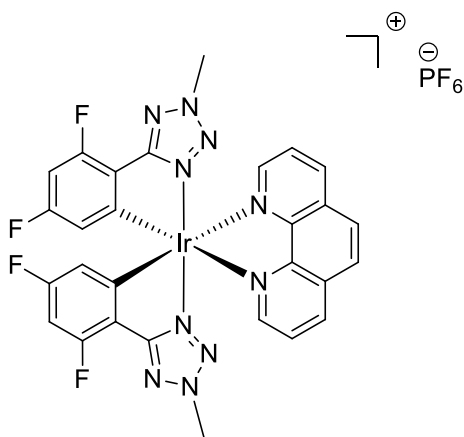


739 [M^+], 145 [M].

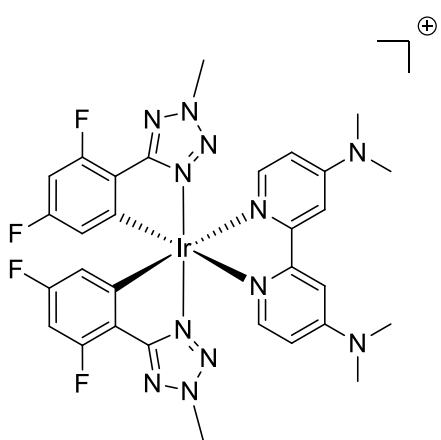
4a: 47.7 mg, Y = 54%. ^1H NMR (CDCl_3 , 400 MHz) δ 9.55 (d, J = 6.2 Hz, 2H), 9.31 (d, J = 8.6 Hz, 2H), 7.95 (bs, 2H), 7.25-7.15 (m, 8H), 7.45 (d, J = 9.8 Hz, 2H), 6.66 (t, J = 8.6 Hz, 2H), 5.72 (d, J = 7.4 Hz, 2H), 4.43 (s, 6H). ^{13}C NMR (CDCl_3 , 100 MHz) δ 171.5 (C, d, J_{CF} = 6 Hz), 164.9 (C, dd, J_{CF} = 12 Hz, J_{CF} = 254 Hz), 159.5 (C, dd, J_{CF} = 12 Hz, J_{CF} = 254 Hz), 156.8 (C), 150.6 (CH), 149.7 (C, d, J_{CF} = 6 Hz), 141.2 (CH), 127.7 (CH), 127.1 (CH), 115.3 (CH, dd, J_{CF} = 4 Hz, J_{CF} = 22 Hz), 115.0 (C, dd, J_{CF} = 4 Hz, J_{CF} = 14 Hz), 99.8 (CH, dd, J_{CF} = 24 Hz, J_{CF} = 28 Hz), 42.1 (CH_3). ^{19}F NMR (CDCl_3 , 400 MHz) δ -112.9 (q, J = 9.8 Hz, 2F), -109.3 (t, J = 9.8 Hz, 2F), -65.0 (s, 6F). ESI-MS:



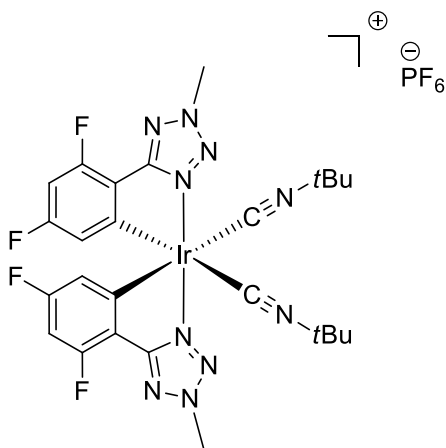
4b: 52.8 mg, Y = 53%. $^1\text{H NMR}$ (CDCl_3 , 400 MHz) δ 8.31 (bs, 2H), 7.92 (d, $J = 5.6$ Hz, 2H), 7.45 (d, $J = 5.6$ Hz, 2H), 6.62 (t, $J = 8.6$ Hz, 2H), 5.73 (d, $J = 6.2$ Hz, 2H), 4.42 (s, 6H), 1.44 (s, 18H). $^{13}\text{C NMR}$ (CDCl_3 , 100 MHz) δ 171.3 (C, d, $J_{\text{CF}} = 6$ Hz), 164.9 (C, dd, $J_{\text{CF}} = 12$ Hz, $J_{\text{CF}} = 254$ Hz), 164.8 (C), 159.5 (C, dd, $J_{\text{CF}} = 12$ Hz, $J_{\text{CF}} = 254$ Hz), 156.3 (C), 150.7 (CH), 150.2 (C, d, $J_{\text{CF}} = 6$ Hz), 125.2 (CH), 121.3 (CH), 115.3 (CH, dd, $J_{\text{CF}} = 4$ Hz, $J_{\text{CF}} = 22$ Hz), 113.7 (C, dd, $J_{\text{CF}} = 4$ Hz, $J_{\text{CF}} = 14$ Hz), 99.6 (CH, dd, $J_{\text{CF}} = 24$ Hz, $J_{\text{CF}} = 28$ Hz), 42.0 (CH_3), 35.8 (C), 30.2 (CH_3). $^{19}\text{F NMR}$ (CDCl_3 , 400 MHz) δ -112.9 (q, $J = 9.8$ Hz, 2F), -109.3 (t, $J = 9.8$ Hz, 2F), -65.0 (s, 6F). ESI-MS: 851 [M^+], 145 [M^-].



4c: 42.7 mg, Y = 47%. $^1\text{H NMR}$ (CD_2Cl_2 , 400 MHz) δ 8.70 (d, $J = 6.8$ Hz, 2H), 8.43 (d, $J = 4.0$ Hz, 2H), 8.22 (s, 2H), 7.88 (bs, 2H), 6.75 (t, $J = 8.0$ Hz, 2H), 5.95 (d, $J = 6.4$ Hz, 2H), 4.30 (s, 6H). $^{13}\text{C NMR}$ (CD_2Cl_2 , 100 MHz) δ 171.5 (C, d, $J_{\text{CF}} = 6$ Hz), 165.0 (C, dd, $J_{\text{CF}} = 12$ Hz, $J_{\text{CF}} = 254$ Hz), 159.5 (C, dd, $J_{\text{CF}} = 12$ Hz, $J_{\text{CF}} = 254$ Hz), 152.2 (C), 148.7 (C, d, $J_{\text{CF}} = 6$ Hz), 147.6 (C), 139.4 (CH), 131.4 (CH), 128.4 (CH), 126.3 (CH), 115.8 (CH, dd, $J_{\text{CF}} = 4$ Hz, $J_{\text{CF}} = 22$ Hz), 114.0 (C, dd, $J_{\text{CF}} = 4$ Hz, $J_{\text{CF}} = 14$ Hz), 99.8 (CH, dd, $J_{\text{CF}} = 24$ Hz, $J_{\text{CF}} = 28$ Hz), 42.0 (CH_3). $^{19}\text{F NMR}$ (CDCl_3 , 400 MHz) δ -112.9 (q, $J = 9.8$ Hz, 2F), -109.3 (t, $J = 9.8$ Hz, 2F), -65.0 (s, 6F). ESI-MS: 763 [M^+], 145 [M^-].



4d: 49.5 mg, Y = 51%. $^1\text{H NMR}$ (CDCl_3 , 400 MHz) δ 8.26 (bs, 2H), 7.34 (d, $J = 4.6$ Hz, 2H), 6.59 (t, $J = 8.0$ Hz, 2H), 6.33 (bs, 2H), 5.74 (d, $J = 6.4$ Hz, 2H), 4.44 (s, 6H), 3.28 (s, 12H). $^{13}\text{C NMR}$ (CDCl_3 , 100 MHz) δ 171.8 (C, d, $J_{\text{CF}} = 6$ Hz), 165.2 (C, dd, $J_{\text{CF}} = 12$ Hz, $J_{\text{CF}} = 254$ Hz), 159.8 (C, dd, $J_{\text{CF}} = 12$ Hz, $J_{\text{CF}} = 254$ Hz), 156.8 (C), 155.4 (C), 153.1 (C, d, $J_{\text{CF}} = 6$ Hz), 149.0 (CH), 115.4 (CH, dd, $J_{\text{CF}} = 4$ Hz, $J_{\text{CF}} = 22$ Hz), 113.7 (C, dd, $J_{\text{CF}} = 4$ Hz, $J_{\text{CF}} = 14$ Hz), 108.0 (CH), 107.8 (CH), 98.9 (CH, dd, $J_{\text{CF}} = 24$ Hz, $J_{\text{CF}} = 28$ Hz), 41.9 (CH_3), 40.3 (CH_3). $^{19}\text{F NMR}$ (CDCl_3 , 400 MHz) δ -112.9 (q, $J = 9.8$ Hz, 2F), -109.3 (t, $J = 9.8$ Hz, 2F), -65.0 (s, 6F). ESI-MS: 825 [M^+], 145 [M^-].



4e: 41.1 mg, Y = 46%. ^1H NMR (CDCl_3 , 400 MHz) δ 6.58 (t, $J = 9.8$ Hz, 2H), 5.57 (d, $J = 7.8$ Hz, 2H), 4.74 (s, 6H), 1.50 (s, 18H). ^{13}C NMR (CDCl_3 , 100 MHz) δ 171.4 (C, d, $J_{\text{CF}} = 6$ Hz), 164.8 (C, dd, $J_{\text{CF}} = 12$ Hz, $J_{\text{C-F}} = 254$ Hz), 162.7 (C), 159.4 (C, dd, $J_{\text{CF}} = 12$ Hz, $J_{\text{C-F}} = 254$ Hz), 152.8 (C, d, $J_{\text{CF}} = 6$ Hz), 114.1 (CH, dd, $J_{\text{CF}} = 4$ Hz, $J_{\text{CF}} = 22$ Hz), 113.0 (C, dd, $J_{\text{CF}} = 4$ Hz, $J_{\text{CF}} = 14$ Hz), 100.4 (CH, dd, $J_{\text{CF}} = 24$ Hz, $J_{\text{CF}} = 28$ Hz), 59.4 (C), 42.1 (CH_3), 30.3 (CH_3). ^{19}F NMR (CDCl_3 , 400 MHz) δ -112.9 (q, $J = 9.8$ Hz, 2F), -109.3 (t, $J = 9.8$ Hz, 2F), -65.0 (s, 6F). ESI-MS: 749 [M^+], 145 [M^-].

Photophysical measurements

The spectroscopic investigations were carried out in spectrofluorimetric grade acetonitrile. The absorption spectra were recorded with a Perkin-Elmer Lambda 950 spectrophotometer. For the photoluminescence experiments, the sample solutions were placed in fluorimetric Suprasil quartz cuvettes (1 cm) and dissolved oxygen was removed by bubbling argon for 20 minutes. The uncorrected emission spectra were obtained with an Edinburgh Instruments FLS920 spectrometer equipped with a Peltier-cooled Hamamatsu R928 photomultiplier tube (PMT) (185-850 nm). An Edinburgh Xe 900 (450 W xenon arc lamp) was used as the excitation light source. The corrected spectra were obtained via a calibration curve supplied with the instrument. The photoluminescence quantum yields (Φ_{PL}) in solution were obtained from the corrected spectra on a wavelength scale (nm) and measured according to the approach described by Demas and Crosby²⁴ using an air-equilibrated water solution of quinine sulfate in 1N H_2SO_4 as reference ($\Phi_{\text{PL}} = 0.546$).²⁵ The emission lifetimes (τ) in the microsecond time range were measured through the time-correlated single photon counting (TCSPC) technique using an HORIBA Jobin Yvon IBH FluoroHub controlling a spectrometer equipped with a pulsed SpectraLED ($\lambda_{\text{exc}} = 370$ nm; FWHM = 11 nm) as excitation source and a red-sensitive Hamamatsu R-3237-01 PMT (185-850 nm) as detector. The analysis of the luminescence decay profiles was accomplished with the DAS6 Decay Analysis Software provided by the manufacturer, and the quality of the fit was assessed with the χ^2 value close to unity and with the residuals regularly distributed along the time axis. To record the 77 K luminescence spectra, samples were put in quartz tubes (2 mm inner diameter) and inserted into a special quartz Dewar flask filled with liquid nitrogen. Solid samples were prepared by drop casting using a dichloromethane solution containing the poly(methyl methacrylate) (PMMA) matrix with 1% wt. of the complex; the thickness of the films was not controlled. Solid-state Φ_{PL} values were calculated by corrected emission spectra obtained from an Edinburgh FLS920 spectrometer equipped with a barium sulfate-coated integrating sphere (diameter of 4 in.) following the procedure described by Würth *et al.*²⁶

Experimental uncertainties are estimated to be $\pm 8\%$ for τ determinations, $\pm 20\%$ for Φ_{PL} , ± 2 nm and ± 5 nm for absorption and emission peaks, respectively.

8.4 Bibliography

-
- ¹ H. Yersin, *Highly Efficient OLEDs with Phosphorescent Materials*; Wiley-VCH: Weinheim, **2008**.
 - ² M. E. Thompson, P. E. Djurovich, S. Barlow, S. Marder, *Comprehensive Organometallic Chemistry III*; Elsevier: Oxford, **2007**; *12*, 101.
 - ³ H. Yersin, A. F. Rausch, R. Czerwieniec, T. Hofbeck, T. Fischer, *Coord. Chem. Rev.* **2011**, *255*, 2622.
 - ⁴ S. Lamansky, P. Djurovich, D. Murphy, F. Abdel-Razzaq, H.-E. Lee, C. Adachi, P. E. Burrows, S. R. Forrest, M. E. Thompson, *J. Am. Chem. Soc.* **2001**, *123*, 4304.
 - ⁵ Y. M. You, S. Y. Park, *J. Am. Chem. Soc.* **2005**, *127*, 12438.
 - ⁶ Y. Chi, P. T. Chou, *Chem. Soc. Rev.* **2010**, *39*, 638.
 - ⁷ R. J. Holmes, S. R. Forrest, T. Sajoto, A. Tamayo, P. I. Djurovich, M. E. Thompson, J. Brooks, Y. J. Tung, B. W. D'Andrade, M. S. Weaver, R. C. Kwong, J. Brown, *J. Appl. Phys. Lett.* **2005**, *87*, 243507.
 - ⁸ V. V. Grushin, N. Herron, D. D. LeCloux, W. J. Marshall, V. A. Petrov, Y. Wang, *Chem. Commun.* **2001**, *16*, 1494
 - ⁹ P. Pla, J. M. Junquera-Hernández, H. J. Bolink, E. Ortí, *Dalton Trans.* **2015**, *44*, 8497.
 - ¹⁰ A. B. Tamayo, S. Garon, T. Sajoto, P. I. Djurovich, I. M. Tsyba, R. Bau, M. E. Thompson, *Inorg. Chem.* **2005**, *44*, 8723.
 - ¹¹ E. Baranoff, S. Fantacci, F. De Angelis, X. Zhang, R. Scopelliti, M. Grätzel, M. K. Nazeeruddin, *Inorg. Chem.* **2011**, *50*, 451.
 - ¹² W.-Y. Lai, J. W. Levell, A. C. Jackson, S.-C. Lo, P. V. Bernhardt, I. D. W. Samuel, P. L. Burn, *Macromolecules* **2010**, *43*, 6986.
 - ¹³ B. Beyer, C. Ulbricht, D. Escudero, C. Friebe, A. Winter, L. Gonzalez, U. S. Schubert, *Organometallics* **2009**, *28*, 5478.
 - ¹⁴ F. Monti, A. Baschieri, I. Gualandi, J. J. Serrano-Pérez, J. M. Junquera-Hernández, D. Tonelli, A. Mazzanti, S. Muzzioli, S. Stagni, C. Roldan-Carmona, A. Pertegás, H. J. Bolink, E. Ortí, L. Sambri, N. Armaroli, *Inorg. Chem.* **2014**, *53*, 7709.
 - ¹⁵ S. Ladouceur, D. Fortin, E. Zysman-Colman, *Inorg. Chem.* **2011**, *50*, 11514.
 - ¹⁶ L. Donato, P. Abel, E. Zysman-Colman, *Dalton Trans.* **2013**, *42*, 8402.
 - ¹⁷ S. Ladouceur, D. Fortin, E. Zysman-Colman, *Inorg. Chem.* **2010**, *49*, 5625.
 - ¹⁸ R. D. Costa, E. Ortí, H. J. Bolink, F. Monti, G. Accorsi, N. Armaroli, *Angew. Chem. Int. Ed.* **2012**, *51*, 8178.

- ¹⁹ N. M. Shavaleev, F. Monti, R. D. Costa, R. Scopelliti, H. J. Bolink, E. Ortí, G. Accorsi, N. Armaroli, E. Baranoff, M. Grätzel, M. K. Nazeeruddin, *Inorg. Chem.* **2012**, *51*, 2263.
- ²⁰ N. M. Shavaleev, F. Monti, R. Scopelliti, A. Baschieri, L. Sambri, N. Armaroli, M. Grätzel, M. K. Nazeeruddin, *Organometallics* **2013**, *32*, 460.
- ²¹ F. Monti, A. Baschieri, E. Matteucci, A. Mazzanti, L. Sambri, A. Barbieri, N. Armaroli, *Faraday Discuss.* **2015**, *185*, 233.
- ²² T. Sajoto, P. I. Djurovich, A. B. Tamayo, J. Oxgaard, W. A. Goddard, M. E. Thompson, *J. Am. Chem. Soc.* **2009**, *131*, 9813.
- ²³ N. M. Shavaleev, F. Monti, R. Scopelliti, N. Armaroli, M. Grätzel, M. K. Nazeeruddin, *Organometallics* **2012**, *31*, 6288.
- ²⁴ G. A. Crosby, J. N. Demas, *J. Phys. Chem.* **1971**, *75*, 991.
- ²⁵ S. R. Meech, D. Phillips, *J. Photochem.* **1983**, *23*, 193.
- ²⁶ C. Wurth, M. Grabolle, J. Pauli, M. Spieles, U. Resch-Genger, *Nat. Protoc.* **2013**, *8*, 1535.

9. Heterometallic Ir(III)₂-Eu(III) complexes: white light emission from a single molecule

In recent years, great attention has been devoted to the development of innovative and low cost technologies for lighting and displays, and one of the most challenging tasks in this field is white light emission.^{1,2,3,4} Materials which reproduce the solar spectrum are the ideal solution for lighting and display applications as they provide the best visual comfort.

White Organic Light Emitting Diodes (WOLEDs) are promising devices to realization of light sources with low energy consumption, since they combine a high efficiency and low costs of production with the interesting feature of being able to produce large emitting surfaces with a good quality of white light. However, lifetime, performances and costs still have to be optimized so that the WOLEDs can become commercially competitive. The development of efficient and stable emitters plays, therefore, a key role in the progress of WOLED technology.

Two different approaches can be pursued in order to obtain a white light emission from organic or organometallic species: (i) single-component materials; (ii) mixture of materials emitting primary colours, *e.g.*, red, green and blue (RGB), or complementary colours (*e.g.*, bluish/green and orange/red). Single materials able to emit over the whole visible spectrum offer the opportunity to prepare high quality white-light sources, due to their stability, the easy devices preparation and reproducibility.^{5,6} However, these compounds are extremely rare,^{7,8} and moreover, with this approach no 'pure' white light has been obtained up to now.^{9,10} Therefore, the white light emission is normally obtained using a mixture of materials,¹¹ involving complex manufacturing protocols and high costs.

Recently, one of the most followed approaches required the use of suitably designed multicomponent individual systems, such as dyad systems, where a luminescent donor with a wide bandgap is used as sensitizer for an emitting acceptor with a smaller bandgap. Higher energy (bluish-green) emission is maintained with concomitant partial energy transfer to the orange-red luminophore. Following this strategy, blue emitting chromophores, such as transition metal complexes, has been used for the photosensitization of Lanthanide ions.¹² The use of d⁶ (especially Ir(III), Ru(II) and Os(II) derivatives) and d⁸ (typically Pt(II)) polypyridyl complexes has been widely studied, due to their suitable features: (i) intense absorption in the visible region; (ii) relatively long lifetimes of the excited states, that can maximize the energy transfer to the Ln(III); (iii) extremely high photophysical, photochemical and thermal stability; (iv) large Stokes-shifts in the visible region, which minimize self-quenching processes. Moreover, the photoluminescent properties of these derivatives can be easily modified by varying the coordination sphere of the central metal; therefore, the emission efficiency, the stability and the emission colour can be improved with a rational design.

The most employed Lanthanide ions show an almost absent absorption in the visible region, while present emission maxima in the UV-Vis region, *i.e.* Eu(III) or Gd(III), or, more frequently, in the NIR region of the spectrum, *i.e.* Nd(III), Yb(III), Er(III) and Pr(III).

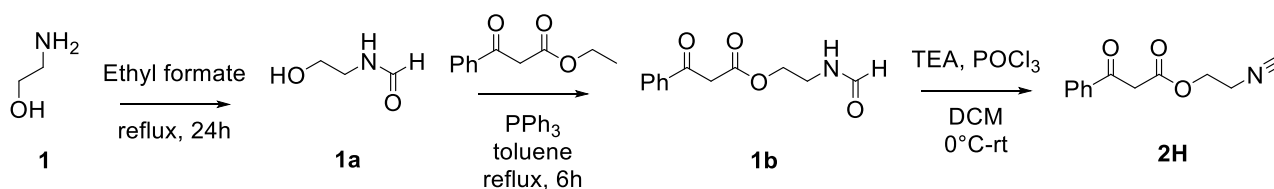
In this context, great attention has been devoted to the use of Ir(III) complexes, whose emission can be easily tuned over the visible spectrum up to the blue region with significant quantum yields. Starting from the pioneering work of DeCola's group,¹³ most researchers prepared different Ir(III)-Eu(III) assemblies^{14,15} with possible white-light emission. Such molecular structures must be carefully designed in order to display a balanced combination of emitted colours, which can be achieved through partial energy transfer between the Ir(III) moiety, represented by a cyclometalated Ir(III) fragment playing the role of a blue emitter and of an antenna for the lanthanide sensitization, and the Eu(III) centre, which is a typical red emitter.¹⁶

Guided by these concepts, during my PhD we prepared three new Ir(III)-Eu(III) dyads made of two peripheral cyclometalated Ir(III) fragments, connected through a central Eu(III) core, and we described how the careful choice of an appropriate set of fluorinated and/or fluorine-free cyclometalating ligands can provide a reliable tool in fine tuning the colour of the combined emission in order to achieve "pure" white light.

9.1 Results and discussion

9.1.1 Synthesis of ligand 2H

We identified the simple ligand **2H** as the right bifunctionalized precursor for the coordination of both the metal centers. In fact, it can coordinate Eu(III) through the β -ketoester group and, at the same time, Ir(III) via the isocyanide moieties. Ligand **2H** was prepared following the synthesis reported in Scheme 1. **1a** was prepared by simple formylation of commercially available 2-aminoethanol (**1**), and the isolated crude was reacted with ethyl benzoylacetate and triphenylphosphine in a transesterification reaction, giving **1b** in 38% yields. This intermediate was subsequently dehydrated with POCl₃ to afford the desired ligand **2H** in 20% yields as a mixture of tautomers, as depicted in Figure 1.



Scheme 1: Synthesis of ligand **2H**

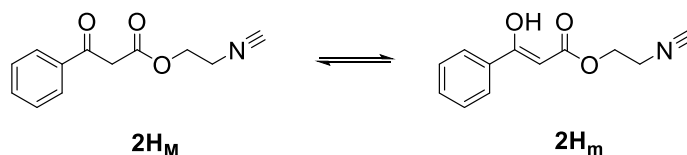
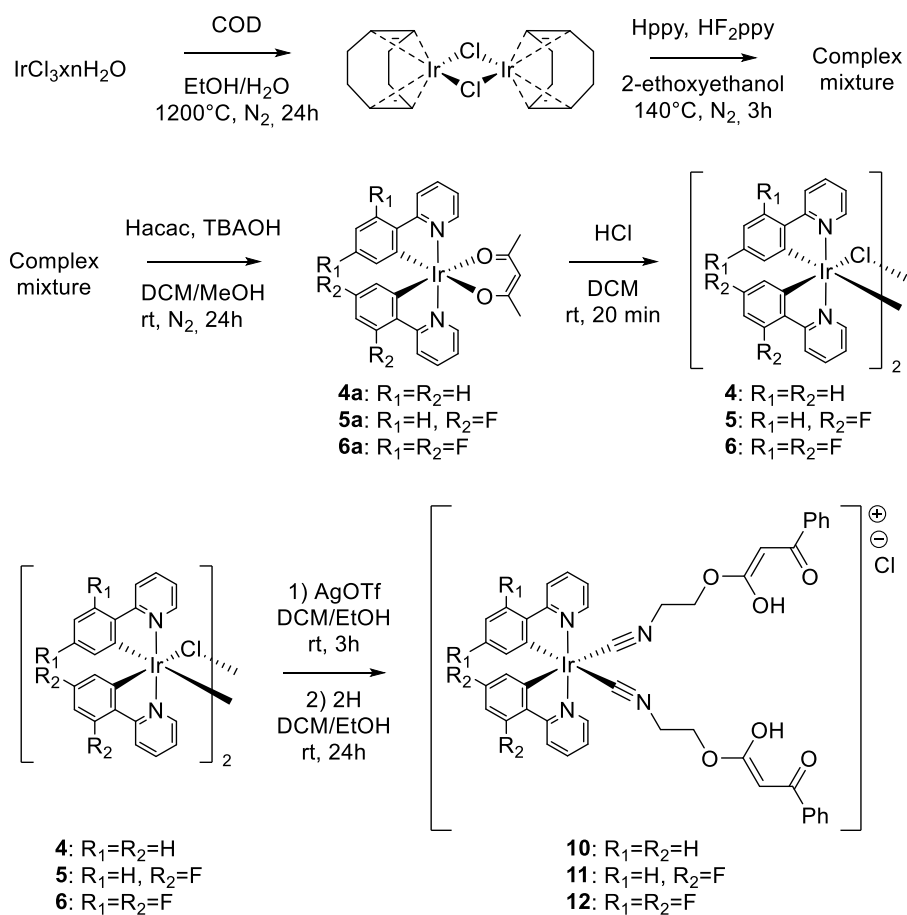


Figure 1: Possible tautomer forms for ligand **2H**

9.1.2 Synthesis of the Ir(III) dimers and Ir(III)-Eu(III) complexes

The synthesis of the complexes is reported in Scheme 2 and Scheme 3. Firstly, we prepared the $[\text{Ir}(\text{COD})(\mu\text{-Cl})_2]$ precursor from reaction of the commercially available $\text{IrCl}_3 \cdot n\text{H}_2\text{O}$ with 1,5-cyclooctadiene, that give the desired product as a red powder in 40% yield.¹⁷ Following a recently reported procedure,¹⁸ we prepared a set of Ir(III) chloro-bridged dimers, with different cyclometalating ligands. Starting from Hppy (2-phenylpyridine) and HF_2ppy (2-(2,4-difluorophenyl)pyridine), after reaction with the $[\text{Ir}(\text{COD})(\mu\text{-Cl})_2]$ precursor, we obtained a complex mixture of Ir-dimers, with a “mixed” composition of the cyclometalated ligands, as reported in Figure 2. This mixture has then been reacted with acetylacetonone (Hacac) in order to brake the chloro-bridge and get three different Ir(III)-acac complexes, that can be easily isolated and separated. Finally, the treatment of the acac-derivative with HCl lead to the formation of the ‘classic’ Ir(III) chloro-bridged dimers. In detail, we obtained two “traditional” precursors, namely $[\text{Ir}(\text{ppy})_2(\mu\text{-Cl})_2]$ (**4**) and $[\text{Ir}(\text{F}_2\text{ppy})_2(\mu\text{-Cl})_2]$ (**6**), and the less conventional “mixed” ligand complex $[\{\text{Ir}(\text{ppy})(\text{F}_2\text{ppy})(\mu\text{-Cl})\}_2]$ (**5**). The reaction of these three dimers **4-6** with ligand **2H** in DCM at room temperature, after Ag(I) mediated halide extraction,¹⁹ gave the three mononuclear Ir(III) model complexes **10-12**.

9. Heterometallic Ir(III)₂-Eu(III) complexes: white light emission from a single molecule



Scheme 2: Synthesis of Ir(III) dimers and Ir(III) model complexes

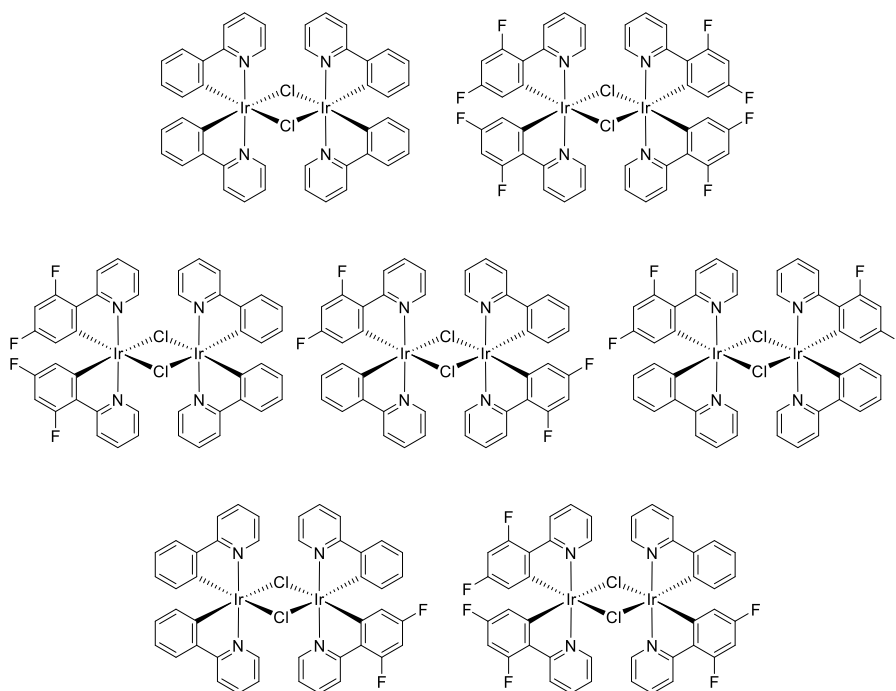
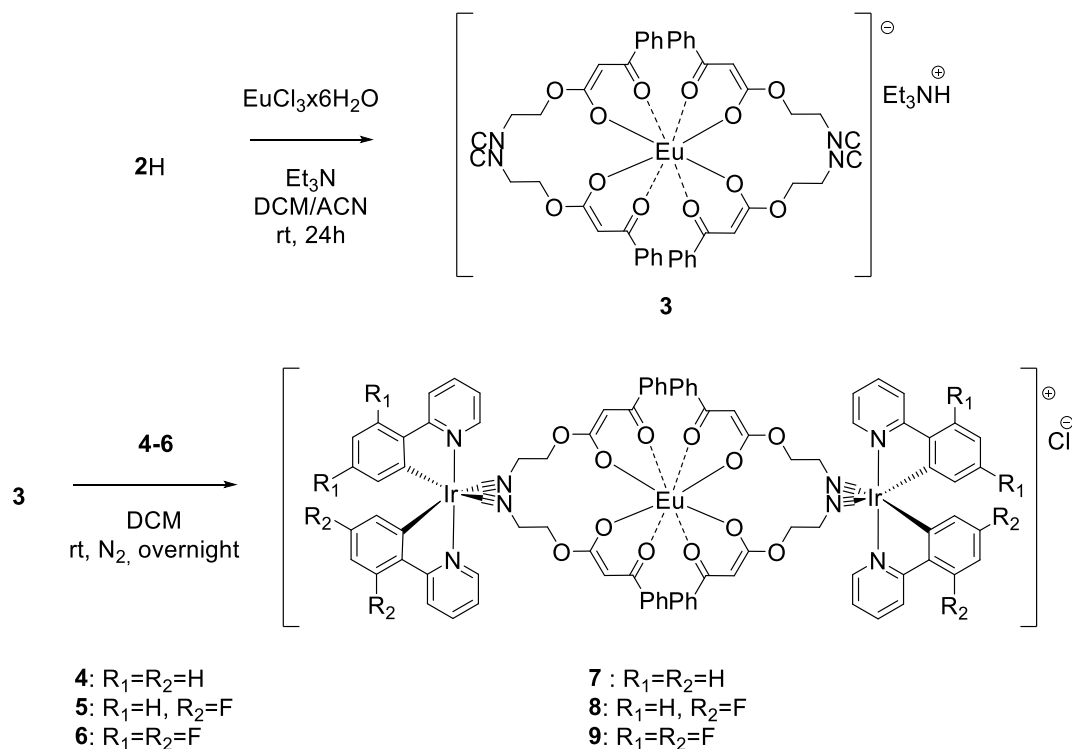


Figure 2: Complex mixture of Ir(III) dimers

2H was then reacted with EuCl₃·6H₂O in a DCM/ACN mixture (5:1) in presence of TEA, giving complex **3** as triethylammonium salt [Eu(**2**)₄][TEAH]. Finally, the reaction of the Eu(III) complex **3** with the dimers **4-6** gave the desired Ir(III)₂-Eu(III) dyads **7-9**.



Scheme 3: Synthesis of Eu(III) complex and Ir(III)-Eu(III) dyads

The formation of the dyads was determined only by ESI-MS analysis. In fact, NMR analysis cannot be performed due to the paramagnetic properties of the Eu(III) ion. In each case, the observed experimental molecular-ion peak pattern was found in excellent agreement with those obtained from the simulation based on natural isotopic abundances,²⁰ as reported in Figure 3 for dyad **7**.

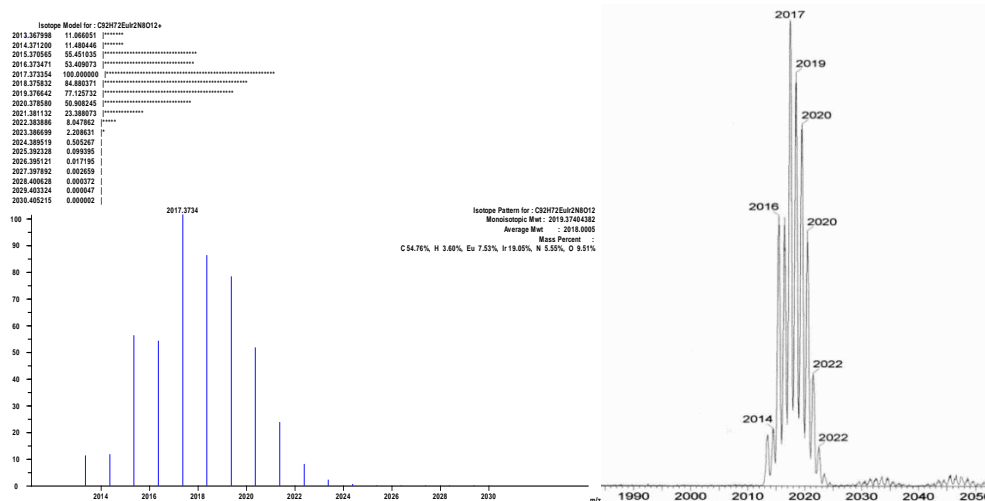


Figure 3: Simulated (left) and measured (right) isotopic pattern for dyad 7

9.1.3 Photophysical properties

The photophysical properties of Ir(III)₂-Eu(III) dyads **7-9** can be analyzed and compared with the properties of the mononuclear building blocks **3** and **10-12**. The photophysical properties of the mononuclear complexes **3** and **10-12** are reported in Table 1.

Table 1: Luminescence properties and photophysical parameters of mononuclear complexes **3** and **10-12**

Complex	Absorption λ_{max} (nm) $10^4\epsilon$ (M ⁻¹ cm ⁻¹)	Emission 298 K					Emission 77K		Solid state	
		λ (nm)	τ (μ s) deair	τ (μ s) air	Φ deair	Φ air	λ (nm)	τ (μ s)	λ (nm)	τ (μ s)
3	246 (7.86)	612	/	86.44 (25%)	/	1%	592	267 (25%)	612	251 (612 nm)
	287 (3.41)			447.42 (75%)			612	573 (75%)		
				(612 nm)			700	(612 nm)		
10	245 (8.00)	455	2.63 (485 nm)	0.81 (485 nm)	14%	5%	449	24,2 (481 nm)	457	0.24 (16%)
	283 (3.67)	485					481		489	2.46 (84%)
	347 (0.77)	511					508		520	(489 nm)
11	247 (10.33)	452	16.71 (484 nm)	0.95 (484 nm)	35%	3%	448	12 (480 nm)	453	1.50 (484 nm)
	282 (4.38)	484					480		484	
	346 (1.06)	510					508		514	
12	242 (9.18)	442	8.64 (470 nm)	1.04 (470 nm)	39%	11%	434	24 (466 nm)	444	0.14 (16%)
	301 (2.57)	470					466		474	1.31 (84%)
		496					502		499	(472 nm)

As reported in Figure 4, the monomeric complexes show a very similar absorption spectra. In detail, complex **3** shows a very intense band centred at 246 nm, related to π - π^* transitions in the chelating ligands, and a less intense band centred at 287 nm, related to the absorption of the phenyl moiety of ligand **2** (¹LC transition). A similar behaviour can be observed also in the case of the three Ir(III) complexes **10-12**. In addition to the already described bands, is possible to observe another absorption band in the region of

346-348 nm, that can be ascribed to MLCT transitions, typical for Ir(III) complexes equipped with ppy or F₂ppy cyclometalating ligands.

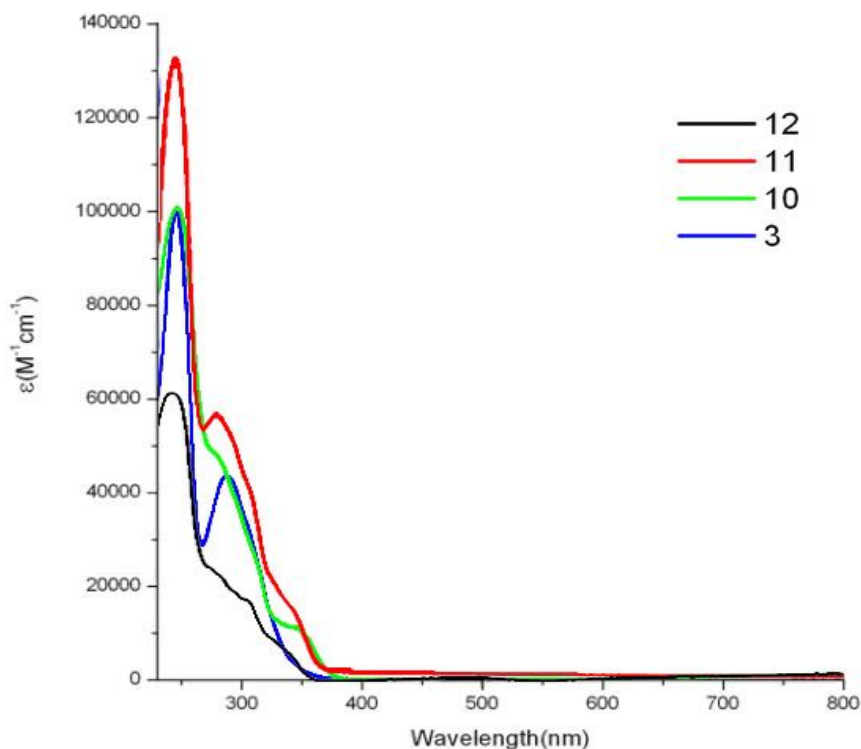


Figure 4: Absorption spectra of mononuclear complexes **3**, **10-12**

The Ir(III) mononuclear species display either blue/green or blue emissions, **10-11** and **12** (Figure 5), respectively, which were owing in all cases to radiative decay from an admixture of triplet ligand centred (³LC) and metal-to-ligand charge transfer (³MLCT) excited states. At 77 K, the emission maxima present a slight blue-shift, to 481 nm (**10**), 480 nm (**11**) and 466 nm (**12**), from which triplet excited state energies of 20800 cm⁻¹ (**10** and **11**) and 21500 cm⁻¹ (**12**) could be determined. Luminescence lifetime decays at room temperature in air-equilibrated DCM are 0.81 μs (**10**), 0.95 μs (**11**) and 1.0 μs (**12**), increased to 2.63 μs, 16.71 μs and 8.64 μs, respectively, in deaerated solutions and to 24.2 μs, 12 μs and 24 μs, respectively, at 77 K. Regarding the luminescence properties of the mononuclear Eu(III) complex **3**, upon excitation of the ligand ¹LC band at 320 nm, the characteristic line-shaped peak at 612 nm (Figure 4), corresponding to the ⁵D₀→⁷F_J (J = 0-4) transition is observed.

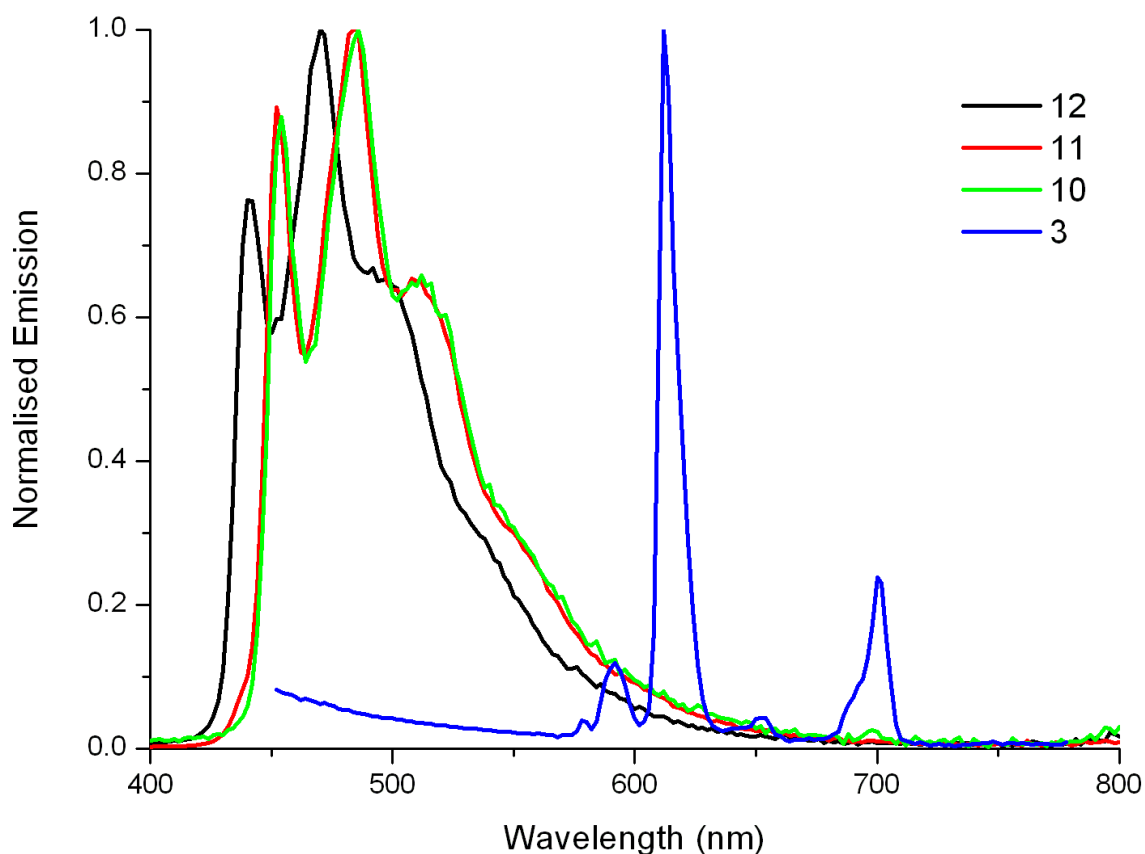


Figure 5: Emission spectra for mononuclear species **3**, **10-12**

The photophysical properties of the dyads systems **7-9** are reported in Table 2.

Table 2: Luminescence properties and photophysical parameters of dyads complexes **7-9**

Complex	Absorption λ_{\max} (nm) $10^4\epsilon$ ($M^{-1} cm^{-1}$)	λ (nm)	Emission 298 K				Emission 77K		Solid state			
			τ (μs) deair	τ (μs) air	Φ deair	Φ air	λ (nm)	τ (μs)	λ (nm)	τ (μs)		
7	240 (9.52)	471	0.26 (470 nm)	0.12 (470 nm)	14%	8%	464	6.0 (464 nm)	611	365.61 (42%)		
	284 (5.18)	504					498				702.81 (58%)	
	375 (0.42)	573(sh) 612					603 (612 nm)				680 (612 nm)	(611 nm)
8	249 (12.10)	465	1.23 (466 nm)	0.30 (466 nm)	43%	14%	465	6.2 (466 nm)	611	311.2 (20%)		
	280 (6.88)	497					495				629.65 (80%)	
	370 (0.81)	530 612					599 (612 nm)				591 (612 nm)	(611 nm)
9	247 (10.69)	452, 482	1.20 (482 nm)	0.30(482 nm)	37%	11%	447	5.8 (479 nm)	612	392.27 (35%)		
	285 (5.04) (sh)	612					479				506 (60%)	679.45 (65%)
	362 (0.87)	613 (612 nm)					506				943 (40%)	(612 nm)
							613	(612 nm)				

Regarding the dyads, it is possible to observe that the absorption profiles of **7-9**, reported in Figure 6, correspond to the sum of the contributions coming from both the Ir(III) and the Eu(III) moieties, as shown in Figure 4.

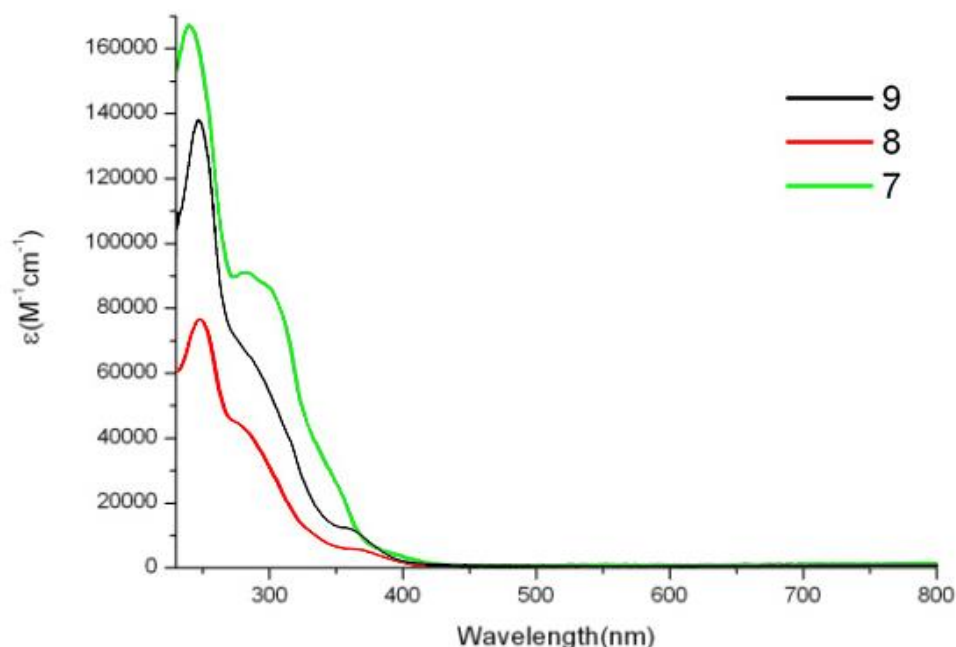


Figure 6: Absorption spectra of dyads **7-9**

The Ir(III)₂-Eu(III) dyads **7-9** displayed a behaviour strictly dependent on the identity of the two end-unit Ir(III) complexes, as shown in Figure 7. Interestingly, the spectral features belonging to the Eu(III) for the three dyads are significantly different from the corresponding mononuclear Eu(III) complex **3**. In particular, the intensity of the $^5D_0 \rightarrow ^7F_2$ transition (centred at 612 nm) compared to the magnetically allowed $^5D_0 \rightarrow ^7F_1$ (centred at 593 nm) suggests a lowering of the symmetry around the Eu(III) centre. A sensible decrease is also observed for the $^5D_0 \rightarrow ^7F_4$ transition, centred at *ca.* 700 nm. This might occur as a consequence of the rigidification of the position of the donor O atoms of the ketoester ligands that find themselves locked when coordinated to the two Ir(III) centres.

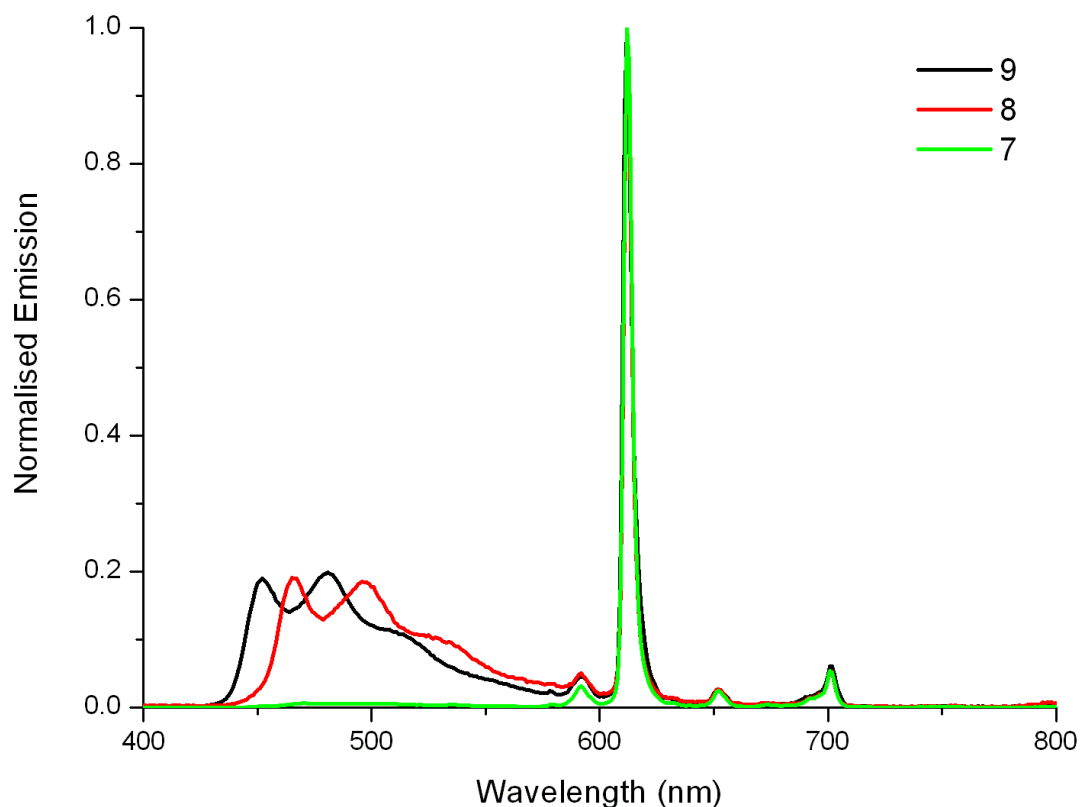


Figure 7: Emission profiles for dyads 7-9

In the case of complex **7**, only emission from the Eu(III) fragment is observed, irrespective of the excitation wavelength (*see below*, Figure 8), with an almost undetectable contribution from the emission of the individual Ir(III) units. It is also notable that the excited state lifetime measured at 470 nm, corresponding to the emission of the Ir(III) moiety, was found to be 0.12 μs , thus shorter than the lifetime of 0.81 μs measured for **10**. This behaviour is attributable to an Ir(III) \rightarrow Eu(III) energy transfer, which is plausible on considering the energy of the Ir(III) triplet state donor, 20800 cm^{-1} , and the $^5\text{D}_0$ accepting state of Eu(III), 17000 cm^{-1} .

Complex **9**, containing the fluorinated Ir(F₂ppy)₂ end-units, displays an emission profile with a contribution from both the Ir(III) centre, at 452 and 482 nm, and the Eu(III) centre, at 612 nm. By monitoring the emission profile with an excitation wavelength ranging between 300 and 350 nm (*see below*, Figure 8), a dominant Ir(III) component is observed. This component is characterized by an excited state lifetime of 0.30 μs , shorter than 1.04 μs measured for complex **12**. This behaviour is consistent with partial Ir(III) \rightarrow Eu(III) energy transfer, which can't be easily quantified due to the inability to selectively excite either the Ir(III) or the Eu(III) moiety in the dyad. The partial nature of the energy transfer could be tentatively ascribed to the raised energy of the Ir(III) triplet state energy, 21500 cm^{-1} , in respect to the value found for **7**. The emitted colour of complex **9** ranges from blue ($\lambda_{\text{exc}} = 300\text{-}330$ nm) to green ($\lambda_{\text{exc}} = ca. 330\text{-}350$ nm).

The dyad **8**, containing the “mixed” fragment [Ir(ppy)(F₂ppy)], shows a behaviour that lies in between the two extreme cases represented by dyads **7** and **9**. Also in this case, the lifetime of the Ir(III) component in the emission is 0.30 μs, shorter than the one found in **11**, 0.95 μs. By spanning the excitation wavelength from 300 to 350 nm (*see below*, Figure 8), is possible to finely balance the blue-emission of the Ir(III) end-units and the red one of the Eu(III) centre. In particular, an almost “pure” white light is observed upon excitation at 320 nm (Commission Internationale de l’Eclairage (CIE) coordinates: X = 0.333, Y = 0.359, Table 3). Due to the dual absorption of Ir(III) and Eu(III) in such a wavelength range, the observed white emission can be probably ascribed to the occurrence of radiative processes arise from the Ir(III) units, the Eu(III) core and from Ir(III)-Eu(III) energy transfer effects.

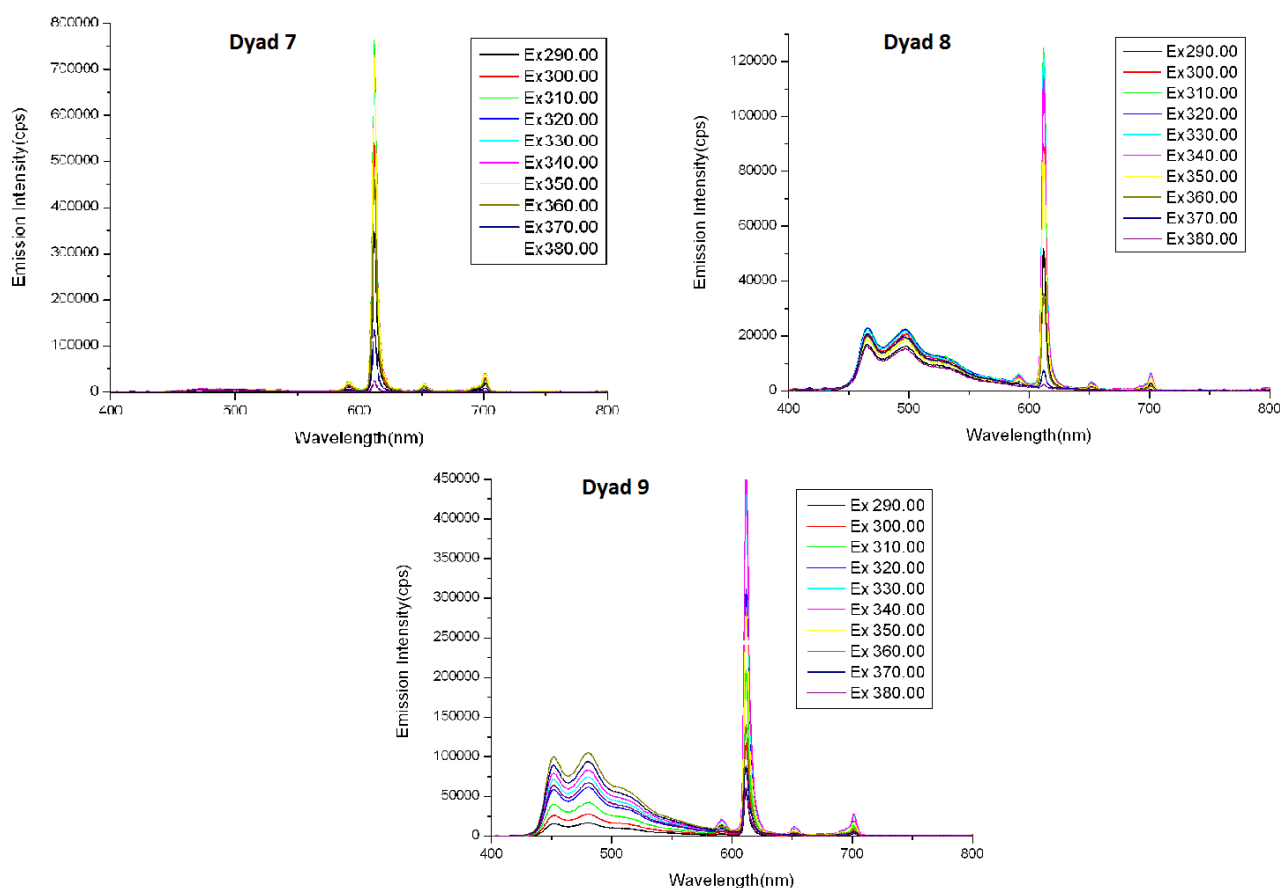


Figure 8: Emission maps of dyads 7-9

The CIE coordinate for each complex at every excitation wavelength are reported in Table 3.

Table 3: CIE coordinates for dyads **7-9**

Complex 7										
λ_{exc} (nm)	290	300	310	320	330	340	350	360	370	380
X	0.611	0.621	0.630	0.629	0.628	0.626	0.629	0.617	0.539	0.356
Y	0.337	0.335	0.335	0.335	0.335	0.335	0.333	0.335	0.342	0.358
Z	0.053	0.044	0.035	0.035	0.037	0.040	0.038	0.049	0.119	0.287

Complex 8										
λ_{exc} (nm)	290	300	310	320	330	340	350	360	370	380
X	0.285	0.313	0.336	0.333	0.338	0.341	0.320	0.250	0.202	0.193
Y	0.364	0.362	0.360	0.359	0.358	0.356	0.356	0.361	0.365	0.362
Z	0.351	0.325	0.304	0.308	0.304	0.303	0.323	0.389	0.433	0.444

Complex 9										
λ_{exc} (nm)	290	300	310	320	330	340	350	360	370	380
X	0.278	0.301	0.316	0.318	0.333	0.328	0.270	0.218	0.204	0.202
Y	0.276	0.278	0.279	0.279	0.281	0.280	0.271	0.263	0.262	0.262
Z	0.445	0.421	0.404	0.403	0.387	0.392	0.459	0.519	0.534	0.536

As observed, a red emission is always recorded for dyad **7**, and the emission is independent from the excitation wavelength. This can be explained with a complete energy transfer between the Ir(III) fragment and the Eu(III) centre. The emitted colour of complex **9** ranges from blue ($\lambda_{\text{exc}} = 300\text{-}330$ nm) to green ($\lambda_{\text{exc}} = ca. 330\text{-}350$ nm) and indicates a partial energy transfer between the two metal centres, with the major contribute arising from the fluorinated Ir(III) fragments. Finally, in dyads **8** is possible to control the contribute of each metal centre in the emission, by varying the excitation wavelength. In detail, an almost “pure” white emission is observed with a $\lambda_{\text{exc}} = 320$ nm, with a perfect balance of the emitted colours.

As expected, the intensity of the Ir(III)-based emission increases for each dyad when measured in deaerated solution or at 77 K. This effect does not cause any particular appreciable variation in the red or blue emissions originating from dyads **7** and **9**, respectively, but it results in the change from white to blue-green in the case of dyad **8**. When measured as neat solid samples at room temperature, all dyads display only red emission, due to the intermolecular quenching effect. In fact, upon dispersion of the dyads within a PMMA matrix (20% w/w), an analogous emission to those in diluted DCM solutions could be measured, and “pure” white emission could be observed from dyad **8** upon excitation at 320 nm (Figure 9).

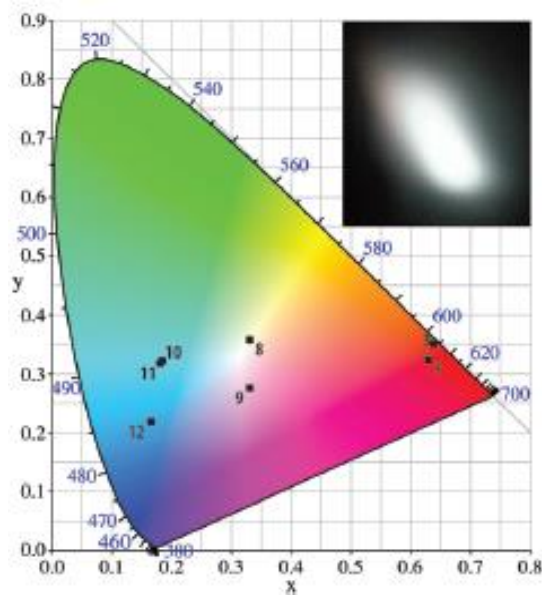


Figure 9: CIE diagram of complexes **3**, **7-12** in DCM solution and white emission of **8** in PMMA matrix

9.2 Conclusions

We have successfully designed and synthesized a bifunctional ligand able to simultaneously coordinate Ir(III) and Eu(III) in order to create new heterometallic complexes, that show the characteristic emission pattern of both metal centers. In particular, an appropriate tuning of the cyclometalating ligands on the Ir(III) units leads to a structure that possesses a perfect balance between the blue and the red emissive component to give an overall white emission. In detail, complex **8** shows white light emission in DCM solution and in the solid state when dispersed within a PMMA matrix. Excitation at 320 nm results in “pure” white light emission in these cases.

9.3 Experimental section

General informations

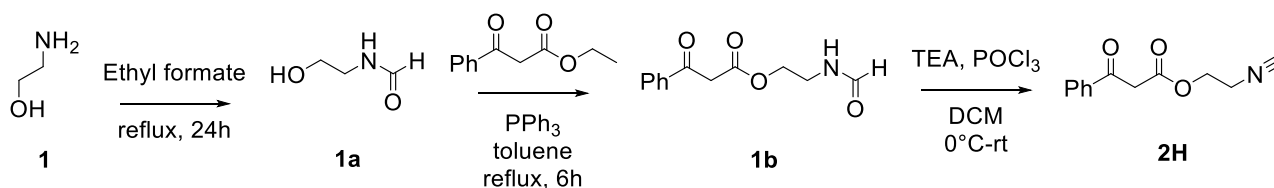
The solvents and chemicals were used as received from sellers, unless otherwise mentioned. NMR spectra were recorded by using a Varian Mercury 400 MHz or a Varian Inova 300 MHz spectrometer with tetramethylsilane as the internal standard. Elemental analyses were performed on a ThermoQuest Flash 1112 series EA instrument. ESI-MS analysis were performed by direct injection of acetonitrile solutions of the compounds using a WATERS ZQ 4000 mass spectrometer. UV/Vis absorption spectra were measured on a Varian Cary 4 double-beam UV-Vis spectrometer and baseline corrected. Steady-state emission spectra were recorded on an Edinburgh FLS920P spectrofluorimeter equipped with a 450 W Xenon arc lamp, double excitation and single emission monochromators and a peltier cooled Hamamatsu R928P

photomultiplier tube (185-850 nm). Emission and excitation spectra were corrected for source intensity (lamp and grating) and emission spectral response (detector and grating) by calibration curve supplied with the instrument. Emission lifetimes were determined on the same Edinburgh instrument with the Time Correlated Single Photon Counting (TCSPC) technique using pulsed picosecond LEDs (ELED 295 or ELED 360, FWHM <800 ps, repetition rates between 10 kHz and 1 MHz) as the excitation source and the above-mentioned R928P PMT as detector. The goodness of fit was assessed by minimizing the reduced χ^2 function and visual inspection of the weighted residuals. The emission quantum yields were determined according to the optically dilute solutions method in ACN solutions with reference to Ru(bpy)₃Cl₂ as the standard (r) according to Equation (1),²¹ where *I* refers to the area of the emission peaks of the complex and the reference, *A* to their absorptions and *n* is the refractive index of the corresponding solvents.

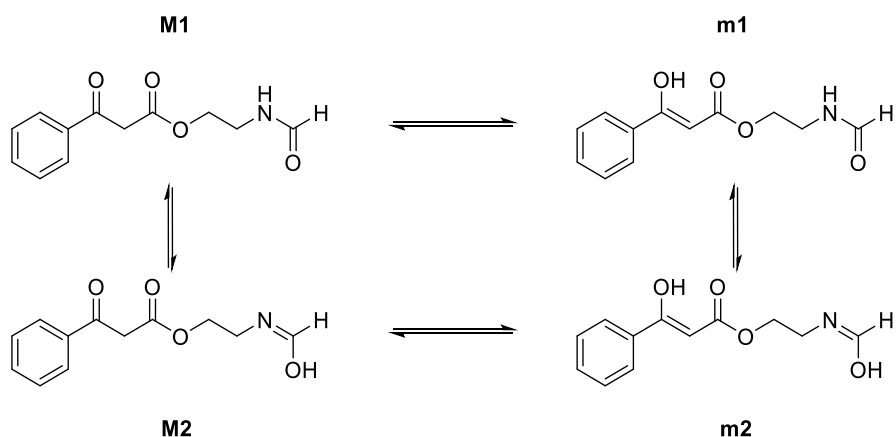
$$\Phi = \Phi_r \frac{I}{I_r} \frac{A_r}{A} \frac{n^2}{n_r^2} \quad (1)$$

Synthesis of ligand 2H

Ligand **2H** was obtained according the following synthetic scheme:

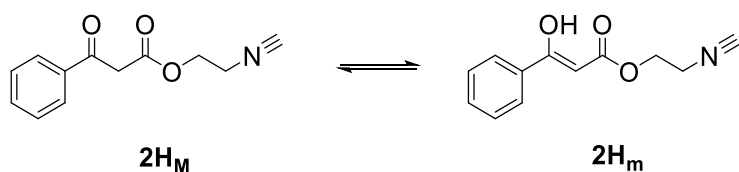


A solution of 2-aminoethanol **1** (2.40 mL, 40.0 mmol) in ethyl formate (4.20 mL) was refluxed for 24 hours. The solution was cooled and the solvent was evaporated to give crude **1a** as brown oil that was used in the next step without purification. To a stirred solution of crude **1a** (3.60 g) and ethyl benzoylacetate (7.00 mL, 40.4 mmol) in toluene (200 mL) triphenylphosphine (1.05 g, 4.0 mmol) was added. The resulting reaction mixture was refluxed and the progress of the reaction was monitored by TLC. After complete conversion of the substrate (6 hours), the solvent was evaporated and the product was purified by column chromatography on silica gel (DCM/MeOH = 97:3) to afford **1b** (3.58 g, 38% yield) as a mixture of keto-enol and amide-imidic acid tautomers at the equilibrium, represented in the following figure as Major (M1, M2) and minor (m1, m2) species. In the ¹H NMR description we indicated with M the sum of M1 and M2 species and with m the sum of m1 and m2 species.



¹H NMR (300 MHz, CDCl₃) δ 12.31 (s, 1H_{m1}), 12.27 (s, 1H_{m2}), 8.17-7.99 (m, 1H_{M+m}), 7.90-7.83 (m, 2H_M), 7.79-7.68 (m, 2H_m), 7.62-7.53 (m, 3H_m), 7.48-7.32 (m, 3H_M), 6.42-5.78 (m, 1H_{M+m}), 5.62 (s, 1H_m), 4.31-4.13 (m, 2H_{M+m}), 4.00 (s, 2H_{M1}), 3.99 (s, 2H_{M2}), 3.60-3.50 (m, 2H_{M+m}). ¹³C NMR (75 MHz, CDCl₃) δ 36.8 (CH₂), 37.2 (CH₂), 40.6 (CH₂), 45.6 (CH₂), 45.8 (CH₂), 62.8 (CH₂), 63.8 (CH₂), 64.6 (CH₂), 86.8 (CH), 126.1 (CH), 128.4 (CH), 128.5 (CH), 128.6 (CH), 128.7 (CH), 128.9 (CH), 131.5 (CH), 131.9 (CH), 132.0 (CH), 132.1 (CH), 132.1 (CH), 134.1 (CH), 135.6 (C), 161.6 (CH), 164.8 (CH), 167.5 (C), 172.1 (C), 172.9 (C), 192.7 (CH), 193.2 (CH).

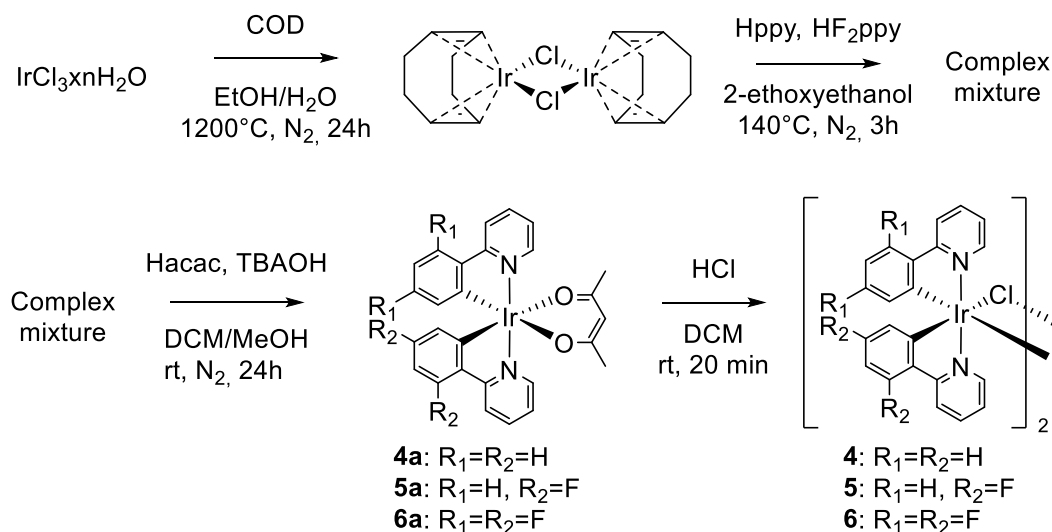
Then a DCM solution (50 mL) of **1b** (3.53 g, 15 mmol) and Et₃N (5.2 mL, 37.5 mmol) was cooled at 0°C, and phosphorous oxychloride (1.4 mL, 15.0 mmol) in 20 mL of DCM was added dropwise over a period of 10 minutes. After the reaction was completed, the reaction was quenched with saturated Na₂CO₃ aqueous solution at 0°C to and the product was extracted with DCM. The organic phase was washed with aqueous NH₄Cl, then dried over anhydrous MgSO₄ and the solvent evaporated. The residue was purified by column chromatography (silica gel, DCM/MeOH=99:1) to give **2** (0.65 g) in 20% yields as a mixture of tautomers **2H_M** and **2H_m** as depicted in the following figure:



¹H NMR (300 MHz, CDCl₃) δ 12.27 (s, 1H_m), 7.97-7.91 (m, 2H_M), 7.91-7.75 (m, 2H_m), 7.66-7.58 (m, 3H_m), 7.55-7.41 (m, 3H_M), 5.75 (s, 1H_m), 4.43-4.26 (m, 2H_{M+m}), 4.09 (s, 2H_M), 3.77-3.50 (m, 2H_{M+m}). ¹³C NMR (75 MHz, CDCl₃) δ 40.6 (t, CH₂), 45.5 (CH₂), 61.0 (CH₂), 62.0 (CH₂), 105.0 (CH), 126.2 (CH), 128.4 (CH), 128.6 (CH), 128.8 (CH), 128.9 (CH), 129.2 (CH), 131.7 (CH), 134.0 (CH), 135.7 (C), 167.1 (CO), 191.9 (CO). Anal. Calculated for C₁₂H₁₁NO₃ (217.22): C, 66.35; H, 5.10; N, 6.45 %. Found C, 66.58; H, 4.94; N, 6.29 %. ESI-MS: 218 [M⁺+1], 240 [M⁺+Na].

Synthesis of Ir(III) dimers 4-6

The synthesis of Ir(III) dimers **4-6** is reported in the following scheme.



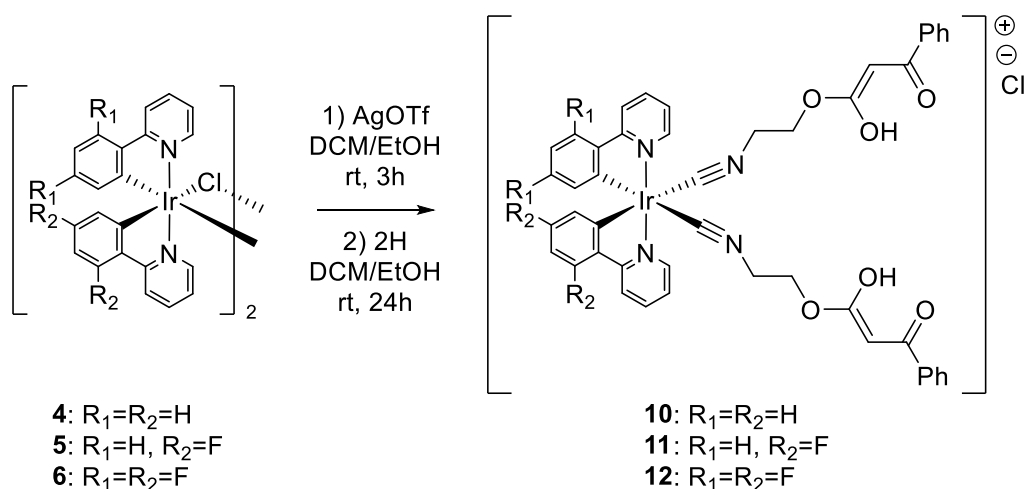
$[\text{Ir}(\text{COD})(\mu\text{-Cl})]_2$ precursor was prepared according to a reported procedure.²² $\text{IrCl}_3 \cdot x\text{H}_2\text{O}$ (150 mg, 0.5 mmol) was dissolved in a 2:1 mixture of EtOH and H_2O (5 mL), then 1,5-cyclooctadiene (0.5 mL, 4.0 mmol) was added and the solution was refluxed in nitrogen atmosphere for 24 hours. The resulting red precipitate was collected and washed with cold MeOH (20 mL). The product was obtained in 40% yields (67.8 mg) and was used in the next step without further purifications. The obtained $[\text{Ir}(\text{COD})(\mu\text{-Cl})]_2$ was dissolved in 1 mL of 2-ethoxyethanol, then 2-phenylpyridine (30 μL , 0.2 mmol) and 2-(2,4-difluorophenyl)pyridine (30 μL , 0.2 mmol) was added and the resulting mixture was refluxed in nitrogen atmosphere for 3 hours. The resulting yellow precipitate was collected and repetitively washed with MeOH (3 x 10 mL), and then dried. The yellow solid (84.1 mg, 0.074 mmol) was dissolved in DCM (6 mL) and added to a mixture of acetylacetone (30 μL , 0.3 mmol) and tetrabutylammonium hydroxide (70 μL , 0.3 mmol) dissolved in a solution of DCM and MeOH 3:1 (4 mL). The resulting mixture was stirred in nitrogen atmosphere for 24 hours. After this time, solvent was evaporated and the crude was purified by column chromatography (silica gel, DCM/Hexane=6:4) to give the desired products **4a**, **5a** and **6a**. Complex **4a** (30.6 mg, 0.05 mmol) was dissolved in DCM (6 mL) and a solution of HCl (2N in Et_2O , 100 μL , 0.15 mmol) was added. The mixture was stirred for 20 minutes, and after this time the solvent was evaporated. The resulting crude was washed with MeOH (5 mL) and filtrated. Dimer **4** was obtained as a yellow solid with an overall yields of 9% (24 mg). The same procedure was repeated with complexes **5a** and **6a**, and the corresponding dimers have been isolated with 11% yields for dimer **5** (26 mg) and 7% for dimer **6** (21 mg).

$[\text{Ir}(\text{ppy})_2(\mu\text{-Cl})]_2$ (**4**): ^1H NMR (400 MHz, CDCl_3) δ 9.26 (dd, $J = 0.8\text{-}6.0$ Hz, 4H), 7.88 (d, $J = 8.0$ Hz, 4H), 7.56 (dt, $J = 1.6\text{-}8.0$ Hz, 4H), 7.51 (dd, $J = 1.2\text{-}8.0$ Hz, 4H), 6.79 (dt, $J = 1.2\text{-}6.0$ Hz, 4H), 6.76 (dt, $J = 1.2\text{-}8.4$ Hz, 4H), 6.58 (dt, $J = 1.2\text{-}8.0$ Hz, 4H), 5.95 (dd, $J = 1.2\text{-}7.6$ Hz, 4H).

[Ir(ppy)(F₂ppy)(μ-Cl)]₂ (**5**): ¹H NMR (400 MHz, CDCl₃) δ 9.20 (dt, *J* = 0.8-5.6 Hz, 4H) 9.13 (dt, *J* = 0.8-5.8 Hz, 4H), 8.25 (d, *J* = 7.6 Hz, 4H), 7.88 (d, *J* = 8.2 Hz, 4H), 7.78-7.73 (m, 8H), 7.50 (ddd, *J* = 1.0-3.2-7.8 Hz, 4H), 6.82-6.74 (m, 12H), 6.59 (m, 4H), 6.26 (m, 4H), 5.82 (d, *J* = 7.8 Hz, 4H), 5.35 (dd, *J* = 1.2-9.2 Hz, 4H).
 [Ir(F₂ppy)₂(μ-Cl)]₂ (**6**): ¹H NMR (400 MHz, CDCl₃) δ 9.11 (ddd, *J* = 0.8-1.6-6.4 Hz, 4H), 8.30 (ddd, *J* = 0.4-0.8-9.2 Hz, 4H), 7.83 (dt, *J* = 1.2-8.4 Hz, 4H), 6.83 (ddd, *J* = 1.2-6.0-7.6 Hz, 4H), 6.34 (ddd, *J* = 2.0-8.8-12.4 Hz, 4H), 5.28 (dd, *J* = 2.0-9.2 Hz, 4H).

Synthesis of Ir(III) complexes 10-12

The synthesis of Ir(III) complexes **10-12** is reported in the following scheme.



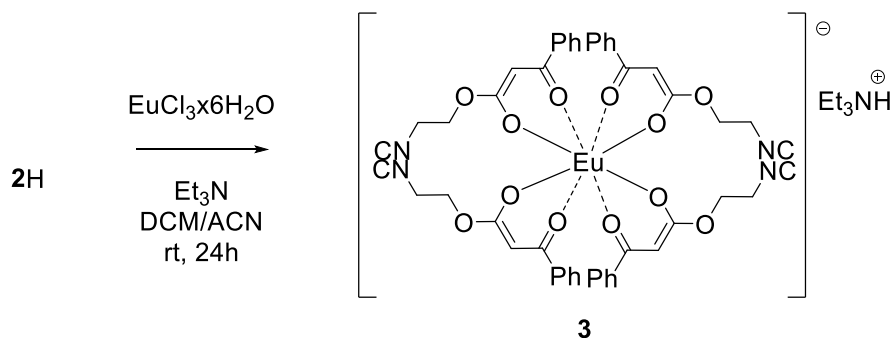
In a 50 ml round-bottom flask equipped with a stirring bar, the Ir(III) dimer **4** (10.7 mg, 0.01 mmol) was dissolved in a mixture of DCM/MeOH 1:1 (4 mL). Then AgOTf (7.7 mg, 0.03 mmol) was added and the mixture was stirred for 3 hours at room temperature. The solution was filtered to remove AgCl and the solvent evaporated. The residual solid was dissolved in 5 mL of DCM and ligand **2** (9.4 mg, 0.04 mmol) was added. After stirring 24 hours at room temperature the solvent was removed. The solid was dissolved in the minimum amount of DCM and Et₂O (10 mL) was added. The obtained precipitate was filtered and dried to give pure **10** (10.8 mg) in 50% yield. ¹H NMR (400 MHz, CDCl₃) δ 12.18 (s, 1H), 9.25-9.15 (m, 2H), 8.00-7.30 (m, 18H), 7.00-6.80 (m, 4H), 6.20-6.10 (m, 2H), 5.42 (s, 1H), 4.50-4.30 (m, 4H), 4.20-4.00 (m, 4H), 3.90-3.80 (m, 4H). Anal. Calculated for C₄₇H₃₈F₃IrN₄O₉S (1084.10): C, 52.07; H, 3.53; N, 5.17 %. Found C, 51.88; H, 3.64; N, 5.33 %. ESI-MS: 935[M⁺], 936 [M⁺+ 1], ESI-MS⁻: 149 [M⁻].

The same procedure was used to obtain **11** (11.6 mg, 52% yield): ¹H NMR (400 MHz, CDCl₃) δ 12.19 (s, 1H_{m1}), 12.16 (s, 1H), 9.25-9.10 (m, 2H), 8.30-8.20 (m, 1H), 8.10-7.20 (m, 16H), 7.00-6.80 (m, 2H), 6.45-6.30 (m, 1H), 6.10-6.00 (m, 1H), 5.75 (s, 1H), 5.65-5.55 (m, 1H), 5.40 (s, 1H), 4.60-4.25 (m, 4H), 4.25-4.00 (m, 4H), 4.00-3.90 (m, 4H). ¹⁹F NMR (400 MHz, CDCl₃) δ -78.19 (s), -106.47 (q, *J*_{CF} = 9.4 Hz), -109.05 (t, *J*_{CF} = 11.0 Hz). Anal. Calculated for C₄₇H₃₆F₅IrN₄O₉S (1120.08): C, 50.40; H, 3.24; N, 5.00 %. Found C, 50.18; H, 3.43; N, 5.21 %. ESI-MS⁺: 971[M⁺], 972 [M⁺+ 1], 149 [M⁻]; and **12** (11.3 mg, 49% yield): ¹H NMR (400 MHz, CDCl₃) δ 12.23 (s, 1H), 9.20-9.15 (m, 2H), 8.35-8.20 (m, 2H), 7.90-7.20 (m, 14H), 6.60-6.40 (m, 2H), 5.74 (s, 1H), 5.55-5.45

(m, 2H), 4.50-4.40 (m, 4H), 4.20-4.10 (m, 4H), 4.00-3.80 (m, 4H). ¹⁹F NMR (400 MHz, CDCl₃) δ -78.10 (s), -106.03 (q, *J*_{CF} = 10.2 Hz), -108.55 (t, *J*_{CF} = 12.4 Hz). Anal. Calculated for C₄₇H₃₄F₇IrN₄O₉S (1156.06): C, 48.83; H, 2.96; N, 4.85 %. Found C, 49.07; H, 2.82; N, 4.99 %. ESI-MS⁺: 1007 [M⁺], 1008 [M⁺¹], ESI-MS⁻: 149 [M⁻].

Synthesis of Europium complex 3

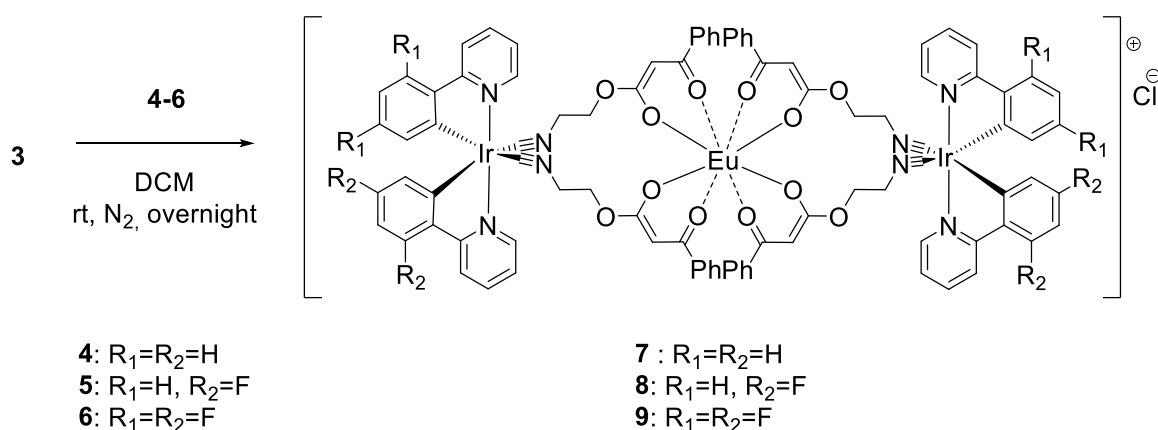
The synthesis of Eu(III) complex **3** is reported in the following scheme.



To a solution of **2** (18.8 mg, 0.08 mmol) in 1.0 mL of DCM and 0.2 mL of ACN, triethylamine (16 μL, 0.117 mmol) was added. After 5 minutes EuCl₃·6H₂O (7.3 mg, 0.02 mmol) was added and the reaction was vigorously stirred overnight at room temperature. Then the solvent was removed and the crude was dissolved in DCM (1 mL) and then Et₂O (5 mL) was added. The precipitated ammonium salt was filtered off and the solution evaporated to give **3** as whitish oil (15.7 mg, 70% yield). Anal. Calculated for C₅₄H₅₆EuN₅O₁₂ (1119.01): C, 57.96; H, 5.04; N, 6.26 %. Found C, 58.10; H, 4.95; N, 6.42 %. ESI-MS: 1017 [M⁻].

Synthesis of the Ir(III)₂-Eu(III) complexes 7-9

The synthesis of Ir(III)-Eu(III) dyads **7-9** is reported in the following scheme.



In a 50 ml round-bottom flask equipped with a stirring bar, Ir(III) dimer **4** (21.4 mg, 0.02mmol) was dissolved in DCM (1mL). Then complex **3** (22 mg, 0.02mmol) was added and the reaction mixture was stirred under N₂ at 30°C overnight. Complex **7** (41.1 mg) was isolated in quantitative yield by precipitation by addition of Et₂O. Anal. Calculated for C₉₂H₇₂ClEuIr₂N₈O₁₂ (2053.45): C, 53.81; H, 3.53; N, 5.46 %. Found C, 54.03; H, 3.72; N, 5.40 %. ESI-MS: 2018 [M⁺].

The same procedure was used for **8** (Anal. Calculated for C₉₂H₆₈ClEuF₄Ir₂N₈O₁₂ (2125.41): C, 51.99; H, 3.22; N, 5.27 %. Found C, 52.26; H, 3.15; N, 5.39 %. ESI-MS: 2089 [M⁺]) and **9** (Anal. Calculated for C₉₂H₆₄ClEuF₈Ir₂N₈O₁₂ (2197.38): C, 50.29; H, 2.94; N, 5.10 %. Found C, 49.93; H, 2.72; N, 5.31 %. ESI-MS: 2161 [M⁺]).

9.4 Bibliography

-
- ¹ J. Kido, M. Kimura, K. Nagai, *Science* **1995**, *267*, 1332.
 - ² Y. Sun, N. C. Giebink, H. Kanno, B. Ma, M. E. Thompson, S. R. Forrest, *Nature* **2006**, *440*, 908.
 - ³ H. C. Su, H. F. Chen, F. C. Fang, C. C. Liu, C. C. Wu, K. T. Wong, Y. H. Liu, S. M. Peng, *J. Am. Chem. Soc.* **2008**, *130*, 3413.
 - ⁴ C. Ulbricht, B. Beyer, C. Friebe, A. Winter, U. S. Schubert, *Adv. Mater.* **2009**, *21*, 4418.
 - ⁵ Y. Liu, M. Nishiura, Y. Wang, Z. M. Hou, *J. Am. Chem. Soc.* **2006**, *128*, 5592.
 - ⁶ J. Y. Li, D. Liu, C. W. Ma, O. Lengyel, C. S. Lee, C. H. Tung, S. Lee, *Adv. Mater.* **2004**, *16*, 1538.
 - ⁷ Q.-Y. Yang, J.-M. Lehn, *Angew. Chem. Int. Ed.* **2014**, *53*, 4572.
 - ⁸ S. Mukherjee, P. Thilagar, *Dyes Pigm.* **2014**, *110*, 2.
 - ⁹ Y. Z. Lee, X. W. Chen, M. C. Chen, A. A. Chen, J. H. Hsu, W. Fann, *Appl. Phys. Lett.* **2001**, *79*, 308.
 - ¹⁰ G. Tu, C. Mei, Q. Zhou, Y. Geng, L. Wang, D. Ma, X. Jing, F. Wang, *Adv. Funct. Mater.* **2006**, *16*, 101.
 - ¹¹ M. C. Gather, A. Köhnen, K. Meerholz, *Adv. Mater.* **2011**, *23*, 233.
 - ¹² M. D. Ward, *Coord. Chem. Rev.* **2007**, *251*, 1663.
 - ¹³ P. Coppo, M. Duati, V. N. Kozhevnikov, J. W. Hofstraat, L. De Cola, *Angew. Chem. Int. Ed.* **2005**, *44*, 1806.
 - ¹⁴ D. Sykes, I. S. Tidmarsh, A. Barbieri, I. V. Sazanovich, J. A. Weinstein, M. D. Ward, *Inorg. Chem.* **2011**, *50*, 11323.
 - ¹⁵ A. H. Shelton, I. V. Sazanovich, J. A. Weinstein, M. D. Ward, *Chem. Commun.* **2012**, *48*, 2749.
 - ¹⁶ S. Petoud, S. M. Cohen, J.-C. G. Bunzli, K. N. Raymond, *J. Am. Chem. Soc.* **2003**, *125*, 13324.
 - ¹⁷ D. Yang, Y. Long, J. Zhang, H. Zeng, S. Wang, C. Li, *Organometallics* **2010**, *29*, 3477.
 - ¹⁸ E. Baranoff, B. F. E. Curchod, J. Frey, R. Scopelliti, F. Kessler, I. Tavernelli, U. Rothlisberger, M. Grätzel, M. K. Nazeeruddin, *Inorg. Chem.* **2012**, *51*, 215.
 - ¹⁹ J. Li, P. I. Djurovich, B. D. Alleyne, M. Yousufuddin, N. N. Ho, J. C. Thomas, J. C. Peters, R. Bau, M. E. Thompson, *Inorg. Chem.* **2005**, *44*, 1713.
 - ²⁰ Molecular Weight Calculator version 6.5, downloaded from <http://ncrr.pnl.gov/software/>
 - ²¹ K. Binnemans, *Chem. Rev.* **2009**, *109*, 4283.
 - ²² D. Yang, Y. Long, J. Zhang, H. Zeng, S. Wang, C. Li, *Organometallics* **2010**, *29*, 3477.

10. New organic white emitters: conjugated carbazole-terpyridine systems

Carbazole (Cbz) and 2,2':6',2''-terpyridine (Tpy) are molecular units of outstanding importance in materials, coordination and supramolecular chemistry. Carbazole is a luminescent molecule,¹ and can be easily functionalized with a large variety of substituents^{2,3} or used for the preparation of polymeric material. For instance, polycarbazoles has been extensively used as hole transporters, electron donors or blue emitters in optoelectronic devices, thanks to their electric and optical properties.^{4,5} On the other hand, 2,2':6',2''-terpyridine and derivatives have been widely studied, especially in the area of metal-supramolecular complexes involving, among others, Ru(II), Os(II) and Zn(II) ions.^{6,7,8} Their optical, electrochemical, luminescent, magnetic, catalytic and therapeutic properties make them attractive for applications in the areas of solar energy conversion, optoelectronic devices, sensors and medicinal chemistry.^{9,10,11,12}

Despite the great number of papers related to Cbz- and Tpy- based organic and inorganic photoactive systems, only a limited numbers of reports studied to properties of systems where these two subunits are combined together.^{13,14,15,16}

In this context, my group decides to prepare different Cbz-Tpy architectures, taking advantage of the electron properties of these subunits. In detail, Cbz shows remarkable electron donor properties, while Tpy is known to be an excellent electron acceptor. The subunits can be directly link together through a conjugated system, in order to prepare D- π -A architectures.^{17,18} D- π -A molecules have found different fields of application in material science, including nonlinear optics and fluorescent probes.^{19,20} One of the key properties of D- π -A systems is the character of their photophysical behaviour. In fact, they may exhibit intramolecular charge-transfer (ICT) that leads to a red-shifts of absorption and/or emission bands related to those arising from the local excited (LE) states centred on the separated moieties.²¹

Preliminary studies carried out on these molecules showed interesting results:²² the chemical and photophysical properties of Cbz-Tpy containing systems can be finely tuned by changing the spacers between the two terminal subunits. In detail, moving from a short distance to a longest one, and changing the conjugation of the linker, is possible to observe very different properties. Moreover, for some of the synthesized molecules, emission of white light was obtained, though with very low quantum yields.

In this context, the goal of the project was to synthesize new carbazole-terpyridine containing systems where the two terminal units are connected with different spacers, both aromatic and triple bonds, in order to change the conjugation degree and trying to obtain more stable architectures, enhancing the white light emission's quantum yields. Furthermore, the presence of the terminal terpyridyl group make these systems suitable for chelating transitions metal, in order to prepare luminescent complexes.

10.1 Results and discussion

10.1.1 Synthesis

In order to explore the effect of the linker on the photophysical properties of Cbz-Tpy containing systems, we designed and synthesized a library of molecules, illustrate in Figure 1, with different aromatic linkers.

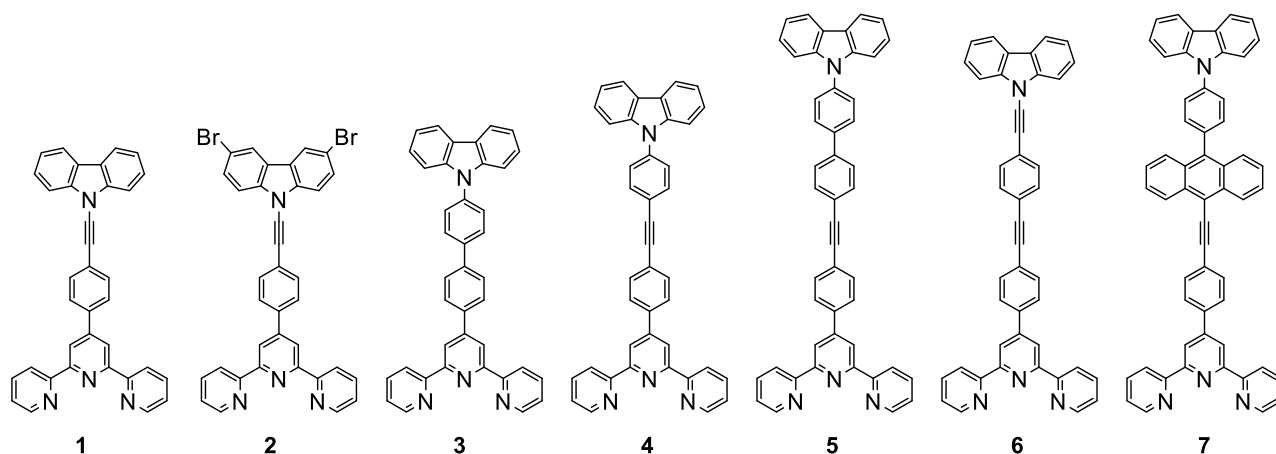


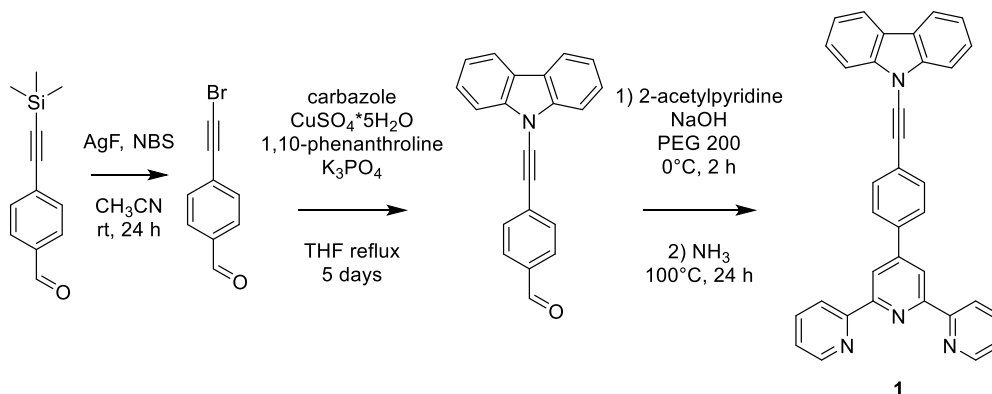
Figure 1: Representation of target carbazole-terpyridine systems

The synthesis of terpyridine-carbazole containing compounds is usually quite difficult. Indeed the biggest problem is the isolation of the final product from the impurities that can be present, generally terpyridine derivatives, with almost the same polarity. For this reason, purification using common strategies, such as column chromatography, generally failed. According with these premises, we opted for precipitation and recrystallization techniques, exploiting the low solubility of structurally complex terpyridines in methanol. However, yields of the purified product are generally low, so an optimization of this step is surely required in the next future.

The synthetic approach usually proceed via a first step where the spacer is formed and functionalized, then the carbazole moiety is linked to the spacer, and, as last step, the terpyridine is formed through a condensation.

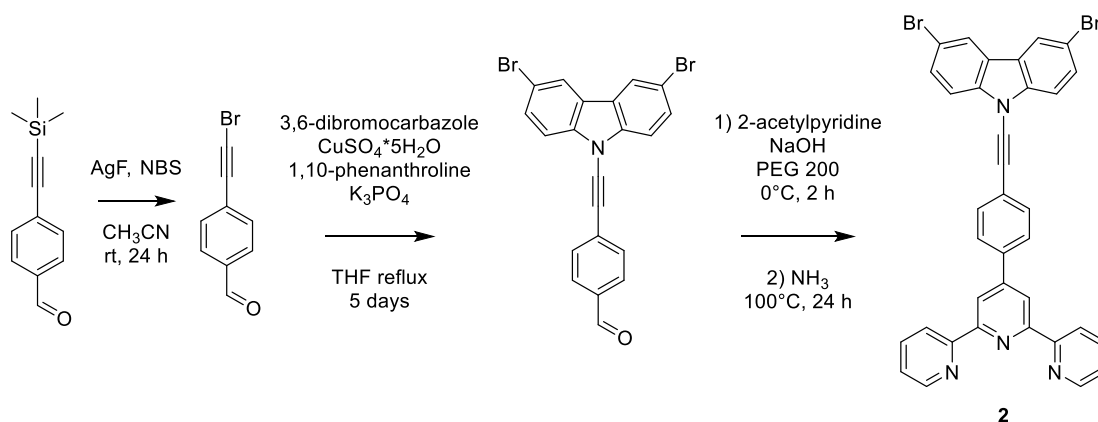
Molecule **1** has been prepared following a described procedure²² and the synthesis is reported in Scheme 1. Starting from TMS-protected ethynyl-benzaldehyde, the α -bromoalkyne derivative has been prepared in 87% yield through treatment with *N*-bromosuccinimide in presence of AgF. This derivative has been then reacted with carbazole in an Ullmann-type coupling, promoted by copper(II) sulphide, giving the desired intermediate in 75% yield. The formed compound has been finally reacted with 2-acetylpyridine in the

presence of KOH and aqueous ammonia as nitrogen source, led to carbazole-terpyridine **1** in 60% yield under mild reaction conditions.



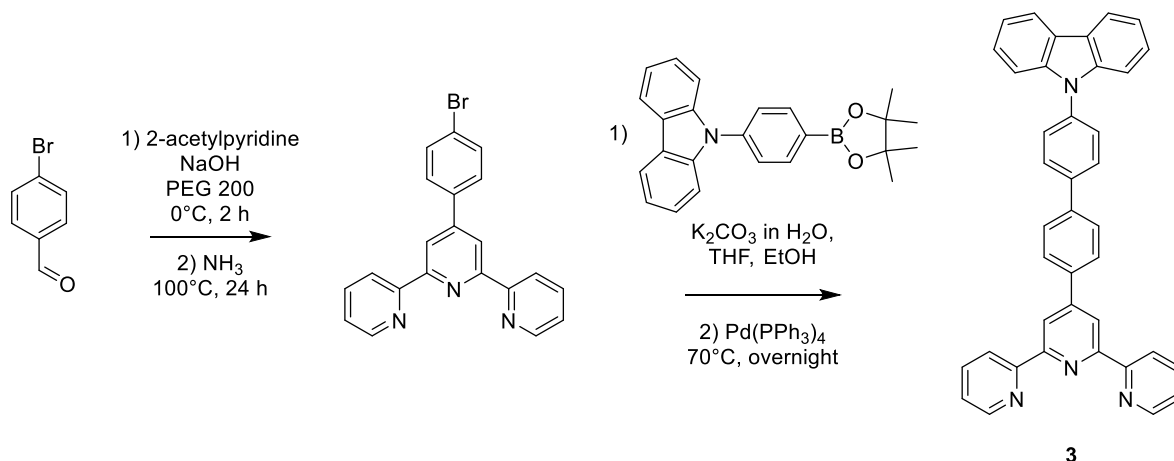
Scheme 1: Synthesis of molecule **1**

For molecule **2**, the synthesis is similar of that described for target molecule **1**, employing 3,6-dibromocarbazole in the Ullmann coupling, giving the bromo-carbazole derivative in 43% yield. The final condensation lead to the isolation of the carbazole-terpyridine system **2** in 30% yield, as reported in Scheme 2.



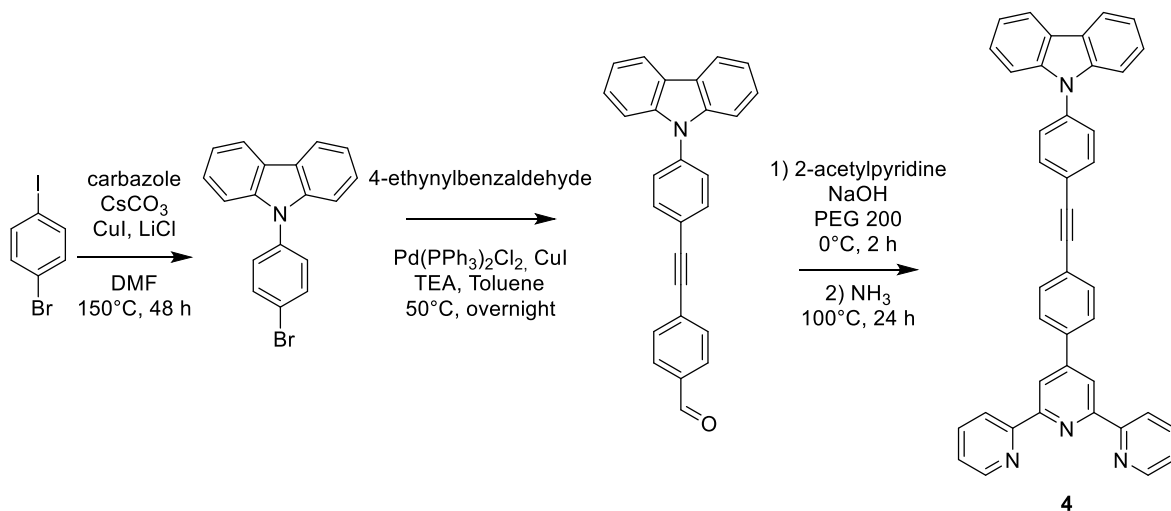
Scheme 2: Synthesis of molecule **2**

Molecule **3** is prepared starting from commercially available *p*-bromo-benzaldehyde. The condensation with 2-acetylpyridine in presence of KOH and ammonia lead to terpyridine intermediate in 73% yield. The following step involve the palladium catalysed Suzuki coupling with 9*H*-carbazole-9-(4-phenyl) boronic acid pinacol ester, in order to obtain the target carbazole-terpyridine **3** in 25% yield, as reported in Scheme 3.



Scheme 3: Synthesis of molecule 3

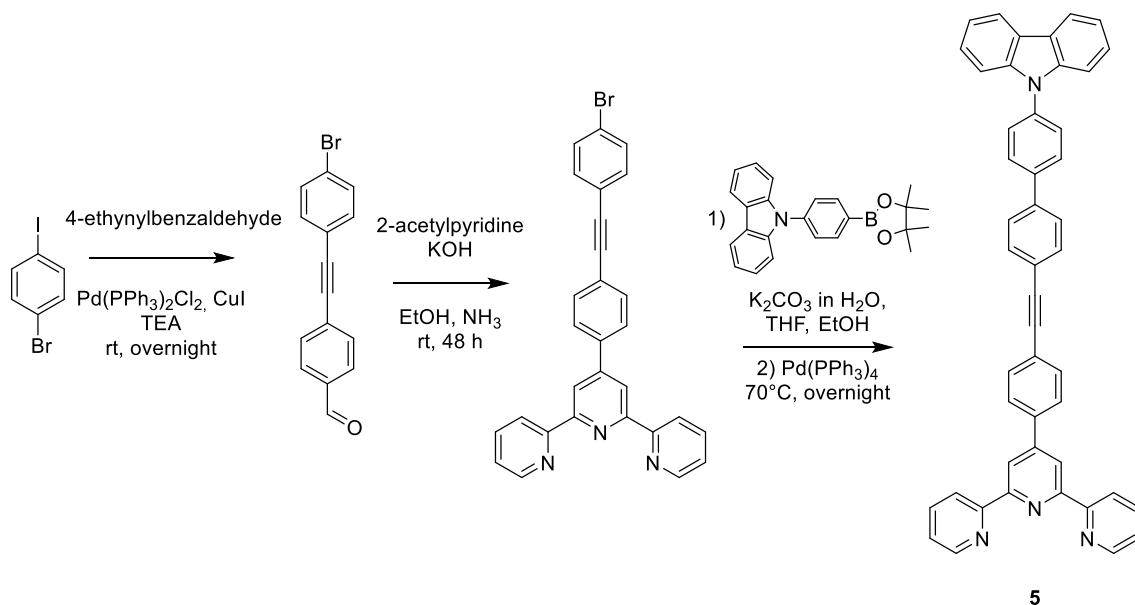
Molecule **4** is prepared starting from *p*-iodo-bromobenzene, which selectively reacts with carbazole in a copper(I) promoted coupling, leaving intact the Br-group.²³ The desired product is obtained in 71% yield. The intermediate is then reacted with *p*-ethynylbenzaldehyde in a palladium-catalysed Sonogashira coupling, which lead to the aldehyde derivative in 22% yield. Finally, the condensation of the obtained compound with 2-acetylpyridine to form the terpyridine moiety in performed, and the desired product **4** can be obtained in 35% yield, as reported in Scheme 4.



Scheme 4: Synthesis of molecule 4

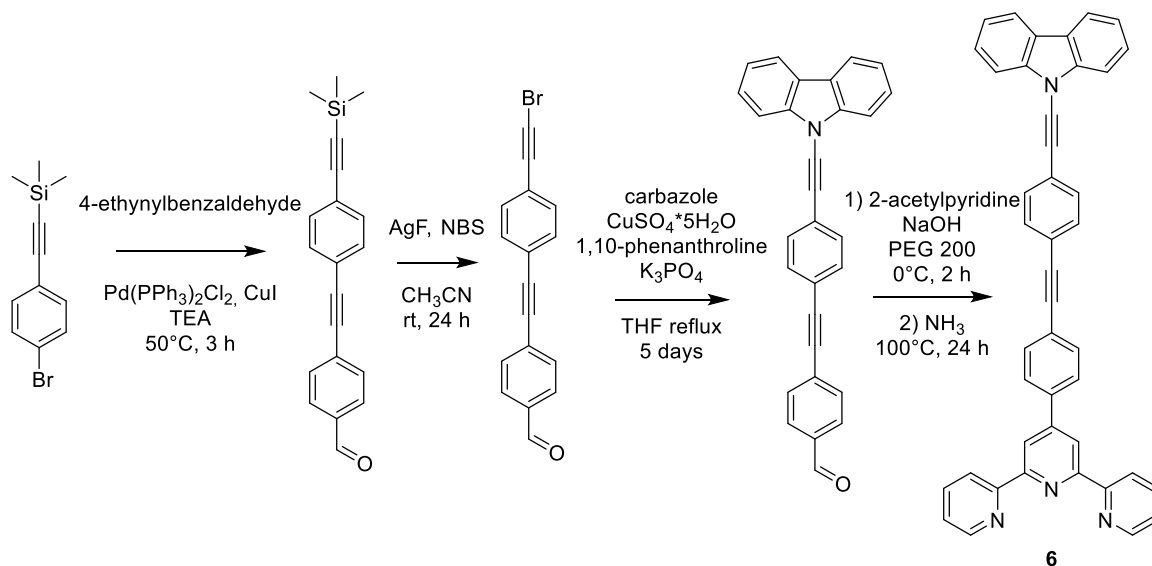
Compound **5** has been prepared following the synthetic procedure reported in Scheme 5. *p*-Iodo-bromobenzene was react in a Sonogashira coupling with *p*-ethynylbenzaldehyde, giving the linker with both aldehyde and bromine functionalities in 94% yield. Then, the terpyridine moiety was synthesized in 15% yield through reaction with 2-acetylpyridine in presence of KOH and ammonia. The final product was then

achieved by Suzuki coupling with 9*H*-carbazole-9-(4-phenyl) boronic acid pinacol ester, which lead to the formation of compound **5** in 30% yield.



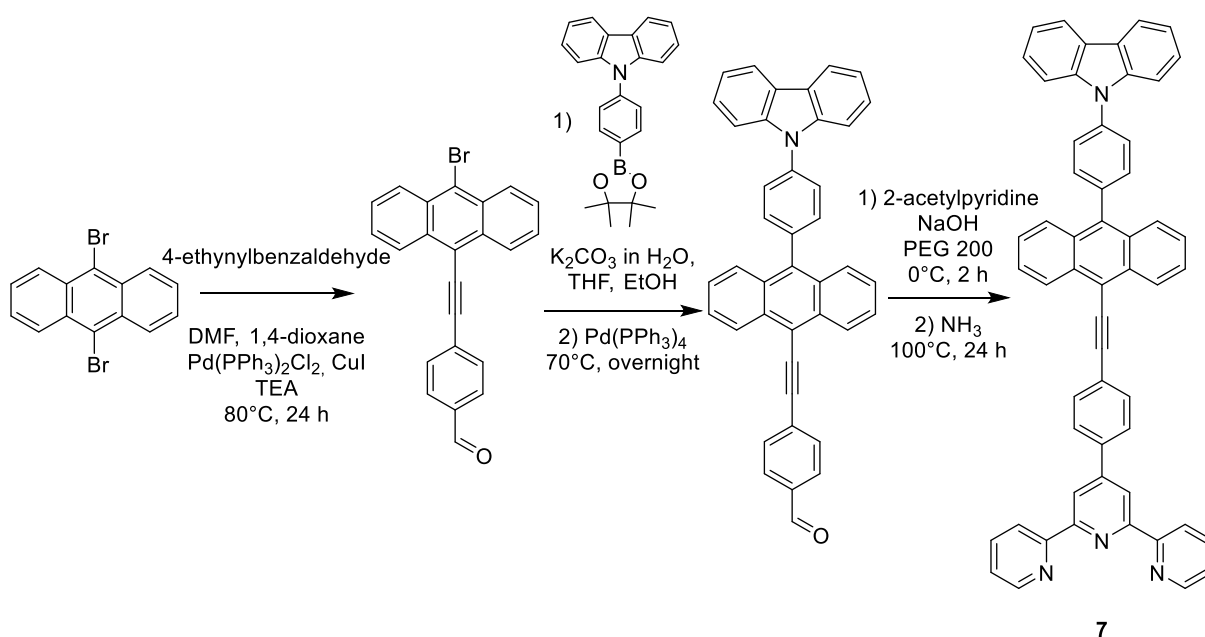
Scheme 5: Synthetic route to molecule **5**

The synthetic procedure for compound **6** is reported in Scheme 6. The TMS-protected *p*-ethynyl-bromobenzene undergoes to palladium-catalysed Sonogashira coupling with *p*-ethynylbenzaldehyde giving the desired product in 44% yield. Then, the desired α -bromoalkyne is synthesized by reaction with *N*-bromosuccinimide and AgF, leading to the isolation of the product in 78% yield. The so obtained intermediate was reacted with carbazole in the Ullmann-type copper(II) catalysed coupling, giving the carbazole derivative in 47% yield. Final condensation with 2-acetylpyridine and ammonia lead to the desired product **6** that can be isolated in 15% yield.



Scheme 6: Synthesis of molecule 6

Finally, we tried to introduce an anthracene moiety as spacer between the two terminal units. The synthetic strategies for compound 7 is reported in Scheme 7. 9,10-Dibromoanthracene was reacted with *p*-ethynylbenzaldehyde in a palladium-catalysed Sonogashira coupling, giving the mono-substituted product in 35% yield. It was then reacted with 9*H*-carbazole-9-(4-phenyl) boronic acid pinacol ester in a Suzuki coupling in order to attach the carbazole moiety to the formed linker, giving the desired derivative in 38% yield. The final condensation of the terminal aldehyde with 2-acetylpyridine lead to the isolation of compound 7 in 15% yield.



Scheme 7: Synthetic route to molecule 7

10.1.2 Photophysical properties

Some preliminary analysis have been carried out, regarding the emission of the synthesized compounds in different solvents. These results are reported in Figure 2 (Emission spectra in toluene, see below) and Figure 3 (Emission spectra in benzonitrile, see below).

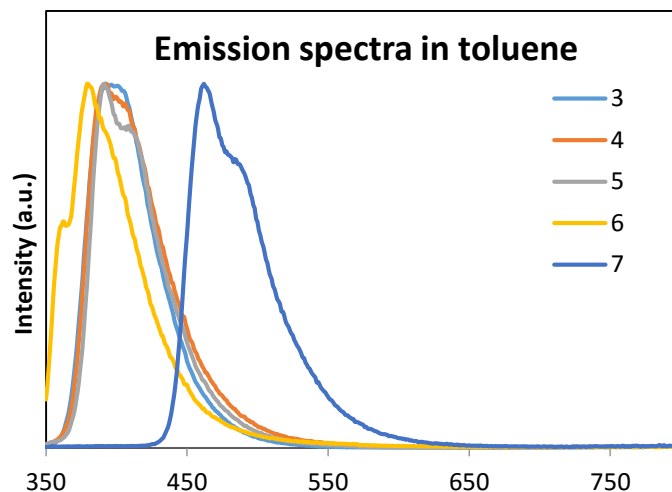


Figure 2: Emission spectra of compounds 3-7 in toluene; $\lambda_{\text{ex}} = 320$ nm

All the compounds display very similar emitting properties, with emission maxima centered in the range between 380-394 nm. A different behaviour can be observed in the case of molecule 7, with an emission maxima centered at 462 nm due to the presence of the anthracene moiety, which is responsible for a red shift of about 80 nm.

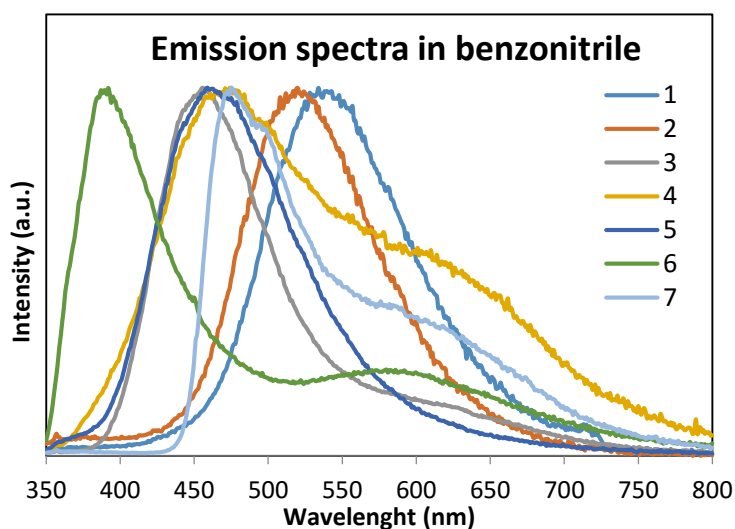


Figure 3: Emission spectra of compounds 3-7 in benzonitrile; $\lambda_{\text{ex}} = 320$ nm

When dissolved in benzonitrile, molecules **1-7** show a different behaviour. The polarity of the solvent shifts the emission maxima towards lower energies, as observed for almost all the compounds except **6**. Moreover, all the bands appear now broader.

Another very interesting feature is the presence of a shoulder that can be observed especially for compounds **4**, **5** and **6**. This shoulder, centered respectively at 578 nm for molecule **6**, 592 nm for molecule **7** and 614 nm for molecule **5**, make these compounds interesting candidates for the generation of white light.

10.2 Conclusions

We have successfully designed and synthesized different carbazole-terpyridine containing compounds, where the two terminal moieties are linked with different conjugated systems.

Compounds **1-7** have been obtained within satisfactory yields, and their photophysical properties have been partially investigated.

Based on these preliminary results, carbazole-terpyridine containing systems **5**, **6** and **7** have shown interesting emitting properties, displaying an almost white emission.

A complete characterization of the photophysical and the electrochemical properties and a theoretical study on such compounds are now going on, in order to well understand the behaviour of these systems and to rationalize the correlation between the structure and the luminescent properties of these architectures.

10.3 Experimental section

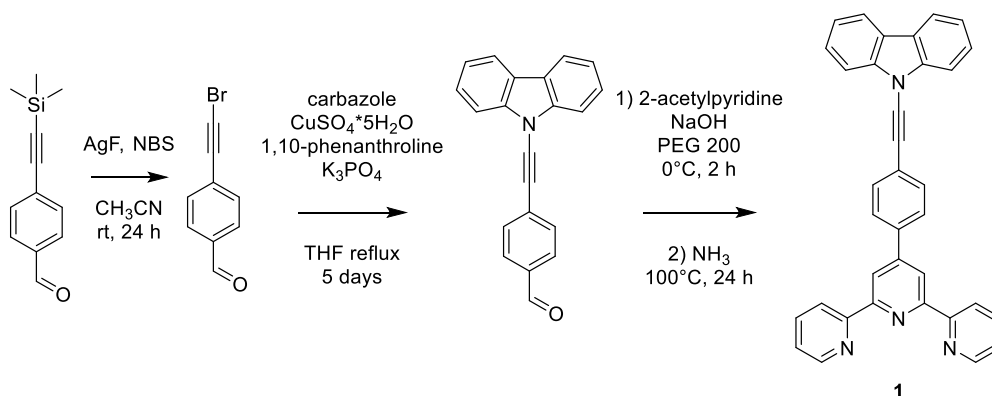
General informations

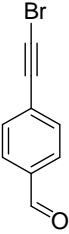
The solvents and chemicals were used as received from sellers, unless otherwise mentioned. NMR spectra were recorded by using a Varian Mercury 400 MHz or a Varian Inova 300 MHz spectrometer with tetramethylsilane as the internal standard. Elemental analyses were performed on a ThermoQuest Flash 1112 series EA instrument. ESI-MS analysis were performed by direct injection of acetonitrile solutions of the compounds using a WATERS ZQ 4000 mass spectrometer. UV/Vis absorption spectra were measured on a Varian Cary 4 double-beam UV-Vis spectrometer and baseline corrected. Steady-state emission spectra were recorded on an Edinburgh FLS920P spectrofluorimeter equipped with a 450 W Xenon arc lamp, double excitation and single emission monochromators and a peltier cooled Hamamatsu R928P photomultiplier tube (185-850 nm). Emission and excitation spectra were corrected for source intensity

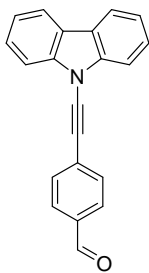
(lamp and grating) and emission spectral response (detector and grating) by calibration curve supplied with the instrument. Emission lifetimes were determined on the same Edinburgh instrument with the Time Correlated Single Photon Counting (TCSPC) technique using pulsed picosecond LEDs (ELED 295 or ELED 360, FWHM <800 ps, repetition rates between 10 kHz and 1 MHz) as the excitation source and the above-mentioned R928P PMT as detector. The goodness of fit was assessed by minimizing the reduced χ^2 function and visual inspection of the weighted residuals. The emission quantum yields were determined according to the optically dilute solutions method in ACN solutions with reference to Ru(bpy)₃Cl₂ as the standard (r) according to Equation (1),²⁴ where I refers to the area of the emission peaks of the complex and the reference, A to their absorptions and n is the refractive index of the corresponding solvents.

$$\Phi = \Phi_r \frac{I}{I_r} \frac{A_r}{A} \frac{n^2}{n_r^2} \quad (1)$$

Synthesis of molecule 1



 **4-(bromoethynyl)benzaldehyde.** 4-((trimethylsilyl)ethynyl)benzaldehyde (1.0 g, 4.95 mmol) and AgF (628 mg, 4.95 mmol) were dissolved in CH₃CN (50 mL). The reaction flask was wrapped in aluminium foil and NBS (881 mg, 4.95 mmol) was added. The mixture was stirred overnight at room temperature. Then the solid was filtered off and washed with CH₃CN (25 mL). The solution was evaporated and the resulting residue was dissolved in Et₂O and washed with water (3 x 25 mL). The organic part was dried on anhydrous MgSO₄ and then evaporated to give product as a white solid in 87% yield (893 mg). ¹H NMR (CDCl₃, 300 MHz) δ 10.01 (s, 1H), 7.83 (d, J = 8.5 Hz, 2H), 7.60 (d, J = 8.3 Hz, 2H).

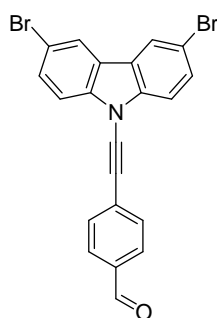
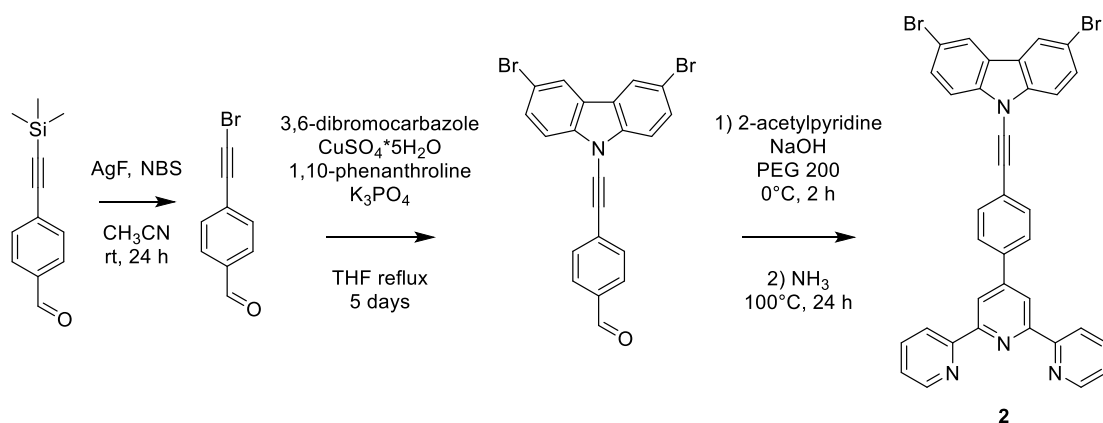


4-((9H-carbazol-9-yl)ethynyl)benzaldehyde. To a solution of 4-(bromoethynyl)benzaldehyde (351.8 mg, 1.68 mmol) in 17 mL of anhydrous THF, carbazole (255.8 mg, 1.53 mmol), K_3PO_4 (648.7 mg, 3.06 mmol), $CuSO_4 \cdot 5H_2O$ (76.4 mg, 0.306 mmol) and 1,10-phenanthroline (110.3 mg, 0.612 mmol) were added. The reaction mixture was purged with nitrogen and heated at 70°C for 5 days. The progress of the reaction was monitored using TLC analysis. Upon completion, the reaction mixture was dried *in vacuo* and the residue was dissolved in water

and extracted with DCM (3 x 15 mL). The combined organic phases were dried with anhydrous $MgSO_4$ and then evaporated. The crude residue was purified on silica gel flash chromatography using a mixture of CH_2Cl_2 /petroleum ether (2:8) to give product as a pale white solid in 75% yield (372.4 mg). 1H NMR ($CDCl_3$, 400 MHz) δ 10.02 (s, 1H), 8.04 (d, $J = 7.6$ Hz, 2H), 7.89 (d, $J = 8.4$ Hz, 2H), 7.74-7.70 (m, 4H), 7.55 (dt, $J_1 = 1.2$ Hz, $J_2 = 7.4$ Hz, 2H), 7.38 (dt, $J_1 = 1.1$ Hz, $J_2 = 7.5$ Hz, 2H).

4'-[4-(9H-Carbazol-9-ylethynyl)phenyl]-2,2':6',2''-terpyridine (**1**). 2-Acetylpyridine (163 μ L, 1.4 mmol) was added to a stirred suspension of crushed NaOH (56 mg, 1.4 mmol) in PEG 200 (1.2 mL) at 0° C. After 30 minutes 4-((9H-carbazol-9-yl)ethynyl)benzaldehyde (166 mg, 0.56 mmol) was added and stirring was continued at 0°C for 2 h. Then concentrated aqueous NH_3 solution (1.8 mL) was added and the suspension stirred at 100°C for 24 h. The precipitate was isolated by vacuum filtration and washed with water (50 mL) and ethanol (10 mL) to give a brown solid. Product **1** was obtained by recrystallization in MeOH in 60% yield (168.1 mg). 1H NMR ($CDCl_3$, 400 MHz) δ 8.79 (s, 2H), 8.76 (d, $J = 5.2$ Hz, 2H), 8.69 (d, $J = 8.0$ Hz, 2H), 8.06 (d, $J = 8.0$ Hz, 2H), 7.97 (d, $J = 8.0$ Hz, 2H), 7.90 (dt, $J_1 = 1.8$ Hz, $J_2 = 8.0$ Hz, 2H), 7.77 (t, $J = 8.8$ Hz, 4H), 7.56 (t, $J = 7.6$ Hz, 2H) 7.38 (t, $J = 6.4$ Hz, 4H); ^{13}C NMR ($CDCl_3$, 100 MHz) δ 156.1 (C), 156.0 (C), 149.4 (C), 149.1 (CH), 140.3 (C), 137.6 (C), 136.9 (CH), 131.6 (CH), 127.3 (CH), 126.8 (CH), 123.9 (CH), 123.8 (C), 123.6 (C), 122.2 (CH), 121.4 (CH), 120.4 (CH), 118.6 (CH), 111.3 (CH), 80.3 (C_{alk}), 74.6 (C_{alk}).

Synthesis of molecule 2

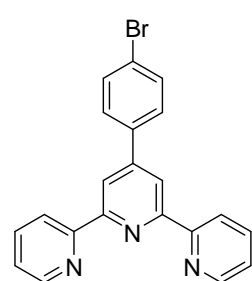
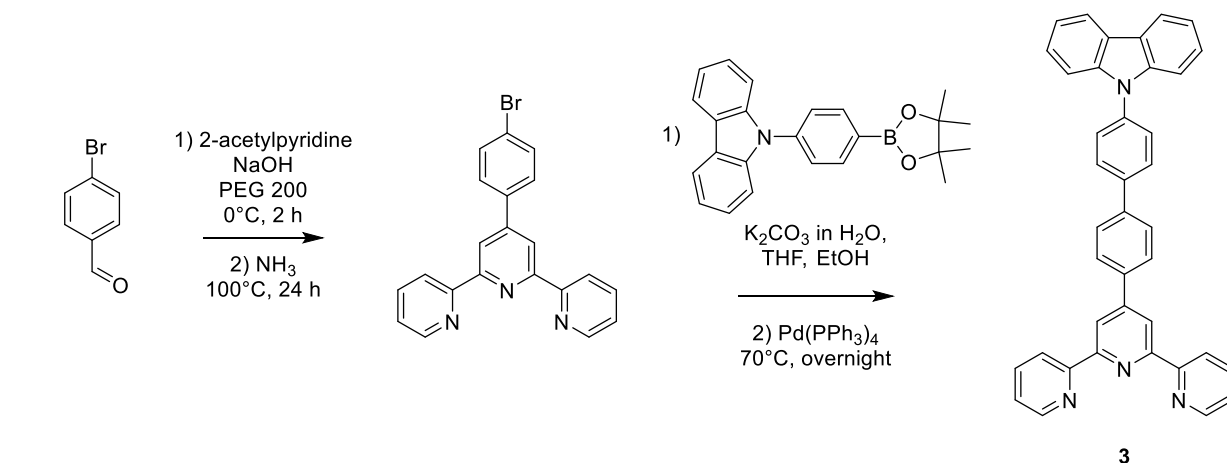


4-((3,6-dibromo-9H-carbazol-9-yl)ethynyl)benzaldehyde. To a solution of 4-(bromoethynyl)benzaldehyde (160.8 mg, 0.77 mmol) in 8 mL of anhydrous THF, 3,6-dibromocarbazole (225.7 mg, 0.7 mmol), K_3PO_4 (294.7 mg, 1.39 mmol), $CuSO_4 \cdot 5H_2O$ (34.9 mg, 0.14 mmol) and 1,10-phenanthroline (54.4 mg, 0.28 mmol) were added. The reaction mixture was purged with nitrogen and heated at 70°C for 5 days. The progress of the reaction was monitored using TLC analysis. Upon completion, the reaction

mixture was dried *in vacuo* and the residue was dissolved in water and extracted with DCM (3 x 15 mL). The combined organic phases were dried with anhydrous $MgSO_4$ and then evaporated. The crude residue was purified on silica gel flash chromatography using a mixture of EtOAc/petroleum (1:9) to give product as a light brown solid in 43% yield (149.8 mg). 1H NMR (CD_3Cl , 400 MHz) δ 10.05 (s, 1H), 8.13 (d, $J = 1.7$ Hz, 2H), 7.92 (d, $J = 8.7$ Hz, 2H), 7.75 (d, $J = 7.8$ Hz, 2H), 7.69 (dd, $J_1 = 1.9$ Hz, $J_2 = 8.4$ Hz, 2H), 7.61 (dd, $J_1 = 0.8$ Hz, $J_2 = 8.4$ Hz, 2H).

4'-[4-((3,6-dibromo-9H-carbazol-9-yl)ethynyl)phenyl]-2,2':6',2''-terpyridine (2). 2-Acetylpyridine (74 μ L, 0.66 mmol) was added to a stirred suspension of crushed NaOH (26.6 mg, 0.66 mmol) in PEG 200 (0.6 mL) at 0°C. After 30 minutes 4-((3,6-dibromo-9H-carbazol-9-yl)ethynyl)benzaldehyde (125.2 mg, 0.28 mmol) was added and stirring was continued at 0°C for 2 h. Then concentrated aqueous NH_3 solution (1.0 mL) was added and the suspension stirred at 100°C for 24 h. The precipitate was isolated by vacuum filtration and washed with water (50 mL) and ethanol (10 mL). The resulting solid was then washed with MeOH to give product **Lig2** as a brown solid in 30% yield (55.1 mg). 1H NMR (CD_3Cl , 400 MHz) δ 8.70 (s, 2H), 8.75 (d, $J = 5.4$ Hz, 2H), 8.70 (d, $J = 7.8$ Hz, 2H), 8.12 (d, $J = 1.8$ Hz, 2H), 7.97 (d, $J = 8.7$ Hz, 2H), 7.90 (dt, $J_1 = 1.8$ Hz, $J_2 = 6.9$ Hz, 2H), 7.74 (d, $J = 8.7$ Hz, 4H), 7.66 (d, $J = 1.8$ Hz, 2H), 7.64 (s, 2H) 7.38 (ddd, $J_1 = 1.3$ Hz, $J_2 = 4.8$ Hz, $J_3 = 7.5$ Hz, 2H); ^{13}C NMR (CD_3Cl , 100 MHz) δ 156.4, 156.3, 149.6, 149.4, 140.6, 137.9, 137.1, 131.9, 127.6, 127.0, 124.1, 124.0, 123.9, 122.4, 121.6, 120.6, 118.8, 111.6, 80.6, 74.8.

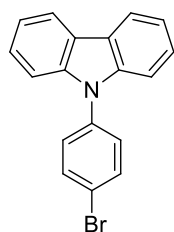
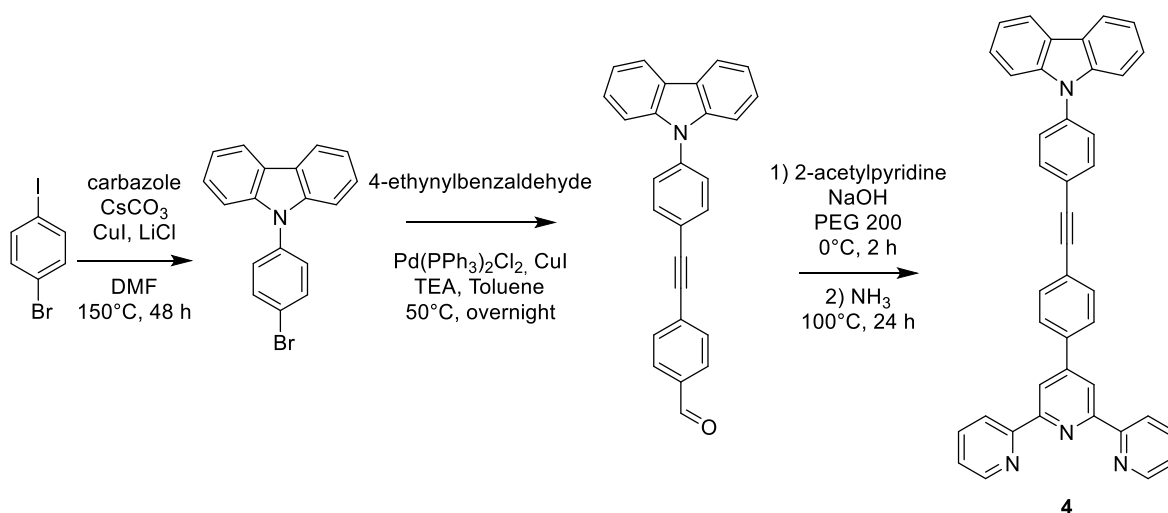
Synthesis of molecule 3



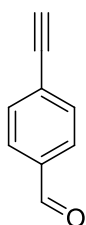
4'-((2,2':6',2''-terpyridin-4'-yl)-[1,1'-biphenyl]-4-yl)-2-bromo-2,2':6',2''-terpyridine (6). 2-acetylpyridine (1.3 mL, 12 mmol) was added to a stirred suspension of crushed NaOH (480.0 mg, 12 mmol) in PEG 200 (10 mL) at 0° C. After 30 minutes 4-bromobenzaldehyde (925.1 mg, 5 mmol) was added and stirring was continued at 0°C for 2 h. Then concentrated aqueous NH₃ solution (15.0 mL) was added and the suspension stirred at 100°C for 24 h. The precipitate was isolated by vacuum filtration and washed with water (50 mL) and ethanol (10 mL) to give product **6** as a white solid in 73% yield (1.42 g). ¹H NMR (CDCl₃, 400 MHz) δ 8.73 (dq, *J*₁ = 0.8 Hz, *J*₂ = 4.8 Hz, 2H), 8.71 (s, 2H) 8.67 (dt, *J*₁ = 1.0 Hz, *J*₂ = 8.0 Hz, 2H), 7.89 (dt, *J*₁ = 1.7 Hz, *J*₂ = 8.0 Hz, 2H), 7.78 (d, *J* = 8.8 Hz, 2H), 7.64 (d, *J* = 8.8 Hz, 2H), 7.36 (ddd, *J*₁ = 1.2 Hz, *J*₂ = 4.8 Hz, *J*₃ = 7.6 Hz, 2H).

9-((2,2':6',2''-terpyridin-4'-yl)-[1,1'-biphenyl]-4-yl)-9H-carbazole (3). To a solution of 4'-((2,2':6',2''-terpyridin-4'-yl)-[1,1'-biphenyl]-4-yl)-2-bromo-2,2':6',2''-terpyridine (194.5 mg, 0.5 mmol) in anhydrous THF (1.5 mL) under nitrogen atmosphere, 9H-carbazole-9-(4-phenyl)boronic acid pinacol ester (184.6 mg, 0.5 mmol), EtOH (63 μl) and K₂CO₃ (2M in water, 250 μl, 0.5 mmol) were added. The solution is degassed with nitrogen and after 10 minutes Pd(PPh₃)₄ (17.3 mg, 0.015 mmol) was added and the solution stirred at 70°C overnight. After the reaction was terminated the solvent was evaporated, distilled water was added, and the resultant solution was extracted with DCM (3 x 15 mL). The collected organic layer was dried over anhydrous MgSO₄ and then evaporated. The residue was purified by alumina column chromatography using a mixture of CH₂Cl₂/MeOH (98:2) to give product **3** as a white solid in 25% yield (69.3 mg). ¹H NMR (CDCl₃, 400 MHz) δ 8.86 (s, 2H), 8.78 (d, *J* = 4.8 Hz, 2H), 8.72 (d, *J* = 8.0 Hz, 2H), 8.09 (d, *J* = 8.8 Hz, 2H), 7.96-7.89 (m, 4H), 7.86 (d, *J* = 8.8 Hz, 2H), 7.69 (d, *J* = 8.0 Hz, 2H), 7.51 (d, *J* = 8.0 Hz, 2H), 7.47-7.37 (m, 4H), 7.32 (dt, *J*₁ = 1.1 Hz, *J*₂ = 8.0 Hz, 2H); ¹³C NMR (CDCl₃, 100 MHz) δ 156.0 (C), 149.7 (C), 149.0 (CH), 141.4 (C), 140.9 (C), 140.8 (C), 139.4 (C), 137.6 (C), 137.2 (CH), 137.2 (C), 128.5 (CH), 127.9 (CH), 127.6 (CH), 127.4 (CH), 126.0 (CH), 124.0 (CH), 123.5 (C), 121.5 (CH), 120.3 (CH), 120.0 (CH), 118.9 (CH), 109.8 (CH).

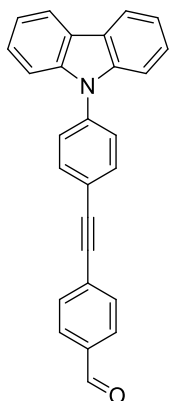
Synthesis of molecule 4



9-(4-bromophenyl)-9H-carbazole. To a solution of 1-bromo-4-iodobenzene (372 mg, 1.32 mmol) in DMF (7 mL), carbazole (200 mg, 1.2 mmol), Cs₂CO₃ (325.8 mg, 1.2 mmol), CuI (22.8 mg, 0.12 mmol) and LiCl (50.7 mg, 1.2 mmol) were added and the resulting solution was stirred at 150°C for 48 hours. After this time water was added and the mixture was extracted with EtOAc (5 x 10 mL). The organic phase was then washed with brine, dried over Na₂SO₄ and the solvent evaporated. The residue was purified by silica gel column chromatography using Hexane as eluent, to give product as a pale yellow solid in 71% yield (272.9 mg). ¹H NMR (CDCl₃, 300 MHz) δ 8.11 (d, *J* = 7.5 Hz, 2H), 7.69 (d, *J* = 9.0 Hz, 2H), 7.44-7.24 (m, 8H).



4-ethynylbenzaldehyde. 4-((trimethylsilyl)ethynyl)benzaldehyde (200 mg, 0.99 mmol) was dissolved in MeOH (10 mL) and the solution was cooled to 0°C. K₂CO₃ (176.4 mg, 1.28 mmol) was then added and the solution was stirred at 0°C for 30 minutes. After this time water was added and the pH was adjusted to 5 using HCl 1M. The mixture was extracted with DCM and the organic phase was washed with brine, dried over Na₂SO₄ and the solvent evaporated to give product as a pale orange solid in quantitative yield (132.4 mg). ¹H NMR (CDCl₃, 300 MHz) δ 10.02 (s, 1H), 7.84 (d, *J* = 8.4 Hz, 2H), 7.64 (d, *J* = 8.4 Hz, 2H), 3.29 (s, 1H).

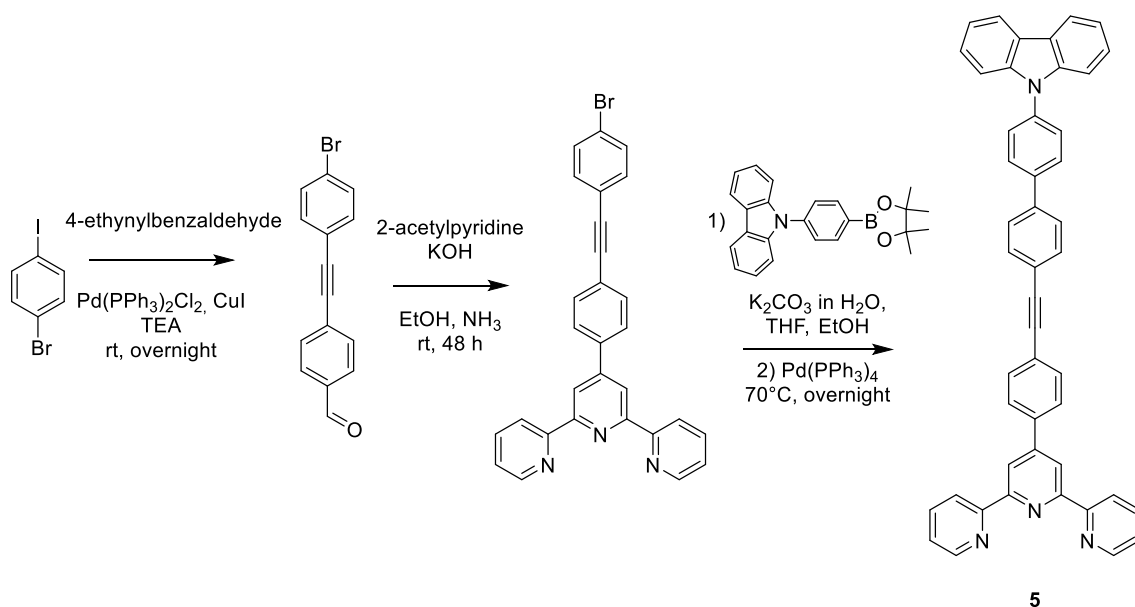


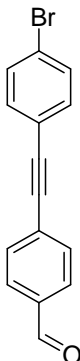
4-((4-(9H-carbazol-9-yl)phenyl)ethynyl)benzaldehyde. In a Schlenk flask, to a solution of **3d** (272.9 mg, 0.85 mmol) in TEA (7 mL) and toluene (1 mL), **2b** (132.2 mg, 1.02 mmol), Pd(PPh₃)₂Cl₂ (59.4 mg, 0.08 mmol) and CuI (16.2 mg, 0.08 mmol) were added and the solution was stirred under nitrogen atmosphere for 24 hours at 50°C. The progress of the reaction was monitored using TLC analysis on silica gel (EP:DCM = 2:1). Upon completion, water was added and the resulting mixture was extracted with DCM (3 x 10 mL). The combined organic phase was then washed with HCl 1M (1 x 10 mL), brine and dried over

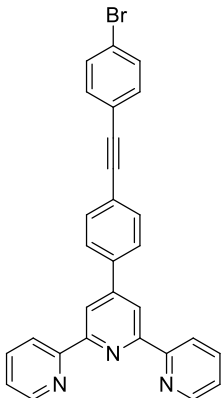
Na₂SO₄. Solvent was evaporated and the residue was purified by silica gel column chromatography using a mixture of CH₂Cl₂/petroleum ether (2:8) to give product **9** as a pale white solid in 22% yield (67.6 mg). ¹H NMR (CDCl₃, 300 MHz) δ 10.05 (s, 1H), 8.16 (d, *J* = 8.1 Hz, 2H), 7.91 (d, *J* = 8.1 Hz, 2H), 7.80 (d, *J* = 8.4 Hz, 2H), 7.73 (d, *J* = 8.4 Hz, 2H), 7.62 (d, *J* = 8.4 Hz, 2H), 7.49-7.40 (m, 4H), 7.35-7.29 (m, 4H).

9-(4-((4-([2,2':6',2''-terpyridin]-4'-yl)phenyl)ethynyl)phenyl)-9H-carbazole (**4**). 2-acetylpyridine (50 μL, 0.42 mmol) was added to a stirred suspension of crushed NaOH (16.7 mg, 0.42 mmol) in PEG 200 (0.5 mL) at 0° C. After 30 minutes 4-((4-(9H-carbazol-9-yl)phenyl)ethynyl)benzaldehyde (67.6 mg, 0.21 mmol) was added and stirring was continued at 0°C for 2 h. Then concentrated aqueous NH₃ solution (0.7 mL) was added and the suspension stirred at 100°C for 24 h. After this time water was added and the mixture was extracted with DCM (3 x 10 mL). The organic phase was then washed with brine, dried over Na₂SO₄. Solvent was evaporated and MeOH was added. The precipitate solid was collected by vacuum filtration and washed with water (50 mL) and ethanol (10 mL) to give product **4** as a white solid in 35% yield (41.2 mg). ¹H NMR (CDCl₃, 400 MHz) δ 8.82 (s, 2H), 8.77 (d, *J* = 4.4 Hz, 2H), 8.72 (d, *J* = 8.0 Hz, 2H), 8.16 (d, *J* = 8.0 Hz, 2H), 7.98 (d, *J* = 8.0 Hz, 2H), 7.93 (t, *J* = 8.0 Hz, 2H), 7.81 (d, *J* = 8.0 Hz, 4H), 7.74 (d, *J* = 8.0 Hz, 2H), 7.61 (d, *J* = 8.0 Hz, 2H), 7.50-7.38 (m, 6H) 7.31 (t, *J* = 7.6 Hz, 2H); ¹³C NMR (CDCl₃, 100 MHz) δ 156.0 (C), 155.9 (C), 149.4 (C), 149.0 (CH), 140.6 (C), 138.4 (C), 137.7 (C), 137.1 (CH), 133.2 (CH), 132.3 (CH), 127.4 (CH), 126.9 (CH), 126.1 (CH), 124.0 (CH), 123.8 (C), 123.6 (C), 122.1 (C), 121.5 (CH), 120.4 (CH), 120.2 (CH), 118.8 (CH), 109.8 (CH), 90.2 (C_{alk}), 90.1 (C_{alk}).

Synthesis of molecule 5



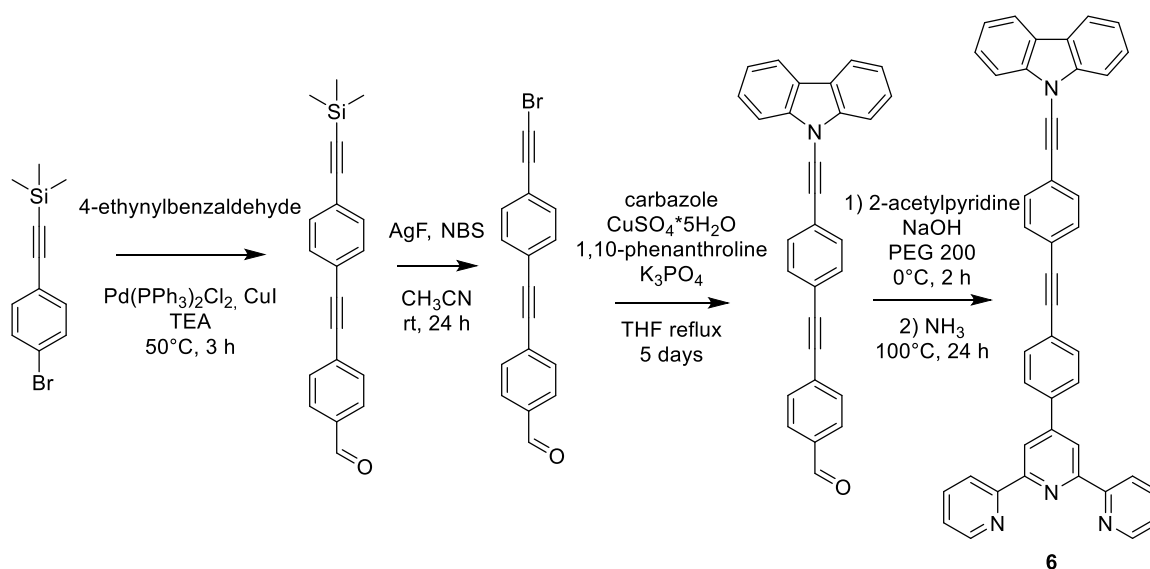
 **4-((4-bromophenyl)ethynyl)benzaldehyde.** In a Schlenk flask, to a solution of 1-bromo-4-iodobenzene (276.1 mg, 0.98 mmol) in TEA (8 mL), carbazole (106.5 mg, 0.82 mmol), Pd(PPh₃)₂Cl₂ (10.9 mg, 0.02 mmol) and CuI (15.7 mg, 0.03 mmol) were added and the solution was stirred under nitrogen atmosphere for 24 hours at room temperature. The progress of the reaction was monitored using TLC analysis on silica gel (EP:EtOAc = 9:1). Upon completion, water was added and pH was adjusted to 5 using HCl 1M. The resulting mixture was extracted with DCM (3 x 10 mL). The combined organic phase was then washed with brine and dried over Na₂SO₄. Solvent was evaporated and the residue was purified by silica gel column chromatography using a mixture of EtOAc/petroleum ether (2:98) to give product as a pale yellow solid in 94% yield (265.2 mg). ¹H NMR (CDCl₃, 300 MHz) δ 10.01 (s, 1H), 7.85 (d, *J* = 8.1 Hz, 2H), 7.65 (d, *J* = 8.1 Hz, 2H), 7.40 (d, *J* = 8.1 Hz, 2H), 7.20 (d, *J* = 8.1 Hz, 2H).

 **4'-4-((4-bromophenyl)ethynyl)phenyl-2,2':6',2''-terpyridine.** 2-acetylpyridine (222 μL, 1.98 mmol) was added to a stirred suspension of crushed KOH (110.9 mg, 1.98 mmol) in EtOH (5 mL). After 30 minutes 4-((4-bromophenyl)ethynyl)benzaldehyde (281.2 mg, 0.99 mmol) was added and stirring was continued for 2 h. Then concentrated aqueous NH₃ solution (1 mL) was added and the suspension stirred at 100°C for 24 h. After this time water was added and the mixture was extracted with DCM (3 x 10 mL). The organic phase was then washed with brine and dried over Na₂SO₄. Solvent was evaporated and MeOH was added. The precipitate solid was collected by vacuum filtration and washed with water (10 mL) and methanol (10 mL) to give product as a brown solid in 15% yield (71.0 mg). ¹H NMR (CDCl₃, 300 MHz) δ 8,76 (s, 2H), 8,74 (dq, *J*₁ = 0.9 Hz, *J*₂ = 4.8 Hz, 2H), 8,68 (dt, *J*₁ =

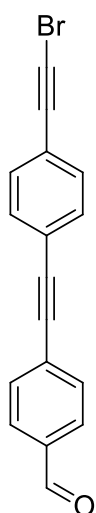
1.1 Hz, $J_2 = 8.1$ Hz, 2H), 7.94-7.86 (m, 4H), 7.67 (d, $J = 8.4$ Hz, 2H), 7.51 (d, $J = 8.4$ Hz, 2H), 7.43 (d, $J = 8.4$ Hz, 2H), 7.40 (ddd, $J_1 = 1.2$ Hz, $J_2 = 4.8$ Hz, $J_3 = 7.5$ Hz, 2H).

9-(4'-((4-([2,2':6',2''-terpyridin]-4'-yl)phenyl)ethynyl)-[1,1'-biphenyl]-4-yl)-9H-carbazole (**5**). To a solution of 4'-((4-bromophenyl)ethynyl)phenyl)-2,2':6',2''-terpyridine (40.0 mg, 0.08 mmol) in THF (0.5 mL) under nitrogen atmosphere, 9H-carbazole-9-(4-phenyl) boronic acid pinacol ester (30.3 mg, 0.08 mmol), EtOH (0.1 ml) and K_2CO_3 (2M in water, 41 μ l, 0.08 mmol) were added. The solution is degassed with nitrogen and after 10 minutes $Pd(PPh_3)_4$ (2.8 mg, 0.002 mmol) was added and the solution stirred at 70°C overnight. After the reaction was terminated the solvent was evaporated, distilled water was added, and the resultant solution was extracted with DCM (3 x 15 mL). The collected organic layer was dried over anhydrous Na_2SO_4 and then evaporated. The residue was purified by silica gel column chromatography using a mixture of $CH_2Cl_2/MeOH$ (99:1), and the resulting fraction were concentrated and the residue dissolved in DCM and washed with MeOH. Product **5** was collected by filtration of the solution as a white solid in 30% yield (16.2 mg). 1H NMR ($CDCl_3$, 400 MHz) δ 8.78 (s, 2H), 8.76 (d, $J = 4.0$ Hz, 2H), 8.70 (d, $J = 8.0$ Hz, 2H), 8.17 (d, $J = 8.0$ Hz, 2H), 7.95 (d, $J = 8.4$ Hz, 2H), 7.90 (dt, $J_1 = 1.6$ Hz, $J_2 = 7.6$ Hz, 2H), 7.86 (d, $J = 8.4$ Hz, 2H), 7.74-7.70 (m, 4H), 7.67 (d, $J = 8.4$ Hz, 2H), 7.51-7.41 (m, 4H), 7.38 (dd, $J_1 = 4.8$ Hz, $J_2 = 7.0$ Hz, 2H), 7.31 (t, $J = 7.0$ Hz, 2H); ^{13}C NMR ($CDCl_3$, 100 MHz) δ 156.1 (C), 156.0 (C), 149.4 (C), 149.1 (CH), 140.8 (C), 140.1 (C), 139.3 (C), 138.2 (C), 137.2 (C), 137.0 (CH), 132.3 (CH), 132.2 (CH), 128.4 (CH), 127.4 (CH), 127.3 (CH), 127.0 (CH), 126.0 (CH), 124.0 (C), 123.9 (CH), 123.5 (C), 122.4 (C), 121.4 (CH), 120.3 (CH), 120.0 (CH), 118.7 (CH), 109.8 (CH), 90.7 (C_{alk}), 90.1 (C_{alk}).

Synthesis of molecule 6

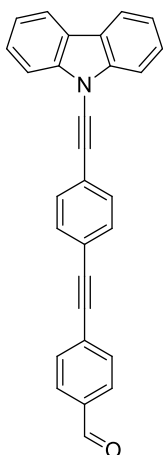


4-((4-((trimethylsilyl)ethynyl)phenyl)ethynyl)benzaldehyde. In a Schlenk flask, to a solution of ((4-bromophenyl)ethynyl)trimethylsilane (291.1 mg, 1.15 mmol) in TEA (3 mL) and toluene (1 mL), 4-ethynylbenzaldehyde (164.4 mg, 1.26 mmol), Pd(PPh₃)₂Cl₂ (40.3 mg, 0.06 mmol) and CuI (11.0 mg, 0.06 mmol) were added and the solution was stirred under nitrogen atmosphere for 3 hours at 50°C. The progress of the reaction was monitored using TLC analysis on silica gel (EP:EtOAc = 2:1). Upon completion, water was added and the resulting mixture was extracted with DCM (3 x 10 mL). The combined organic phase was then washed with HCl 1M (1 x 10 mL), brine and dried over Na₂SO₄. Solvent was evaporated and the residue was purified by silica gel column chromatography using a mixture of EtOAc/petroleum ether (2:98) to give product as a pale yellow solid in 44% yield (150.2 mg). ¹H NMR (CDCl₃, 300 MHz) δ 10.02 (s, 1H), 8.86 (d, *J* = 8.4 Hz, 2H), 7.66 (d, *J* = 8.4 Hz, 2H), 7.51-7.43 (m, 4H), 0.26 (s, 9H).



4-((4-(bromoethynyl)phenyl)ethynyl)benzaldehyde.

4-((4-((trimethylsilyl)ethynyl)phenyl)ethynyl)benzaldehyde (117.5 mg, 0.39 mmol) and AgF (49.3 mg, 0.39 mmol) were dissolved in CH₃CN (10 mL). The reaction flask was wrapped in aluminium foil and NBS (69.2 mg, 0.39 mmol) was added. The mixture was stirred overnight at room temperature. Then the solid was filtered off and washed with CH₃CN (10 mL). The solution was evaporated and the resulting residue was dissolved in Et₂O and washed with water (3 x 25 mL). The organic part was dried on anhydrous Na₂SO₄ and then evaporated to give product as a white solid in 78% yield (93.2 mg). ¹H NMR (CDCl₃, 300 MHz) δ 10.02 (s, 1H), 8.87 (d, *J* = 8.4 Hz, 2H), 7.67 (d, *J* = 8.4 Hz, 2H), 7.49 (d, *J* = 8.4 Hz, 2H), 7.44 (d, *J* = 8.4 Hz, 2H).

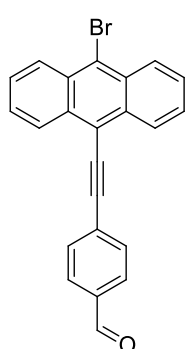
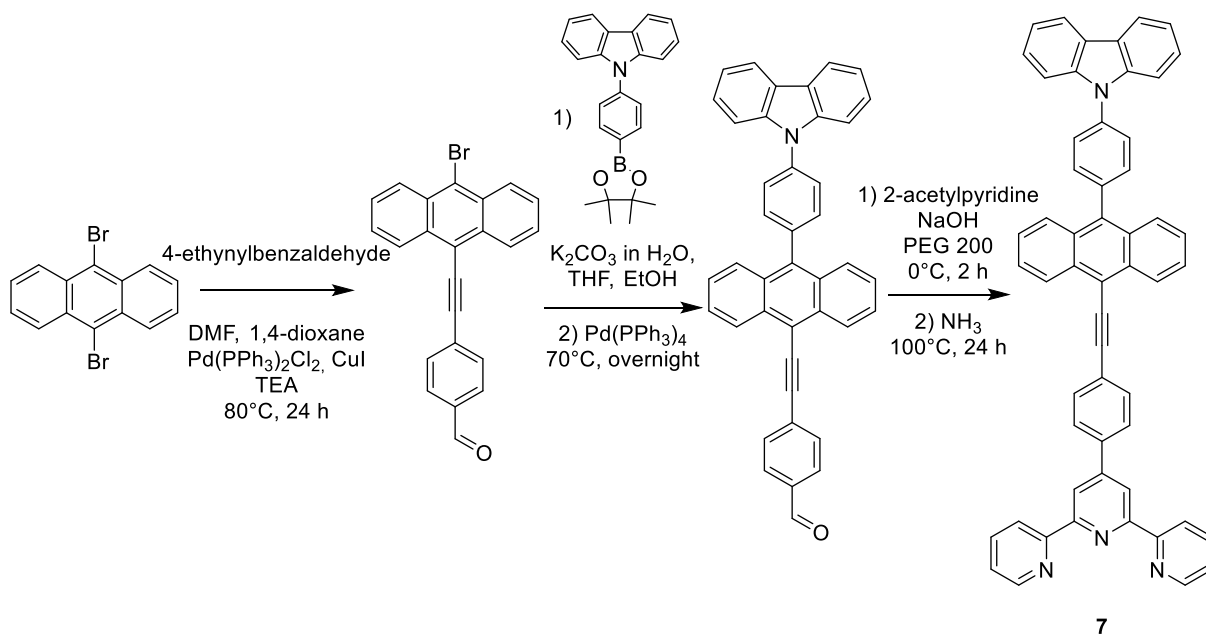


4-((4-((9H-carbazol-9-yl)ethynyl)phenyl)ethynyl)benzaldehyde. To a solution of 4-((4-(bromoethynyl)phenyl)ethynyl)benzaldehyde (93.2 mg, 0.30 mmol) in anhydrous THF (7 mL), carbazole (45.9 mg, 0.27 mmol), K_3PO_4 (116.5 mg, 0.55 mmol), $CuSO_4 \cdot 5H_2O$ (13.7 mg, 0.06 mmol) and 1,10-phenanthroline (19.8 mg, 0.11 mmol) were added. The reaction mixture was purged with nitrogen and heated at 70°C for 5 days. The progress of the reaction was monitored using TLC analysis. Upon completion, the reaction mixture was dried *in vacuo* and the residue was dissolved in water and extracted with DCM (3 x 15 mL). The combined organic phases were dried with anhydrous Na_2SO_4 and then evaporated. The crude residue was purified on silica gel flash chromatography using a mixture of

Hexane/EtOAc (95:5) to give product as a pale yellow solid in 47% yield (55.8 mg). 1H NMR ($CDCl_3$, 400 MHz) δ 10.04 (s, 1H), 8.06 (d, $J = 8.4$ Hz, 2H), 7.89 (d, $J = 8.4$ Hz, 2H), 7.74 (d, $J = 8.4$ Hz, 2H), 7.70 (d, $J = 8.4$ Hz, 2H), 7.59-7.50 (m, 2H), 7.45-7.35 (m, 2H), 7.28-7.21 (m, 4H).

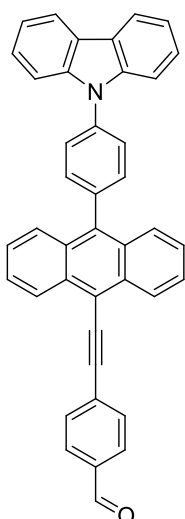
9-((4-((4-((2,2':6',2''-terpyridin)-4'-yl)phenyl)ethynyl)phenyl)ethynyl)-9H-carbazole (**6**). 2-acetylpyridine (50 μ L, 0.42 mmol) was added to a stirred suspension of crushed NaOH (17.2 mg, 0.42 mmol) in PEG 200 (1.5 mL) at 0°C. After 30 minutes 4-((4-((9H-carbazol-9-yl)ethynyl)phenyl)ethynyl)benzaldehyde (55.8 mg, 0.14 mmol) was added and stirring was continued at 0°C for 2 h. Then concentrated aqueous NH_3 solution (1.5 mL) was added and the suspension stirred at 100°C for 24 h. After this time water was added and the mixture was extracted with DCM (3 x 10 mL). The organic phase was then washed with brine, dried over Na_2SO_4 . Solvent was evaporated and MeOH was added. The precipitate solid was collected by vacuum filtration and washed with water (50 mL) and ethanol (10 mL) to give product **6** as a pale yellow solid in 15% yield (12.6 mg). 1H NMR ($CDCl_3$, 400 MHz) δ 8.77 (s, 2H), 8.75 (dq, $J_1 = 1.0$ Hz, $J_2 = 4.8$ Hz, 2H), 8.69 (dt, $J_1 = 1.0$ Hz, $J_2 = 8.0$ Hz, 2H), 8.05 (d, $J = 8.0$ Hz, 2H), 7.94 (d, $J = 8.4$ Hz, 2H), 7.74 (d, $J = 8.0$ Hz, 2H), 7.70 (d, $J = 8.0$ Hz, 4H), 7.61 (d, $J = 1.6$ Hz, 4H), 7.55 (dt, $J_1 = 1.1$ Hz, $J_2 = 7.6$ Hz, 2H), 7.37 (t, $J = 6.8$ Hz, 4H); ^{13}C NMR ($CDCl_3$, 100 MHz) δ 156.2 (C), 156.1 (C), 149.4 (C), 149.2 (CH), 140.3 (C), 138.4 (C), 136.9 (CH), 132.2 (CH), 131.7 (CH), 131.1 (CH), 127.3 (CH), 126.8 (CH), 123.9 (C), 123.8 (CH), 123.7 (C), 123.0 (C), 122.4 (C), 122.2 (CH), 121.4 (CH), 120.4 (CH), 118.7 (CH), 111.3 (CH), 90.8 (C_{alk}), 90.6 (C_{alk}), 80.9 (C_{alk}), 74.7 (C_{alk}).

Synthesis of molecule 7



4-((10-bromoanthracen-9-yl)ethynyl)benzaldehyde. In a Schlenk flask, to a solution of 9,10-dibromoanthracene (645.2 mg, 1.92 mmol) in DMF (10 mL) and 1,4-dioxane (4 mL), 4-ethynylbenzaldehyde (249.6 mg, 1.92 mmol), TEA (0.5 mL), Pd(PPh₃)₂Cl₂ (28.0 mg, 0.04 mmol) and CuI (19.1 mg, 0.10 mmol) were added and the solution was stirred under nitrogen atmosphere for 24 hours at 80°C. The progress of the reaction was monitored using TLC analysis on silica gel (EP:EtOAc = 9:1). Upon completion, water was added and the resulting mixture was extracted with DCM (3 x 10 mL). The combined organic phase

was then washed with HCl 1M (1 x 10 mL), brine and dried over Na₂SO₄. Solvent was evaporated and the residue was purified by silica gel column chromatography using a mixture of petroleum ether/EtOAc (95:5) to give product as a yellow solid in 35% yield (253.2 mg). ¹H NMR (CDCl₃, 300 MHz) δ 10.09 (s, 1H), 8.71-8.57 (m, 4H), 7.95 (q, *J* = 8.4 Hz, 4H), 7.71-7.63 (m, 4H).



4-((10-(4-(9H-carbazol-9-yl)phenyl)anthracen-9-yl)ethynyl)benzaldehyde. To a solution of 4-((10-bromoanthracen-9-yl)ethynyl)benzaldehyde (253.2 mg, 0.66 mmol) in THF (1.5 mL) under nitrogen atmosphere, 9H-carbazole-9-(4-phenyl) boronic acid pinacol ester (242.7 mg, 0.66 mmol), EtOH (65 μl) and K₂CO₃ (2M in water, 330 μl, 0.66 mmol) were added. The solution is degassed with nitrogen and after 10 minutes Pd(PPh₃)₄ (19.0 mg, 0.02 mmol) was added and the solution stirred at 70°C overnight. After the reaction was terminated the solvent was evaporated, distilled water was added, and the resultant solution was extracted with DCM (3 x 15 mL). The collected organic layer was dried over anhydrous Na₂SO₄ and then evaporated. The residue was purified by silica gel column

chromatography using a mixture of CH₂Cl₂/EP (1:9) to give product as a yellow solid in 38% yield (106.9 mg). ¹H NMR (CDCl₃, 300 MHz) δ 10.10 (s, 1H), 8.77 (d, *J* = 9 Hz, 2H), 8.22 (d, *J* = 7.8 Hz, 2H), 7.98 (dd, *J*₁ = 8.7 Hz, *J*₂ = 12.3 Hz, 4H), 7.88-7.81 (m, 4H), 7.72-7.65 (m, 6H), 7.57-7.48 (m, 4H), 7.36 (dt, *J*₁ = 1.0 Hz, *J*₂ = 7.5 Hz, 2H).

9-(4-(10-((4-([2,2':6',2''-terpyridin]-4'-yl)phenyl)ethynyl)anthracen-9-yl)phenyl)-9H-carbazole (7). 2-acetylpyridine (66 μL, 0.59 mmol) was added to a stirred suspension of crushed NaOH (24.0 mg, 0.59 mmol) in PEG 200 (1.0 mL) at 0° C. After 30 minutes 4-((10-(4-(9H-carbazol-9-yl)phenyl)anthracen-9-yl)ethynyl)benzaldehyde (106.9 mg, 0.20 mmol) was added and stirring was continued at 0°C for 2 h. Then concentrated aqueous NH₃ solution (3 mL) was added and the suspension stirred at 100°C for 24 h. After this time water was added and the mixture was extracted with DCM (3 x 10 mL). The organic phase was then washed with brine, dried over Na₂SO₄. Solvent was evaporated and MeOH was added. The precipitate solid was collected by vacuum filtration and washed with water (50 mL) and ethanol (10 mL). Then it was purified by silica gel column chromatography using a mixture of CH₂Cl₂/MeOH (95:5) to give product **7** as a yellow solid in 15% yield (22.3 mg) ¹H NMR (CDCl₃, 400 MHz) δ 8.83 (d, *J* = 10.8 Hz, 4H), 8.79 (d, *J* = 4.8 Hz, 2H), 8.72 (d, *J* = 8.0 Hz, 2H), 8.22 (d, *J* = 8.0 Hz, 2H), 8.05 (d, *J* = 8.0 Hz, 2H), 7.96 (d, *J* = 8.0 Hz, 2H), 7.92 (d, *J* = 8.0 Hz, 4H), 7.84 (t, *J* = 8.0 Hz, 4H), 7.69 (t, *J* = 8.4 Hz, 6H), 7.55-7.49 (m, 4H) 7.42-7.34 (m, 4H); ¹³C NMR (CDCl₃, 100 MHz) δ 156.0 (C), 149.5 (C), 149.1 (CH), 140.8 (C), 138.4 (C), 137.6 (C), 137.5 (C), 137.4 (C), 137.3 (C), 137.1 (CH), 132.7 (CH), 132.4 (C), 132.2 (CH), 130.1 (C), 127.5 (CH), 127.2 (CH), 127.1 (CH), 126.9 (CH), 126.6 (CH), 126.1 (CH), 126.0 (CH), 124.4 (C), 124.0 (CH), 123.6 (C), 121.5 (CH), 120.5 (CH), 120.2 (CH), 118.8 (CH), 117.7 (C), 109.9 (CH), 88.1 (C_{alk}), 77.2 (C_{alk}).

10.4 Bibliography

- ¹ S. M. Bonesi, R. Erra-Balsells, *J. Lumin.* **2001**, *93*, 51.
- ² A. R. Katritzky, G. W. Rewcastle, L. M. V. Demiguel, *J. Org. Chem.* **1988**, *53*, 794.
- ³ S. E. Creutz, K. J. Lotito, G. C. Fu, J. C. Peters, *Science* **2012**, *338*, 647.
- ⁴ J. L. Li, A. C. Grimsdale, *Chem. Soc. Rev.* **2010**, *39*, 2399.
- ⁵ N. Blouin, M. Leclerc, *Acc. Chem. Res.* **2008**, *41*, 1110.
- ⁶ S. Encinas, L. Flamigni, F. Barigelletti, E. C. Constable, C. E. Housecroft, E. R. Schofield, E. Figgemeier, D. Fenske, M. Neuburger, J. G. Vos, M. Zehnder, *Chem.-Eur. J.* **2002**, *8*, 137.
- ⁷ J. E. Beves, E. C. Constable, C. E. Housecroft, C. J. Kepert, D. J. Price, *CrystEngComm* **2007**, *9*, 456.
- ⁸ B. Bozic-Weber, E. C. Constable, N. Hostettler, C. E. Housecroft, R. Schmitt, E. Schonhofer, *Chem. Commun.* **2012**, *48*, 5727.
- ⁹ A. Wild, A. Winter, F. Schlutter, U. S. Schubert, *Chem. Soc. Rev.* **2011**, *40*, 1459.

- ¹⁰ M. W. Cooke, G. S. Hanan, *Chem. Soc. Rev.* **2007**, *36*, 1466.
- ¹¹ K. M. C. Wong, V. W. W. Yam, *Coord. Chem. Rev.* **2007**, *251*, 2477.
- ¹² I. Eryazici, C. N. Moorefield, G. R. Newkome, *Chem. Rev.* **2008**, *108*, 1834.
- ¹³ G. Accorsi, N. Armaroli, F. Cardinali, D. Wang, Y. X. Zheng, *J. Alloys Compd.* **2009**, *485*, 119.
- ¹⁴ S. H. Hwang, P. S. Wang, C. N. Moorefield, L. A. Godinez, J. Manriquez, E. Bustos, G. R. Newkome, *Chem. Commun.* **2005**, 4672.
- ¹⁵ A. Maier, H. Fakhrnabavi, A. R. Rabindranath, B. Tieke, *J. Mater. Chem.* **2011**, *21*, 5795.
- ¹⁶ A. C. Ribou, T. Wada, H. Sasabe, *Inorg. Chim. Acta* **1999**, *288*, 134.
- ¹⁷ R. Gompper, H. U. Wagner, *Angew. Chem. Int. Ed. Engl.* **1988**, *27*, 1437.
- ¹⁸ M. Kivala, F. Diederich, *Acc. Chem. Res.* **2009**, *42*, 235.
- ¹⁹ S. Barlow, S. R. Marder, in *Functional Organic Materials*, ed. T. J. J. Müller, U. H. F. Bunz, Wiley-VCH, Weinheim, **2007**, pp. 393-437.
- ²⁰ C. Aurisicchio, B. Ventura, D. Bonifazi, A. Barbieri, *J. Phys. Chem. C* **2009**, *113*, 17927.
- ²¹ Z. R. Grabowski, K. Rotkiewicz, W. Rettig, *Chem. Rev.* **2003**, *103*, 3899.
- ²² A. Baschieri, L. Sambri, I. Gualandi, D. Tonelli, F. Monti, A. Degli Esposti, N. Armaroli, *RSC Advances* **2013**, *3*, 6507.
- ²³ J. H. Cho, Y.-S. Ryu, S. H. Oh, J. K. Kwon, E. K. Yum, *Bull. Korean Chem. Soc.* **2011**, *32*, 2461.
- ²⁴ K. Binnemans, *Chem. Rev.* **2009**, *109*, 4283.

11. A mesoionic carbene as neutral ligand for phosphorescent cationic Ir(III) complexes

1,2,3-triazol-5-ylidene derivatives have recently emerged as a new class of so-called mesoionic or abnormal carbenes (MICs or aNHCs),¹ and have found a wide range of applications as ligands in metal complexes, typically to be used in the area of homogeneous catalysis.^{2,3}

The success of this class of ligands is based on a combination of favorable features, such as strong donor character (even higher than their NHC analogues) and the fact that the regioselective copper(I) catalyzed 'click' cycloaddition of alkynes with azides (CuAAC) allows easy preparation of the triazole precursors.⁴ Subsequent *N*-alkylation and deprotonation of the readily obtained 1,2,3-triazoles afford the desired mesoionic carbene ligands.⁵

The synthesis of 1,2,3-triazoles entails a large variety of aryl wingtip derivatives. Among them, phenyl-triazoles (**A**) and pyridyl-triazoles (**B**) are extensively utilized as bidentate cyclometalating⁶ and ancillary⁷ ligands, respectively, in luminescent transition metal complexes (Figure 1). Similarly, the corresponding triazolylidene derivatives **C** and **D** have been recently used as bidentate cyclometalating and donor ligands to afford Ru(II)^{3a} and Ir(III)^{3a,3c,3d} complexes employed in various catalytic processes. However, applications of pyridyl derivatives **D** in other fields are still scarce and few examples of pyridyl-1,2,3-triazol-5-ylidene Ru(II)- complexes as photosensitizers appeared only recently.⁸

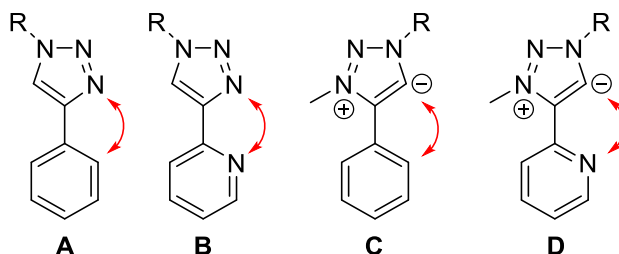


Figure 1: Examples of 1,2,3-triazole derivatives as bidentate ligands; the coordination sites are pointed out

Based on our interest in luminescent compounds^{7d-e,9} and with the aim of widening our library of organic chelating ligands,¹⁰ we envisaged the possibility of using **D**-type 1,2,3-triazol-5-ylidene derivatives as ligands for phosphorescent Ir(III) complexes.

Most luminescent Ir(III) coordination compounds reported in the literature contain bidentate ligands. This is due to easy synthetic accessibility and to the possibility of varying functional groups on the ligand skeleton, enabling a rational tuning of the photophysical properties.

In particular, ortho-metalated phenyl pyridines and their analogues typically serve as monoanionic bidentate ligands and have enabled the preparation of large number of cyclometalated Ir(III) complexes

since the pioneering works of Thompson.¹¹ These compounds are the best choice as triplet emitters in electroluminescent devices,¹² due to their strong and tunable luminescence output all across the whole visible spectral region, by modifying the chemical nature of the ligands.

By contrast, Ir(III) complexes containing only chelating neutral ligands such as 2,2'-bipyridine - with, for instance, general formula $[\text{Ir}(\text{L-L})_2\text{Cl}_2]^+$ and $[\text{Ir}(\text{L-L})_2(\text{L}'\text{-L}')^{3+}]$ - are relatively rare, most probably due to the harsh reaction conditions and the laborious purifications needed in the presently available synthetic routes.¹³ However, recently, renovated interest in such compounds has sparked,¹⁴ particularly due to their possible applications as antimicrobial agents¹⁵ and DNA-intercalators.¹⁶

Even dianionic ligands are still rather uncommon in Ir(III) complexes, with some recent examples involving dianionic C⁻C,¹⁷ N⁻N⁻¹⁸ and S⁻S⁻¹⁹ chelators, in combination with neutral or monoanionic cyclometalating derivatives.

Herein, we report the first example of a 4-pyridyl-1,2,3-triazolylidene derivative as a neutral donor ligand to obtain the cationic phosphorescent Ir(III) complexes $[\text{Ir}(\text{tripz})_2\text{Cl}_2]^+$ (**3**, tripz = 1-benzyl-3-methyl-4-(pyridin-2-yl)-1*H*-1,2,3-triazolylidene) and $[\text{Ir}(\text{tripz})_2(\text{b-trz})]^+$ (**5**, H₂b-trz = di(1*H*-tetrazol-5-yl)methane) through a simple synthetic procedure (Scheme 1). In the latter, the bis-tetrazolate dianionic chelating ligand **4** is used to obtain a luminescent complex.

11.1 Results and discussion

11.1.1 Synthesis of complexes **3** and **5**

The synthetic route to **3** and **5** is reported in Scheme 1. We identified ligand **2** (Scheme 1) as the MIC precursor able to behave as a bis-chelating ligand, as it contains a 2-pyridyl-1,2,3-triazolylidene unit and exhibits a benzyl group as *N*-substituent, which can avoid competing coordination and favors cyclometalation.²⁰

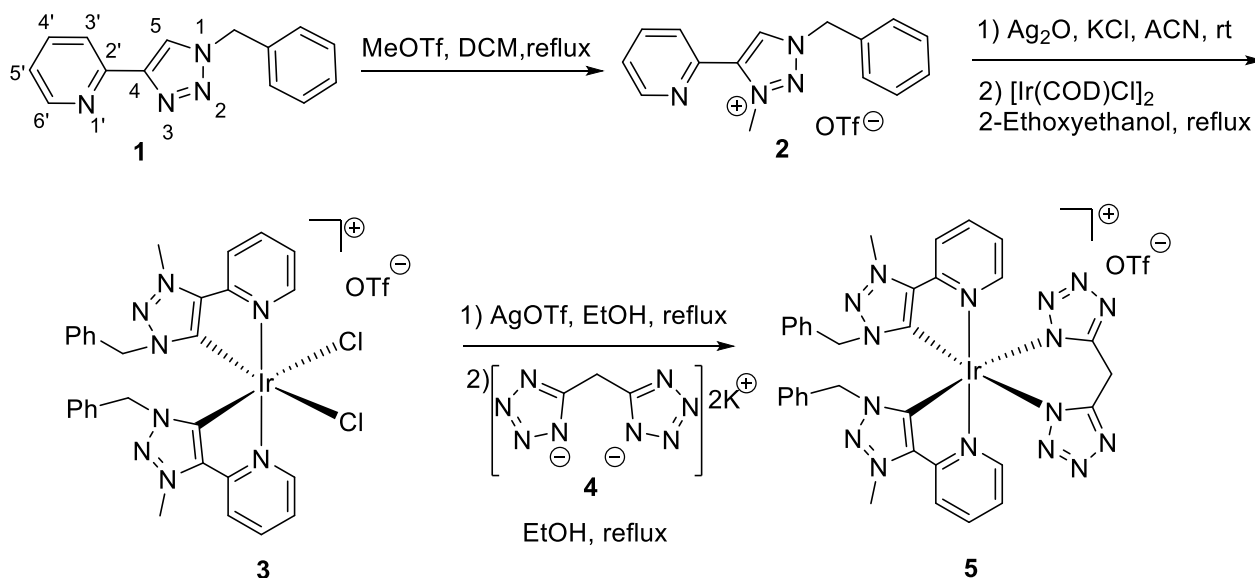
The pyridyl triazole **1** is obtained from the click reaction between benzyl-azide and 2-ethynyl-pyridine.²¹ It reacts regioselectively with MeOTf to give the mono-methylated triazolium salt **2**.

Standard approaches²² to obtain a chloride-bridged Ir(III) dimer by direct reaction of **2** with $\text{IrCl}_3 \cdot x\text{H}_2\text{O}$ or with the more reactive $[\text{Ir}(\text{COD})\text{Cl}]_2$ failed.

Considering that the coordination of 1,2,3-triazol-5-ylidene carbenes to a metal is generally achieved through transmetalation from a Ag-MIC complex,²³ we performed the C-H bond activation of the MIC precursor **2** by reaction with Ag₂O in acetonitrile in the absence of light,²⁴ to get the corresponding -triazolylidene complex which was directly used in the next step without purification.

The Ag-Ir transmetalation was performed by reaction of the Ag-derivative of **2** with $[\text{Ir}(\text{COD})\text{Cl}]_2$ ²⁵ at reflux in 2-ethoxyethanol. Complex **3** was obtained as an air-stable yellow solid and its structure was confirmed by NMR, MS and X-ray analysis (see below). The ¹H NMR most diagnostic evidences of the Ir-complex formation were the disappearance of the triazolium H-5 proton, the observation of the characteristic AB resonance pattern of the benzylic protons, some high-field shifts due to the π stacking and the down-field shift of the H-6' proton.

Complex **3** is rather stable but, upon halide extraction with AgOTf, it reacts with the dianionic ligand **4**, which is derived from the deprotonation of di(1*H*-tetrazol-5-yl)methane.²⁶ This affords complex **5** in good yields (Scheme 1). Any attempts to obtain **5** as crystals suitable for X rays analysis failed, and its structure was established by NMR and mass analysis and supported by DFT calculations (see below).



Scheme 1: Synthesis of complexes **3** and **5**

11.1.2 Structural characterization

Single crystals of complex **3** were obtained as trifluoromethanesulphonic salt by slow diffusion of Et₂O in DCM/acetonitrile solution. The compound crystallizes in the monoclinic *C*₂/*c* space group and the crystal cell contains a molecule of acetonitrile and a water molecule. The structure of the cation showed the same arrangement of the two ligands around a pseudo octahedral iridium ion (see Figure 2). The two pyridinic nitrogen occupy the two apical position, therefore leading to a *trans* arrangement. The two chlorine atoms occupy two adjacent equatorial positions, whereas the two remaining are filled by the triazolylidenes. The two benzyl moieties are arranged in a parallel-stacked conformation with the two ligands. The structure is

reported in Figure 2 and the corresponding crystallographic parameters in Table 1, and they are very similar to other iridium complexes reported in the literature.²⁷

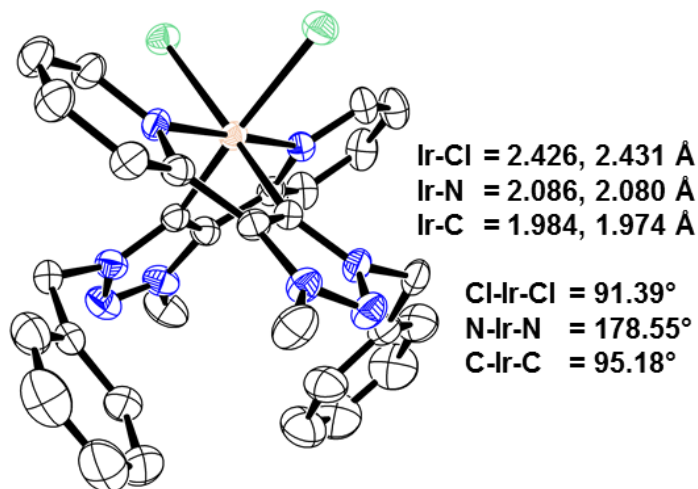


Figure 2: Experimental X-ray structures of complex **3**. ORTEP representations are at the 50% probability. Counter anion, solvents, and hydrogen atoms are omitted for the sake of clarity

Table 1: Crystallographic parameters for **3**

	3
Formula	C ₃₀ H ₂₈ N ₈ Cl ₂ Ir, C ₁ F ₃ O ₃ S, C ₂ H ₃ N, O ₁
F _w	969.83
T, K	298
λ, Å	0.71073 (Mo-Kα)
Crystal system	Monoclinic
Space group	C ₂ /c
a, Å	21.6091(12)
b, Å	12.3435(7)
c, Å	28.5466(15)
α, deg	90.000
β, deg	100.2300(10)
γ, deg	90.000
Cell volume, Å ³	7493.2(7)
Z	8
D _c , g cm ⁻³	1.719
μ, mm ⁻¹	3.827
F(000)	3824

h, k, l max	27, 15, 36
Crystal size, mm	0.25, 0.15, 0.05
θ limits, °	1.45 to 26.00
Reflections collected	40629
Independent reflections	8049
Data/restraints/parameters	8049/0/481
Weight. Scheme	0.0272 6.7122
GOF on F^2	1.009
R_1 ($I > 4\sigma(I)$)	0.0607
w R_2 (all data)	0.0722
Peak/hole, e \AA^{-3}	0.811 and -0.487
Notes:	The crystal cell contains a water molecule (O100), but the two hydrogens could not be experimentally found.

^1H NMR for compounds **3** (top) and **5** (bottom) are reported in Figure 3. The role of the triazolylidene derivative as MIC ligand is confirmed by the number of the aromatic protons in the spectra (total = 9H) and in particular by the absence of the singlet related to the triazole moiety, which can be usually find at 9.26 ppm (as for compound **2**). The presence of the ancillary ligand **4** in complex **5** is corroborate by the presence of the singlet centred at 4.7 ppm, typical for the ditetrazolymethane derivative. Variation in chemical shifts can also be observed for the benzyl- CH_2 -system and for the protons of the pyridyl-moiety.

11. A mesoionic carbene as neutral ligand for phosphorescent cationic Ir(III) complexes

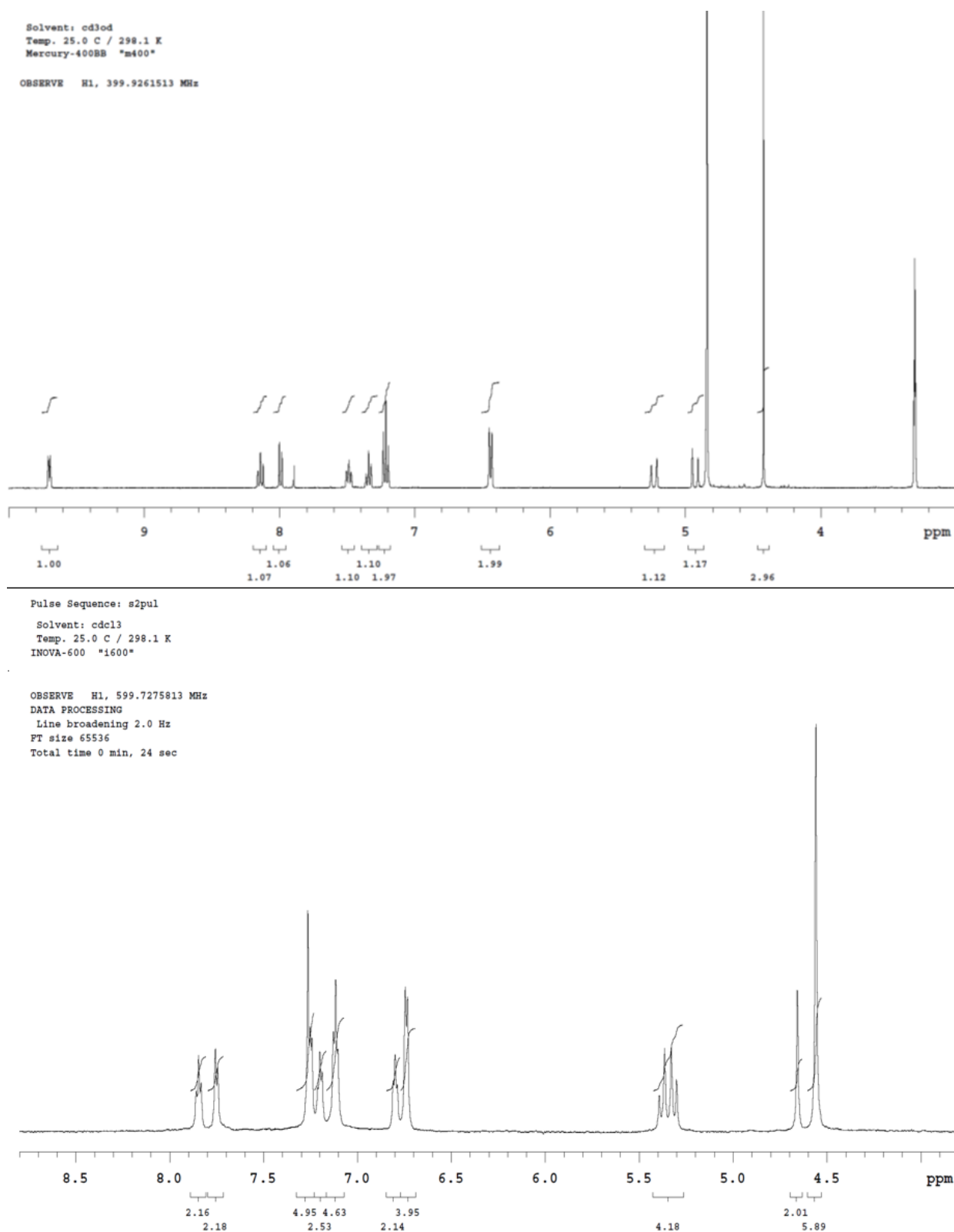


Figure 3: ^1H NMR for complexes **3** (top) and **5** (bottom)

11.1.3 Electrochemical properties

The electrochemical properties of the Ir(III) complexes **3** and **5** were investigated by cyclic (CV) and square wave (SWV) voltammetry in acetonitrile solutions ($c \approx 4 \times 10^{-4}$ M) at 298 K. The redox potentials, measured relative to the ferrocene/ferrocenium (Fc/Fc⁺) redox couple, are collected in Table 2, while selected voltammograms are reported in Figure 4.

Upon scanning of the anodic region, complex **3** displays a one-electron oxidation wave, which can be formally assigned to the Ir^{III}/Ir^{IV} redox couple, though it should be noted that the HOMO is also delocalized over the phenyl moieties of the ligand (see below, Figure 7). The oxidation couple observed at $E = +1.40$ V was quasi-reversible at all scan rates tested (0.01-0.5 V/s), with peak-to-peak separation $\Delta E_{pp} = 0.10$ -0.08 V. On the other hand, complex **5** show an almost irreversible mono-electronic redox process at +1.62 V. When scanned cathodically, two almost irreversible one-electron reduction waves are observed for both complexes at about -1.8 and -2.0 V ($\Delta E_{pp} = 0.10$ and 0.15 V, respectively, almost independent from the scan rate between 0.01-2.00 V/s). These are assigned to the stepwise reduction of the two MIC ligands on the basis of the theoretical data presented below (*vide infra*). The oxidation potentials of complexes **3** and **5** are considerably more positive, by ca. 0.53 V and 0.75 V, respectively, than that of the model cationic complex **[Ir(ppy)₂(bpy)]⁺** (where Hppy = 2-phenyl pyridine and bpy = 2,2'-bipyridine) ($E = +0.87$ V), while the first reduction potential is quite similar.²⁸ Thus, the presence of the mesoionic carbene ligand has a strong stabilization effect on the HOMO with respect to ppy, which underpins a radical change of the nature of the HOMO itself in the case of **3** (see below). On the contrary, the LUMO energy is almost unchanged. Notably, the electrochemical HOMO-LUMO gap (ΔE_{redox}) correlates very well with the energy difference calculated by the DFT method (see below, Table 3), which provides a basis for the understanding of the electronic features of our Ir(III) complexes.

Table 2: Electrochemical data of complexes **3** and **5** determined by SWV in room-temperature acetonitrile solution +0.1 M TBAPF₆

Complex	Electrochemical data ^a [V]		
	E_{ox}	E_{red}	ΔE_{redox} ^b
[Ir(ppy)₂(bpy)]⁺	+0.87 ^c	-1.78 ^c	2.65
3	+1.40	-1.82, -1.98	3.22
5	+1.62	-1.82, -2.05	3.44

^a All redox potentials are reported with respect to the Fc⁺/Fc couple (estimated errors: ± 20 mV). ^b $\Delta E_{redox} = E_{ox} - E_{red}$.

^c Data from ref 28.

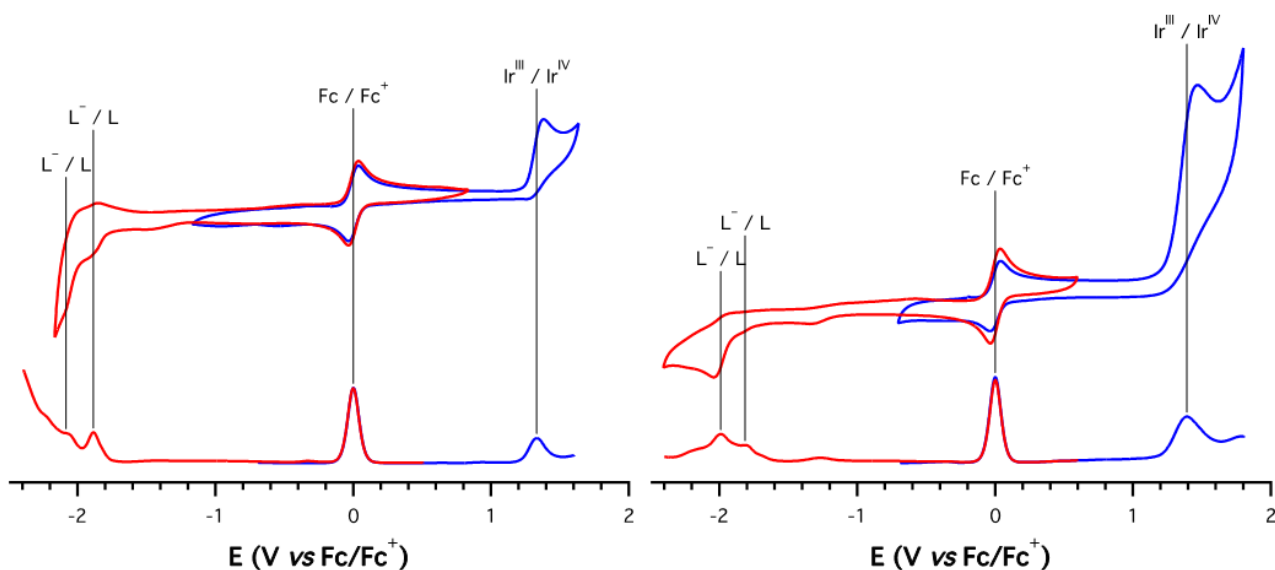


Figure 4: Anodic (blue) and cathodic (red) cyclic (top traces) and square wave (bottom traces) voltammetry scan of complexes **3** (left) and **5** (right) in CH₃CN solution at 298 K

11.1.4 Ground-state theoretical calculations

The structural and electronic properties of **3** and **5** were investigated by means of density functional theory (DFT) calculations at the M06/6-31G(d)&LANL2DZ(Ir)^{29,30,31,32} level of theory considering acetonitrile solvation effects using the polarizable continuum model (PCM).³³ The ground-state geometries of both complexes were fully optimized without symmetry constraints. The accuracy of the computational method is validated by the comparison between the available X-ray structure of **3** and its theoretically calculated one.³⁴ Accordingly, Figure 5 clearly shows that the experimental and computed geometries are virtually superimposable as mathematically proved by the extremely small minimized value of the root-mean-square deviation calculated for all the atomic positions (only 0.148 Å). This value is even smaller (0.084 Å) if the phenyl moieties of **3** are excluded from the minimization process since their position is relatively undefined in the experimental X-ray structure.

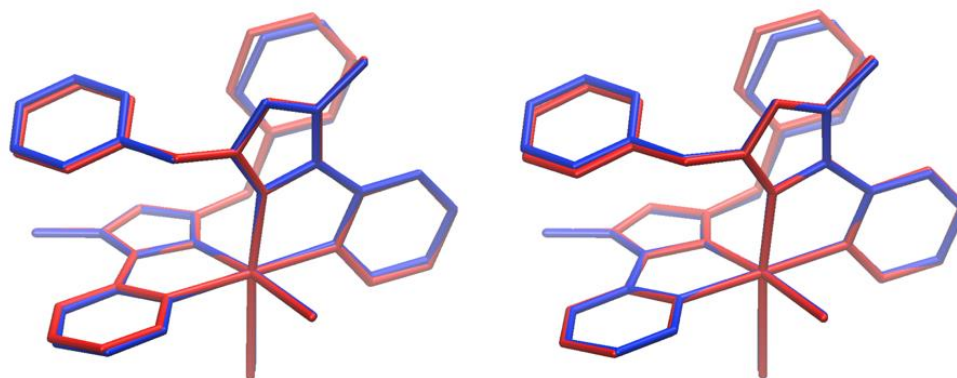


Figure 5: Structural overlay (H atoms omitted) between the experimental X-ray structure of the cationic part of complex **3** (blue) and the theoretically computed one (red). The structural overlay is calculated by minimizing the root-mean-square deviation (RMSD) of all the atomic positions (left, RMSD = 0.148 Å) or, alternatively, by excluding the phenyl moieties from the minimization process because of their relatively undefined position (due to high thermal motion) in the experimental data (right, RMSD = 0.084 Å)

It is noteworthy that the fully optimized ground-state geometry of **3** displays a perfect C_2 symmetry, while the experimental one belongs to the C_1 point group. The lack of symmetry in the X-ray structure can be attributed to the presence of the triflate counterion and/or solvent molecules in the crystal lattice, rather than to intermolecular interactions within **3** (*vide supra*). On the other hand, the replacement of the two chloride ligands with the chelating bis-anionic ligand **4** in **5**, removes the C_2 symmetry of the complex due to the lack of planarity of the ligand **4** itself, induced by the presence of the methylene bridge linking the two tetrazolate moieties.

As mentioned above, we could not obtain suitable crystals for X-ray structural determination of **5**, therefore a direct experimental proof of the coordination mode of ligand **4** upon chelation of the iridium metal center is not available. There are three possibilities: (i) both tetrazole moieties coordinate the iridium metal through the nitrogens in position 1 on the tetrazole ring; (ii) same as before using the nitrogens in position 2; (iii) the two tetrazole moieties are not equivalent, with one coordinating through the nitrogen in position 1 and the other one through the nitrogen in position 2. The latter hypothesis is not compatible with NMR data; in fact, for instance, the ^{13}C -NMR spectrum of the complex shows only one signal associated to the C-5 tetrazolic carbon. Notably, DFT calculations suggest that the most probable scenario is (i) because all geometry optimizations starting from three different initial guesses, representative of the three above mentioned isomers, converge on the same structure depicted in Figure 6.

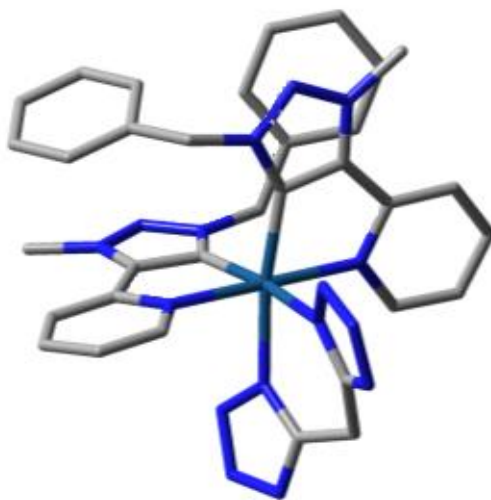


Figure 6: Calculated structure for complex 5

Figure 7 displays the energy diagram and the topology of the frontier molecular orbitals of both **3** and **5**, together with those computed for the archetypal complex $[\text{Ir}(\text{ppy})_2(\text{bpy})]^+$ as reference.

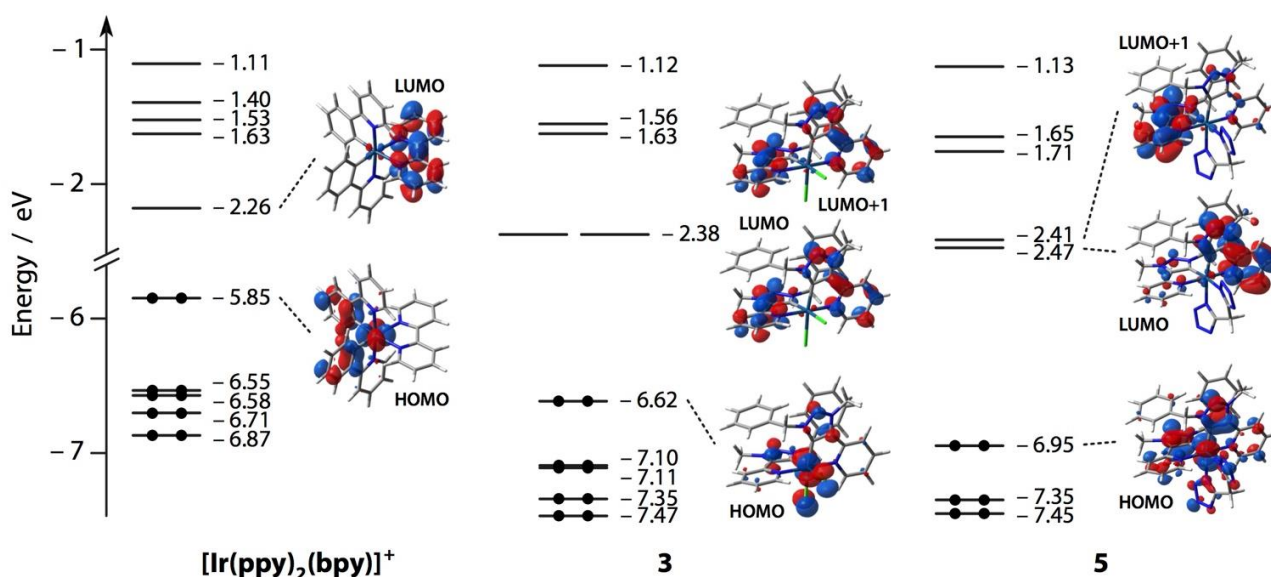


Figure 7: Energy diagram showing the energy values of the frontier Kohn-Sham molecular orbitals of **3** and **5** in acetonitrile, together with those computed for the archetypal complex $[\text{Ir}(\text{ppy})_2(\text{bpy})]^+$; for some relevant orbitals, the corresponding isosurface is also displayed for the sake of clarity (isovalue = $0.04 \text{ e}^{1/2} \text{ bohr}^{-3/2}$)

Normally, in cyclometalated cationic iridium(III) complexes, the HOMO is mainly localized on the metal center and on the moiety of the cyclometalating ligands involved in the Ir–C bond, as found for $[\text{Ir}(\text{ppy})_2(\text{bpy})]^+$ and **5**. Interestingly, this is not the case for **3**, where the HOMO, but also the HOMO-1 and the HOMO-2, are basically π^* orbitals respectively involving one of the three iridium d_π orbitals (pseudo- t_{2g})

and a different linear combination of the chlorides 3p orbitals (Figure 7). This results in a strong stabilization of the HOMO (-0.80 eV), if compared to the archetypal complex. The HOMO energy is even lower in the case of **5** (-1.10 eV vs. **[Ir(ppy)₂(bpy)]⁺**) because this π^* orbital, now involving the iridium metal center and the triazole moiety, is strongly stabilized by the ligand field exerted by the bis-anionic ligand **4**.

On the other hand, in both **3** and **5**, the LUMO and LUMO+1 are centered on the two mesoionic carbene ligands and are virtually isoenergetic (fully degenerate in the case of **3**, displaying C_2 symmetry). The effect of the chloride ligands or of the chelating **4** unit is negligible in altering the LUMO and LUMO+1 energy of the two complexes ($\Delta E \approx 0.05$ eV). The scenario is completely different in the case of the archetypal complex **[Ir(ppy)₂(bpy)]⁺** where the LUMO is centered on the 2,2'-bipyridine ancillary ligand (**bpy**). All the calculated energy levels are reported in Table 3.

Table 3: HOMO and LUMO energy levels calculated by DFT

Complex	DFT calculated energy ^a [eV]		
	E_{HOMO}	E_{LUMO}	ΔE_{DFT}^b
[Ir(ppy)₂(bpy)]⁺	-5.85	-2.26	3.59
3	-6.65	-2.39	4.26
5	-6.95	-2.47	3.48

^a DFT calculations were carried out at the M06/6-31G(d) & LANL2DZ(Ir) level of theory in acetonitrile, using PCM.

^b $\Delta E_{\text{DFT}} = E_{\text{LUMO}} - E_{\text{HOMO}}$.

In short, DFT calculations suggest that **3** and **5** should display a ligand-centered (LC) emission, unlike **[Ir(ppy)₂(bpy)]⁺** which exhibits a metal-to-ligand charge-transfer (MLCT) band. The largest HOMO-LUMO energy gap is predicted for **5** (4.48 eV), to be compared with 4.26 eV for **3**. These theoretical findings are in line with both the electrochemical data (see CV and SWV measurements, Table 2).

11.1.5 Photophysical properties and excited-state characterization

Photoluminescence studies in solution were carried out in spectroscopic grade acetonitrile. The absorption spectra of **3** and **5** are reported in Figure 8.

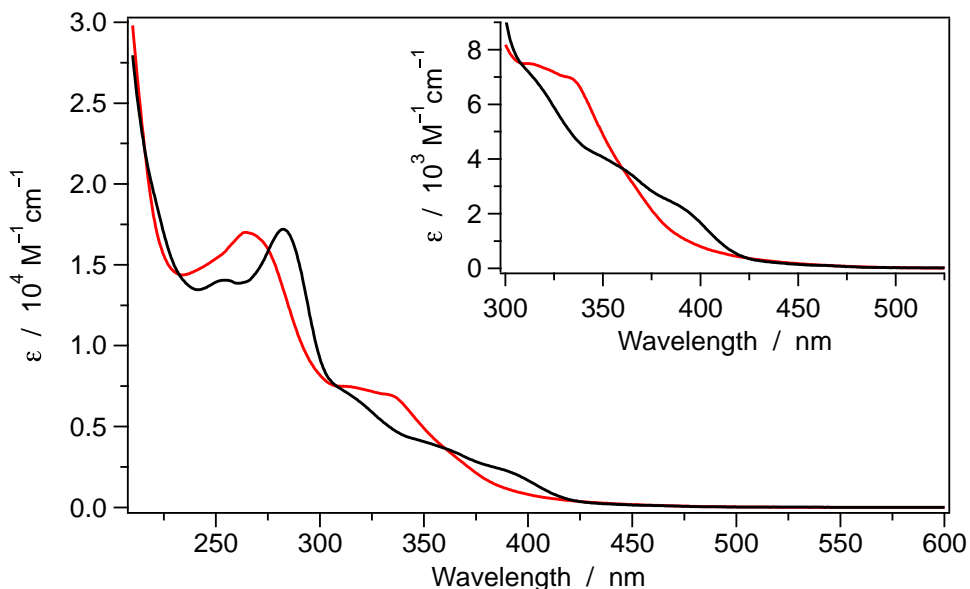


Figure 8: Absorption spectra of **3** (black) and **5** (red) in acetonitrile at 298 K. The lowest-energy transitions are magnified in the inset

Both compounds exhibit a similar absorption profile in the spectral window between 210 and 300 nm. Therefore, these strong absorption bands are primarily attributed to spin-allowed $^1(\pi-\pi^*)$ ligand-centered (LC) transitions mainly involving the two identical mesoionic carbene ligands, with some likely contribution from ^3LC forbidden transitions, enabled by the heavy-atom effect of the iridium center ($\zeta_{\text{Ir}} = 3909 \text{ cm}^{-1}$).^{12,35} At longer wavelengths ($\lambda > 300 \text{ nm}$; Figure 8, magnified region), several weaker and broader bands are present but their qualitative attribution is less straightforward, therefore TD-DFT calculations have been performed to rigorously assess their nature. In agreement with experimental data, theoretical estimations predict a more red-shifted absorption onset in the case of **3**. In fact, the $S_0 \rightarrow S_1$ and $S_0 \rightarrow S_2$ vertical excitations, that are mainly responsible for the lowest-energy absorption band in both complexes, are estimated to occur at 382 and 378 nm for **3**, and at 349 and 345 nm for **5**. In both compounds, the $S_0 \rightarrow S_1$ predominantly involve a HOMO \rightarrow LUMO excitation, while the $S_0 \rightarrow S_2$ transitions can be described as HOMO \rightarrow LUMO+1 electron promotion (see Figure 7 for orbital topologies). As a consequence, in the case of complex **3**, the lowest-energy absorption band in the inset of Figure 8 can be assigned to a ligand-to-ligand charge-transfer (LL'CT) transition from the chlorines to the mesoionic carbene ligands. On the contrary, for complex **5**, the band mainly originates from a LC transition involving the two carbene ligands. Anyway, it

must be stressed that a strong MLCT component is always present in both cases since the iridium d_{π} orbitals strongly contribute to the HOMO of both complex **3** and **5**.

The emission spectra of **3** and **5** are reported in Figure 9 both in acetonitrile solution at 298 K (full) and at 77 K (dashed), while the luminescence properties and photophysical parameters are summarized in Table 4.

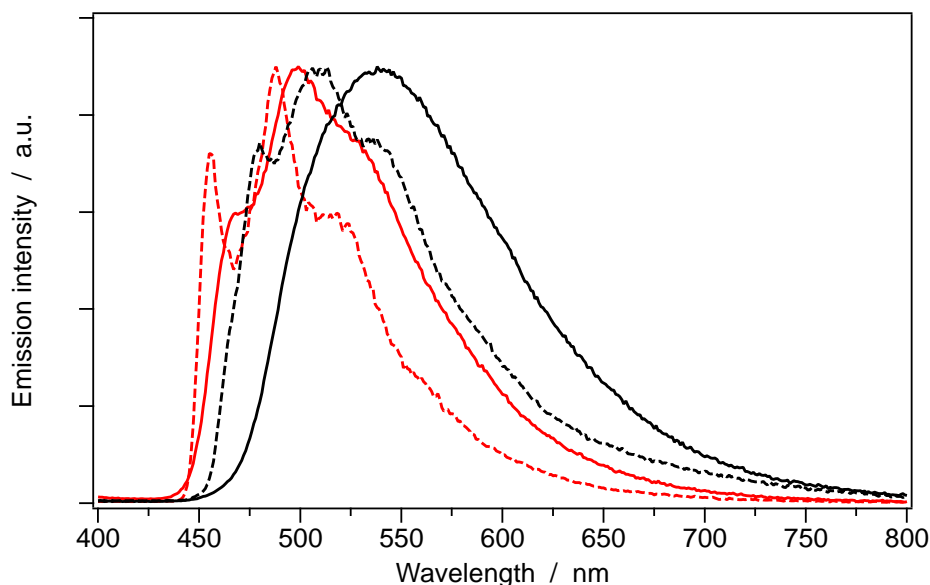


Figure 9: Corrected emission spectra of **3** (black) and **5** (red) in acetonitrile at 298 K (full) and at 77 K (dashed)

The room-temperature emission spectrum of **5** is more structured if compared to that of **3**, probably due to the presence of the bis-tetrazolate chelating ligand that can increase the rigidity of the related complex. This is also reflected in a less pronounced hypsochromic shift when lowering the temperature from 298 K to 77 K. Moreover, it should be stressed that, at low temperature, also the emission spectrum of **3** displays a pronounced vibronic structure with the main progression displaying a frequency similar to that observed for **5** (*i.e.*, 1441 vs. 1358 cm^{-1}). Such vibrational frequency can be associated to the aromatic C=C stretching of the mesoionic carbene ligands, indicating that the emitting state is probably a ^3LC state in both complexes, not involving the ancillary ligands.³⁶

Table 4: Luminescence properties and photophysical parameters of complexes **3** and **5**

	Oxygen-free solution CH ₃ CN 298 K			Rigid matrix CH ₃ CN, 77 K		1% PMMA matrix 298 K		
	λ_{em} [nm]	Φ_{em}^a [%]	τ [μ s]	λ_{em} [nm]	τ [μ s]	λ_{em} [nm]	Φ_{em}^b [%]	τ [μ s]
3	538	1.4	5.90	456, 488, 515	11.8	552	3.1	4.6
5	470 ^(sh) , 499	11.7	3.77	480, 509, 537	20.5	475 ^(sh) , 502	20	7.9

^a [Ru(bpy)₃]Cl₂ as reference (PLQY = 2.8%); ^b determined using an integrating sphere.

In order to assess the nature of the emitting state, the lowest triplet state of each complex was optimized using an unrestricted DFT approach. As expected, the spin-density distributions reported in Figure 10 indicate that the lowest triplet excited state of both complexes has a strong LC nature (centered on the neutral pyridyl-triazolylidene ligand) with some ³MLCT contribution from the iridium d_π orbitals. In both cases, the topology of the spin-density contours is compatible with a HOMO→LUMO excitation (see Figure 7 for comparison). The calculated emission energies are computed to be 2.26 eV (548 nm) and 2.32 eV (535 nm) for **3** and **5**, respectively. These values well compare with the mean photon energy of the emission spectra recorded in room-temperature acetonitrile solution (*i.e.*, 2.21 eV and 2.38 eV for **3** and **5**, respectively). According to theoretical indications, the blue shift observed in the case of **5** can be ascribed to the stronger stabilization of the iridium d_π orbitals induced by the bis-tetrazolate ancillary ligand compared to the two chloride atoms, rather than to a different nature of the triplet excited state.

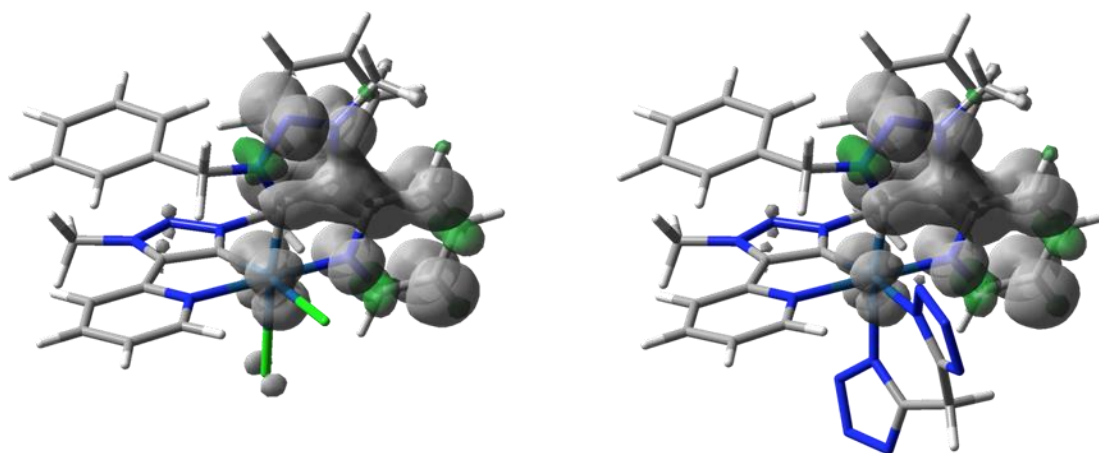


Figure 10: Spin-density distribution for the lowest-energy triplet state (T_1) of complex **3** (left) and **5** (right), computed in acetonitrile using the PCM-UM06/6-31G(d)& LANL2DZ(Ir) level of theory; isovalue: 0.002 e bohr⁻³

Despite both complexes emit from a similar ³LC state, their photoluminescence quantum yields (PLQYs) in room-temperature acetonitrile solutions are considerably different (Table 4). **5** exhibits a PLQY around 12%, a value which is comparable with that of the archetypal complex [Ir(ppy)₂(bpy)]⁺, whereas the PLQY of the

dichloro-precursor **3** is one order of magnitude lower. However, such a low quantum yield is in line with literature data reported for other cyclometalated iridium(III) complexes equipped with chloride ions as ligands.³⁷

In Figure 11 are reported the room-temperature emission spectra of **3** and **5** in poly(methyl methacrylate) (PMMA, 1% by weight). The emission profiles are comparable with those recorded in acetonitrile solution at 298 K and only a slight red-shift is observed when the complexes are embedded in the polymeric matrix, further corroborating the hypothesis of a ligand-centered emitting state with a small MLCT contribution.

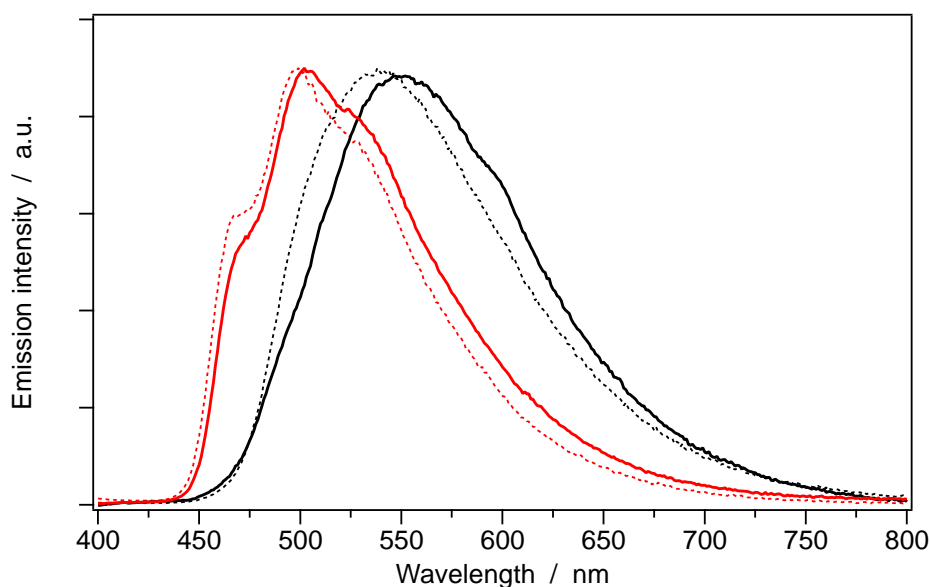


Figure 11: Corrected emission spectra of complex **3** (black) and **5** (red) in 1% PMMA matrix recorded at 298 K (full lines) and compared to the ones in room-temperature acetonitrile solutions (thin dashed lines)

11.2 Conclusions

Cationic luminescent Ir(III) complexes carrying a mesoionic carbene (MIC) as neutral ligand and two chlorides or a chelating bis-tetrazolate derivative as anionic ancillary ligands have been obtained for the first time.

A simple procedure to synthesize derivatives **3** and **5** has been set up through transmetalation of the *in situ*-generated Ag-carbene and $[\text{Ir}(\text{COD})\text{Cl}]_2$. The complexes have been obtained in satisfactory yields and fully characterized. DFT calculations indicate that luminescence originates from ligand-centered (LC) excited states and all the theoretical findings are in line with both the electrochemical data and the electronic absorption spectra. In particular, the presence of the bis-tetrazolate ligand in **5** induces a blue shift in the emission compared to complex **3**. Photoluminescence quantum yields are comparable to those of the

archetypal complex $[\text{Ir}(\text{ppy})_2(\text{bpy})]^+$ and of other cyclometalated iridium(III) complexes carrying chloride ligands, respectively.

This work gives entry to a new class of phosphorescent Ir(III) complexes which can now be expanded by rationally changing the mesoionic carbene and/or the ancillary ligands, in order to enhance the luminescent properties and potential applications thereof.

11.3 Experimental section

General synthetic procedures

Analytical grade solvents and commercially available reagents were used as received, unless otherwise stated. Chromatographic purifications were performed using 70-230 mesh silica. ^1H , ^{13}C , NMR spectra were recorded on a Varian Inova 300 MHz, on a Mercury 400 MHz or on an Inova 600 MHz spectrometer. Chemical shifts (δ) are reported in ppm relative to residual solvent signals for ^1H and ^{13}C NMR (^1H NMR: 7.26 ppm for CDCl_3 ; ^{13}C NMR: 77.0 ppm for CDCl_3). ^{13}C NMR spectra were acquired with ^1H broad band decoupled mode. Coupling constants are given in Hertz. Elemental analyses were performed on a ThermoQuest Flash 1112 series EA instrument. ESI-MS analysis were performed by direct injection of acetonitrile solutions of the compounds using a WATERS ZQ 4000 mass spectrometer

Synthesis of 2-(1-benzyl-1H-1,2,3-triazol-4-yl)pyridine (1)

Benzylbromide (1.4 mL, 11.7 mmol) and NaN_3 (1.9 g, 29.2 mmol) were dissolved in DMSO (30 mL) and the resulting solution was stirred at room temperature for 24 hours. After this time, water (30 mL) was added and the resulting mixture was extracted with DCM (4 x 15 mL). The collected organic phase was washed with water (30 mL) and brine (30 mL), dried over Na_2SO_4 and concentrated giving a pale yellow oil, which was used without further purifications. The resulting benzylazide was dissolved in a mixture of 1:1 *t*BuOH/water (60 mL) and 2-ethynylpyridine (1.8 mL, 17.5 mmol), $\text{CuSO}_4 \cdot \text{H}_2\text{O}$ (1.2 g, 4.7 mmol) and sodium ascorbate (378.2 mg, 1.75 mmol) were added. The resulting mixture was stirred at room temperature for 24 hours and then the solvent was removed under vacuum. The crude was dissolved in DCM (30 mL) and ammonia solution (30 mL) was added. Stirring was performed for additional 24 hours. Water (30 mL) was added to the reaction and the mixture was extracted with DCM (3 x 20 mL). The collected organic phase was washed with brine, dried over Na_2SO_4 and concentrate. The crude was purified on silica gel flash chromatography using a mixture of CH_2Cl_2 /methanol (95:5) to give product **1** in 93% yield (2.7 g). ^1H NMR (CDCl_3 , 300 MHz) δ 8.53 (d, $J = 4.8$ Hz, 1H), 8.17 (d, $J = 8.1$ Hz, 1H), 8.05 (s, 1H), 7.76 (dt, $J_{\text{HH}} = 1.8$ Hz, $J_{\text{HH}} = 7.8$ Hz, 1H) 7.40-7.31 (m, 5H), 7.21 (ddd, $J_{\text{HH}} = 0.9$ Hz, $J_{\text{HH}} = 5.1$ Hz, $J_{\text{HH}} = 7.5$ Hz, 1H), 5.58 (s, 2H). ^{13}C NMR

(CDCl₃, 400 MHz) δ 150.2 (C), 149.3 (CH), 148.7 (C), 136.9 (CH), 134.3 (C), 129.2 (CH), 128.8 (CH), 128.3 (CH), 122.8 (CH), 121.9 (CH), 120.2 (CH), 54.4 (CH₂).

Synthesis of 1-benzyl-3-methyl-4-(pyridin-2-yl)-1H-1,2,3-triazol-3-ium-trifluoromethanesulfonate (2)

2-(1-benzyl-1H-1,2,3-triazol-4-yl) pyridine **1** (200 mg, 0.85 mmol) was dissolved in DCM (3 mL) and MeOTf (480 μ L, 4.24 mmol) was slowly added. The resulting solution was refluxed for 24 hours under nitrogen atmosphere. The solvent was then evaporated and the crude was washed with Et₂O (5 mL) and DCM (5 mL). Product **2** was isolated by silica gel flash chromatography using a mixture of CH₂Cl₂/methanol (95:5) in 58.9% yield (199.6 mg). ¹H NMR (CD₃OD, 400 MHz) δ 9.26 (s, 1H), 8.83-8.80 (m, 1H), 8.07-7.99 (m, 2H), 7.65-7.56 (m, 3H), 7.53-7.45 (m, 3H), 5.91 (s, 2H), 4.65 (s, 3H). ¹³C NMR (CD₃OD, 100 MHz) δ 152.0 (CH), 145.3 (C), 143.4 (C), 140.1 (CH), 134.1 (C), 131.7 (CH), 131.3 (CH), 131.2 (CH), 130.8 (CH), 127.8 (CH), 126.5 (CH), 122.1 (CF₃, J_{CF} = 319.8 Hz), 59.3 (CH₂), 42.6 (CH₃). Anal. Calculated for C₁₆H₁₅F₃N₄O₃S (400.38): C, 48.00; H, 3.78; N, 13.99%. Found: C, 48.94; H, 3.89; N, 14.21%.

Synthesis of complex [Ir(tripz)₂Cl₂]⁺ (3)

1-benzyl-3-methyl-4-(pyridin-2-yl)-1H-1,2,3-triazol-3-ium-trifluoromethanesulfonate **2** (100 mg, 0.25 mmol) was dissolved in acetonitrile (15 mL). KCl (186.5 mg, 2.5 mmol) and Ag₂O (202.8 mg, 0.875 mmol) was added. The resulting mixture was stirred in nitrogen atmosphere for 2 days in absence of light. After this time the resulting solid was removed by filtration and washed with ACN (10 mL). The solution was then evaporated under vacuum giving the silver derivative as a white solid that was added to a solution of di- μ -chlorobis(1,5-cyclooctadiene)diiridium ([Ir(COD)Cl]₂) (67.2 mg, 0.1 mmol) in 2-ethoxyethanol (3 mL). The resulting solution was refluxed for 24 hours under nitrogen atmosphere. The black precipitate was filtered off and the resulting solution was concentrated under vacuum. The crude was washed with Et₂O (5 mL) and the pale yellow precipitate was collected and dried. Then MeOH (5 mL) was added and the resulting solid was filtered off. The solvent was evaporated giving a yellow oil. Recrystallization from DCM/Et₂O gave product **3** as a yellow solid in 40.6% yield (21.6 mg). ¹H NMR (CD₃OD, 400 MHz) δ 9.71 (d, J_{HH} = 6.0 Hz, 2H), 8.15 (dt, J_{HH} = 1.2 Hz, J_{HH} = 8.0 Hz, 2H), 8.00 (dq, J_{HH} = 0.8 Hz, J_{HH} = 8.0 Hz, 2H), 7.49 (t, J_{HH} = 6.8 Hz, 2H), 7.35 (t, J_{HH} = 7.6 Hz, 2H), 7.22 (t, J_{HH} = 7.6 Hz, 4H), 6.45 (d, J_{HH} = 7.6 Hz, 4H), 5.24 (d, J_{HH} = 16.8 Hz, 2H), 4.93 (d, J_{HH} = 16.8 Hz, 2H), 4.43 (s, 6H). ¹⁹F NMR (CD₃OD, 300 MHz) δ -80.0 (s). ¹³C NMR (CD₃OD, 150 MHz) δ 155.0 (CH), 151.5 (C), 150.1 (C), 141.4 (CH), 137.7 (C), 135.2 (C), 129.8 (CH), 129.5 (CH), 126.5 (CH), 126.4 (CH), 123.2 (CH), 56.2 (CH₂), 39.7 (CH₃). Anal. Calculated for C₃₁H₂₈Cl₂F₃IrN₈O₃S (912.79): C, 40.79; H, 3.09; N, 12.28%. Found: C, 41.04; H, 2.98; N, 11.89%. ESI-MS: 763 [M-CF₃SO₃]⁺.

Synthesis of ligand di(1H-tetrazol-5-yl)methane (H₂-4)

Malononitrile (12.0 g, 182 mmol), NaN₃ (26 g, 400 mmol) and dimethylamine hydrochloride (32.6 g, 400 mmol) were dissolved in DMF and the resulting solution was stirred at 110 °C for 24 hours. The precipitate

was filtered off and the solution was evaporated under reduced pressure. The resulting solid was dissolved in 1M HCl until a pH value of 1 and the resulting precipitate was collected and well dried. MeOH (30 mL) and active carbon were added and the resulting mixture was stirred overnight. The black precipitate was filtered off and the solvent was evaporated giving product as a white solid in 60% yield (16.6 g). ^1H NMR (CD_3OD , 300 MHz) δ 5.30 (s, 2H). ^{13}C NMR (CD_3OD , 75 MHz) δ 155.3 (C), 21.2 (CH_2).

Synthesis of complex $[\text{Ir}(\text{tripz})_2(\text{b-trz})]^+$ (**5**)

Complex **3** (21.6 mg, 0.028 mmol) was dissolved in EtOH (4 mL) and AgOTf (22.0 mg, 0.085 mmol) was added. The resulting mixture was refluxed for 24 hours. Then the formed black solid was filtered off and the solution was added to a mixture of di(1*H*-tetrazol-5-yl)methane (**H₂-4**, 4.3 mg, 0.028 mmol) and KOH (5 mg, 0.085 mmol) in EtOH (2 mL) previously stirred for 30 min at room temperature. The resulting solution was refluxed at 90 °C for 4 hours and then the solvent was evaporated. The crude was purified by aluminium oxide flash chromatography using a mixture of CH_2Cl_2 /methanol (95:5) to give product as a yellow solid in 77.2% yield (21.6 mg). ^1H NMR (CDCl_3 , 600 MHz) δ 7.84 (t, $J_{\text{HH}} = 7.8$ Hz, 2H), 7.75 (d, $J_{\text{HH}} = 7.8$ Hz, 2H), 7.24 (d, $J_{\text{HH}} = 6.0$ Hz, 2H), 7.20 (t, $J_{\text{HH}} = 7.2$ Hz, 2H), 7.11 (t, $J_{\text{HH}} = 7.2$ Hz, 4H), 6.79 (t, $J_{\text{HH}} = 7.2$ Hz, 2H), 6.73 (d, $J_{\text{HH}} = 7.2$ Hz, 4H), 5.37 (d, $J_{\text{HH}} = 16.8$ Hz, 2H), 5.31 (d, $J_{\text{HH}} = 16.8$ Hz, 2H), 4.65 (s, 2H), 4.55 (s, 6H). ^{19}F NMR (CD_3OD , 300 MHz) δ -80.0 (s). ^{19}F NMR (CD_3OD , 600 MHz) δ -80.0 (s). ^{13}C NMR (CDCl_3 , 150 MHz) δ 154.6 (C), 151.1 (C), 151.0 (CH), 149.0 (C), 141.1 (C), 139.9 (CH), 133.7 (C), 128.7 (CH), 127.9 (CH), 125.6 (CH), 124.7 (CH), 121.8 (CH), 56.2 (CH_2), 39.4 (CH_3), 29.7 (CH_2). Anal. Calculated for $\text{C}_{34}\text{H}_{30}\text{F}_3\text{IrN}_{16}\text{O}_3\text{S}$ (991.98): C, 41.17; H, 3.05; N, 22.59%. Found: C, 40.71; H, 2.97; N, 21.93%. ESI-MS: 843 $[\text{M}-\text{CF}_3\text{SO}_3]^+$.

Electrochemistry

Voltammetric experiments were performed in a three-electrodes cell (BioLogic SVC-2 cell, Pt working electrode, Pt pseudo-reference, Pt counter electrode) using a Metrohm AutoLab PGSTAT 302 electrochemical workstation in combination with the NOVA software package. The measurements were carried out at 298 K in CH_3CN solution with sample concentration ca. 4×10^{-4} M, using 0.1 M tetrabutylammonium hexafluorophosphate (Sigma-Aldrich, electrochemical grade) as the supporting electrolyte. Oxygen was removed from the solutions by bubbling argon for 10 minutes before each scan. Ferrocene was added as the internal reference at the end of each set of measurements. Cyclic voltammograms (CV) were recorded at scan rates between 0.01 and 2 V/s to check reversibility; square-wave voltammograms (SWV) were recorded with scan rate = 25 mV/s, SW amplitude = 20 mV and frequency = 25 Hz.

Computational details

Density functional theory (DFT) calculations were carried out using the D.01 revision of the Gaussian 09 program package in combination with the M06 hybrid meta exchange-correlation functional. The 6-31G(d)

basis set was selected for C, H, N and Cl atoms; on the other hand, the “double- ζ ” quality LANL2DZ basis sets and the related pseudopotential were adopted for the Ir metal center. All the complexes were fully optimized in acetonitrile both in the electronic ground state (S_0) and in the lowest triplet state (T_1) by using the polarizable continuum model (PCM). A frequency calculation was always used to confirm that the stationary point found by the geometry optimization was actually corresponding to a minimum on the potential energy surface (no imaginary frequencies). Time-dependent DFT calculations (TD-DFT)³⁸ at the same level of theory used for geometrical optimization, were employed to simulate the absorption spectra of all the molecules in their optimized S_0 geometry. The first 100 singlet and 25 triplet vertical excitations were computed for the complexes. To investigate the nature of the T_1 state, geometry optimizations and related frequency calculations were performed at the spin-unrestricted UM06 level of theory, imposing a spin multiplicity of 3. The emission energy from the lowest triplet excited state was estimated by subtracting the SCF energy of the T_1 state in its minimum conformation from that of the singlet ground state having the same geometry of T_1 . All the pictures of molecular orbitals and spin-density surfaces were created using GaussView 5.³⁹ The structural overlap of the X-ray crystal structure of 3 and the theoretically computed one is obtained using the VMD program by minimising the root-mean-square deviation (RMSD) of all the atomic positions, except hydrogen.

Photophysical measurements

The spectroscopic investigations were carried out in spectrofluorimetric grade acetonitrile. The absorption spectra were recorded with a Perkin-Elmer Lambda 950 spectrophotometer. For the photoluminescence experiments, the sample solutions were placed in fluorimetric Suprasil quartz cuvettes (1 cm) and dissolved oxygen was removed by bubbling argon for 20 minutes. The uncorrected emission spectra were obtained with an Edinburgh Instruments FLS920 spectrometer equipped with a Peltier-cooled Hamamatsu R928 photomultiplier tube (PMT) (185-850 nm). An Edinburgh Xe 900 with 450 W xenon arc lamp was used as the excitation light source. The corrected spectra were obtained via a calibration curve supplied with the instrument. The photoluminescence quantum yields (PLQY) in solution were obtained from the corrected spectra on a wavelength scale (nm) and measured according to the approach described by Demas and Crosby,⁴⁰ using an air-equilibrated water solution of $[\text{Ru}(\text{bpy})_3]\text{Cl}_2$ as reference (PLQY = 2.8 %)⁴¹ was used as standard. The emission lifetimes (τ) in the nanosecond and microsecond ranges were measured through the time-correlated single photon counting (TCSPC) technique with the use of the same luminescence spectrometer described above and equipped with a laser diode as the excitation source (1 MHz; $\lambda_{\text{exc}} = 407$ nm; 200 ps time resolution after deconvolution) and the aforementioned PMTs as detectors. The analysis of the luminescence decay profiles was accomplished with the software provided by the manufacturer, and the quality of the fit was assessed with the χ^2 value close to unity and with the residuals regularly distributed along the time axis. To record the 77 K luminescence spectra, samples were put in quartz tubes

(2 mm inner diameter) and inserted into a special quartz Dewar flask filled with liquid nitrogen. The poly(methyl methacrylate) (PMMA) films containing 1% (w/w) of the complex were drop-cast from dichloromethane solutions. The thickness of the films was not controlled. Solid-state PLQY values were calculated by corrected emission spectra obtained from an Edinburgh FLS920 spectrometer equipped with a barium sulfate-coated integrating sphere (diameter of 4 in.) following the procedure described by Würth *et al.*⁴² Experimental uncertainties are estimated to be $\pm 8\%$ for τ determinations, $\pm 10\%$ for Φ_{PL} , ± 2 nm and ± 5 nm for absorption and emission peaks, respectively.

11.4 Bibliography

¹ a) P. Mathew, A. Neels, M. Albrecht, *J. Am. Chem. Soc.* **2008**, *130*, 13534; b) G. Guisado-Barrios, J. Bouffard, B. Donnadieu, G. Bertrand, *Angew. Chem. Int. Ed.* **2010**, *49*, 4759.

² a) J. D. Crowley, A. Lee, K. J. Kilpin, *Aust. J. Chem.* **2011**, *64*, 1118; b) K. F. Donnelly, A. Petronilho, M. Albrecht, *Chem. Commun.* **2013**, *49*, 1145; c) J. M. Aizpurua, R. M. Fratila, Z. Monasterio, N. Pérez-Esnaola, E. Andreieff, A. Irastorza, M. Sagartzazu-Aizpurua, *New J. Chem.* **2014**, *38*, 474; and cited references.

³ Selected examples of catalytic applications: a) A. Bolje, S. Hohloch, M. van der Meer, J. Košmrlj, B. Sarkar, *Chem. Eur. J.* **2015**, *21*, 6756; b) D. Mendoza-Espinosa, R. González-Olvera, G. E. Negrón-Silva, D. Angeles-Beltrán, O. R. Suárez-Castillo, A. Álvarez-Hernández, R. Santillan *Organometallics* **2015**, *34*, 4529; c) A. Petronilho, A. Llobet, M. Albrecht, *Inorg. Chem.* **2014**, *53*, 12896; d) R. Maity, S. Hohloch, C.-Y. Su, M. van der Meer, B. Sarkar, *Chem. Eur. J.* **2014**, *20*, 9952; e) R. Lalrempuia, N. D. McDaniel, H. Müller-Bunz, S. Bernhard, M. Albrecht, *Angew. Chem. Int. Ed.* **2010**, *49*, 9765.

⁴ V. V. Rostovtsev, L. G. Green, V. V. Fokin, K. B. Sharpless, *Angew. Chem. Int. Ed.* **2002**, *41*, 2596; b) C. W. Tornøe, C. Christensen, M. Meldal, *J. Org. Chem.* **2002**, *67*, 3057; c) F. Himo, T. Lovell, R. Hilgraf, V. V. Rostovtsev, L. Noodleman, K. B. Sharpless, V. V. Fokin, *J. Am. Chem. Soc.* **2005**, *127*, 210.

⁵ R. H. Crabtree, *Coord. Chem. Rev.* **2013**, *257*, 755; and cited references.

⁶ a) B. Beyer, C. Ulbricht, D. Escudero, C. Friebe, A. Winter, L. Gonzalez, U. S. Schubert, *Organometallics* **2009**, *28*, 5478; b) S. Ladouceur, D. Fortin, E. Zysman-Colman, *Inorg. Chem.* **2011**, *50*, 11514; c) J. M. Fernández-Hernández, C.-H. Yang, J. I. Beltrán, V. Lemaury, F. Polo, R. Fröhlich, J. Cornil, L. De Cola, *J. Am. Chem. Soc.* **2011**, *133*, 10543; d) M. de Barros e Silva Botelho, J. M. Fernandez-Hernandez, T. B. de Queiroz, H. Eckert, L. De Cola, A. S. S. de Camargo, *J. Mater. Chem.* **2011**, *21*, 8829; e) J. M. Fernández-Hernández, J. I. Beltrán, V. Lemaury, M.-D. Gálvez-López, C.-H. Chien, F. Polo, E. Orselli, R. Fröhlich, J. Cornil, L. De Cola, *Inorg. Chem.* **2013**, *52*, 1812; f) L. Donato, P. Abel, E. Zysman-Colman, *Dalton Trans.* **2013**, *42*, 8402.

⁷ a) E. Orselli, R. Q. Albuquerque, P. M. Fransen, R. Fröhlich, H. M. Janssen, L. De Cola, *J. Mater. Chem.* **2008**, *18*, 4579; b) M. Felici, P. Contreras-Carballada, Y. Vida, J. M. M. Smits, R. J. M. Nolte, L. De Cola, R. M.

- Williams, M. C. Feiters, *Chem. Eur. J.* **2009**, *15*, 13124; c) M. Mydlak, C. Bizzarri, D. Hartmann, W. Sarfert, G. Schmid, L. De Cola, *Adv. Funct. Mater.* **2010**, *20*, 1812; d) A. Baschieri, S. Muzzioli, V. Fiorini, E. Matteucci, M. Massi, L. Sambri, S. Stagni, *Organometallics* **2014**, *33*, 6154; e) M. Naddaka, E. Locatelli, D. Colecchia, L. Sambri, I. Monaco, A. Baschieri, F. Sasdelli, M. Chiariello, E. Matteucci, P. Zani, M. Comes Franchini, *RSC Advances* **2015**, *5*, 1091.
- ⁸ a) S. Sinn, B. Schulze, C. Friebe, D. G. Brown, M. Jäger, E. Altuntaş, J. Kübel, O. Guntner, C. P. Berlinguette, B. Dietzek, U. S. Schubert, *Inorg. Chem.* **2014**, *53*, 2083; b) V. Leigh, W. Ghattas, R. Lalrempuia, H. Müller-Bunz, M. T. Pryce, M. Albrecht, *Inorg. Chem.* **2013**, *52*, 5395.
- ⁹ A. Baschieri, S. Muzzioli, E. Matteucci, S. Stagni, M. Massi, L. Sambri, *Dalton Trans.* **2015**, *44*, 37.
- ¹⁰ a) F. Monti, A. Baschieri, I. Gualandi, J. J. Serrano-Pérez, J. M. Junquera-Hernández, D. Tonelli, A. Mazzanti, S. Muzzioli, Stefano Stagni, C. Roldan-Carmona, A. Pertegás, H. J. Bolink, E. Ortí, L. Sambri, N. Armaroli, *Inorg. Chem.* **2014**, *53*, 7709; b) F. Monti, A. Baschieri, E. Matteucci, A. Mazzanti, L. Sambri, A. Barbieri, N. Armaroli, *Faraday Discuss.* **2015**, *185*, 233.
- ¹¹ a) S. Lamansky, D. Murphy, F. A. Razzaq, H. E. Lee, C. Adachi, P. E. Burrows, S. R. Forrest, M. E. Thompson, *J. Am. Chem. Soc.* **2001**, *123*, 4304; b) S. Lamansky, P. Djurovich, D. Murphy, F. A. Razzaq, R. Kwong, I. Tsyba, M. Bortz, B. Mui, R. Bau, M. E. Thompson, *Inorg. Chem.* **2001**, *40*, 1704.
- ¹² R. D. Costa, E. Ortí, H. J. Bolink, F. Monti, G. Accorsi, N. Armaroli, *Angew. Chem. Int. Ed.* **2012**, *51*, 8178.
- ¹³ I. M. Dixon, J. P. Collin, J.-P. Sauvage, L. Flamigni, S. Encinas, F. Barigelletti, *Chem. Soc. Rev.* **2000**, *29*, 385.
- ¹⁴ S. Soman, J. C. Manton, J. L. Inglis, Y. Halpin, B. Twamley, E. Otten, W. R. Browne, L. De Cola, J. G. Vos, M. T. Pryce, *Chem. Commun.* **2014**, *50*, 6461.
- ¹⁵ a) M. Pandrala, F. Li, M. Feterl, Y. Mulyana, J. M. Warner, L. Wallace, F. R. Keene, J. G. Collins, *Dalton Trans.* **2013**, *42*, 4686; b) M. Pandrala, F. Li, L. Wallace, P. J. Steel, B. Moore II, J. Autschbach, J. G. Collins, F. R. Keene, *Aust. J. Chem.* **2013**, *66*, 1065.
- ¹⁶ S. Stimpson, D. R. Jenkinson, A. Sadler, M. Latham, D. A. Wragg, A. J. H. M. Meijer, J. A. Thomas, *Angew. Chem. Int. Ed.* **2015**, *54*, 3000.
- ¹⁷ K. R. Lee, M.-S. Eum, C. S. Chin, S. Lee, I. J. Kim, Y. S. Kim, Y. Kim, S.-J. Kim, N. H. Hur, *Dalton Trans.* **2009**, 3650.
- ¹⁸ J.-L. Liao, Y. Chi, Z.-T. Sie, C.-H. Ku, C.-H. Chang, M. A. Fox, P. J. Low, M.-R. Tseng, G.-H. Lee, *Inorg. Chem.* **2015**, *54*, 10811.
- ¹⁹ V. H. Nguyen, H. Q. Chew, B. Su, J. H. K. Yip, *Inorg. Chem.* **2014**, *53*, 9739.
- ²⁰ K. F. Donnelly, R. Lalrempuia, H. Müller-Bunz, M. Albrecht, *Organometallics* **2012**, *31*, 8414.
- ²¹ J. D. Crowley, P. H. Bandeen, L. R. Hanton, *Polyhedron* **2010**, *29*, 70.
- ²² B. J. Coe, M. Helliwell, J. Raftery, S. Sanchez, M. K. Peers, N. S. Scrutton, *Dalton Trans.* **2015**, *44*, 20392.
- ²³ E. C. Keske, O. V. Zenkina, R. Wang, C. M. Crudden, *Organometallics* **2012**, *31*, 456.

- ²⁴ S. Hohloch, L. Suntrup, B. Sarkar, *Organometallics* **2013**, *32*, 7376.
- ²⁵ D. Yang, Y. Long, J. Zhang, H. Zeng, S. Wang, C. Li, *Organometallics* **2010**, *29*, 3477.
- ²⁶ V. Y. Zubarev, R. E. Trifonov, V. V. Poborchii, V. A. Ostrovskii, *Chem. Heterocycl. Compd.* **2006**, *42*, 469.
- ²⁷ B. J. Coe, M. Helliwell, J. Raftery, S. Sanchez, M. K. Peers, N. S. Scrutton, *Dalton Trans.* **2015**, *44*, 20392.
- ²⁸ S. Ladouceur, E. Zysman-Colman, *Eur. J. Inorg. Chem.* **2013**, 2985.
- ²⁹ M. J. Frisch, G. W. Trucks, H. B. Schlegel, G. E. Scuseria, M. A. Robb, J. R. Cheeseman, G. Scalmani, V. Barone, B. Mennucci, G. A. Petersson, et al. *Gaussian 09, Revision D.01*, Gaussian, Inc.: Wallingford CT, 2009.
- ³⁰ a) Y. Zhao, D. G. Truhlar, *Theor. Chem. Acc.* **2008**, *120*, 215; b) Y. Zhao, D. G. Truhlar, *Accounts Chem. Res.* **2008**, *41*, 157.
- ³¹ a) G. A. Petersson, A. Bennett, T. G. Tensfeldt, M. A. Al-Laham, W. A. Shirley, J. Mantzaris, *J. Chem. Phys.* **1988**, *89*, 2193; b) M. M. Francl, W. J. Pietro, W. J. Hehre, J. S. Binkley, M. S. Gordon, D. J. DeFrees, J. A. Pople, *J. Chem. Phys.* **1982**, *77*, 3654.
- ³² P. J. Hay, W. R. Wadt, *J. Chem. Phys.* **1985**, *82*, 299.
- ³³ a) J. Tomasi, M. Persico, *Chem. Rev.* **1994**, *94*, 2027; b) J. Tomasi, B. Mennucci, R. Cammi, *Chem. Rev.* **2005**, *105*, 2999; c) C. J. Cramer, D. G. Truhlar, in *Solvent Effects and Chemical Reactivity*, eds. O. Tapia and J. Bertrán, Springer Netherlands, 2002, vol. 17, pp. 1-80.
- ³⁴ W. Humphrey, A. Dalke, K. Schulten, *J. Mol. Graph Model.* **1996**, *14*, 33.
- ³⁵ T. Hu, L. He, L. Duan, Y. Qiu, *J. Mater. Chem.* **2012**, *22*, 4206.
- ³⁶ a) G. H. Allen, R. P. White, D. P. Rillema, T. J. Meyer, *J. Am. Chem. Soc.*, **1984**, *106*, 2613; b) J. V. Caspar, T. D. Westmoreland, G. H. Allen, P. G. Bradley, T. J. Meyer, W. H. Woodruff, *J. Am. Chem. Soc.* **1984**, *106*, 3492; c) E. M. Kober, J. V. Caspar, R. S. Lumpkin, T. J. Meyer, *J. Phys. Chem.* **1986**, *90*, 3722; d) H. Amouri, J. B. Waern, R. Caspar, A. Barbieri, C. Sabatini, A. Zanelli, F. Barigelletti, *Dalton Trans.* **2007**, 2179.
- ³⁷ L. Flamigni, A. Barbieri, C. Sabatini, B. Ventura, F. Barigelletti, *Top. Curr. Chem.* **2007**, *281*, 143.
- ³⁸ a) R. E. Stratmann, G. E. Scuseria, M. J. Frisch, *J. Chem. Phys.* **1998**, *109*, 8218; b) M. E. Casida, C. Jamorski, K. C. Casida, D. R. Salahub, *J. Chem. Phys.* **1998**, *108*, 4439; c) R. Bauernschmitt, R. Ahlrichs, *Chem. Phys. Lett.* **1996**, *256*, 454.
- ³⁹ R. Dennington, T. Keith and J. Millam, *GaussView, Version 5*, (2009) Semichem Inc., Shawnee Mission, KS, USA.
- ⁴⁰ G. A. Crosby, J. N. Demas, *J. Phys. Chem.* **1971**, *75*, 991.
- ⁴¹ K. Nakamaru, *Bull. Chem. Soc. Jpn.* **1982**, *55*, 2697.
- ⁴² C. Wurth, M. Grabolle, J. Pauli, M. Spieles, U. Resch-Genger, *Nat. Protoc.* **2013**, *8*, 1535.

12. Ir complexes for in vitro imaging on glioblastoma cell line

Early cancer detection is today the best possibility to increment patients' survival rate. However, many forms of cancer are still very difficult to detect with common techniques, due to their nature or location in the body, so remain practically untreatable.¹ Up to now, one of the most common techniques in cancer detection is the use of diagnostic contrast agents, but they present some limitations, especially due to their poor selectivity for infected tissues, with consequences in diagnosis sensitivity. In recent years, the development of tumor-targeted contrast agents, based on biocompatible nanoparticle formulations, have led to encouraging results in terms of sensitivity and specificity for tumor imaging.²

In the past few years, the use of phosphorescent iridium(III) complexes have rapidly grown for cellular imaging, intracellular sensing, gene delivery and cancer cell detection.^{3,4} Key advantages for these complexes, compared to organic luminophores for bioimaging, are the compatibility with time-gated bioimaging techniques, that completely eliminate the sample-autofluorescence background signals, and the large Stokes shifts in the visible region, join with the possibility of fine tuning the physical and chemical properties by simple modification of the ligands. Indeed, these complexes show an intense, long-living and environmental-sensitive emission, that allows their employment as reporters of their local surrounding and intracellular biological events.^{3,4} Unfortunately, many Ir(III) complexes present a high cytotoxicity. However, this problem can be prevented by incorporation and/or linkage of them into biologically compatible nanocarriers,^{5,6,7} such as cholesterol based nanocarriers. This class of nanocarriers are of a great potential for biomedical applications, but the fabrication of an amphiphilic structure through the attachment of a hydrophilic tail to the cholesterol hydrophobic macrostructure is necessary in order to create water dispersible nanocarriers.^{8,9,10} The use of Polyethylene (PEG) as a stabilizing agent for nanoparticles in aqueous media thanks to its hydrophilicity have been widely studied, but very few examples of pure PEG functionalized cholesterol particles have been reported, due to the oversized dimension of the nanoparticles or the needed of additional surfactants for their stabilization.^{11,12,13}

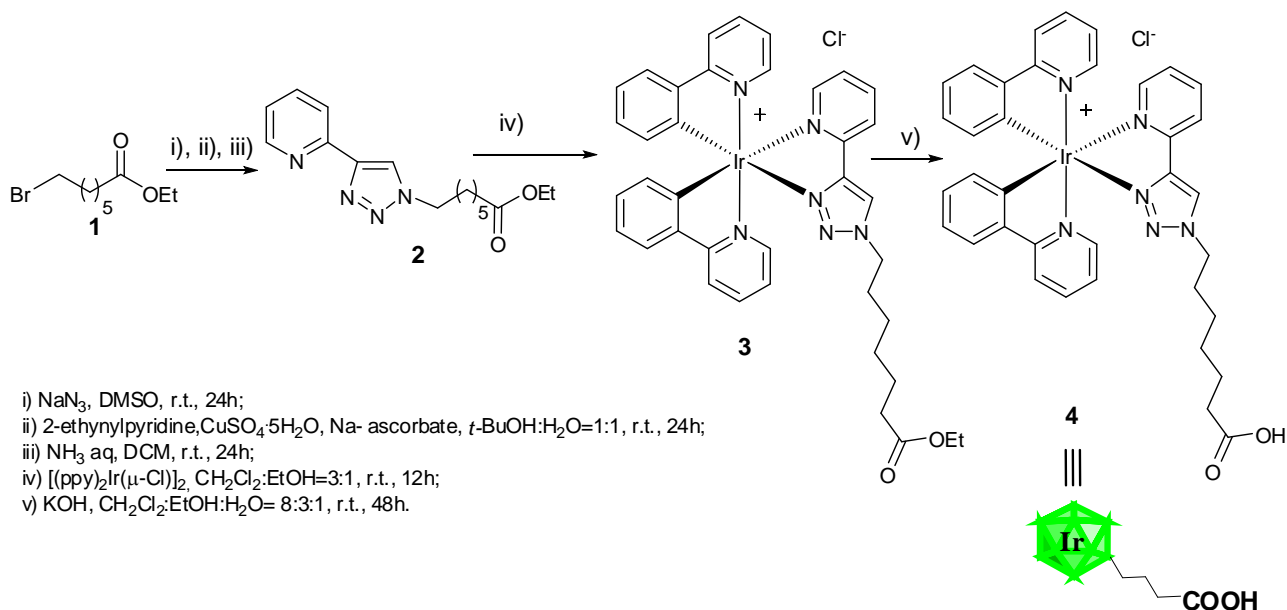
In this project, I have synthesized an Iridium(III) complex with a terminal carboxylic acid group able to be linked to the outer shell of cholesterol-PEG based nanocarriers or to be encapsulated inside their lipophilic core. In both cases, Ir(III) complexes is shield by the nanocarrier, and is possible to monitoring their positions into a cancer cell line, U87MG, derived from human glioblastoma multiforme.

12.1 Results and discussion

12.1.1 Synthesis of Iridium complex

The object of the project was to synthesize a cationic luminescent Ir(III) complex bearing a lipophilic tail with a terminal carboxylic acid group. As ligand for the Ir(III) complex we choose a pyridin-1,2,3-triazole derivative, easily obtained *via* a click reaction. In fact, the Cu(I)-catalyzed azide-alkyne cycloaddition (CuAAC),^{14,15} proved to be a very effective method to regioselectively afford 1,4-substituted-1,2,3-triazoles from azides and terminal alkynes with a wide range of substituents. Furthermore, 4-pyridine-1,2,3-triazole derivatives has been widely employed as ancillary ligands in the formation of emitting Ir(III) complexes, with good photophysical properties.^{16,17}

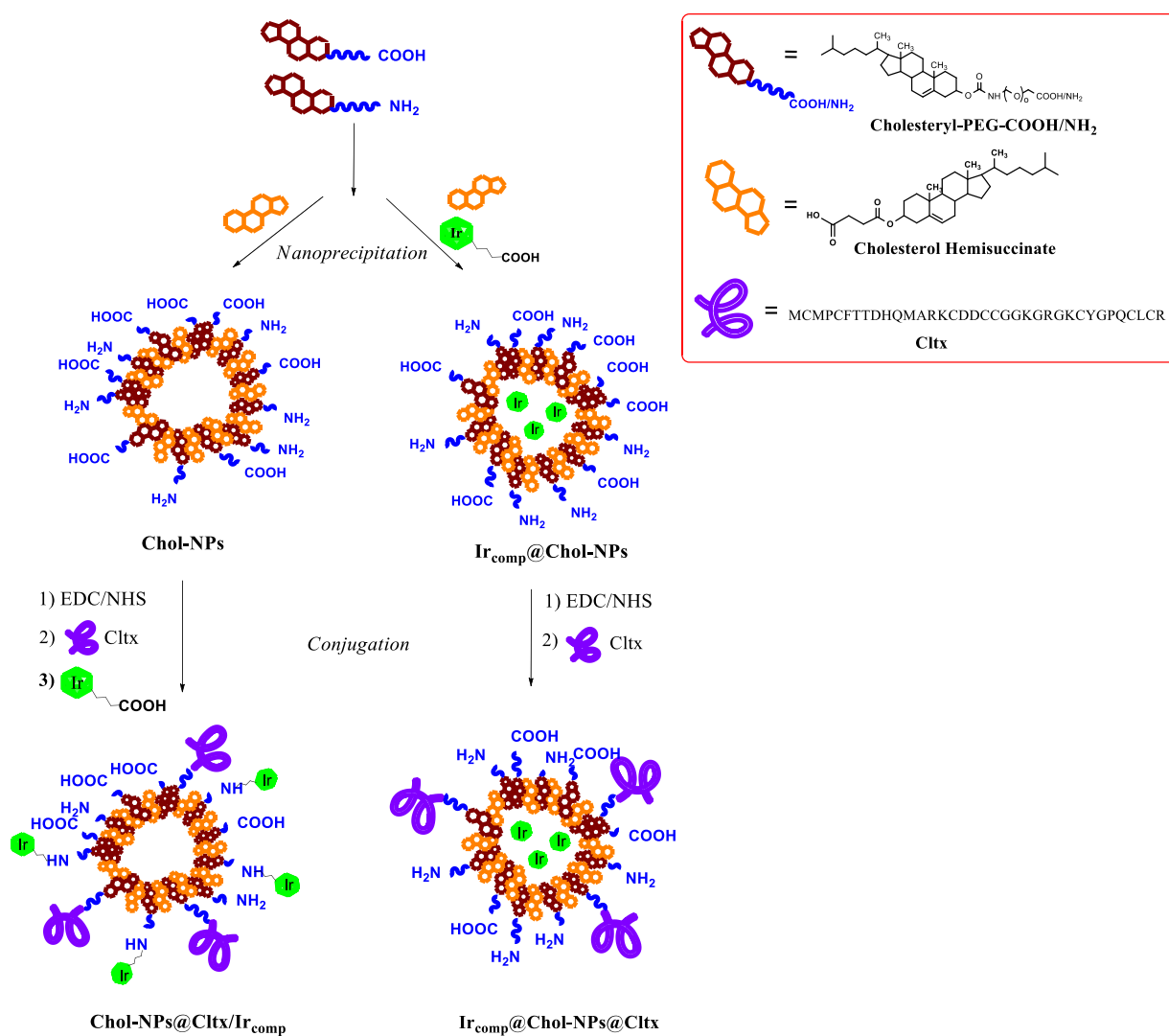
The synthesis of complex **4** is reported in Scheme 1. Starting from commercially available ethyl 7-bromoheptanoate (**1**), NaN₃ was added and the corresponding azide was isolated in quantitative yield. The crude azide was then reacted with 2-ethynylpyridine under Huisgen cycloaddition conditions to give the bidentate compound **2** in 95% yield. Ligand **2** was used as ancillary ligand to prepare the complex **3**. The cyclometalated μ -dichloro-bridged iridium precursor [Ir(C[^]N)₂Cl]₂, where C[^]N is ppy = 2-phenylpyridine, was dissolved in a 3:1 mixture of DCM and EtOH, then **2** was added and the reaction mixture was stirred at room temperature for 72 hours. After purification of the crude by washing with Et₂O, the pure product **3** was isolated in 96% yield. Finally, ester saponification was performed through treatment with KOH, giving the target complex **4** in 96% yield.



Scheme 1: Synthesis of target Ir(III) complex

12.1.2 Synthesis of the nanoparticles

The process is reported in Scheme 2. Two PEG-cholesterol based amphiphilic macrostructures, with carboxylic acid or amino terminal groups have been prepared by reaction of cholesteryl chloroformate and two different PEG polymer, giving desired Chol-PEG-COOH and Chol-PEG-NH₂ copolymer. Through nanoprecipitation techniques, nanocarriers have been prepared. Nanoprecipitation in presence of the Ir(III) complex lead to Ir_{comp}@Chol-NPs, where Ir is contained in the nanocarrier. Chol-NPs@Ir_{comp}, where the Ir complex is linked to the outer sphere of the nanoparticle, are prepared through the reaction of empty nanocarrier, with terminal -NH₂ group on the surface and the iridium complex **4**. Both Ir(III)-containing nanoparticles have been then decorated in the outer sphere with Cltx (Chlorotoxin), a 36-aminoacid peptide very used as targeting agent for glioma cell lines.^{18,19,20,21}



Scheme 2: Schematic representation of the final nanoparticles preparation

12.1.3 ζ potential and hydrodynamic diameter

Characterization data for synthesized nanocarriers are summarized in Table 1. The empty nanocarrier (Chol-NPs, entry 1) shows a small hydrodynamic diameter of 52.4 nm with a ζ potential of -23.3 mV, negative for the presence of deprotonated carboxylic acid groups and not protonated amino groups in the NPs outer sphere. Similar ζ potential was measured also for the Iridium(III) complex-containing nanocarrier ($\text{Ir}_{\text{comp}}@$ Chol-NPs, entry 2), however with an increase in the hydrodynamic diameter of about 10 nm. Functionalization of NPs' outer shell with Cltx and Ir(III) complex results in little change in hydrodynamic diameter, 53.8 nm, and an increase in the ζ potential, -32.3 mV (entry 4), indicative of successfully conjugation. Similar ζ potential was also measured for $\text{Ir}_{\text{comp}}@$ Chol-NPs@Cltx, with a value of -33.2 mV, but in this case, a sensible increase in hydrodynamic diameter is detected, up to 76 nm.

Table 1: ζ potential and hydrodynamic diameter for synthesized nanocarriers

Entry	Sample	DLS [nm]	ζ potential [mV]
1	Chol-NPs	52.4 \pm 2.0	-23.3
2	$\text{Ir}_{\text{comp}}@$ Chol-NPs	63.9 \pm 1.3	-20.4
3	$\text{Ir}_{\text{comp}}@$ Chol-NPs@Cltx	75.9 \pm 0.5	-33.2
4	Chol-NPs@Cltx/ Ir_{comp}	53.8 \pm 2.1	-32.3

12.1.4 Photophysical characterization

The photophysical properties of Chol-NPs@Cltx/ Ir_{comp} and $\text{Ir}_{\text{comp}}@$ Chol-NPs@Cltx in water have been investigated and are reported in Figure 1. The absorption spectra are very similar to this of the free Ir(III) complex **4**. The bands in the 250-300 nm region are assigned to spin allowed ligand-centered transitions ^1LC ($\pi-\pi^*$) localized in the triazole-pyridine and phenyl-pyridine ligands. The weaker absorption bands in the 350–420 nm region belong to spin allowed $^1\text{MLCT}$ and spin forbidden $^3\text{MLCT}$ transitions. As observed for **4**, both Chol-NPs@Cltx/ Ir_{comp} and $\text{Ir}_{\text{comp}}@$ Chol-NPs@Cltx exhibited intense phosphorescence with maxima at 484 and 512 nm, with quantum yields (Φ) of 31% and 23%, respectively, and lifetimes of 1.46 ns and 1.41 ns, respectively.

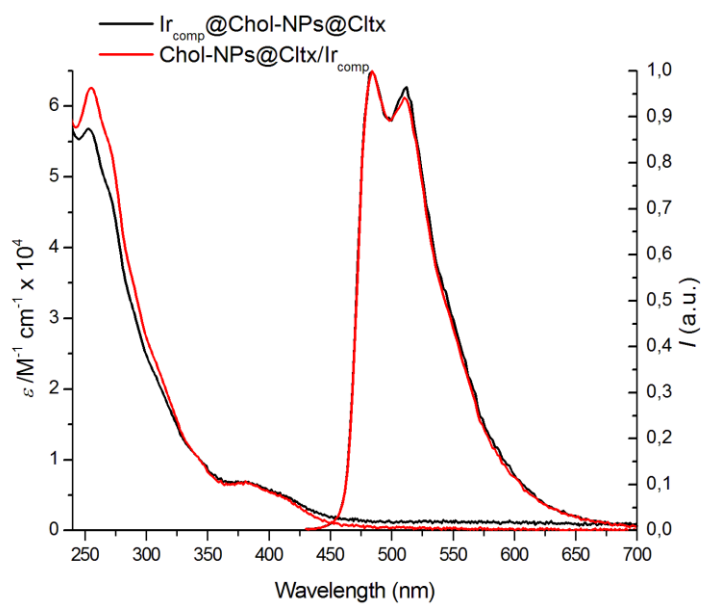


Figure 1: Absorption and normalized emission spectra ($\lambda_{\text{exc}} = 386 \text{ nm}$) of $\text{Ir}_{\text{comp}}@ \text{Chol-NPs}@ \text{Cltx}$ and $\text{Chol-NPs}@ \text{Cltx}/ \text{Ir}_{\text{comp}}$ in air equilibrated water solution at room temperature

12.1.5 Internalization of Ir(III)-NPs

Glioblastoma multiforme cancer cells have been treated with the prepared NPs, in order to demonstrate the effective ability of them to be internalized (Figure 2).

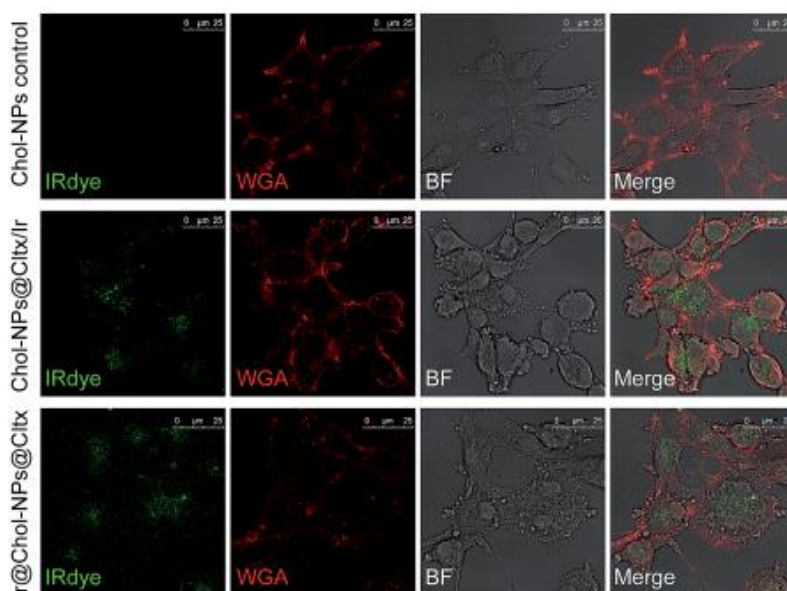


Figure 2: Internalization of iridium(III)-containing NPs into glioma-derived U87MG cells. $\text{Chol-NPs}_{\text{control}}$, $\text{Chol-NPs}@ \text{Cltx}/ \text{Ir}_{\text{comp}}$ and $\text{Ir}_{\text{comp}}@ \text{Chol-NPs}@ \text{Cltx}$ (0.1 mg/mL) were incubated with U87MG cells for 24 h, respectively. Cells were then fixed and subjected to confocal microscopy. NPs are visualized in green, while wheat germ agglutinin (WGA), a lectin that binds to sialic acid and *N*-acetylglucosaminyl residues on the cell surface, is visualized in red. The results shown are averages of triplicate samples from a typical experiment. Measurement bar in confocal images is 25 micrometers.

As a result, Chol-NPs@Cltx/Ir_{comp} was found to be more selective toward the U87MG cells than Ir_{comp}@Chol-NPs@Cltx nanocarriers, principally due to the different stability of the NPs. However, when the Ir(III) is covalently linked, as in the case of Chol-NPs@Cltx/Ir_{comp}, NPs is more stable and no NPs can be found outside of the cells (green dots, see Figure 2, right bottom, Merge image), thing that can be observed for NPs where Ir(III) is entrapped in the nanocarrier, as for Ir_{comp}@Chol-NPs@Cltx (Figure 2, right central, Merge image).

12.2 Conclusions

We have successfully synthesized an opportunely functionalized pyridine-triazole ancillary ligand suitable for Iridium complexation, with a terminal carboxylic acid group. The ligand has been used to prepare a phosphorescent Ir(III) complex, that has been fully characterized. Complex **4** has been used in the preparation of two different cholesterol-PEG based nanoparticles, one with the Ir(III) complex encapsulated in the empty core, and one with the Ir(III) complex covalently linked to the outer sphere. Both the NPs show good photophysical properties and the ability to be internalized in cancer cells. Applications of the described nanosystem in nanomedicine and drug delivery are still under investigation.

12.3 Experimental section

Materials and methods

CH₂Cl₂ and CHCl₃ were passed through basic alumina prior to use. Chromatographic purifications were performed using 70-230 mesh silica. ¹H NMR and ¹³C NMR spectra were recorded using CDCl₃ or DMSO solutions at 300, 400 and 600 MHz for ¹H and 75.46, 100.6 and 150.92 MHz for ¹³C. Chemical shifts (δ) are reported in ppm relative to CHCl₃ (δ = 7.26 for ¹H and δ = 77.0 for ¹³C). ¹³C NMR spectra were acquired with ¹H broad band decoupled mode. The following abbreviations are used to indicate the multiplicity: s, singlet; d, doublet; t, triplet; q, quartet; quint, quintet; oct, octet; m, multiplet; b, broad signal. Fourier transform infrared (FTIR) spectra were recorded on a Perkin-Elmer Spectrum 2000. Mass spectra (MS) were obtained with an electrospray ionization source (ESIMS). All the ESIMS spectra were performed using MeOH as the solvent. Elemental analyses were performed using Flash EA1112 Automatic Elemental Analyzer CE instruments. All reactions were carried out in air and using undistilled solvent without any precautions to exclude moisture, unless otherwise mentioned. UV/Vis absorption spectra were measured on a Varian Cary 4 double-beam UV-Vis spectrometer and baseline corrected. Steady-state emission spectra were recorded on an Edinburgh FLS920P spectrofluorimeter equipped with a 450 W Xenon arc lamp, double excitation and single emission monochromators and a peltier cooled Hamamatsu R928P photomultiplier tube (185–850

nm). Emission and excitation spectra were corrected for source intensity (lamp and grating) and emission spectral response (detector and grating) by calibration curve supplied with the instrument. Emission lifetimes were determined on the same Edinburgh instrument with the Time Correlated Single Photon Counting (TCSPC) technique using pulsed picosecond LEDs (ELED 309.6, FWHM <800 ps, repetition rates between 10 kHz and 1 MHz) as the excitation source and the above-mentioned R928P PMT as detector. The goodness of fit was assessed by minimizing the reduced χ^2 function and visual inspection of the weighted residuals. The emission quantum yields were determined according to the optically dilute solutions method in aqueous solutions with reference to Ru(bpy)₃Cl₂ as the standard (r) according to Equation (1)²² where *I* refers to the area of the emission peaks of the complex and the reference, *A* to their absorptions and *n* is the refractive index of the corresponding solvents.

$$\Phi = \Phi_r \frac{I}{I_r} \frac{A_r}{A} \frac{n^2}{n_r^2} \quad (1)$$

Synthesis of **2**

To a solution of ethyl 7-bromoheptanoate **1** (1.19 g, 5.0 mmol) in DMSO (17 ml) NaN₃ (650 mg, 10 mmol) was added. The mixture was left to stir at room temperature for 24 hours, then 75 ml of water and 75 ml of EtOAc were added. The aqueous layer was separated and extracted with EtOAc (3 x 50 ml). The collected organic phases were dried over MgSO₄ and the solvent evaporated. The obtained crude azide showed good purity at ¹H NMR analysis [(CDCl₃, 300 MHz) δ 4.07 (q, *J*_{HH} = 7.2 Hz, 2H), 3.21 (t, *J*_{HH} = 6.9 Hz, 2H), 2.25 (t, *J*_{HH} = 7.7 Hz, 2H), 1.64-1.50 (m, 4H), 1.38-1.28 (m, 4H), 1.21 (t, *J*_{HH} = 7.1 Hz, 3H). ¹³C NMR (CDCl₃, 75 MHz) δ 173.6 (CO), 60.2 (CH₂), 51.3 (CH₂), 34.1 (CH₂), 28.6 (CH₂), 28.5 (CH₂), 26.3 (CH₂), 24.7 (CH₂), 14.2 (CH₃).] and therefore it was directly employed in the next step without further purification. The crude azide was dissolved in a 1:1 *t*BuOH/H₂O mixture (25 ml) and CuSO₄·5H₂O (62 mg, 0.25 mmol), Na-(L)-ascorbate (324 mg, 1.5 mmol) and ethynyl pyridine (0.56 mL, 5.5 mmol) were added. After 24 hours stirring at room temperature, the solvent was removed under vacuum and aqueous NH₃ (35 ml) and DCM (35 ml) were added and the mixture was left to stir overnight. Therefore, after separation of the phases, the aqueous layer was extracted with DCM (3 x 25 ml). The collected organic layers were dried over MgSO₄, filtered and the solvent removed under vacuum. The crude product was purified by flash chromatography (EtOAc/DCM=6/4 and DCM/MeOH=9/1) to give 1.43 g (4.7 mmol, 95% yields from **1**) of **2** as a pale yellow solid. ¹H NMR (CDCl₃, 300 MHz) δ 8.58 (dq, *J*_{HH} = 4.9 Hz, *J*_{HH} = 0.9 Hz, 1H), 8.18 (dt, *J*_{HH} = 8.0 Hz, *J*_{HH} = 1.1 Hz, 1H), 8.12 (s, 1H), 7.78 (td, *J*_{HH} = 7.8 Hz, *J*_{HH} = 1.9 Hz, 1H), 7.23 (ddd, *J*_{HH} = 7.5 Hz, *J*_{HH} = 4.9 Hz, *J*_{HH} = 1.3 Hz, 1H), 4.42 (t, *J*_{HH} = 7.1 Hz, 2H), 4.12 (q, *J*_{HH} = 7.1 Hz, 2H), 2.28 (t, *J*_{HH} = 7.3 Hz, 2H), 2.03-1.91 (m, 2H), 1.70-1.53 (m, 2H), 1.42 - 1.35 (m, 4H), 1.25 (t, *J*_{HH} = 7.1 Hz, 3H). ¹³C NMR (CDCl₃, 100 MHz) δ 173.5 (CO), 150.3 (C), 149.3

(CH), 148.3 (C), 136.8 (CH), 122.7 (CH), 121.7 (CH), 120.2 (CH), 60.2 (CH₂), 50.3 (CH₂), 34.0 (CH₂), 30.0 (CH₂), 28.4 (CH₂), 26.1 (CH₂), 24.6 (CH₂), 14.2 (CH₃).

Synthesis of complex 3

In a 25 ml round-bottom flask equipped with a stirring bar, ligand **2** (14 mg, 2.5 equiv) was dissolved in a 3:1 mixture of CH₂Cl₂/EtOH (5 mL) and the dimer [(ppy)₂Ir(μ-Cl)]₂ (20 mg, 0.019 mmol) was added. The mixture was left to stir at room temperature for 72 hours. Then the solvent was evaporated and the crude product was washed with Et₂O to remove the excess of ligand to give 30 mg of pure **3** (96% yields). ¹H NMR (CDCl₃, 400 MHz) δ 10.9 (s, 1H), 9.19 (d, *J*_{HH} = 7.9 Hz, 1H), 7.99 (t, *J*_{HH} = 7.8 Hz, 1H), 7.91 (dd, *J*_{HH} = 8.2 Hz, *J*_{HH} = 4.1 Hz, 2H), 7.79-7.71 (m, 3H), 7.69-7.63 (m, 3H), 7.45 (d, *J*_{HH} = 6.2 Hz, 1H), 7.21 (t, *J*_{HH} = 6.9 Hz, 1H), 7.05-6.83 (m, 6H), 6.32 (dd, *J*_{HH} = 12.2 Hz, *J*_{HH} = 7.6 Hz, 2H), 4.46 (oct, *J*_{HH} = 7.1 Hz, 2H), 4.12 (q, *J*_{HH} = 7.5 Hz, 2H), 2.23 (t, *J*_{HH} = 7.5 Hz, 2H), 1.95 (quint, *J*_{HH} = 7.5 Hz, 2H), 1.51 (quint, *J*_{HH} = 7.7 Hz, 2H), 1.32-1.14 (m, 7H). ¹³C NMR (CDCl₃, 100 MHz) δ 173.6 (CO), 168.4 (C), 167.7 (C), 150.2 (C), 150.1 (C), 149.4 (CH), 149.3 (CH), 148.5 (C), 148.3 (CH), 146.6 (C), 143.7 (C), 143.6 (C), 139.7 (CH), 137.9 (CH), 137.8 (CH), 131.8 (CH), 131.7 (CH), 130.6 (CH), 130.0 (CH), 129.3 (CH), 125.8 (CH), 125.0 (CH), 124.6 (CH), 124.3 (CH), 123.1 (CH), 122.7 (CH), 122.6 (CH), 122.1 (CH), 119.4 (CH), 119.3 (CH), 60.2 (CH₂), 50.2 (CH₂), 34.1 (CH₂), 29.6 (CH₂), 28.2 (CH₂), 25.9 (CH₂), 24.7 (CH₂), 14.2 (CH₃).

Synthesis of complex 4

In a 25 ml round-bottom flask equipped with a stirring bar, the complex **3** (30 mg, 0.036 mmol) was dissolved in 2 mL of DCM. A solution of KOH (33 mg, 0.582 mmol) in a 3:1 mixture of EtOH/H₂O (1 mL) was added and mixture was left to stir at room temperature overnight. Then the solvent was evaporated and the crude product was neutralized with diluted HCl (1M). The aqueous layer was extracted with DCM (3 x 10 ml). The collected organic layers were dried over MgSO₄, filtered and the solvent removed under vacuum to give 28 mg (0.0346 mmol, 96% yields) of pure **4** as a pale yellow solid. ¹H NMR (CDCl₃, 400 MHz) δ 10.41 (s, 1H), 9.08 (d, *J*_{HH} = 6.1 Hz, 1H), 8.02 (t, *J*_{HH} = 7.8 Hz, 1H), 7.91 (dd, *J*_{HH} = 8.2 Hz, *J*_{HH} = 4.1 Hz, 2H), 7.81-7.71 (m, 3H), 7.70-7.62 (m, 3H), 7.48 (d, *J*_{HH} = 6.2 Hz, 1H), 7.21 (t, *J*_{HH} = 6.9 Hz, 1H), 7.10-6.83 (m, 6H), 6.32 (dd, *J*_{HH} = 12.2 Hz, *J*_{HH} = 7.6 Hz, 2H), 4.46 (oct, *J*_{HH} = 7.1 Hz, 2H), 2.44 (t, *J*_{HH} = 7.5 Hz, 2H), 1.95 (quint, *J*_{HH} = 7.5 Hz, 2H), 1.67 (quint, *J*_{HH} = 7.7 Hz, 2H), 1.42-1.21 (m, 4H). ¹³C NMR (CDCl₃, 100 MHz) δ 174.9 (CO), 167.3 (C), 166.6 (C), 149.0 (2C), 148.6 (CH), 148.3 (CH), 147.5 (C), 147.3 (CH), 145.5 (C), 142.7 (C), 146.6 (C), 138.8 (CH), 137.1 (CH), 136.9 (CH), 130.8 (CH), 130.7 (CH), 129.6 (CH), 129.0 (CH), 127.5 (CH), 125.0 (CH), 123.6 (2CH), 123.3 (CH), 122.3 (CH), 121.8 (CH), 121.6 (CH), 121.2 (CH), 118.4 (2CH), 51.0 (CH₂), 33.3 (CH₂), 28.3 (CH₂), 26.8 (CH₂), 24.3 (CH₂), 23.5 (CH₂). ESI-MS : 775 [M⁺]. Elemental Analysis: C, 53.28; H, 4.21; Cl, 4.39; Ir, 23.68; N, 10.35; O, 3.92.

12.4 Bibliography

- ¹ D. M. Parkin, F. Bray, J. Ferlay, P. Pisani, *Ca-Cancer J. Clin.* **2005**, *55*, 74.
- ² X. Wang, L. Yang, Z. Chen, D. M. Shin, *Ca-Cancer J. Clin.* **2008**, *58*, 97.
- ³ Y. You, *Curr. Opin. Chem. Biol.* **2013**, *17*, 699.
- ⁴ K. K. Lo, K. Y. Zhang, *RSC Adv.* **2012**, *2*, 12069.
- ⁵ H. Wu, T. Yang, Q. Zhao, J. Zhou, C. Li, F. Li, *Dalton Trans.* **2011**, *40*, 1969.
- ⁶ C. W. Lai, Y.-H. Wang, C.-H. Lai, M.-J. Yang, C.-Y. Chen, P.-T. Chou, C.-S. Chan, Y. Chi, Y.-C. Chen, J.-K. Hsiao, *Small* **2008**, *4*, 218.
- ⁷ Z. Zhou, D. Li, H. Yang, Y. Zhub, S. Yang, *Dalton Trans.* **2011**, *40*, 11941.
- ⁸ Y. Wang, H. Wang, G. Liu, X. Liu, Q. Jin, J. Ji, *Macromol. Biosci.* **2013**, *13*, 1084.
- ⁹ J.-H. Lee, S.-W. Jung, I.-S. Kim, Y.-I. Jeong, Y.-H. Kim, S.-H. Kim, *Int. J. Pharm.* **2003**, *251*, 23.
- ¹⁰ B. Luppi, T. Cerchiara, F. Bigucci, R. Basile, V. Zecchi, *J. Pharm. Pharmacol.* **2004**, *56*, 407.
- ¹¹ Y. Maitani, A. Nakamura, T. Tanaka, Y. Aso, *Int. J. Pharm.* **2012**, *427*, 372.
- ¹² M. A. Maslov, T. O. Kabilova, I. A. Petukhov, N. G. Morozova, G. A. Serebrennikova, V. V. Vlassov, M. A. Zenkova, *J. Controlled Release* **2012**, *160*, 182.
- ¹³ S. Winzen, M. Bernhardt, D. Schaeffel, A. Koch, M. Kappl, K. Koynov, K. Landfester, A. Kroeger, *Soft Matter* **2013**, *9*, 5883.
- ¹⁴ V. V. Rostovtsev, L. G. Green, V. V. Fokin, K. B. Sharpless, *Angew. Chem. Int. Ed.* **2002**, *41*, 2596.
- ¹⁵ F. Himo, T. Lovell, R. Hilgraf, V. V. Rostovtsev, L. Noodleman, K. B. Sharpless, V. V. Fokin, *J. Am. Chem. Soc.* **2005**, *127*, 210.
- ¹⁶ E. Orselli, R. Q. Albuquerque, P. M. Fransen, R. Frohlich, H. M. Janssen, L. De Cola, *J. Mater. Chem.* **2008**, *18*, 4579.
- ¹⁷ A. Baschieri, S. Muzzioli, V. Fiorini, E. Matteucci, M. Massi, L. Sambri, S. Stagni, *Organometallics* **2014**, *33*, 6154.
- ¹⁸ E. Locatelli, F. Broggi, J. Ponti, P. Marmorato, F. Franchini, S. Lena, M. Comes Franchini, *Adv. Healthcare Mater.* **2012**, *1*, 342.
- ¹⁹ A. Pucci, E. Locatelli, J. Ponti, C. Uboldi, V. Molinari, M. Comes Franchini, *J. Nanopart. Res.* **2013**, *15*, 1818.
- ²⁰ E. Locatelli, W. Bost, M. Fournelle, J. Llop, L. Gil, F. Arena, V. Lorusso, M. Comes Franchini, *J. Nanopart. Res.* **2014**, *16*, 2304.
- ²¹ E. Locatelli, M. Naddaka, C. Uboldi, G. Loudos, E. Fragogeorgi, V. Molinari, A. Pucci, T. Tsotakos, D. Psimadas, J. Ponti, M. Comes Franchini, *Nanomedicine* **2014**, *9*, 839.
- ²² K. Binnemans, *Chem. Rev.* **2009**, *109*, 4283.